MICROBIAL CATALYSIS FOR THE PRODUCTION OF HYDROXY- AND AMINO-FATTY ACIDS

Eden Silva e Souza, B.Sc., M.Sc.

School of Biomolecular and Biomedical Science

Head of School: Professor Dr. Cormac Murphy

Principal Supervisor: Dra. Tanja Narančić

A thesis submitted to University College Dublin in fulfilment of the

requirements for the degree of Doctor of Philosophy

October 2024

TABLE OF CONTENTS

Abbreviations

1-PEA	1-phenylethylamine
2ABA	2-aminobutyric acid
2AHA	2-aminohexanoic acid
2AOA	2-aminooctanoic acid
2ADA	2-aminodecanoic acid
2HBA	2-hydroxybutyric acid
2HHA	2-hydroxyhexanoic acid
2HOA	2-hydroxyoctanoic acid
3ABA	3-aminobutyric acid
3HBA	3-hydroxybutyric acid
3HBAd	3-hydroxybutyric acid dehydrogenase
3OBA	3-oxobutyric acid / acetoacetate
AA	Amino acid
AADH	Amino acid dehydrogenases
abs	Absorbance
ADH	Alcohol dehydrogenase
Aib	2-aminoisobutyric acid
AMP	Antimicrobial peptide
AMR	Antimicrobial resistance
ANOVA	Analysis of Variance
AP	Acetophenone
ATCC	American Type Culture Collection
ATP	Adenosine triphosphate
BCA	Bicinchoninic acid
Bch	3-hydroxyisobutyryl-CoA hydrolase gene from *Bacillus cereus*
bLf	Bovine lactoferrin
bLfcin	Bovine lactoferricin
LFcin	Bovine lactoferricin nonameric peptide
Bp	Base pair
BSA	Bovine serum albumin
CAMP	Cationic antimicrobial peptide
Carb	Carbenicillin
CD	Circular dichroism
CDW	Cell dry weight

CE	Cell extract
Cec	Cecropin family of antimicrobial peptides
CFE	Cell free extract
CFU	Colony forming unit
Chl	Chloramphenicol
CoA	Coenzyme A
CRISPR	Clustered regularly interspaced short palindromic repeats-associated protein 9
CV_TA	Transaminase *CV2025* from *Chromobacterium violaceum*
Dap	3-diaminopropionic acid
DDH	D-lactate from *Haloferax mediterranei*
DMSO	Dimethyl sulfoxide
DNA	Deoxyribonucleic acid
DS	Downstream region
dsDNA	Double-stranded DNA
DTNB	5,5′-dithiobis (2-nitrobenzoic acid)
EC	Enzyme Commission number
FMN	Flavin mononucleotide
g	Gram
gDNA	Genomic DNA
Gen	Gentamycin
Glu	Glucose
GO	Glycolate oxidase from S*pinacia oleracea*
h	Hour
HFA	Hydroxy fatty acids
hLf	Human lactoferrin
hLfcin	Human lactoferricin
HPLC	High-performance liquid chromatography
HRP	Horseradish peroxidase
IC_{50}	Half-maximal inhibitory concentration
IPTG	Isopropyl-β-D-1-thiogalactopyranoside
kDa	Kilodalton
Kb	Kilobase
K_{cat}	Catalytic constant
KEGG	Kyoto Encyclopaedia of Genes and Genomes
Kg	Kilogram

km	Kanamycin
K_m	Michaelis-Menton constant
kV	Kilovolts
L	Liter
LA	Lactic acid
L-ala	L-alanine
LB	Luria-Bertani medium
LDH	Lactate dehydrogenase
LeuDH	Leucine dehydrogenase from *Bacillus thuringiensis*
LFcin	Lactoferricin
Lf	Lactoferrin
LPS	Lipopolysaccharide
M	Molar
MBC	Minimum bactericidal concentration
Methyl-3OBA	Methyl-3-oxobutyric acid / methyl-acetoacetate
mg	Milligram
MIC	Minimum inhibitory concentration
min	Minute
mL	Millilitre
mM	Millimolar
MOA	Mode of action
MPA	3-mercaptopropionic acid
min	Minute
mg	Milligram
mM	Millimolar
NAD^+	Nicotinamide adenine dinucleotide (oxidised form)
NADH	Nicotinamide adenine dinucleotide (reduced form)
ncAA	Non-coded amino acid
NCTC	National Collection of Type Cultures
ng	Nanogram
OD	Optical density
OPA	*o*-phthalaldehyde
PAGE	Polyacrylamide gel electrophoresis
PBS	Phosphate buffered saline
PC	Phosphatidylcholine
PCR	Polymerase chain reaction

PDB	Protein data bank
PE	Phosphatidylethanolamine
PET	Polyethylene terephthalate
pH	Negative logarithm of hydrogen ion concentration
PhaA	Acetoacetyl-CoA thiolase gene (*phaA*)/protein from *Cupriavidus necator*
PHA	Polyhydroxyalkanoate
PHB	Polyhydroxybutyrate
PLA	Polylactic acid
PLP	Pyridoxal 5′-phosphate
PMP	Pyridoxamine 5'-phosphate
PNP	Pyridoxine 5′-phosphate
PS	Phosphatidylserine
Pyr	Pyruvate
(*R*)3HBA	(*R*)-3-hydroxubutyric acid
RBC	Red blood cell
RBS	Ribosomal binding site
SEM	Scanning electron microscopy
rpm	Revolutions per minute
(*S*)3HBA	(*S*)-3-hydroxubutyric acid
s	Second
SD	Standard deviation
SDS-PAGE	Sodium dodecyl sulfate polyacrylamide gel electrophoresis
SEM	Scanning electron microscopy
sgRNA	Single guide RNA
SM	Sphingomyelin
spec	Spectinomycin
TA	Transaminase
TCA	Tricarboxylic acid cycle
TesB	Thioesterase gene/protein from *E. coli* K12
TEM	Transmission electron microscopy
TEMED	TEMED
Tet	Tetracycline
TNB	5-thio-2-nitrobenzoic acid
US	Upstream region
V	Volt
Vmax	Maximum velocity

v/v	Volume per volume
w/v	Weight per volume
°C	Degree Celsius
%	Percentage
Å	Angstroms
α	Alpha
β	Beta
ε	Molar (absorption) extinction coefficient
µg	Microgram
µL	Microliter
µM	Micromolar
Φ	Phi
Ψ	Psi
θ	Theta
ω	Omega

Amino acids

Amino acid	3-letter abbreviation	1-letter abbreviation
Alanine	Ala	A
Arginine	Arg	R
Asparagine	Asn	N
Aspartic acid	Asp	D
Cysteine	Cys	C
Glutamic acid	Glu	E
Glutamine	Gln	Q
Glycine	Gly	G
Histidine	His	H
Isoleucine	Ile	I
Leucine	Leu	L
Lysine	Lys	K
Methionine	Met	M
Phenylalanine	Phe	F
Proline	Pro	P
Serine	Ser	S
Threonine	Thr	T
Tryptophan	Trp	W
Tyrosine	Tyr	Y
Valine	Val	V

Declaration of authorship

I hereby certify that the submitted work, excepting the constructs for 3-hydroxybutyric acid synthesis, is my own work and this research was completed while registered as a candidate for the degree stated on the Title Page, and I have not obtained a degree elsewhere on the basis of the research presented in this submitted work.

Declaration of collaboration

Some elements of this research counted with the collaboration of other researcher groups.

The CD spectroscopy was carried out with Dr. Marc Devocelle at the Department of Chemistry, Royal College of Surgeons in Ireland, Ireland.

The transaminase screening was performed with help from Dr. Elaine O'Reilly, School of Chemistry, University College Dublin, Ireland.

Abstract

This study focused on the microbial synthesis of 3-hydroxybutyric acid (3HBA), which is industrially relevant but can also be converted into non-coded amino fatty acids. Synthetic operons combining the acetoacetyl-CoA thiolase gene (*phaA*) from *C. necator*, either the (*R*)- (*phaB*) or (*S*)-3-hydroxybutyryl-CoA dehydrogenase gene (*paaH1*) from *C. necator*, and thioesterase (*tesB*) from *E. coli* or 3-hydroxyisobutyryl-CoA hydrolase (*bch*) from *B. cereus* were previously developed in our laboratory to synthesize 3HBA from glucose. While successful, 3HBA synthesis produced acetate as a by-product of overflow metabolism. To address acetate co-production, genes encoding phosphotransacetylases Pta and EutD were targeted for deletion using modified CRISPR-Cas9 methods.

Testing in flasks revealed that the Δ*pta* mutant showed no 3HBA synthesis, while the double deletion Δ*eutD*Δ*pta* produced 1.2-fold less acetate but also decreased product yield by 2.3-fold. The Δ*eutD* mutant increased product yield by 1.3-fold, but acetate levels rose as well.

To optimize 3HBA synthesis further, a bioprocess was developed. Aerobic fermentation with BL21_*tesB_RHBD* yielded 6.89 g/L of 3HBA when protein expression was induced at higher densities, representing a 4.6-fold increase from previous flask conditions. Although flask cultivation showed poor results, the Δ*eutD_tesB_RHBD* strain in the bioprocess achieved a 1.6-fold increase compared to BL21, resulting in 11.2 g/L (R)3HBA while maintaining acetate at about 1 g/L.

Additionally, a cascade reaction was designed to convert 3HBA to 3-oxobutyric acid (3OBA) and then to the non-coded amino acid 3-amino butyric acid (3ABA). Since 3OBA is an intermediate in 3HBA synthesis, it was hypothesized that replacing 3-hydroxybutyryl-CoA with an ω-transaminase (CV_TA) known for 3OBA-methyl ester conversion would yield 3ABA from glucose. However, the new pathway did not produce 3ABA, as CV_TA only acted on the methyl ester form of 3OBA. Screening of three commercially available transaminases identified ATA-117 as a promising candidate, with molecular docking suggesting its potential interaction with 3OBA but not 3OBA-CoA due to unfavorable interactions in the active site.

A one-pot cascade reaction was also tested to produce α-amino fatty acids and 3ABA from hydroxy fatty acids. Five enzymes were evaluated for hydroxy fatty acid oxidation

to provide substrates for transaminase reactions. The two alcohol dehydrogenases (ADHs) did not exhibit activity towards the target substrates. While glycolate oxidase (GO) exhibited activity with all tested 2-hydroxy fatty acids, both GO and CV_TA showed mutual inhibition in one-pot assays. Two lactate dehydrogenases were cloned, but their activity remained untested due to time constraints.

The potential applications of non-coded amino acids (ncAAs) are numerous. Here their application was tested regarding the enhancement of antimicrobial peptide activity. Based on previous research, a nonapeptide derived from bovine lactorerricin was modified by adding ncAAs with acyl chains ranging from C4 to C10 at the C- or N-terminus. The modified peptides were tested against *E. coli*, *B. subtilis*, *P. aeruginosa*, *S. typhimurium*, and *S. aureus* using minimal inhibitory concentration (MIC) and minimal bactericidal concentration (MBC) assays, along with electron microscopy to assess peptide-bacteria interactions. Results indicated a correlation between increased antimicrobial peptide potency and fatty amino acid chain length. While modifications at N- and C-terminals exhibited varying effects i.e. in some instances the C-terminal modification had a more profound effect, while in others the N-terminal modification appeared more powerful, no consistent pattern emerged. SEM and TEM images showed membrane damage in *E. coli* and *B. subtilis*, suggesting membrane disruption as the primary action mechanism. Circular dichroism analysis revealed that ncAA incorporation did not alter the peptide's secondary structure in physiological or membrane mimicking environments.

Chapter 1

Introduction

1. Introduction

1.1. Biocatalysis

Catalysts promote the conversion of a substrate to its respective product without being consumed in the reaction. They enhance reaction kinetics but do not affect thermodynamics (Ney, Jawad Nasim et al. 2018). Chemical synthesis has been the "gold standard" process to produce valuable industrial compounds. However, it often requires toxic solvents or expensive metals, leading to toxic by-products and increased costs (Kharissova, Kharisov et al. 2019). For example, lactic acid (LA), also known as 2-hydroxypropanoic acid, is a chiral compound, widely used in food, pharmaceutical and chemical industries (Gezae Daful, Loridon et al. 2024). Several chemical methods describe the synthesis of LA, including from petroleum sources. Nonetheless, commercial LA has only been synthesized from its derivatives, such as esters and propionic acid, and it is usually obtained as a racemic product (Ojo and De Smidt 2023). The microbial synthesis of LA, often achieved by fermentation, is carried out under milder conditions when compared to chemical catalysis, can produce optically pure enantiomers and uses cheap feedstocks, like sugars (Gezae Daful, Loridon et al. 2024)

As many of the molecules used in daily life are derived from petroleum, a non-renewable source, the scientific community has made significant efforts to find better alternatives to produce these materials. Currently, it is possible to obtain similar biobased molecules.

The use of biological components, such as cells or enzymes, can greatly reduce toxic waste without compromising efficiency (Thakkar, Mhatre et al. 2010). The application of purified enzymes, cell lysates, or whole cells to obtain a desired product is defined as biocatalysis (Hughes and Lewis 2018). Biocatalysts have emerged as an alternative to achieve green chemistry, which promotes a more sustainable chemical production (Sun, Zhang et al. 2018). However, this comes with caveats that will be discussed shortly. The relevance of biological catalysis is observed in the number of publications and patents over the years. Less than 100 publications were found about this topic in 2000; while only in 2015, more than 800 publications were found in databases (Rossino, Robescu et al. 2022). Additionally, according to the International Mining and Resources Conference (IMARC) data, biocatalytic processes in Europe produced 52.4

kilo tons of products in 2023 and is estimated to reach 72.1 kilo tons in 2032 (IMARC 2024).

The increased focus in biobased processes can be attributed to several factors. For example, the 'Safe and Sustainable by Design' is a voluntary program created by the European Commission to incentivise industries to search for alternatives that reduce the impact of production in health, environment and climate (EuropeanCommission 2024). Along those lines, consumers' views on sustainable practices help to shift the production towards biobased or biodegradable products. For instance, the willingness of a consumer to buy a biobased product can be affected by the price, place of residence and age. In general, more campaigns for the general public are needed to increase the knowledge about biobased/biodegradable products (Ruf, Emberger-Klein et al. 2022). The highly anticipated Biotech Act, a legislation expected to simplify the regulatory processes and improve the lab-to-industry translation, will be put in place in 2025 and it will significantly contribute to the growth of biobased industries and bioeconomy.

The use of plastics is likely one of the best examples for the applicability of biocatalysis. Plastics are an essential aspect of modern society and its production is estimated to reach 760 million mega tons in 2050 (Gross and Enck 2021). The synthetic polymer polyethylene terephthalate (PET) was initially used to produce textile fibres, and it is mostly now known to compose the PET bottles. Industrially PET is obtained from the condensation of terephthalic acid and ethylene glycol derived from petroleum, a non-renewable source. The chemical synthesis of PET often uses antimony trioxide as a catalyst, as well as salts of titanium, germanium, cobalt, or manganese, which are toxic and produce toxic by-products. Furthermore, PET bottle, which is the most common form of the polymer, can be recycled, but it is non-degradable (Al-Sabagh 2016). On the other hand, biocatalysis offers the possibility of producing polyhadroxyalkanoates (PHAs), polyesters found in some bacteria species, such as *Cupriavidus necator*, or many species belonging to the genus *Pseudomonas*, and possess similar properties to synthetic plastic and can be produced by microorganisms (Sikkema, Cal et al. 2023).

Notable advances in genomics have enabled the discovery of uncultivable organisms (Cross, Campbell et al. 2019) as well as the identification of new genes and proteins

through sequence mining for enzymes and secondary metabolites (Sekurova, Schneider et al. 2019). Metagenomics, for instance, has helped to elucidate the pathways for the synthesis of PHAs from waste-water (Li, Huang et al. 2023). While enzymes, either in pure form or as whole-cell catalysts, can significantly increase reaction rates (Benkovic 2003), their use presents challenges mainly due to low stability and enzymatic efficiency. The structure and function of enzymes have been shaped by evolution for millions of years. They are usually part of metabolic pathways, accustomed to low substrate and product concentration, and frequently, negatively regulated by the presence of the product. In biocatalysis, high substrate load, fast reaction, stability under process-like conditions etc. are key desirable features in enzymes. In this context, protein engineering is crucial to broaden substrate range, enhance enzymatic stability, and achieve higher product yields. Rational protein engineering and directed evolution are commonly used methods (Ali, Ishqi et al. 2020).

The industrial application of enzymes depends on the cost of production and purification, and their susceptibility to environmental variables, such as thermo- and proteolytic stability (Garzon-Posse, Becerra-Figueroa et al. 2018). In some instances, the use of whole-cell biocatalysts over pure enzymes can contribute to cost reduction, as purification steps can be avoided, and cells provide an optimal environment for enzymatic activity (Schmid 2001). Having in mind better performance of enzymes with lower substrate load, whole-cell biocatalysts offer advantages, such as, multi-step reactions with cofactor regeneration, while still providing high selectivity regarding the product stereo- and regioselectivity (de Carvalho 2017).

Additionally, the use of biocatalysts ranges from the valuable monomers to polymers. As mentioned earlier, PLA is a biodegradable polymer that can serve as an alternative to petroleum-based polymers. PLA can be composed of DL-lactic acid (DL-LA), L-lactic acid (L-LA), or D-lactic acid (D-LA) (Tsuji and Kondoh 2017). LA is a product of microbial carbon metabolism, containing both a hydroxyl and a carboxyl group. Due to these functional groups, LA can serve as scaffold to synthesize various molecules, like acrylic acid, an unsaturated carboxylic acid used to produce plastics, textiles, and paints (Wojcieszak, Bonnotte et al. 2020), showcasing that one biobased molecule can have a myriad of applications increasing its value

Other molecules, such as hydroxy fatty acids (HFAs), monomers found in PHAs also have multiple application potential. HFAs are found in various natural sources and can be used to produce biodiesel, biopolymers, nylons, resins, waxes, and more (Takeuchi, Kishino et al. 2016). While the PHA producers have all the relevant genes to produce HFAs, there are usually multiple pathways present, and the pathways to use these valuable molecules as carbon and energy substrate. Therefore, recombinant expression of the machinery required for the synthesis of HFAs in the "neutral" context can be employed as a strategy. For instance, it has been demonstrated that by recombinantly overexpressing acyl-acyl carrier protein from plants or bacteria in *E. coli*, the production of medium chain length ω-HFAs can be achieved (Xiao, Yue et al. 2018). Furthermore, a similar approach involving the overexpression of a thioesterase to produce free fatty acids and a fatty acid hydroxylase to obtain HFAs has been used (Wang, Li et al. 2012). This process was further improved by overexpressing the acetyl-CoA carboxylase (*accase*) and thioesterase (*tesA*) genes, and deleting the gene (*fadD*), which encodes an acyl-CoA synthetase responsible for HFA degradation (Cao, Cheng et al. 2016).

Although biocatalysis presents all the advantages mentioned, there are drawbacks for its large-scale use. Claims that biocatalysis is "greener" when compared to chemical synthesis are often not supported by metrics (Domínguez De María 2021). Water is the solvent commonly used in biocatalysis. However, researchers do not consider that the waste-water resultant from biochemical reactions contains salts, solvents and by-products, thus making the resultant waste not clean. Other disadvantages of biocatalysis include the lower selectivity of whole-cells compared to purified enzymes, and difficulties in protein immobilization (Rossino, Robescu et al. 2022). Yet, biocatalysis still offers great advantages over chemical synthesis.

1.1.1. β-Hydroxybutyric acid

β-Hydroxybutyric acid (3-hydroxybutyric acid - 3HBA) is a chiral hydroxy fatty acid composed of four carbons (Figure 1.1). It is naturally produced by some bacterial species and found in plants and animals, including humans (Mierziak, Burgberger et al. 2021). Microbes can synthesize 3HBA via two routes: (1) endogenous synthesis of poly-3-hydroxybutyrate (PHB) followed by enzymatic depolymerization to 3HBA; or

recombinant synthesis where a (2) β-ketothiolase condenses two acetyl-CoA molecules from the TCA cycle into acetoacetyl-CoA, which is then reduced to 3-hydroxybutyryl-CoA by acetoacetyl-CoA reductase, followed by removal of the CoA group by a thioesterase (Biernacki, Riechen et al. 2017) (Figure 1.2.).

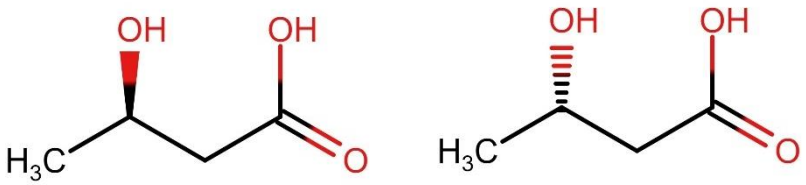

Figure 1. 1. Chemical structure of (*R*)-3-hydroxybutyric acid (left) and (*S*)-3-hydroxybutyric acid (right).

In animals, 3HBA is produced as an intermediate in the fatty acid degradation pathway (Lehninger, Sudduth et al. 1960) and can be secreted by degradation of PHB produced in the microbiome (Bonartsev, Voinova et al. 2018). In plants, the metabolism of 3HBA is yet to be elucidated. However, β-ketothiolase and acetoacetyl-CoA-reductase, known to participate in 3HBA synthesis in bacteria, are activated in plants. Furthermore, in these organisms, 3HBA is involved in metabolic processes related to environmental stress resistance, though its roles are not fully understood (Mierziak, Burgberger et al. 2021). Bacteria produce 3HBA via the first route mentioned above by polymerizing (*R*)-3-hydroxybutyryl-CoA under stress conditions as a form of carbon storage polymer (PHB) (Vicente, Proença et al. 2023). PHB, part of the polyhydroxyalkanoates, has a range of industrial applications (Diniz, Mourão et al. 2023).

3HBA has been investigated for its medical applications. Studies show 3HBA has positive effects on hypertension (Chakraborty, Galla et al. 2018), colorectal cancer (Dmitrieva-Posocco, Wong et al. 2022) and as an anti-aging compound (Wang, Chen et al. 2021). 3HBA is also a precursor in the synthesis of 4-acetoxy-2-azetidinone, an intermediate for carbapenem antibiotics, an industry worth $20.73 million in China in

2020 (Ye, Yang et al. 2022). 3HBA is also a precursor for ethyl-3-hydroxybutyrate, which imparts a fruity flavour and aroma to wine (Ortega, López et al. 2001).

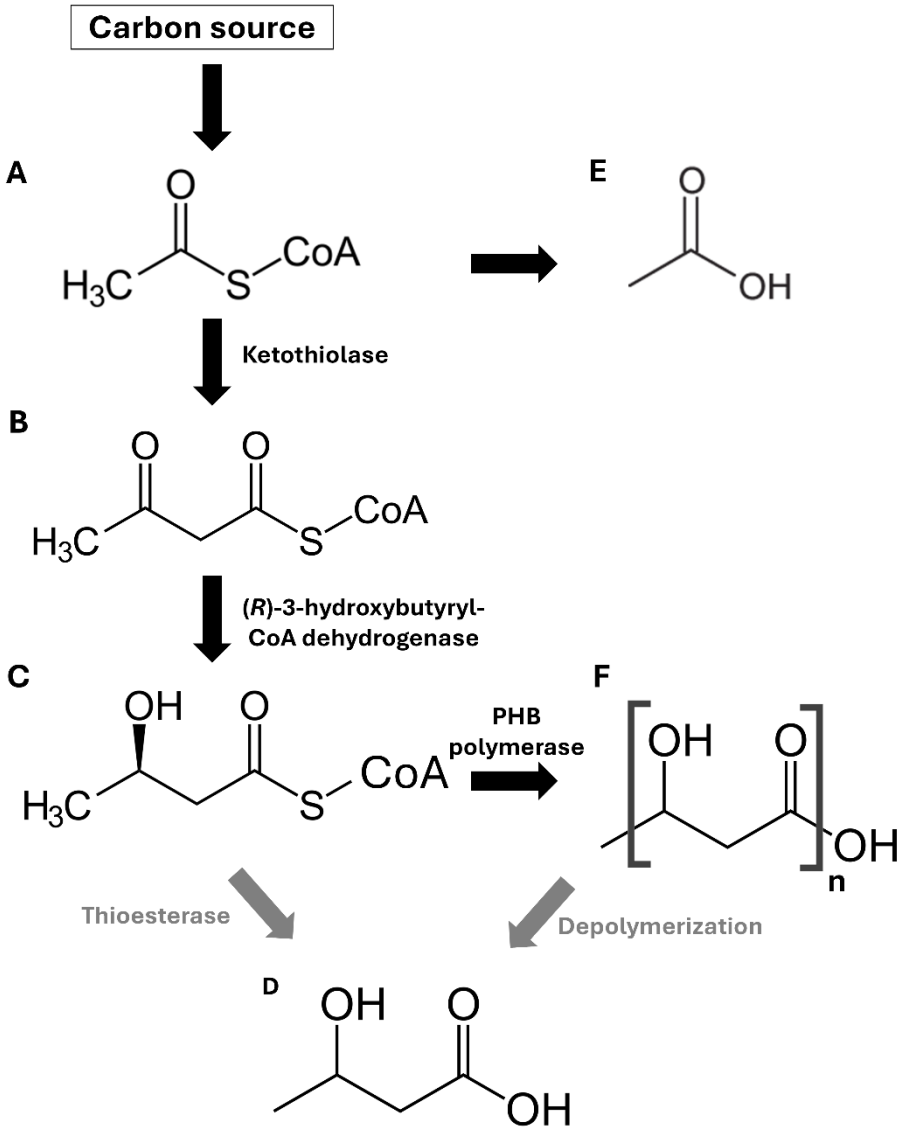

Figure 1. 2. Routes to obtain 3-hydroxybutyric acid natively (black arrows) or recombinantly (grey arrows) from a carbon source that can be sugar, CO_2, or acetate. The native synthesis uses (A) acetyl-CoA produced in TCA cycle, which can be secreted as (E) acetate or be condensed to (B) acetoacetyl-CoA, which is the converted to (C) (*R*)-3-hydroxybutyryl-CoA. A PHB polymerase uses (C) to produce (F) PHB. (F) can be recombinantly bio-, thermo- or chemically depolymerized to (D) 3HBA or the -CoA group in (C) can be cleaved by a thioesterase.

1.1.2. Synthesis of 3HBA

The synthesis of 3HBA and other chiral molecules can be achieved by chemical or biological methods. Chemical synthesis of hydroxy fatty acids is hindered by low yields, use of toxic/expensive catalysts, and multi-step methodologies, making it undesirable on a large scale, use of toxic and, or expensive chemical catalysts. For example, using commercial long-chain aldehydes as substrate, Bourboula and colleagues developed a chemical process where the substrates were converted to an epoxy by an imidazolidinone organocatalyst, which was further converted to 3-hydroxy fatty acids, using vinylmagnesium, and fatty γ-lactones by or ozonolysis, a process where an alkane is converted to a carbonyl (Bourboula, Limnios et al. 2019). Although using an organocatalyst makes the process less toxic, biocatalysis can further improve it. Biological synthesis offers stereo- and chemoselectivity, the use of cheaper substrates, and mild conversion conditions (Biernacki, Riechen et al. 2017).

Recombinant synthesis of PHB can be achieved in model organisms like *E. coli* (Saito, Imai et al. 2022). Natural PHB producers use a ketothiolase to condensate two acetyl-CoA (A) molecules, produced in the TCA cycle, into acetoacetyl-CoA (B); which is then converted by an (*R*)-3-hydroxybutyryl-CoA dehydrogenase into (*R*)-3-hydroxybutyryl-CoA (C); this intermediate is polymerised by a PHB polymerase (F) (Figure 1.2). Using chemical or recombinantly expressing depolymerases, or by using chemical or thermal methods, it is possible to obtain (*R*)3HBA. Additionally, by combining the genes involved in the synthesis of (*R*)-3-hydroxybutyryl-CoA and overexpressing a thioesterase, it is also possible to recombinantly obtain (*R*)3HBA. (Figure 1.2).

Several thermal methods for depolymerising PHB are described. PHB is a crystalline polymer and depending on its monomer composition, the crystallinity may be higher or lower. A temperature higher than 170 to 180 °C is usually required to depolymerise PHB, which makes the process very energy costly (Špitalský, Lacík et al. 2006). Another study aimed to produce methyl-3-hydroxybutyrate and methyl-3-methoxybutyrate from PHB. Obtaining methyl-3-hydroxybutyrate was possible by mixing PHB with methanol and sulfuric acid. However, for the synthesis of methyl 3-methoxybutyrate, a thermo-step at 175 °C was needed to produce crotonic acid followed by its conversion to methyl crotonate, using an acid, and finally to methyl-3-methoxybutyrate, using sodium methoxide (Parodi 2021). Enzymatic methods to depolymerize PHB are usually more efficient as they can operate at 70 °C and do not

require hash chemicals, making the process more efficient (Rodríguez-Contreras, Calafell-Monfort et al. 2012).

However, producing the polymer and then depolymerizing it increases costs and time, leading to studies focusing on direct recombinant synthesis of 3HBA (Gulevich, Skorokhodova et al. 2021). Therefore, a more direct route, which circumvents the polymerisation of 3HBA would be advantageous over the above methods. Various hosts have been employed for heterologous expression of the enzymes involved in the 3HBA synthesis. The synthesis of 3HBA was attempted in the dimorphic yeast *Blastobotrys* (*Arxula*) *adeninivorans*, an unfrequently used organism in metabolic processes, but known to be efficient in recombinant protein expression. The genes of three bacterial thiolases (*atoBp*, *thlp*, *phaAp*), three endogenous yeast thiolases (*akat1p*, *akat2p*, *akat4p*) and a reductase from *C. necator* (*phaB*) were cloned in different combinations and expressed in *B. adeninivorans*. Constructs were prepared combining a thiolase and the reductase mentioned for the synthesis of 3HBA. Permeabilized cells were used for single protein activity and results revealed that high thiolase enzymatic activity does not always correlate with high 3HBA synthesis, which can be explained by specific thiolase optimum conditions (pH optimum, kinetic parameters, etc.). The highest 3HBA concentration was observed when Thl and PhaB were coexpressed, and it reached 4.84 g/L, however after a very long incubation of 214 h in flask experiments. Altering the bioprocess conditions led to 3.76 g/L of 3HBA produced in a shorter time of 89 h (Biernacki, Riechen et al. 2017).

E. coli was also employed as a host for 3HBA synthesis. *E. coli* is a well-characterized production host, that is amenable to genetic manipulation. For example, a β-ketothiolase (*phbA*) and acetoacetyl-CoA reductase (*phbB*) from *C. necator* were combined with butyrate kinase gene (*buk*), which removes the -CoA, and phosphotransbutyrylase (*ptb*), that converts 3-hydroxybutyryl-CoA to 3-hydroxybutyryl-phosphate, both genes from *Clostridium acetobutylicum*. The four genes were combined in the vector pBHR69 and *phaA* and *phaB* were ligated to the vector pBHR68, pUC18 and pkk233-3, while *buk* and *ptb* were ligated to pBBR1MCS-2. Different plasmids were used to verify which combination resulted in the highest 3HBA concentration. The constructs were introduced into *E. coli* DH5α for 3HBA synthesis, and, in most cases, induction of protein expression by isopropyl-β-D-1-thiogalactopyranoside (IPTG) negatively affected 3HBA yields. However, this effect

was not analysed (Gao, Wu et al. 2002). *E. coli* offers a shorter incubation period and higher product concentration in comparison to the previous strategy where yeast was used. In this work, under fed-batch conditions, cells produced 12 g/L 3HBA over 48 h from 60 g/L glucose (Gao, Wu et al. 2002). The product formation was accompanied however with quite high acetate byproduct, reaching 8.5 g/L in the above process. The byproduct formation is a non-desirable characteristic, and in this case the byproduct is of similar characteristics as 3HBA. Overall, this complicates the downstream processing and increases the cost of the process. However, it was observed in the case of membrane separation that the difference in hydrophobicity between acetic acid and 3HBA is an important factor for separation (Choudhari, Cerrone et al. 2015).

Another study focused on 3HBA production investigated a strategy in which the genes encoding the enzymes involved in each of the steps separately versus a strategy in which the genes were cloned together, under the same promoter (Lee, Park et al. 2008). A β-ketothiolase from *C. necator* H16, an (*S*)-3-hydroxybutyryl-CoA dehydrogenase (*hbd*) from *Clostridium acetobutylicum* ATCC824 or *C. necator* and 3-hydroxyisobutyryl-CoA hydrolase (*bch*) from *Bacillus cereus* ATCC14579 were cloned as a synthetic operon in pET21a (pET21a_*bch_phaA_hbd*) under expression of the strong promoter T7, or in two plasmids with *bch* cloned in pET28b and *phaA* and *hbd* in pTac. The synthetic operon appeared to be more efficient in producing 0.61 g/L (*S*)3HBA over 48 h, compared to the production using the two plasmid strategy, where 0.10 or 0.22 g/L of (*S*)3HBA were produced depending on the *hbd* gene used (Lee, Park et al. 2008).

While strides were made toward the biotechnological production of 3HBA, it is important to recognise the factors that are affecting the production. It appears that glucose excess and high cell density influence 3HBA yield. Nonetheless, acetic acid is produced under these conditions, meaning that valuable carbon is diverted from the target product. To understand how to minimise carbon spillage as acetic acid, it is important to understand the steps involved in the byproduct synthesis.

1.1.3. Acetate metabolism in *E. coli*

Overflow metabolism refers to the production of wasteful by-products during growth (Millard, Enjalbert et al. 2021). When grown in anaerobic condition or in excess

fermentative sugars, even under aerobic conditions, *E. coli* produces acetate as one of the by-products of overflow metabolism (Harden 1901). Currently, it is accepted that the acetate pathway is redundant, meaning that several genes are involved in its secretion and consumption, and the overflow metabolism is the result of a coordination at the genetic, transcriptional, and posttranslational levels. Acetate was also linked to the pathogenicity of *E. coli* strains, as it helps to maintain the gut microbiota as it can be used as carbon source (Bernal, Castaño-Cerezo et al. 2016) and inhibits the growth of other bacteria by increasing the acidity of the environment in which *E. coli* is better at tolerating when in high glucose concentration (Sengupta, Ekka et al. 2017).

In *E. coli*, acetate can be produced by: (1) the decarboxylation of pyruvate via pyruvate oxidase (PoxB) (Abdel-Hamid, Attwood et al. 2001); or (2) by the oxidative decarboxylation of pyruvate to acetyl-CoA by a variety of routes: in one of the routes a phosphotransacetylase, either Pta or EutD, converts acetyl-CoA to acetyl-P, which is then released as acetate by acetate kinase (AckA) (Figure 1.3). The latter is the main route for acetate excretion, involving the reversible phosphorylation/dephosphorylation by phosphate acetyltransferases Pta or EutD (EC: 2.3.1.8). Both enzymes contain the PTA_PTB domain found in acetyl- and butyryltransferases (Bologna, Andreo et al. 2007). The acetate formed can be directly converted to acetyl-CoA by acetyl-CoA synthetase (Acs), which is mostly active through the acetate recycling system Pta-AckA-Acs when glucose concentration is low (Millard, Enjalbert et al. 2021).

The genes *eutD* and *pta* have been characterized in *E. coli* (Bologna, Campos-Bermudez et al. 2010, Campos-Bermudez, Bologna et al. 2010). While both enzymes perform the same reaction, EutD is significantly more efficient in the reversible conversion of acetyl-CoA to acetyl-P, whereas Pta is considered a housekeeping enzyme. A 17 gene-*eut* operon contains *eutD,* which is involved in ethanolamine metabolism in *E. coli* (Jallet, Soldan et al. 2024). It was shown that deletion of both *eutD* and *pta* limits *E. coli* growth in minimal media with acetate as the carbon source. (Bologna, Campos-Bermudez et al. 2010), demonstrating the role of these two enzymes in acetate assimilation/production (Millard, Enjalbert et al. 2021).

Another enzyme, AckA, an acetate kinase (Enzyme Commission (EC) 2.7.2.1) was also associated with acetate overflow metabolism as it catalyses the reversible

conversion of acetyl-CoA to acetate (Millard, Enjalbert et al. 2021). A study using deletion mutants for the genes involved in the acetate pathway observed that the bidirectional AckA-Pta pathway controls acetate secretion and consumption in *E. coli* and can maintain the acetate flux alone (Enjalbert, Millard et al. 2017).

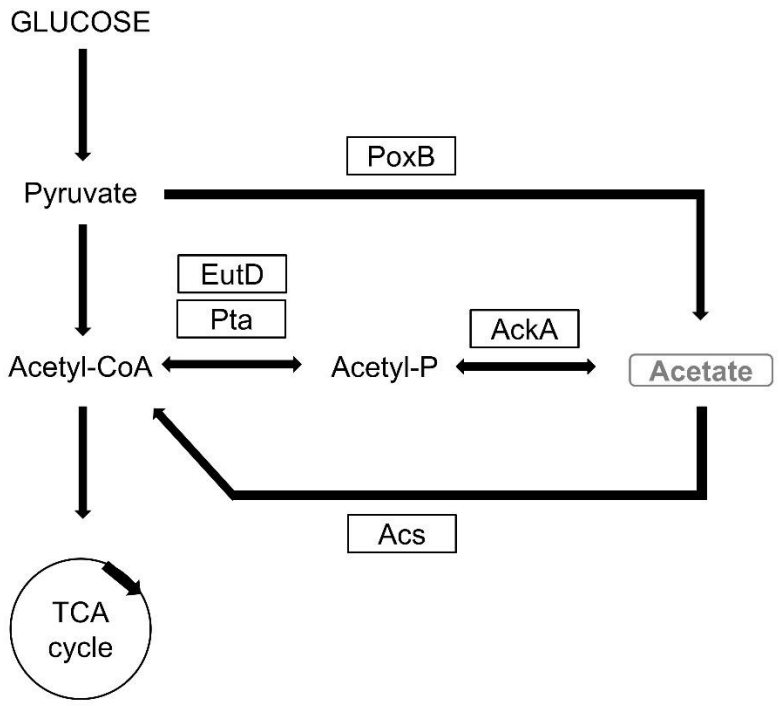

Figure 1. 3. An overview of acetate metabolism in *E. coli*. Carbon and energy substrates, such as glucose, are converted into acetyl-CoA, a central metabolic intermediate. In overflow metabolism, acetyl-CoA is converted to acetyl-phosphate by one phsphotransacetylase (EutD or Pta), which is converted to acetate by acetate kinase (AckA). In the other route, pyruvate can be directly converted to acetate by a pyruvate decarboxylase (PoxB). The acetate formed by either route can be converted back to acetyl-CoA by Acetyl-CoA synthetase (Acs)

Thus, disruption of this pathway represents an opportunity to reduce carbon spillage as acetate and diverge these carbons towards a target product. Acetate is produced up to 8 mM (0.47 g/L), when the metabolism changes from production to its consumption. When in glucose excess, acetate and glucose can be consumed simultaneously during exponential growth and glucose excess, where acetate seems

to be firstly produced when glucose is in excess and later used as an energy source (Enjalbert, Millard et al. 2017). As *eutD* and *pta* are the genes involved in the conversion of acetyl-CoA to acetyl-P, the deletion of these genes can drastically reduce acetate formation by this route.

Therefore, if 3HBA production is to be favoured, acetate as a byproduct is to be limited via engineering efforts aimed at reducing acetyl-CoA conversion into acetate.

1.2. Chiral amines

While 3HBA has interesting applications as discussed above, this, and other hydroxy fatty acids could be used as a substrate in a two-enzyme cascade reaction to produce chiral amines. Enantiomerically pure amines are found among all kingdoms of life and are used as building blocks for pharmaceuticals and agrochemicals (Musa, Hollmann et al. 2019). Global production of amino acids reached 10.3 million tons in 2021 and is expected to rise to 13.8 million tons by 2027 (IMARC group, 2022). Amines can have antimicrobial activity (Baidin, Owens et al. 2021), are used as food supplements (Harty, Zabriskie et al. 2018), or scaffolds for the synthesis of 40 % of fine chemicals industrially produced in 2022 in the United States (Liu, Kong et al. 2022).

Rivastigmine, (*S*)-3-[1-(dimethylamino)ethyl]phenyl ethyl (methyl) carbamate, is a potent drug used for the treatment of dementia and Alzheimer's. Although widely used, an industrial-scale method for Rivastigmine synthesis was only developed in 2013. This method involves five steps starting from *m*-hydroxyacetophenone substrate and requires an iridium spiro pyridine–aminophosphine catalyst, which is expensive and has 84 % yield (Yang, Xie et al. 2014).

Chiral amines can be grouped into aliphatic or aromatic amines and further divided into α, β, or γ depending on the position of the NH_2 group. These amines can be synthesized by diastereoisomeric crystallisation, asymmetric reduction of imines or enamines, asymmetric addition to ketimines or nitriles, amination of ketones, nucleophilic addition, and C–H insertion by using a chemo, organo- or biocatalyst (Ghislieri and Turner 2013, Yin, Shi et al. 2020). Chemical catalysis usually involves hydrogenation of enamines or imines (Nugent and El-Shazly 2010), but it can be expensive or rely on solvents and/or rare or toxic catalysts. For instance, a method for

the amination of aryl halides uses palladium as a catalyst in a process that occurs at 90 °C (McCann, Reichert et al. 2020). Another method involves the amination of phenols at temperatures ranging from 120 to 140 °C using rhodium as a catalyst (Chen, Kang et al. 2022).

Biocatalysts, being biodegradable and operable under mild conditions and in aqueous solutions, are a preferable alternative (Bell, Finnigan et al., 2021). Biocatalysts are stereospecific, but differently from chemical catalysts, that require pure substrates, biocatalysts can use the isomer they are specific to in a racemic mixture to produce chiral products (Cui, Gao et al. 2024). There are several enzymes that can be used to synthesise chiral amines, and they come with certain advantages and challenges. Amination reactions with biocatalysts are often performed by amine (EC1.4.1.28) or amino acid dehydrogenases (AADHs - EC: 1.4.1.) or transaminases (TA - EC 2.6.1) (Azofra, Tran et al. 2020, Liu, Kong et al. 2022), but also amine oxidases and imine reductases are used less frequently (Vikhrankar, Satbhai et al. 2024).

Members of the amino acid dehydrogenase superfamily use 1,4-dihydronicotinamide adenine dinucleotide ($NADP^+$/NADPH) as cofactor and catalyse the reversible amination of α-keto acids to their corresponding α-amino acids (Chen, Jiang et al. 2009). The superfamily of AADH (EC Number 1.4.1.X) comprise glutamic acid, valine, tryptophan, leucine, and phenylalanine dehydrogenases (Zhou, Xu et al. 2022). The tridimensional structure and mechanism of action is similar between the five mentioned groups. These proteins have two subunits with two domains each. One domain binds to the substrate, while the other binds the cofactor. The active site is positioned in a cleft between these two domains (Son, Kim et al. 2015). Although AADH are naturally involved in the metabolism of amino acids, they have been engineered for increased substrate specificity. For instance, the active site of a less common β-amino acid dehydrogenase, naturally active towards aliphatic substrates, was subjected to rounds of mutagenesis so it could catalyse β-aromatic substrates (Liu, Feng et al. 2023). The major drawback of using amine dehydrogenases in general is the yield limited to 50 % and low stereoselectivity, especially when multiple dehydrogenases are in play. This issue can be improved by addition of cofactor regeneration and formate removal (Stewart 2001, Bachosz, Zdarta et al. 2023).

Transaminases (TAs) are pyridoxal 5'-phosphate (PLP) dependent enzymes that transfer amino groups from donors (amines or imines) to acceptors (ketones, aldehydes, or keto acids) (John 1995). TAs form a superfamily divided into α- or ω-transaminases. α-TAs form α-amino acids, placing the amine group in the α position relative to the carboxyl group (Voss, Xiang et al. 2020). ω-TAs have broader applicability and can aminate aldehydes, ketones, or keto acids (Kelly, Pohle et al. 2018).

PLP is stabilized in the active site via Schiff's base with K288 and further stabilized by D259, Y153, and V261 (Humble, Cassimjee et al. 2012). TA activity proceeds in two steps (Figure 1.4). In the first half-reaction, the amino group is transferred from the amino donor to PLP forming pyridoxamine 5'-phosphate (PMP) and releases a keto by-product. In the second half-rection, the amino group is transferred from PMP to the keto acceptor resulting in the corresponding amino acid, and PLP is regenerated. (Xu, Tang et al. 2020).

The interest in TAs as biocatalysts stems from their broad specificity and capacity to accept a range of non-native donors and acceptors. A notable example of TA use is in the synthesis of an antidiabetic drug sitagliptin. The large-scale chemical synthesis of sitagliptin was first described by Merck and included the asymmetric hydrogenation of an enamine in 8 steps to produce sitagliptin phosphate with 52 % yield. The β-amino acid component of sitagliptin was obtained by hydrolysis of a lactam or ester substrate by lithium hydroxide and used rhodium as catalyst (Hansen 2005).

A TA-based biocatalyst was developed through protein engineering which replaced rhodium used for the asymmetric hydrogenation of an enamine (Savile 2010). The implementation of the biocatalytic step increased the process enantioselectivity and abolished the need for specific equipment used to remove the catalyst. The method engineered an ω-TA from *Arthrobacter* sp. and resulted in a TA version with 27 mutations, which has larger binding pocket with higher specificity towards the target substrate prositagliptin ketone. The use of the biocatalytic step improved sitagliptin synthesis efficiency by 53 % (kg/L/day) compared to the chemical process. This success boosted research in TA modifications for improved substrate specificity towards large amines, for instance (Savile 2010, Meng, Ramírez-Palacios et al. 2021).

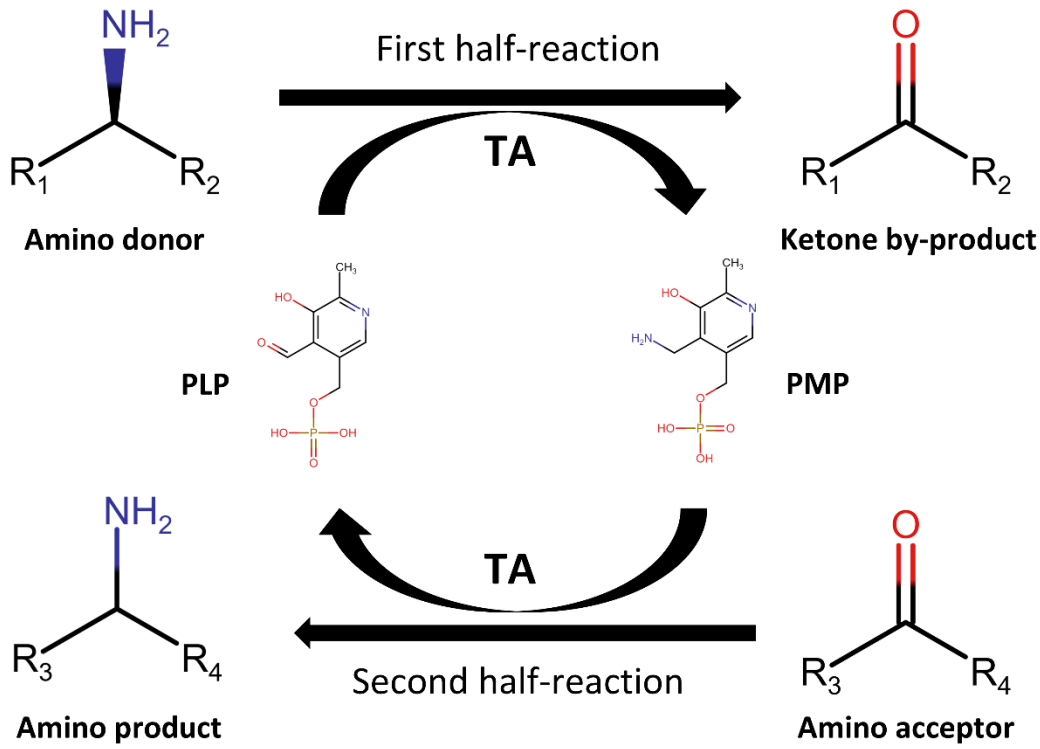

Figure 1. 4. Generic transaminase catalysed reaction. In this figure the amino group is transferred from an amino donor to pyridoxal 5'-phosphate (PLP), that becomes pyridoxamine 5'-phosphate (PMP), in the first-half reaction. In the second part of the reaction, the amino group is transferred from PMP to the amino acceptor, while PLP is regenerated.

However, while there are numerous examples of the use of TAs to synthesise valuable chiral amines, there are still several challenges related to their activity. For example, the thermodynamic equilibrium and TA inhibition by pyruvate are the major challenges. Both can be circumvented by adding a pyruvate removing system such as lactate dehydrogenase (Stewart 2001). In addition to the abovementioned case of sitagliptin production, where protein engineering techniques were employed to expand the substrate range, the frequently low activity could be also addressed by implementing cascade reactions. Inspired by natural reactions, which all occur in the cellular environment, artificial biocatalytic cascades combine two or more enzymes in the same reaction pot without removal of the intermediates (Jongkind, Fossey-Jouenne et al. 2022). Although this an advantage over the chemical process, all enzymes used in

a cascade have to be compatible with regards to optimal pH, solvents and temperature and the overall process has to be energy favourable (France, Hepworth et al. 2017)

Cascade reactions can be divided into linear, parallel and orthogonal cascades. Linear cascades are the ones which take place in one pot without removal of the components. In parallel cascades, the formation of the primary target occurs simultaneously with the formation of a secondary target product. Orthogonal cascades are similar to the parallel cascades and a cosubstrate is converted to an intermediate, which is converted to a secondary product, the difference between orthogonal and parallel cascades is the participation of the co-substrate in the main reaction. Lastly, cyclic cascades, where a secondary product is converted back to the starting substrates (Simon, Richter et al. 2014).

Genes from different sources can be recombinantly expressed in a model host to produce a desired compound. For example, (Skalden, Peters et al. 2015) combined into a linear cascade an enoate reductase from *Saccharomyces carlsbergensis* with a TA from *Vibrio fluvialis* to produce (*R*1,*S*3)-1-amino-3-methylcyclohexanes with 87 % conversion.

In another study, a phenylalanine dehydrogenase from *B. badius* was tested with a range of aliphatic and aromatic secondary alcohols and deemed suitable for the cascade. As this dehydrogenase is NADP+/NADPH dependent, an alcohol dehydrogenase from *Aromatoleum aromaticum*, wild type and mutated to have the inverse stereoselectivity, was investigated to complement the cascade under the same conditions (cofactor, temperature, pH, etc.). This cascade was able to aminate aliphatic (medium, long and branched) and aliphatic alcohols with conversion up to 96 %. The by-product of this cascade was only water, and the cofactor was regenerated by a glucose dehydrogenase.

These examples highlight the applicability of artificial cascade reactions. Nonetheless. There are challenges involved in combining these enzymes. For example, the reaction conditions (pH, buffer, salts) have to match for all enzymes present, the product or intermediates cannot inhibit enzymatic activity, among others. There are solutions available. Enzyme immobilization can increase protein activity and reduce protein interactions with non-target substrates. Compartmentalization also offers a solution so each reaction can occur to its maximum yield (Gruber, Marques et al. 2017).

1.2.1. Non-coded amino acids (ncAAs)

Non-coded amino acids (ncAAs), unnatural or non-canonical amino acids, are so called because they are not genetically encoded as the other 22 amino acids (selenocysteine, pyrrolysine and the other 20 standard amino acids) (Martínez-Rodríguez, Torres et al. 2020). Despite not being part of the genetic code, ncAAs are valuable building blocks in various industrial applications (Mathew and Yun 2012). ncAAs encompass a variety of structures, including α-AAs (Almahboub, Narancic et al. 2018), β-AAs (Parthasarathy, Savka et al. 2019), D-AAs (Du, Wey et al. 2023), and homo amino acids (Sun, Zhang et al. 2018). These amino acids can be involved in various processes, ranging from the direct use as food supplements (Fernandes, Osório et al. 2023), to the modification of proteins to increase stability, for instance (Deepankumar, Nadarajan et al. 2015).

Organisms produce ncAAs as analogues, intermediates or metabolites of the synthesis of coded amino acids (Zou, Li et al. 2018). For instance, β-alanine is produced in plants from spermidine and spermine, and it plays a role in environmental stress response. In humans, β-ala, produced in the liver or ingested from meat, is a precursor for carnosine synthesis, with studies highlighting its supplementation for muscle recovery and strength (Harris, Tallon et al. 2006). Other ncAAs, like proline derivatives and homoserine, are naturally produced as metabolites of coded amino acids (Wu, Bazer et al. 2011, Ferla and Patrick 2014).

ncAAs can be categorized into two classes based on their structure: (1) analogues or derivatives, which are similar to the canonical amino acids, and (2) surrogates, which are structurally different from coded amino acids (Blaskovich 2016, Guo and Berglund 2017). Although cells do not have the machinery to specifically add ncAAs to a peptide chain, some of the ncAAs can still be found in proteins. In one of the known mechanisms, an aminoacyl-tRNA synthetase paired with a canonical amino acid can also pair its tRNA with an analogue ncAA, for instance, the leucine-tRNA synthetase which can also naturally, but less efficiently, charge azaleucine to tRNA (Lemeignan, Sonigo et al. 1993).

Chemical synthesis is still largely used to produce ncAAs. However, chemical synthesis makes use of expensive and/or toxic reaction components. The

enantioselective reduction of enamines or imines is a widely used method, but it requires a metal catalyst that can be rhodium or iridium (Ortiz, Shezaf et al. 2022). For instance, the chemical synthesis of 2-aminobutyric acid (2ABA) uses sodium cyanide and propionaldehyde, the first can cause environmental contamination and is toxic to humans (Patent 102050750). In another study, the fluorescent ncAA L-3-(6-acetylnaphthalen-2-ylamino)-2-aminopropanoic acid was accomplished by a 6-step method, which resulted in aa 12-fold increase in comparison to the previous method available and 51 % total yield with high purity towards the L-enantiomer. Nonetheless, this method used two toxic catalysts, copper(I) iodide and triphenylphosphine, and temperatures ranging from 0 to 140 °C, which increases energy costs and makes it risky for the environment and people operating it (Xiang and Wang 2011).

Amino fatty acids are part of the ncAAs, can be naturally produced and have biotechnological applications. However, their bioavailability, or time they are available in the body after administration, is poor, and therefore they are difficult to fully characterize (Hueber, Gimbert et al. 2022). Generally, an amide bond combines a fatty acid and an amine creating fatty acid amides, which is a lipid family (Ni, Bhandari et al. 2021). Chemically, fatty nitriles, which can be obtained from a reaction between ammonia and triglycerides, fatty esters or fatty acids, can be hydrogenated and result in fatty amines under high temperature and the presence of a catalyst (ie. silica or metal-based) (Zhang and Madbouly 2016) and that process can be extrapolated for amino fatty acids, but it still has the drawbacks mentioned for chemical synthesis.

Biocatalysis can be applied for the synthesis of ncAAs, as well. In this context, whole cell biocatalysts have been used as a mean for efficient amino production, especially after the last decade, that has been named as “Fourth Wave of Biocatalysis” (Bornscheuer 2018). Cells overexpressing native or recombinant proteins can be used to bioproduce ncAAs.

Various enzymes have been employed for the synthesis of ncAAs. Amine dehydrogenases have been used in reductive amination to produce complex amino acids from primary or secondary alcohols, generating water as the only by-product and using nicotinamide cofactors (Wang, Sundara Sekar et al. 2021). In another example, a D-mandelate dehydrogenase from *Lactobacillus brevis* was engineered for improved activity and combined with an L-leucine dehydrogenase from *B. cereus* to

produce ncAAs, such as, D-2-aminopentanoic acid and 2ABA with 94 % conversion rate (Liu, Zhou et al. 2020)

There are multiple reports on metabolic engineering to produce amino fatty acids. A threonine deaminase and an engineered glutamate dehydrogenase were coupled to produce (*S*)-2-aminobutyric acid. They were further combined with a carboxylic acid reductase and an aldehyde reductase to produce (*S*)-2-aminobutanol in *Saccharomyces cerevisiae*. This method produced 0.40 ± 0.02 mg/L (*S*)-2-aminobutyric acid and 0.42 ± 0.07 mg/L (*S*)-2-aminobutanol (Weber, Hatsch et al. 2017). The synthesis of this ncAA is of relevance as it is a precursor of drugs such as Levetiracetam, Ethambutol and Brivaracetam (Xu, Li et al. 2019). A more recent method relied on BL21 as a host. L-Threonine was converted to 2-oxobutyric acid, by an L-threonine deaminase, and used to produce 2-aminobutyric acid. High-throughput screening was used to identify a leucine dehydrogenase active to 2-oxobutyric acid was undertaken and identified an enzyme from *Exiguobacterium sibiricum* as candidate in aminating 2-oxobutyric acid. The gene of leucine dehydrogenase was subjected to mutagenesis aiming to improve the tolerance to the substrate, which can inhibit the enzyme. After 24 h 95 % conversion was observed (Chen, Zhu et al. 2021).

ncAAs can be applied as single molecules, to compose other molecules or to modify peptides and proteins. The ncAA pomaglumetad (LY-404,039) is a glutamate analogue that was observed to be efficient in the treatment of schizophrenia (Patil, Zhang et al. 2007). 2,4-diaminobutyric acid, on the other hand, composes the structure of the antibiotics polymyxin B and colistin (Velkov, Roberts et al. 2013). Almahboub and collaborators showed the application of 2-aminooctanoic acid in potentiating the antimicrobial activity of a short peptide. ncAAs can yet be used to label proteins, such as norleucine and O-[11C]methyl-l-tyrosine (Iwata, Furumoto et al. 2003, Anderhuber, Fladischer et al. 2016), as protein inhibitor like tert-leucine (Soth, Hermann et al. 2013) and to compose the structure of several other drugs.

Testing the applicability of ncAAs in modifying proteins results in novel or improved activities and creates the bases for the *in vivo* incorporation of ncAAs to proteins. Addition of ncAAs to peptides and proteins allows the expansion of the genetic code and, thus, broaden the range of biological functions (Kohrer 2013). For instance, by using a method for bioprospecting an N-oxigenase and aminoacyl-tRNA

synthetase/tRNA, and further genomic engineering, Butler et al., (2023) engineered an *E. coli* strain able to synthesise para-amino-L-phenylalanine from glucose and its incorporation to a protein (Butler, Sen et al. 2023). The genetic incorporation of ncAAs was first accomplished in *E. coli* (Wang, Brock et al. 2001) and later it was achieved in *Saccharomyces cerevisiae* (Chin, Cropp et al. 2003). Both cases used an evolved aminoacyl-tRNA synthetase and tRNA pair to incorporate the amino acid in the peptide chain. Ever since these successful cases, other methods have been investigated, selective pressure incorporation, for example (Du, Li et al. 2022).

1.3. Antimicrobial chemotherapy

The development of antimicrobial drugs is thought to be one of the most important breakthroughs in the twentieth century (Katz and Baltz 2016). The history of antimicrobial drugs begins with Paul Ehrlich's research on arsenic compounds as antimicrobial agents, which led to the discovery of sulfonamides. This compound class has the functional group (*R*-SO_2-NH_2), which is responsible for the antimicrobial activity (Siddique 2013). Sulfonamide drugs, or just sulfa drugs, act at the level of the bacterial folic acid metabolism, inhibiting competitively dihydropteroate synthase, responsible for the conversion of *p*-aminobenzoic acid to dihydropterin pyrophosphate (Henry 1943). The use of sulfonamides as antimicrobial drugs reduced as newer more efficient drugs were discovered (Weinstein 1957).

In the late 1920s Alexander Fleming was a member of St. Mary Hospital, in London, where he would study antiseptics and microbiology (Fleming 1922). While working on lysozyme's antimicrobial activity on *Staphylococcus aureus*, Fleming noticed a contamination by blue mould (*Penicillium notatum*). Around the fungus growth area, there was a zone of inhibition for bacteria, which led to the discovery of penicillin (Fleming 1929).

Penicillin's discovery started what is known as "the golden era of antimicrobial therapy". Between the decades of 1950 and 1960 the information on antimicrobial molecules increased at fast pace and about half of antimicrobial drugs in use today were discovered in that period (Davies 2006). Although pharmaceutical companies invested a great deal on antimicrobial drugs during the golden era, they are losing interest in these drugs in the past decades due to strict health regulations and an

imbalance between the investment required to produce a new drug and low profit due to low market prices (Klug, Idiris et al. 2021). These problems related to investment in new antibiotics can be associated to the fact that these drugs are only used for a short period and have low market cost compared with drugs used for chronic disease, for example (Bartlett, Gilbert et al. 2013). As a result, the number of approved antimicrobial drugs has decreased drastically in the last decades, showing a reduction in discovery of about 40 % in the number of drugs when compared with the 1980's (Dheman, Mahoney et al. 2020).

1.3.1. Antimicrobial resistance

In addition to the decrease in the number of new antibiotics being discovered, the continuous use of antimicrobial drugs in the treatment or infectious diseases has selected microorganisms, which are drug resistant (Sykes 2010). Antimicrobial resistance (AMR), defined as microbes surviving to a defined antimicrobial drug concentration, is a challenge that poses one of the greatest threats to human health, development, and food security (Acar and Röstel 2001, Leistner 2014). Drug misuse, incomplete antimicrobial treatment, over and self-prescription, and antimicrobial overuse in agriculture and livestock are the main agents to accelerate AMR (Michael, Dominey-Howes et al. 2014, Clifford, Desai et al. 2018).

AMR happens naturally. Bacteria may acquire a series of mechanisms to resist the effect caused by antimicrobials such as blocking the target-drug interaction (Lewis 2013). Vancomycin is known to interact with D-alanyl-D-alanine, present in bacterial cell wall of *S. aureus*. The mechanism of resistant of vancomycin resistant *S. aureus* (VRSA) is based on substituting D-alanyl-D-alanine by D-alanyl-D-lactate, which vancomycin has lower affinity to (Gardete and Tomasz 2014) Microbes can also actively expel the antimicrobials by expressing efflux pumps, as it is the case with tetracycline resistant *E. coli* (McMurry 1980). In addition, inactivation of the antibiotic or modified target structure are observed as well (Lewis 2013). A well-studied example regarding gene acquisition is the case of methicillin resistant *S. aureus* (MRSA). This strain expresses a protein named penicillin-binding protein 2a (PBP2a). The acquisition of this gene, that encodes a transpeptidase allows that peptidoglycan

crosslinking continues in *S. aureus* in the presence of β-lactam antibiotics (Fishovitz, Hermoso et al. 2014).

It is estimated that by 2050 the AMR treatment costs may increase from $300 billion to $1 trillion and result in 10 million deaths per year around the world (O'Neill 2015, WorldBank 2016). Thus, new approaches to treat microbial infections are required to reduce these damages.

1.3.2. Antimicrobial peptides

Antimicrobial peptides (AMPs) are small peptides found in plants (Iqbal, Khan et al. 2019), bacteria (Martínez 2016), fungi (Xiong, Hady et al. 2011), insects, archaea (Besse, Peduzzi et al. 2015), (Feng, Fei et al. 2020), and humans (Friberg, Haaber et al. 2020). To date, 3940 AMPs (https://wangapd3.com/main.php) are deposited in the Antimicrobial Peptide Database (APD3), with shown activity against bacteria, fungi, viruses, and cancer cells (Wang, Li et al. 2016). Due to their multifunctionality and diversity, AMPs offer a great opportunity for the development of new antimicrobials.

One of the most remarkable characteristics of AMPs is their broad-spectrum activity against microbes. They show a general pathogen recognition pattern, such as, recognising components of cellular membrane (Hancock 2002). For example, nisin is an AMP with two domains, the N-terminal domain has high affinity towards lipid II, only found in bacteria, and the C-terminal domain is responsible for the pore forming activity (Musiejuk and Kafarski 2023). Furthermore, AMPs may target bacterial membrane based on lipidic charge: as the outer leaflet of mammalian cells have zwitterionic, and bacterial membranes have negatively charged phospholipids, AMPs mostly interact with the negatively charged pattern (Querinjean 1971). Besides the role of AMPs in the innate immune response, by killing microbes directly, it has been observed they can act as immunomodulatory molecules (Nijnik and Hancock 2009). LL-37 is a human cationic AMP that has shown transcriptional immunomodulatory activity, by regulating genes involved in chemokine secretion and increasing the expression of chemokine receptors (Scott, Davidson et al. 2002).

While AMPs are very diverse, there are chemical features common to most of them. Amphipathicity, hydrophobicity and cationicity have been directly related to antimicrobial and cytotoxic activity (Powers and Hancock 2003).

AMPs' sequence is usually rich in lysine and arginine residues, giving AMPs positive net charge ranging from at least +2 (Hancock 1997, Haney and Hancock 2013). Introduction of additional positively charged residues can increase the antimicrobial activity (Hilpert, Volkmer-Engert et al. 2005).

Hydrophobicity is another important feature, as hydrophobic residues comprise about 50 % of amino acids in AMPs (Stark, Liu et al. 2002). Hydrophobic amino acid residues often appear between each 2-4 residues, which helps to create the α-helical structure (Schmidtchen, Pasupuleti et al. 2014), possibly important for the pore formation in bacterial membrane (Spaar, Munster et al. 2004).

AMP can be modified to have increased or decreased hydrophobicity, which includes amino acid replacement or addition of fatty acid groups. Lipidation is used as a strategy to increase the hydrophobicity of an AMP. Usually, addition of a lipidic group is achieved on lysine or an N-terminal residue (Rounds and Straus 2020). For example, C-terminal conjugation of hexanoic or octanoic acid to the peptide K5L7 had little effect in toxicity, but significantly increased the antimicrobial activity (Rosenfeld 2010). The chimeric AMP CM15 cecropin A-mellitin) was subjected to substitution of A10 and V14 by D-lysine, single and combined substitution, with an additional substitution on leucine at position 4. Results revelled that all substitutions increase the mean residue hydrophobicity and hydrophobic moment. Additionally, the mean residue hydrophobicity correlates with microbial activity against *E. coli* and *P. aeruginosa*. Furthermore, haemolytic activity and peptide hydrophobicity had inverse correlation. The authors claim the reduced helicity caused by the substitutions resulted in reduced antimicrobial activity, but drastically reduced the toxicity of the peptides, which is a positive outcome (Kaminski and Feix 2011). This last example demonstrates how more than one physicochemical characteristic can be altered to improve activity.

Based on their secondary structure, AMPs can be classified into four groups: all α peptides only have α-helices, all β, which are composed of β-sheets, mixed structures (αβ), which are composed of both α-helices and β-sheets or unstructured/linear peptides, which do not form helices or β-sheets (Kumar, Kizhakkedathu et al. 2018). Amphipaticity is a characteristics of AMPs associated with selectivity and antimicrobial activity. Amphipathic α-helical AMPs are ubiquitous, being found from amphibian skin to AMPs synthesized by human ribosomes, and represent the most abundant class

of AMPs (Tossi, Sandri et al. 2000). Amphipathic α-helices can be naturally structured or unstructured in the presence of a polar solvent, and assume the helical conformation only when in contact with the membrane phospholipids (Fernández-Vidal 2007). While amphipathicity was shown to have more prominent effect than hydrophobicity on antimicrobial activity, it simultaneously decreases AMP's specificity and leads to increase in haemolytic activity (Chen, Guarnieri et al. 2007).

β-sheet is the second most common structural arrangement in AMPs. These AMPs are characterized by the presence of disulfide bonds (Dhople, Krukemeyer et al. 2006). An AMP family named defensins includes a variety of cationic peptides usually stabilized by three intramolecular disulfide bonds; however, the number and pattern of disulfide bridges can be correlated to the source organism. For instance, α and β defensins have three disulfide bonds, while θ defensins also have three disulfide bonds, they are cyclic and can be found in evolutionary older primates (Kumar, Kizhakkedathu et al. 2018). The relevance of cysteine residues, involved in disulfide bond formation, was demonstrated in the case of AMP NCR247. Here, four cysteine residues were replaced by serine, which meant that while the charge was the same, the formation of S-S bonds was prevented, causing a 10-fold reduction in antimicrobial activity of NCR247 (Haag, Kerscher et al. 2012).

The third structural arrangement, which contains both α and β structures, can also be exemplified by a subcategory of defensins. In this case, the structure is composed of an α-helix connected by two disulfide bridges to two or three antiparallel β-strands. For peptides containing the αβ motif, the S-S bridges are known to stabilize the structure and are important for activity. αβ-defensins are usually found in invertebrates, fungi, and plants (Dias and Franco 2015).

1.3.4.2. Lactoferricin

Lactoferrin (Lf), an iron-binding glycoprotein, was first identified in cow milk in the late 1930's and has since been identified in other mammals and in fish (Sorensen 1940, Torres 2006). Its sequence comprises 703 amino acids, which fold into one protein chain (Querinjean 1971).In general Lf is composed of two globular lobes connected by an α-helix. Lf is also N-glycosylated and the level of glycosylation and sugars involved depend on the source of the protein (Karav, German et al. 2017). Lf exhibits

antibacterial and antifungal activity, both widely studied, with highlights for anti-*Candida* spp. activity (Nikawa 1993, Xu 1999).

Bovine lactoferricin (bLfcin), a 25-residue peptide (Figure 1.5.) (FKCRRWQWRMKKLGAPSITCVRRAF), comprises residues 17 to 41 of the bovine LF (bLf) with a disulfide bond between cysteine residues C19 and C36 (Sinha, Kaushik et al. 2013). It was postulated that bLfcin folds as an anti-parallel β-sheet, different to what is observed in the intact protein Lf, which folds as an α-helix (Hwang, Zhou et al. 1998). Another difference is that bLFcin exhibits bactericidal activity, as opposed to bLf, which has bacteriostatic activity (Rainard 1987, Kutila, Pyörälä et al. 2003). Human Lfcin (hLfcin) and bLfcin differ in length, as hLfcin is 49-residues long. Sequence differences may account for different structural arrangements: bLfcin adopts an amphipathic β-sheet conformation in aqueous solution, while hLfcin arranges in a random-coiled structure in the same solvent (Hunter, Demcoe et al. 2005, Bruni, Capucchio et al. 2016).

Several studies test and modify different portions of Lfcin for improved activity. Lfcin is obtained via proteolysis of Lf and it is 25-amino acid peptide. However, its activity is attributed to 11 residues positioned in the N-terminus (Chapple 1998). Nonetheless, only six amino acids out of the 11 also show antimicrobial activity for bLfcin (Hossain, Dohra et al. 2021). The Lfcin mode of action is still under debate, but it is thought to be caused by interaction between the positively charged AMP with negatively charged bacterial membrane components: lipoteichoic and teichoic acid in Gram-positive, and lipopolysaccharide (LPS) in Gram-negative bacteria (Samuelsen, Haukland et al. 2004). Atomic force microscopy revealed that the 25-mer bLfcin creates membrane blisters in Gram-negative bacteria (Lehrer 1998), and transmission electron microscopy observed the cytoplasmatic localization of bLfcin suggesting that it is internalized (Haukland, Ulvatne et al. 2001). The synthesis of protein, DNA and RNA was measured by using isotopes of lysine, thymidine and uridine, respectively. Decrease in DNA synthesis was observed in *E. coli* treated with Lfcin and decrease of RNA, DNA, and protein were observed for *Bacillus subtilis* even in sub-lethal concentrations for both cases (Ulvatne, Samuelsen et al. 2004).

bLfcin exerts anticancer activity as well (Liscano, Oñate-Garzón et al. 2020). The toxicity of bLfcin towards cancer cells was first reported to acute monocytic leukaemia

THP-1, where the peptide induces cells to produce reactive oxygen species (ROS) and activates calcium and magnesium endonucleases, leading to apoptosis (Yoo, Watanabe et al. 1997). Cancer cells appear to have negatively charged surface, which facilitates the peptide-cell interaction (Le, Chen et al. 2019). Besides antibacterial and anticancer activity, bLfcin exerts antiviral (Andersen, Jenssen et al. 2004), antifungal (Wakabayashi, Hiratani et al. 1996, Gifford, Hunter et al. 2005), anti-inflammatory (Drago-Serrano 2018), and antihelmintic activity (León-Sicairos, Ordaz-Pichardo et al. 2017).

Although not many reports describe them, the drawbacks observed in most AMPs can be extrapolated for Lfcin. These disadvantages include susceptibility to proteolysis, short life-time and low bioavailability (Drayton, Kizhakkedathu et al. 2020). Since the late 1990's the design of synthetic analogues of bLfcin has been investigated and the antibacterial activity was related to the secondary structure, peptide length, and net charge (Rekdal 1999). It also appears that truncated Lf peptides have higher antimicrobial activity than the full sequence molecule (Bellamy 1992). The 6-mer variant of bLfcin (RRWQWR) was observed to be degraded by proteases after 2 h. The modification through C-terminal amidation increased its antimicrobial activity, while N-terminal acetylation improved proteolysis resistance, (Nguyen, Chau et al. 2010), showcasing that the modifications can have extremely positive effect on both activity and stability of AMPs.

Nine amino acid residues (LFcin - RRWQWRMKK; Fig 1.5B) were said to confer bLfcin its activity and exhibit higher antibacterial activity than the parent peptide (Wakabayashi, Matsumoto et al. 1999). N-acylation or synthesis of the same sequence with D-amino acids resulted in improved antibacterial and antifungal activity compared to bLfcin (Wakabayashi, Matsumoto et al. 1999). Therefore, this core peptide represents an excellent model to investigate the effect of modifications on its structure and function.

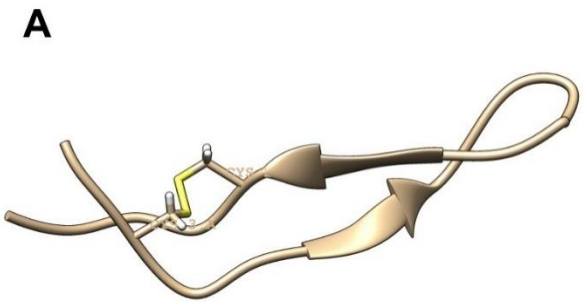

Figure 1. 5. The structure of bovine lactoferricin (bLfcin) with 25 amino acids. The disulfide bond between Cys3 and Cys20 is shown in yellow. Protein Data Bank (PDB) ID 1LFC. Figure created on UCSF Chimera 1.15.

1.3.4.3. AMP's mode of action

AMPs can exhibit their effect on microorganisms with high selectivity, which makes them an appealing molecule class for antimicrobial development. A series of models have been proposed to explain AMPs' mode of action (MOA), with pore forming and non-pore forming models being the two major classes of membranolytic mechanisms and non-membranolytic involving targets other than the membrane (Wimley 2010).

Pore formation is mostly driven by electrostatic and hydrophobic interactions between peptides or the peptides and phospholipids and are generally divided into toroidal pores and barrel-stave pores. It is said a barrel-stave pore when peptides line up with the hydrophilic portion oriented towards the pore lumen to form pore. While in toroidal pores both the peptides change the membrane curvature and interact with the phospholipids cooperatively creating the pore. The major difference between the two types is the participation of lipids in the toroidal pore (Aslam, Firdos et al. 2022).

Membranolytic non-pore forming models are explained by the carpet (Figure 1.6 c) or detergent model (Figure 1.6. d). The carpet model is explained by AMPs lying parallel to the membrane surface and interacting with the lipids head group, this model is highly dependent on the peptide-to-lipid ratio. As for the detergent model, AMPs orient parallel to the membrane surface and create nanopores that disrupts the membrane in a detergent-like mode leading to micelle formation (Aslam, Firdos et al. 2022). There are similarities between the detergent and carpet model and some authors consider both only as carpet model (Singh, Choudhary et al. 2022). However, the carpet model

is also thought to be one of the steps for the toroidal pore formation (Lee, N. Hall et al. 2015).

For the pore-forming mechanisms, the peptides start at a low peptide-to-lipid molar ratio where AMPs lie parallel to the bacterial membrane. Unstructured AMPs or AMPs with a defined secondary structure may go through conformational changes when in contact with membranes, assuming all α, all β, or αβ mixed structural arrangements. That is the case of plantaricin A, a 26-amino acid long peptide, that is unstructured in aqueous solution, but assumes an α-helical conformation in the presence of negatively charged membranes, but not in the presence of zwitterionic lipids (Zhao, Sood et al. 2006). When peptide-to-lipid ratio increases, AMPs insert into the membrane in what is named the “I state”. As an example, melittin and its analogues only insert into bacterial membrane at high peptide-to-lipid ratio (Woo and Lee 2017).

The barrel-stave model proposes that after helical AMPs insert in the membrane, the hydrophobic region on the peptide interacts with hydrophobic lipid portion, while the hydrophilic regions of the peptide create a transmembrane channel/pore, where cell content overflows (Figure 1.6. a) (Hughes and Lewis 2018, Kumar, Kizhakkedathu et al. 2018). The second pore model to explain AMP`s MOA is the “toroidal model” (Figure 1.6. b). In this model, the peptides insert into the membrane in a fashion that the polar face of the AMP interacts with the polar head of membrane`s phospholipids (Figure 1.6) (Yamauchi, Wakabayashi et al. 2006). Magainins are AMPs initially isolated from *Xenopus laevis* and were observed to induce the curvature of lipids in the bacterial membrane that coincides with the toroidal pore model (Hallock 2003).

Additionally, it was observed that upon interaction of the core amino acids of LL-37, comprising of 12 residues, with bacterial membrane the α-helical short peptide assemblies into a densely packed supramolecular transmembrane pore. The interaction between the helices mostly relies on the amphipathicity (Engelberg and Landau 2020).

The carpet or detergent-like (figure 1.6 c-d) model were observed to be the MOA of the lipopeptide surfactin. It was observed that surfactin acts mostly on the outer membrane where the peptides insert (Heerklotz and Seelig 2007). Furthermore, it was observed that that the acyl chains in the peptide interact with the phospholipids in the membrane increasing the fluidity and thus causing the detergent-like effect (Carrillo,

Teruel et al. 2003). Synthetic (Oren and Shai 2000) or naturally (Stella, Mazzuca et al. 2004) acylated AMPs have been observed to self-aggregate which can potentialize the micelle formation. Other AMPs, such as aurein, are known to disrupt bacterial membrane in a detergent-like way (Chen and Mark 2011)

Additionally, activity may not be related to membrane lysis/permeabilization. In this case, AMPs can enter the cell via endocytosis or direct penetration. In the first case, peptides enter the cell via lipid vesicles called macropinosomes, which are formed by a refolding of the bacterial membrane. When internalized, AMPs are released and perform antimicrobial activity through interaction with specific targets (Madani, Lindberg et al. 2011).

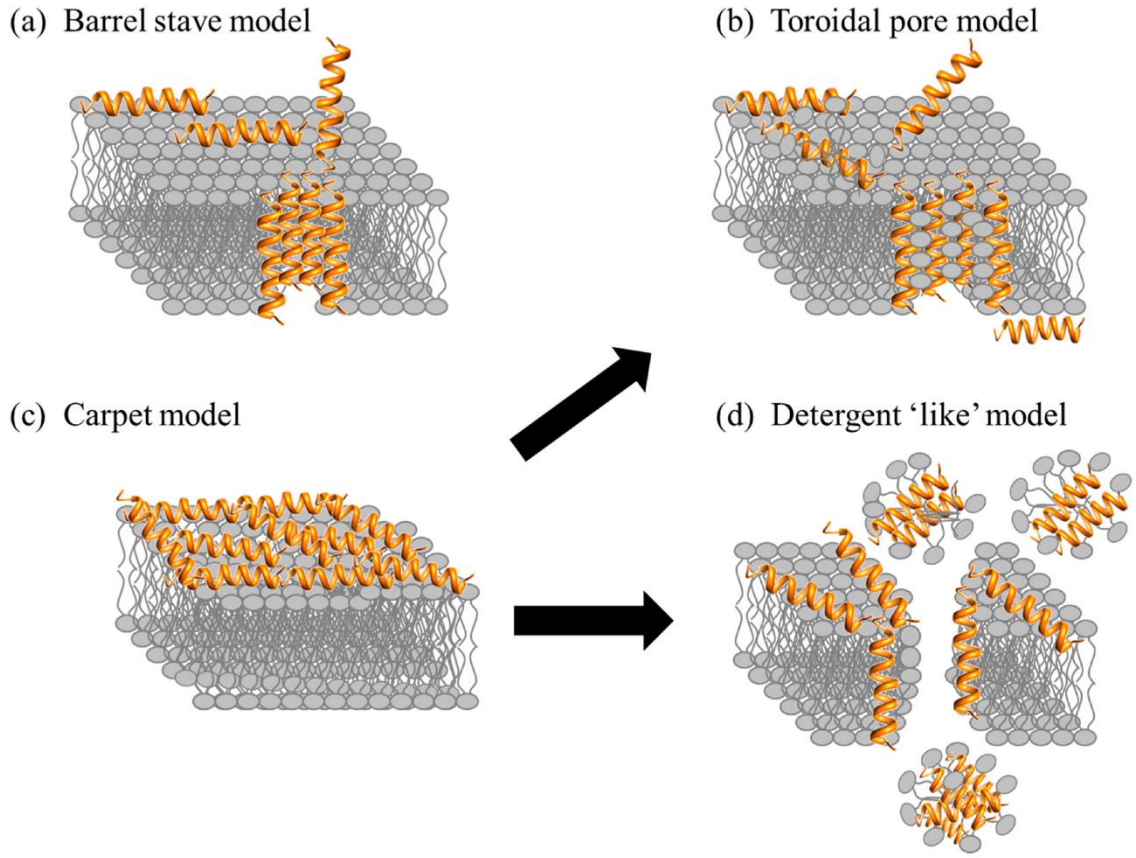

Figure 1. 6. Mode of action of antimicrobial peptides. Pore forming (a and b) and non-pore forming (c and d) models explaining the interaction between antimicrobial peptides microbial membrane and, consequently, their mode of action. Image created by (de Carvalho 2017).

In direct penetration, AMPs are transported across bacterial membrane through increased membrane permeabilization caused by high peptide density. For instance, an AMP named NK-18 was observed to have dual activity on increasing membrane permeability and damage, and binding to DNA after internalization, observed through fluorescent labelling and agarose gel (Yan, Wang et al. 2013) . Other reports indicate the presence of intracellular alternative targets for other AMPs, such as, bacterial ribosomes, inhibition of nucleic acid or protein biosynthesis, protein inhibitors, and mechanisms of cell division (Ishikawa, Kubo et al. 1992, Park 1996, Le, Fang et al. 2017)

It was also demonstrated that AMPs may trigger immunomodulatory responses (Engelberg and Landau 2020). For instance, the host defence peptide LL-37 and human β-defensin-2 (hbD2), hbD3, and lysozyme were noted to form complexes with double stranded DNA (dsDNA) and mediate a response by activation of toll-like receptors 9 (TLR9) and plasmacytoid dendritic cells (pDCs), respectively. LL-37 condenses with dsDNA forming an aggregated structure, which is internalized by the pDC endocytic pathway, where it may induce IFN-α (Lande, Gregorio et al. 2007, Lande, Chamilos et al. 2015). This shows that AMPs can act by neutralising the pathogen or by stimulating the immune system to produce a pro-inflammatory response.

1.3.4.4. Cytotoxicity of AMPs

Mammalian plasmatic membranes are mainly made up of four phospholipids: phosphatidylcholine (PC), sphingomyelin (SM), phosphatidylethanolamine (PE), and negatively charged phosphatidylserine (PS) (Van Meer, Voelker et al. 2008). The extracellular portion of the membrane (outer leaflet) is mostly composed of PC, SM, and PE, while PE and little amounts of PC, anionic PS and phosphatidylinositol are the components of the intracellular portion (inner leaflet) (Vance 2015). As the main phospholipid in the outer leaflet of mammalian cells is zwitterionic PC, AMPs interact weakly with them. The interaction relies on the physicochemical properties abovementioned. Although the mechanism of interaction between AMPs and host cells is not yet fully understood, it was observed that AMPs interact with negative ions

present in red blood cells membrane (Smirnova, Kolodkin et al. 2020). Cancer cells may display alterations in membrane composition that lead to increased proportion of anionic phospholipids in the outer leaflet that may explain AMP activity towards cancer cells (Hoskin and Ramamoorthy 2008)

However, the cross-talk still can occur and AMPs in that case exhibit a cytotoxic effect. This is facilitated via the same MOA. For example, indolicidin, a short, cationic, hydrophobic AMP with a broad-spectrum antimicrobial activity also results in haemolysis, vacuolization of the cytoplasm, and detachment of cell monolayer, that can be the result of its MOA of increasing membrane permeabilization (Vaucher, da Motta Ade et al. 2010). On the other hand, the AMP CAP18, a cathelicidin α-helical peptide, shows antimicrobial activity with low toxic effect against horse erythrocytes (Ebbensgaard, Mordhorst et al. 2018). The cytotoxic activity depends on the physicochemical properties and MOA of each AMP. Amino acid content (ie. proline) may affect the balance between antimicrobial and haemolytic activity, as well. For instance, the peptide P14, with a proline, presents higher antimicrobial activity than its analogue P14A, with an Ala, substitution of proline by Ala in the peptide due to charge and structural arrangement provided by proline. Furthermore, the parent peptide and analogue exhibited low cytotoxic activity against red blood cells. This was attributed to the MOA of these AMPs being dependent on membrane interaction, which has little or no effect in mammalian cells (Suh 1999). As abovementioned, cationicity is one of the most important physicochemical aspects for AMP selectivity and activity (Huang, He et al. 2014).

Haemolytic activity and antimicrobial activity, as well as susceptibility to proteolysis, can be improved by modifications such as, fluorination (Guo, Miao et al. 2024), acylation (Li, Yang et al. 2021) and PEGylation (Moreira Brito, Carvalho et al. 2022).

1.3.4.3. Modification of AMPs by non-coded amino acids

Reduced toxicity and higher antimicrobial activity are observed for second generation AMPs in a broad field named peptidomimetics (Fjell, Hiss et al. 2011). Peptidomimetics aims to design enhanced peptides that mimics natural AMPs` function, MOA, and structure. These peptides are often formed by addition of ncAAs or cyclization of linear peptides (Mendez-Samperio 2014). ncAAs can greatly increase physicochemical

properties and structural diversity of AMPs (Bhonsle 2013), as well as improve metabolic stability and bioavailability, and AMP resistance to proteolysis (Hancock 1998, Oh 1999).

Substitutions of L-AAs in AMPs by its D- isomers have been evaluated. Only by replacing L-AAs by D-AAs in the polar face or non-polar face of the α-helix, it was possible to reduce haemolytic activity (Jiang, Wang et al. 2023). By replacing all amino acids by their D- isomers, the antimicrobial activity of an AMP increased by 32-fold against multidrug resistant bacteria and their biofilm (Mohamed, Brezden et al. 2017). D-amino acids, such as D-alanine (Figure 1.7. A), can positively affect the secondary structure without altering the positive net charge and hydrophobicity (Lee 2002).

An AMP called S1 was N-terminally modified with the bulky ncAA β-naphthylalanine (Figure 1.7. B) and tested for synergistic activity with commercial antibiotics. It was observed that the native AMP and antibiotics alone had no or limited antimicrobial activity. However, addition of this bulky amino acid to S1 enhanced the activity against all bacteria tested alone and even more when combined with conventional antibiotics (Wu, Peng et al. 2021).

2-aminoisobutyric acid (Aib – Figure 1.7. C), naturally found in AMPs peptaibols, when used to replace each amino acid in temporin-1Dra, bar K11 and K12 residues that are known to be important for activity, increased antimicrobial and cytolytic activity against hepatoma-derived cells at different levels depending on the position of the substitution. Moreover, substitution in some positions caused the cytotoxic activity against red blood cells and fibroblast to increase, also depending on the position. the authors attribute these results to increased stability of the AMP in the presence of Aib, which is the result of stringency in movement promoted by Aib (Michael Conlon, Al-Kharrge et al. 2007).

Fatty acids have been employed to promote the hydrophobic interaction between the peptide and membrane. Modification of an inactive AMP with fatty acids ranging from 10 to 16 carbons (decanoic to palmitic acid) led to peptide becoming active (Malina and Shai 2005). However, it was shown that when long chain fatty acids were used, increased haemolytic activity was also observed (Malina and Shai 2005). Another challenge with the use of fatty acids to modify AMPs stems from the fact that only certain positions can be modified i.e. N-terminus, or lysine (Jain, Smith et al. 2015)

and arginine (Albada 2012) residues, or specific adapters are needed to facilitate the acylation.

Our group has recently developed a strategy to produce non-coded fatty amino acids, which remove the need for adapters and facilitate direct modification of C-terminus in addition to N-terminal modification (Almahboub, Narancic et al. 2018). Furthermore, it was demonstrated that the C-terminal modification has a more pronounced effect, reducing the minimal inhibitory concentration (MIC) needed to exert effect compared to N-terminally modified and unmodified peptide. It however remained unclear how is this effect achieved. Understanding the effect of the modification on the peptide structure, and the MOA would prove highly beneficial in further development of AMPs as therapeutics.

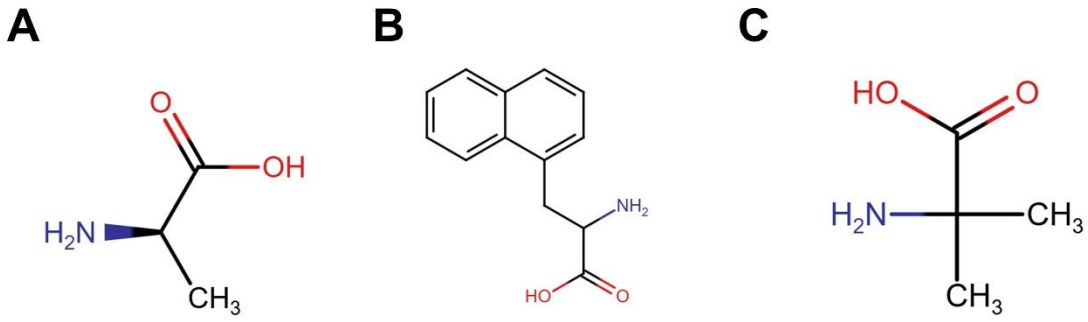

Figure 1. 7. Non-coded amino acid structure. Chemical structure of the analogue non-coded amino acid (A) D-alanine; and surrogates (B) β-naphthylalanine and (C) 2-aminoisobutyric acid.

1.4. Aims of the project

This project had a two-pronged approach. As ncAAs are recognised as powerful molecules that could be used standalone, or to modify AMPs, the first part of the theses aimed to develop a system to produce ncAAs from a cheap substrate, such as, sugars. To this end, building on a synthetic pathway previously developed in our research group, we aimed to metabolically engineer *E. coli* as a host for the conversion of glucose to 3-aminobutyric acid. The abovementioned synthetic pathway focuses on the production (*R*)- and (*S*)-3-hydoxybutyric acid, and it was observed that the activity of the pathway is associated with a byproduct, acetate formation. Therefore, the first specific aim was to remove/decrease the byproduct formation through engineering and

bioprocess development. Secondly, by modifying or expanding the enzyme cascade encoded by this synthetic pathway, the aim was to divert the carbon to 3-aminobutyric acid production.

The research of our group also previously demonstrated that α-non-coded fatty amino acids could be produced employing a transaminase biocatalyst. The work presented here aimed to explore cascade reactions to synthesise these ncAAs, thereby expanding the range of starting substrates.

Finally, to address the effect of AMP modification by these ncAAs, with emphasis on the effect of the fatty amino acid chain length, the aim was to generate understanding of the hydrophobicity threshold, the effect on the structure of the modified AMP, as well as the effect on cytotoxicity.

1.4.1. Specific aims

i. To engineer *E. coli* BL21 to improve 3-hydroxy butyric acid production from glucose as a feedstock.
ii. To develop a cascade reaction or engineer a strain to produce 3-aminobutyryc acid, a β-amino acid, from glucose.
iii. To develop a cascade reaction using 2-hydroxy fatty acids as substrates and biosynthesise α-non-coded amino acids.
iv. To modify bovine lactoferricin B core amino acids with α-non-coded amino acids ranging from 2 to 10 carbons in the acyl chain.
v. To evaluate the peptides' antimicrobial activity against *Escherichia coli*, *Salmonella typhimirium*, *Bacillus subtilis*, *Pseudomonas aeruginosa*, and *Staphylococcus aureus*.
vi. To evaluate AMPs structural changes caused by the ncAAs modification.

Chapter 2

Material and methods

2. Material and methods

2.1. Materials

GeneRuler 1 kb Plus DNA Ladder, 6X DNA Loading Dye, GeneJET Genomic DNA Purification Kit, GeneJET Plasmid Miniprep Kit, GeneJET Gel Extraction Kit and restriction enzymes were obtained from Fisher Scientific (Ireland). Bugbuster® protein Extraction Reagent, was purchased from Merck Chemicals (UK). Oligonucleotide primers were obtained from Merck (Ireland). 2-hydroxyhexanoic acid (2HHA) (racemic mix) was acquired from AA blocks (USA). SafeView Nucleic acid stain was purchased from NBS Biologicals (UK). Tetramethylethylenediamine (TEMED), Sodium Dodecyl Sulfate (SDS) mix acrylamide: bis-acrylamide, Trizma base, lactic acid, 2-hydroxybutyrate (2HBA) (racemic mix), 2-hydroxyoctanoic acid (2HOAA) (racemicmix), (*S*)-3-hydroxybutyric acid (*S*)3HBA, (*R*)-3-hydroxybutyric acid (*R*)3HBA**,** 6xHis Tag monoclonal antibody HRP conjugate were purchased from Sigma-Aldrich (Ireland). ECL DualVue Western Blotting markers, Perfect protein western markers, S-protein HRP conjugate were purchased from Cytiva, (Sweden). EZ-Run prestained Rec protein ladder was sourced from Thermo Fisher Scientific (Dublin, Ireland). ReadyBlue Protein Gel Stain was purchased from Merck (Ireland). The filter used for protein purification was purchased from Filtropur, Sarsteat, (Ireland). Lysogeny Broth (LB), isopropyl β-D-1-thiogalactopyranoside (IPTG), Na_2HPO_4, Imidazole, NaCl, $(NH_4)_2S_2O_8$, Methanol, carbenicillin were obtained form from Fisher Scientific (Ireland). Q5 High-Fidelity 2x Master Mix was purchased from New England Biolabs, (UK). DNA Assembly Master Mix was obtained from New England Biolabs Inc., (UK). Polyvinyl difluoride (PVDF) transfer membrane and Pierce® ECL Western Blotting substrate kit were obtained from ThermoFisher Scientific, (USA). Skimmed milk was obtained from Oxoid (UK). All other chemicals were purchased from Sigma-Aldrich (Ireland). The powdered enzymes ATA-117, ATA-217 and ATA-113 were purchased from Codexis® (USA).

2.2. Methods

2.2.1. Media, culture conditions and strains

Bacteria strains used in this study are listed in Table 2.1. A single colony from a fresh plate was cultivated in 3 mL Lysogeny broth (LB) at 37 °C, 200 rpm, from 16-18 hours.

LB broth was prepared by mixing 20 g/L and LB agar was prepared by mixing LB powder 20 g/L with agar 15 g/L. The mixture was homogenized and autoclaved prior to use. The overnight culture was used for long term storage by preparing glycerol stocks (30 % v/v glycerol) and kept at -70 °C. When a fresh culture was needed, the glycerol stock was streaked on an LB agar plate (LB with 1.5 % w/v agar). Overnight cultures were prepared by inoculating a fresh colony in a 13 mL tube (Sarstedt; Germany) containing 3 mL LB. Except when stated differently, tubes were incubated at 37 °C with shaking at 200 rpm for approximately 16-18 h. Appropriate antibiotic was added when required.

For aerobic cultivations in a bioreactor, a rich media containing 5 g/L yeast extract, 10 g/L tryptone, 5 g/L KH_2PO_4, 3 g/L K_2HPO_4, 1.6 g/L $(NH_4)_2SO_4$, 1.7 g/L citric acid, and 4 mL Ramseys trace elements (per litre: 4 g $ZnSO_4 \cdot 7H_2O$; 1 g $MnCl \cdot 4H_2O$; 0.2 g $Na_2B_4O_7 \cdot 10H_2O$; 0.3 g $NiCl_2 \cdot 6H_2O$; 1 g $Na_2MoO_4 \cdot 2H_2O$; 1 g $CuCl \cdot 2H_2O$; 7.6 g $FeSO_4 \cdot 7H_2O$; added to the medium after autoclaving).

Whenever needed, the medium was supplemented with kanamycin 50 µg/mL (km50), carbenicillin 50µg/mL (carb50) gentamicin 20 µg/mL (gen20), tetracycline 15 µg/mL (tet15), spectinomycin 50 µg/mL (spec50).

2.2.2. Growth conditions for 3HBA and 3ABA synthesis

For the synthesis of 3-hydroxybutyric acid (3HBA) 1 mL overnight culture of *E. coli* BL21 recombinantly expressing *tesB_RHBD, tesB_SHBD, bch_RHBD or bch_SHBD*, and for the synthesis of 3-amino butyric acid (3ABA) (Table 2.3), 1 mL of overnight BL21_ABA, was inoculate 100 mL LB broth or M9 medium pH (64 g/L Na_2HPO_4, 15 g/L KH_2PO_4, 2.5 g/L NaCl) supplemented with 10 g/L glucose, 2 mM MgSO4 and 0.1 mM $CaCl_2$ in a 250 mL Erlenmeyer flask. Flasks were incubated at 37 °C at 200 rpm until cells reached mid-exponential growth (OD_{600nm}=0.3-0.5). The flasks were then incubated at 4 °C for 30 min and protein expression induced by adding 0.5 mM IPTG followed by incubation at 30 °C for 24 or 48 h. One millilitre of sample was collected in determined intervals to analyse 3ABA (Section 2.7.2.) or glucose, acetic acid and 3HBA (Section 2.7.1.)

Table 2. 1. Bacterial strains used in this study.

Strain	Genotype	Source
DH5α	*Escherichia coli* DH5α F- endA1 glnV44 thi-1 recA1 relA1 gyrA96 deoR nupG Φ80dlacZΔM15 Δ(lacZYA-argF)U169, hsdR17(rK- mK+), λ–	Novagen
DH5α_SADH	*E. coli* DH5α harbouring the SADH construct	This study
DH5α_RADH	*E. coli* DH5α harbouring the RADH construct	This study
DH5α_GO	*E. coli* DH5α harbouring the CV_TA construct	This study
DH5α_CV_TA	*E. coli* DH5α harbouring the CV_TA construct	(Almahboub, Narancic et al. 2018)
DH5α_ABA	*E. coli* DH5α harbouring the ABA operon	This study
DH5α_3HBAdAf	*E. coli* DH5α harbouring the pET45b_3HBDdAf	This study
DH5α_3HBAdPp	*E. coli* DH5α harbouring the pET45b_3HBDdAf	This study
DH5α_pET	*E. coli* DH5α harbouring pET45b(+) vector	This study

DH5α_*tesB_RHBD*	*E. coli* DH5α harbouring the *tesB_RHBD* operon	(Liu 2020)
DH5α_*tesB_SHBD*	*E. coli* DH5α harbouring the *tesB_SHBD* operon	(Liu 2020)
DH5α_*bch_RHBD*	*E. coli* DH5α harbouring the *bch_RHBD* operon	(Liu 2020)
DH5α_*bch_SHBD*	*E. coli* DH5α harbouring the *bch_RHBD* operon	Novagen
BL21	*E. coli* BL21 (DE3) F– ompT gal dcm lon hsdSB(rB- mB-) araB::T7RNAP-tetA	
E. coli DH5*α λpir*	*supE44, ΔlacU169 (ΦlacZΔM15), recA1, endA1, hsdR17, thi-1, gyrA96, relA1, λpir phage lysogen*	*Novagen*
E. coli HB101/pRK 600	Helper strain in a tripartite conjugation, Chl^R	*Novagen*
BL21_SADH	*E. coli* BL21 (DE3) expressing SADH construct	This study
BL21_RADH	*E. coli* BL21 (DE3) expressing RADH construct	This study
BL21_CV_TA	*E. coli* BL21 (DE3) expressing the CV_TA construct	Almahboub *et al*., (2017)
BL21_GO	*E. coli* BL21 (DE3) expressing the GO construct	This study
BL21_L-LDH	*E. coli* BL21 (DE3) expressing the D-lactate dehydrogenase from *E. coli*	This study
BL21_L-DDH	*E. coli* BL21 (DE3) expressing the D-lactate dehydrogenase from *Haloferax mediterranei*	This study

BL21_ABA	*E. coli* BL21 (DE3) expressing *tesB_phaA_CV2025* for 3-aminobutyric acid synthesis	This study
BL21_3ABA	*E. coli* BL21 (DE3) expressing *CV2025_tesB_phaA* for 3-aminobutyric acid synthesis	This study
Bacillus subtilis ATCC6633	Bacillus subtilis subsp. s*pizizenii* ATCC6633	DSMZ
E. coli NCTC9001	*E. coli* NCTC9001; Serovar o1:k1(l1):h7	DSMZ
Pseudomonas aeruginosa ATCC27853	*Pseudomonas aeruginosa* (Schroeter) ATCC27853	DSMZ
Salmonella typhimurium NCTC12023	*Salmonella enterica* subsp. *enterica* serotype Typhimurium NCTC12023	DSMZ
BL21_pET45b	*E. coli* BL21 (DE3) harbouring empty pET-45b	This study
BL21_*tesB_RHBD*	*E. coli* BL21 (DE3) expressing the *tesB_phaA*_RHBD operon	(Liu 2020)
BL21_*tesB_SHBD*	*E. coli* BL21 (DE3) expressing the *tesB_phaA*_SHBD operon	(Liu 2020)
BL21_*bch_RHBD*	*E. coli* BL21 (DE3) expressing the *bch_phaA*_RHBD operon	(Liu 2020)
BL21_*bch_SHBD*	*E. coli* BL21 (DE3) expressing the *bch_phaA*_SHBD operon	(Liu 2020)

Δ*eutD*	*E. coli* BL21 (DE3) Δ*eutD*	This study
Δ*pta*	*E. coli* BL21 (DE3) Δ*pta*	This study
Δ*eutD*Δ*pta*	*E. coli* BL21 (DE3) Δ*eutD*Δ*pta*	This study
ΔeutD_tesB_RHBD	*E. coli* BL21 (DE3) Δ*eutD* expressing the *tesB_phaA*_RHBD operon	This study
ΔeutD_tesB_SHBD	*E. coli* BL21 (DE3) Δ*eutD* expressing the *tesB_phaA*_SHBD operon	This study
Δ*eutD_bch_RHBD*	*E. coli* BL21 (DE3) Δ*eutD* expressing the *bch_phaA*_RHBD operon	This study
Δ*eutD_bch_SHBD*	*E. coli* BL21 (DE3) Δ*eutD* expressing the *bch_phaA*_SHBD operon	This study
Δ*pta_tesB_RHBD*	*E. coli* BL21 (DE3) Δ*pta* expressing the *tesB_phaA*_RHBD operon	This study
Δ*pta_tesB_SHBD*	*E. coli* BL21 (DE3) Δ*pta* expressing the *tesB_phaA*_SHBD operon	This study
Δ*eutD*Δ*pta_tesB_RHBD*	*E. coli* BL21 (DE3) Δ*eutD*Δ*pta* expressing the *tesB_phaA*_RHBD operon	This study
Δ*eutD*Δ*pta_tesB_SHBD*	*E. coli* BL21 (DE3) Δ*eutD*Δ*pta* expressing the *tesB_phaA*_SHBD operon	This study

2.2.3. Bioreactor set up

The synthesis of 3HBA was scaled up to 1 L fermentation using F0-Baby (Bionet® Spain). LB was used in batch or fed-batch fermentations.

Initially, 3 mL overnight pre-culture was grown at 37 °C for 6 h and 1 mL of the pre-inoculum was used to inoculate 2 x 50 mL LB in a 250 mL Erlenmeyer flask, which were incubated overnight at 37 °C, 200 rpm. The inoculum was then added to the medium (10 % v/v) with 100 µg/mL and 0.2 g/L $MgSO_4$. In a batch process, glucose was added at the start (10 g/L), while in a fed-batch process 20 g/L glucose were added in batch. Cells were grown at 37 °C until OD_{600nm} reached 5-7 for lower cell density, or OD_{600nm}=15, for higher cell density. When the appropriate OD_{600nm} was reached, 5-7 for low cell density and 14-16 for high cell density, the temperature was brought down to 30 °C and protein expression induced with 0.5 mM IPTG. Two mL of sample were collected in determined intervals to measure glucose consumption and 3HBA/Acetate production and OD_{600nm}.

For fed-batch fermentations, the conditions were as above, but a feed bottle with 1 mL $MgSO_4$ (200 g/L stock concentration), was added to 100 mL glucose (500 g/L stock concentration). Glucose was provided with a feed rate of approximately 2 g/L/h, while $MgSO_4$ was fed at about 0.005 g/L/h.

In both cases pH was controlled by automatic addition of 15 % sulfuric acid and 25 % ammonium hydroxide. When the required OD_{600nm} was reached, protein expression was induced by adding 0.5 mM IPTG.

The rates were calculated as in the equation below, where Δx is the difference in acetate, glucose, 3HBA or OD_{600nm} and Δt is the time where the samples were analysed. This variation was calculated between all time points collected (ie. acetate 3 h - acetate 2 h / 3 h - 2 h) and used to analyse the average glucose consumption and intervals where cell growth and 3HBA synthesis were maximized.

$$\frac{\Delta x}{\Delta t}$$

2.3. Recombinant DNA techniques

2.3.1. Genomic DNA isolation

The genomic DNA (gDNA) of BL21 was isolated using GeneJET Genomic DNA Purification Kit (Thermo Fisher Scientific) following the manufacturer's instructions. The concentration and quality of extracted gDNA was assessed with BioDrop µLite (Lab plan, Kildare, Ireland).

2.3.2. Polymerase chain reaction (PCR)

Polymerase chain reaction (PCR) was used to amplify DNA fragments. The reaction mix consisted of 12.5 µL of polymerase Q5 High-Fidelity 2x Master Mix (New England Biolabs, UK), 0.5 µM of each primer and 1-10 ng DNA template, and 1 µL dimethyl sulfoxide (DMSO), in a total volume of 25 µL.

PCR was carried out using a ProFlexTM PCR System (Applied Biosystem, Carlsbad, USA) under a thermocycling condition consisting of initial denaturation at 98 °C for 30 s, then 30 cycles of denaturation at 98 °C for 10 s, annealing at 56-65 °C for 30 s, elongation at 72 °C using 10 s/kb, followed by a final incubation at 72 °C for 2 min. Annealing temperature and elongation time were adapted appropriately according to specific primer melting temperature (Tm) and DNA product size. The PCR product was separated and visualized on 1 % (w/v) agarose gel, which was stained with 0.1 µg/mL SafeView Nucleic acid stain. GeneRuler 1 kb Plus DNA Ladder (Thermo Fisher Scientific) was used as a molecular weight marker to estimate the size of DNA.

2.3.3. Gene Cloning

The genes encoding a glycolate oxidase GO from *Spinacia oleracea* (GenBank XM_022011288.1), *S*- and *R*-specific alcohol dehydrogenases (ADH) from *Aromatoleum aromaticum* (SADH - GenBank: CR555306) and *L. brevis* (RADH - GenBank: LS483405), respectively (Mutti *et al*., 2015), *ldhA* gene that encodes a D-lactate dehydrogenase from *E. coli* BL21 (DE3) (L-LDH) (AM946981.2) and D-lactate dehydrogenase from *Haloferax mediterranei* (L-DDH) (DQ223970.1) were purchased from Twist Bioscience (UK). These were then cloned into pET45b (NovoGene) using Gibson assembly (2.3.4.). All of the primers used to create homology regions are listed in Table 2.2 A and the constructs obtained in Table 2.3. PCR reaction was performed

on a ProFlexTM PCR System (Applied Biosystem, Carlsbad, USA). PCR product was analysed on a 1 % (w/v) agarose gel stained with 0.1 µg/mL SafeView Nucleic acid stain. PCR was performed as described in section 2.3.2.

2.3.4. Gibson Assembly

Gibson assembly was used to ligate the target genes to the vector of interest. The Gibson mixture consisted of a 10 µL reaction containing 50 ng of the amplified vector with overhanging nucleotides complementary to the target gene, 100 ng of the target gene PCR product also with overhanging nucleotides, 5 µL of the Gibson Assembly® Master Mix (NEB #E2621S/L/X). The reactions were incubated in Thermoblock (Thermomixer comfort, Eppendorf, Germany) at 50 °C for 1 h.

2.3.5. Design of a synthetic operon to produce 3-aminobutyric acid Aminobutyric acid operon (ABA operon)

3ABA operon includes the genes for hydrolase TesB, ketothiolase PhaA and the transaminase CV_TA (*CV_2025*). The genes were separated by the ribosome binding site 1 and 2, which was purchased from Sigma (Ireland). Two different order of genes were attempted: *tesB*_RBS1_*phaA*_RBS2_*CV_2025* (ABA operon), and *CV_2025*_RBS1_*tesB*_RBS2_*phaA* (3ABA operon), using the primers shown in Table 2.2. B. Fragments were PCR amplified as in Section 2.3.2. and Gibson assembled as in Section 2.3.4. The constructs generated are shown in Table 2.3.

Table 2. 2. List of primers used in this study.

Primer name	Sequence (5'-3')	Application
A. Primers used for to produce the constructs for protein expression		
pET_SADH_F	GAGACACTGACTCGAGTCTGGTAAAGAAACC	Cloning
pET_ADH_R	TTGCGTCATTGGATCCGGACTCTTGTCG	Cloning
SADH_F	GATGACGACGACAAGAGTCCGGATCCAATGACGCAAAGACTGAAGGACAAG	Cloning
SADH_R	GTTTCTTTACCAGACTCGAGTCAGTGTCTCACCATACCGC	Cloning
pET_RADH_F	CGCTCAATAACTCGAGTCTGGTAAAGAAACC	Cloning
pET_RADH_R	GTTTGACATTGGATCCGGACTCTTGTCG	Cloning
RADH_R	GATGACGACGACAAGAGTCCGGATCCAATGTCAAACCGGTTAGATGGAAAAG	Cloning
RADH_R	GTTTCTTTACCAGACTCGAGTTATTGAGCGGTATAACCACCATC	Cloning
pET_GO_F	CTCGAGTCTGGTAAAGAAAC	Cloning
pET_GO_R	GGATCCGGACTCTTGTCG	Cloning
GO_F	GATGACGACGACAAGAGTCCGGATCCAATGGAGATCACAAATGTG	Cloning
GO_R	GTTTCTTTACCAGACTCGAGTTATAATCTGGCAACAGC	Cloning
pET_LLDH_F	ACTGGTTTAACTCGAGTCTGGTAAAGAA	Cloning
pET_LLDH_R	GAGTTTCATTGGATCCGGACTCTTGT	Cloning
LLDH_F	TCCGGATCCAATGAAACTCGCCGTTTA	Cloning
LLDH_R	CAGACTCGAGTTAAACCAGTTCGTTC	Cloning
pET_LDDH_F	CGTGGTGTAACTCGAGTCTGGTAA	Cloning
pET_LDDH_R	GATGTGCATTGGATCCGGACTCTT	Cloning
LDDH_F	TCCGGATCCAATGCACATCGAA	Cloning
LDDH_R	AGACTCGAGTTACACCACGCG	Cloning
pET45_3hbaAf_F	AGCACGCTAACTCGAGTCTGGTA	Cloning

pET45_3hbaAf_R	TTTCAGCATTGGATCCGGACT	Cloning
3hbadAf_F	GTCCGGATCCAATGCTGAAAGGTAAAAAA	Cloning
3hbaAf_R	CAGACTCGAGTTAGCGTGCTGT	Cloning

B. **Primers used to amplify fragments and construct the ABA operon (tesB_phaA_CV2025) or 3ABA operon (*CV2025_phaA_tesB*).**

pet_ABA_F	GGCTTAGCTCGAGTCTGGTAAAGAA	Cloning for ABA operon
pet_ABA_R	TTTAGCGCCTGACTCATGGATCCGG	Cloning for ABA operon
CV_TA_ABA_R	ACCAGACTCGAGCTAAGCCAGCC	Cloning for ABA operon
CV_TA_ABA_F	AGGAGTGGACATGCAGAAGCAACGT	Cloning for ABA operon
tesB_phaa_ABA_R	TTGCTTCTGCATGTCCACTCCTTGA	Cloning for ABA operon
tesB_phaa_ABA_F	TCCGGATCCATGAGTCAGGCGCTAA	Cloning for ABA operon
3ABA_pet_F	CGCAAATAACTCGAGTCTGGTAAA	Cloning for 3ABA operon
3ABA_pet_R	CTTCTGCATGGATCCGGACTCT	Cloning for 3ABA operon
3ABA_cvta_F	AGAGTCCGGATCCATGCAGAAGCAA	Cloning for 3ABA operon
3ABA_cvta_R	GCGCCTGACTCATAGCCACCCCTC	Cloning for 3ABA operon
3ABA_tesB_phaA_F	GAGGGGTGGCTATGAGTCAGG	Cloning for 3ABA operon
3ABA_tesB_phaA_R	TTTACCAGACTCGAGTTATTTGCG	Cloning for 3ABA operon
RBS1	AATGAAATTGTCATGAGGGGATATTTTGTTCATCCCCCA CCTAACTTCTTTGCTTCAGCTAAATCTTGTGTGGTGAAAA TCTTACTACCCGCAAATAGCGGTATAAAATCGAGGCTAT ATAGTAGTGTAATTACAGCTACTATATAGCCTTTTTTATTT AATTATTTTTAATAAAATTTAATTTTATTAAATCCATTTTTG TGCTACACTGATTTTAATCAAATATTCTAAAAATAAAAAG GAGGGGTGGCT	Cloning for 3ABA operon

RBS2	GGAAGGGGTTTTCCGGGGCCGCGCGCGGTTGGCGCGG ACCCGGCGACGATAACGAAGCCAATCAAGGAGTGGAC	Cloning for 3ABA operon

C. **List of primers and sgRNA used on CRISPR three-plasmid methodology for the knock out of 1017 bp *eutD* and knock-in of the RHBD operon.**

pKNOCK_F	CTGCAGGAATTCGATATCAAGCTTATC	Cloning
pKNOCK_R	GGATCCACTAGTTCTAGAGCGG	Cloning
US_F	GCTCTAGAACTAGTGGATCCTTTCGAGCTAAACAGCCAC GAC	Cloning
US_R	AGTCGTATTATCATAGGGATTGCCAGTTAGCC	Cloning
DS_F	TATGGGCTGAACGGTCCCGTTCTGGAC	Cloning
DS_R	TTGATATCGAATTCCTGCAGTGTCACTGCTTTGCATTTTC AGC	Cloning
T7_Bch_PhaA_RHBD_F	ATCCCTATGATAATACGACTCACTATAGGGGAATTGTGA G	Cloning
T7_Bch_PhaA_RHBD_R	ACGGGACCGTTCAGCCCATATGCAGGCC	Cloning
pKNOCK_A	ATGGGAATTCCCCTCCACCGC	Verification
pKNOCK_B	CCCTCGAGGTCGACGGTATCGATA	Verification
Flank_F	CGCGAAAGTTATTGCTTGAGACGGGT	Verification
Flank_R	AACGGCGTCATCCAGTGACGC	Verification
Target _F	ATGATTATTGAACGTTGTCGTGAACTGGCGTTG	Verification
Target _R	GTAAACTGCTTTCGCGGTTCACTTCTGTC	Verification
	GTCCTAGGTATAATACTAGT	Cloning
118sgRNA	GTTGCGAGCGCCCGCCAGAG	
	GTTTTAGAGCTAGAAATAGCAAGTTAAAATAAGGCTAGT	
	CCGTTATCAACTTGAAAAAGTGGCACCGAGTCGGTGCTT	

118sgRNA_F	GTCCTAGGTATAATACTAGTGTTGCGAGCGCCC	Cloning
pgRNA(2.5kb)_F	GTTTCGGTCAAGGCTGGCAGGT	Cloning
pgRNA(2.5kb)_R	ACTAGTATTATACCTAGGACTGAGCTAGCTGTCAAAGAT CTTTAGAATTC	Cloning
T7_RNApol_R	GGTCATATCGTTACCTTGCGGGTT	Verification
T7_RNApol_F	GCATTTATGCAAGTTGTCGAGGCTGA	Verification
Km_F	GCCCTGAATGAACTCCAAGA	Verification
Km_R	CTCGTCAAGAAGGCGATAGAAG	Verification

D. **Primers used for the construction of pKNOCK and pgRNA for deletion of 854 bp of the *eutD* gene.**

sgRNA_DEL	ACATTGGCCTTGCCCTGTAG	
118DEL_pgRNA	GTCCTAGGTATAATACTAGT ACATTGGCCTTGCCCTGTAG GTTTTAGAGCTAGAAATAGCAAGTTAAAATAAGGCTAGT CCGTTATCAACTTGAAAAAGTGGCACCGAGTCGGTGCTT	Cloning
sgRNA integration (in the 200bp kept)	ATCCGGAAAAACCACTCTGG	Cloning
118 pgRNA integration (in the 200bp kept)	GTCCTAGGTATAATACTAGT ATCCGGAAAAACCACTCTGG GTTTTAGAGCTAGAAATAGCAAGTTAAAATAAGGCTAGT CCGTTATCAACTTGAAAAAGTGGCACCGAGTCGGTGCTT	Cloning
RNA_seq_R	CAGCCAAGCTGGAGACCGTTT	Verification
US_del_F	TAGTGGATCCGCGATGAACAT	Cloning
US_del_R	GGACCGTTCAGCCATGCGGATCAATCA	Cloning
DS_del_F	TCCGCATGGCTGAACGGTCC	Cloning
DS_del_R	ATTCCTGCAGTGTCACTGCTTTG	Cloning
pKNOCK_del_F	AGCAGTGACACTGCAGGAATTCGATATC	Cloning
pKNOCK_del_R	TGTTCATCGCGGATCCACTAGTTCTAGAG	Cloning

Flanking_del_F	GTTGACGATGAACAGCAGCAGCC	Cloning
Flanking_del_R	CCAGTGACGCGAAAACGCCCATC	Cloning
500bp_pgRNA_F	AAGTGGCACCGAGTCGGTGCTTTTTTT	Cloning
500bp_pgRNA_R	GCCGTATTACCGCCTTTGAGTGAGC	Cloning
118pgRNA_del_F	GTCCTAGGTATAATACTAGTACATTGGCCTTG	Cloning
pgRNA_F (linear plasmid 3129bp)	GCTCACTCAAAGGCGGTAATACGGC	Cloning
New flank_F	GATCCATCTCCCTGCGGACAGTC	Cloning
New flank_R	CAGCAATGGCTAACTGGCGCATTGCC	Verification
Gen_F	TGCATCACTTCTTCCCGTATG	Verification
Gen_R	AAGTTAGGTGGCTCAAGTATGG	Verification
Target_del_F	AACCTCGCAATGCGGGAAGAATT	Verification
Target_del_R	TTCAACCAGTGTTTGTAAACTGCTTT	Verification

E. **Primers used for *pta* knockout with ~800 bp upstream and downstream homologous regions.**

pta US(500 bp)_F	ATGAGCGTTGACGCAATCAACAAACTGCTG	Cloning
pta US(500 bp)_R	GCTTGCGCATGGTTTATCCTCTTTCGTTACC	Cloning
pta DS(500 bp)_F	AGGATAAACCATGCGCAAGCCGGTTAACGA	Cloning
pta DS(500 bp)_R	TCGTTAGTCAGAATGCGAAATGAGTGTGGATCTACG	Cloning
sg1	CAGCATAATAATACGGGACA	Cloning
sg2	AGGGATCAGCATAATAATAC	Cloning
pTarget (118bp) pta_sg1	GTCCTAGGTATAATACTAGTCAGCATAATAAT ACGGGACAGTTTTAGAGC	Cloning
pTarget (118bp) pta_sg2:	GTCCTAGGTATAATACTAGTAGGGAT CAGCATAATAATACGTTTTAGAGCTAGAAATAGCAAGTTA AAA	Cloning

pTargrt(1.5kb)_F	ATCGACATTGATCTGGCTATCTTGCTGACAAAAGC	Cloning
PTargrt(1.5kb)_R	ACTAGTATTATACCTAGGACTGAGCTAGCTGTCAAGGATC	Cloning
pTarget(0.6kb)_F	GTGGCACCGAGTCGGTGCTTTTTT	Cloning
pTarget(0.6kb)_R	GCAAGATAGCCAGATCAATGTCGATCGTGG	Cloning
pta_Flank_F	AAGGTCTGGTCATGGGTACCCGTT	Verification
pta Flank_R	TCGTGAACAGCTGTACGCGGTGA	Verification

F. **Primers used for *pta* knockout with upstream and downstream with ~500 bp and pTarget providing the sgRNA.**

pta US(500 bp)_F	ATGAGCGTTGACGCAATCAACAAACTGCTG	Cloning
pta US(500 bp)_R	GCTTGCGCATGGTTTATCCTCTTTCGTTACC	Cloning
pta DS(500 bp)_F	AGGATAAACCATGCGCAAGCCGGTTAACGA	Cloning
pta DS(500 bp)_R	TCGTTAGTCAGAATGCGAAATGAGTGTGGATCTACG	Cloning
pTarget (118bp) pta_sg1	GTCCTAGGTATAATACTAGTCAGCATAATAATACGGGACAGTTTTAGAGC	Cloning
pTarget (118bp) pta_sg2:	GTCCTAGGTATAATACTAGTAGGGATCAGCATAATAATACGTTTTAGAGCTAGAAATAGCAAGTTAAAA	Cloning
pTargrt(1.5kb)_F	ATCGACATTGATCTGGCTATCTTGCTGACAAAAGC	Cloning
PTargrt(1.5kb)_R	ACTAGTATTATACCTAGGACTGAGCTAGCTGTCAAGGATC	Cloning
pTarget(0.6kb)_F	GTGGCACCGAGTCGGTGCTTTTTT	Cloning
pTarget(0.6kb)_R	GCAAGATAGCCAGATCAATGTCGATCGTGG	Cloning
pta_Flank_F	AAGGTCTGGTCATGGGTACCCGTT	Verification
pta Flank_R	TCGTGAACAGCTGTACGCGGTGA	Verification

G. **Primers used for the genomic integration of the SHBD operon.**

sgRNA integration	ATCCGGAAAAACCACTCTGG	sgRNA

118 pgRNA_SHBDint_F	GTCCTAGGTATAATACTAGT ATCCGGAAAAACCACTCTGG GTTTTAGAGCTAGAAATAGCAAGTTAAAATAAGGCTAGT CCGTTATCAACTTGAAAAAGTGGCACCGAGTCGGTGCTT	Cloning
US_SHBDint_F	CTATGAAAGATTTCATCACCGATGCA	Cloning
US_SHBDint_R	AGTGAGTCGTATTATGCGTTCCCCC	Cloning
DS_SHBDint_F	GAACGGGACCGTTCACTCGAG	Cloning
DS_int_R	TGTCACTGCTTTGCATTTTCAGC	Cloning
SHBD_usds_2_F	GAACGCATAATACGACTCACTATAGGG	Cloning
SHBD_usds__2_ R	CCGTTCACTCGAGTTACTTGCTATAGA	Cloning
SHBD_usds_F	TGGGGGAACGCATAATACGAC	Cloning
SHBD_usds_R	ACGGGACCGTTCACTCGAGTTA	Cloning
Flanking_SHBDint_F	CATCCAGCGTGAAATTCCTGTATG	Verification
phaAA_F	AAGGCCGGCAAGTTTGACGAAGAG	Verification
phaAA_R	CTCTTCGTCAAACTTGCCGGCCTT	Verification
phaA_F	GGGTGGCTATGACTGACGTTGTCA	Verification
phaA_R	TGACAACGTCAGTCATAGCCACCC	Verification
Target_int_F	ATGATTATTGAACGTTGTCGT	Verification
Target_int_R	GCCATGCGGATCAATCAC	Verification
pTarget_int _118 bp_1 (Synthego)	GTCCTAGGTATAATACTAGT TCCGGAAAAACCACTCTGGC GTTTTAGAGCTAGAAATAGCAAGTTAAAATAAGGCTAGT CCGTTATCAACTTGAAAAAGTGGCACCGAGTCGGTGC	Cloning
pTarget_int _118 bp_2 (EuPaGDT)	GTCCTAGGTATAATACTAGT ATCCGGAAAAACCACTCTGG GTTTTAGAGCTAGAAATAGCAAGTTAAAATAAGGCTAGT CCGTTATCAACTTGAAAAAGTGGCACCGAGTCGGTGCTT	Cloning

Table 2. 3. List of vectors and constructs used in this study.

Vector/construct	Description	Reference
pET45b	pET-45b(+) expression vector under T7 promoter, $Carb^R$	Novagen
pET45b_CV_TA	pET-45b containing *CV2025* gene from *Chromobacterium violaceum,* $Carb^R$	(Almahboub, Narancic et al. 2018)
pET45b_SADH	pET-45b containing ADH gene from *Aromatoleum aromaticum*, $Carb^R$	This study
pET45b_RADH	pET-45b containing ADH gene from *Lactobacillus brevis,* $Carb^R$	This study
pET45b_GO	pET-45b containing GO gene from *Spinacia oleracea*, $Carb^R$	This study
pET45b_LLDH	pET-45b containing *ldhA* gene from *E. coli*, $Carb^R$	This study
pET45b_LDDH	pET-45b containing lactate dehydrogenase gene from *Haloferax mediterranei*, $Carb^R$	This study
tesB_RHBD operon	pET-45b containing the synthetic operon with *tesB_phaA_RHBD* genes	(Liu 2020)
tesB_SHBD operon	pET-45b containing the synthetic operon with *tesB_phaA_SHBD* genes	(Liu 2020)
bch_RHBD operon	pET-45b containing the synthetic operon with *bch_phaA_RHBD* genes	(Liu 2020)
bch_SHBD operon	pET-45b containing the synthetic operon with *bch_phaA_SHBD* genes	(Liu 2020)
3ABA	pET-45b containing the synthetic operon with *CV2025_tesB_phaA* genes	This study
ABA operon	pET-45b containing the synthetic operon with *tesB_phaA_CV2025* genes	This study
pCas9_gen	pCas9/λRed recombineering plasmid with constitutively expressed Cas9 and the araBAD promoter expressing αβγ, $Gent^R$	Cook *et al*., (2018)
pCas9_km	pCas9/λRed recombineering plasmid with constitutively expressed Cas9 and the araBAD promoter expressing αβγ, km^R	This study
pKNOCK	Repair plasmid, Km^R	Addgene
pgRNA	sgRNA plasmid, Tet^R	Cook *et al*., (2018)
pKNOCK_US_T7_Bch_PhaA_RHBD_DS	Repair plasmid containing the construct to be inserted, Km^R	This study

pTarget	*pMB1 aadA* sgRNA-*pMB1*	(Jiang, Chen et al. 2015)

2.3.6. Preparation of chemically competent cells and heat shock transformation

Chemically competent cells were prepared according to Hanahan (1983), with modifications (Hanahan 1983). An overnight culture of the required *E. coli* strain was used to inoculate 50 mL LB (2 % v/v) and grown at 30 °C, 200 rpm until OD_{600nm} reached mid-exponential phase (0.3-0.5). Cells were then cooled on ice for 10 min and harvested at 10000 rpm, 4 °C for 15 min (Sorvall RC-5, refrigerated floor centrifuge, England). The supernatant was discarded, and cells resuspended in 10 mL ice-cold 0.1 M $CaCl_2$ and incubated on ice for 30 min. The cells were centrifuged as above, and the was washed in 10 mL 0.1 M $CaCl_2$. Finally, cells were harvested and resuspended in 3 mL 0.1 M $CaCl_2$ and 1 mL 50 % glycerol. Aliquots of 200 µL were stored at -80 °C.

One hundred microliters of competent *E. coli* cells were thawed on ice and mixed with 50-100 ng construct or 5 µL Gibson mixture. The mixture was gently homogenized and incubated on ice for 30 min. After that, the mixture was transferred to a 42 °C water bath for heat shock for 60-90s, followed by a 2 min incubation on ice. 900 µL of LB was added to the mixture and it was incubated at 37 °C for 1 h under 200 rpm shaking. Finally, 300 µL of the transformation product was incubated overnight on selective plate containing the appropriate antibiotic.

2.3.7. Electrocompetent cells preparation and electroporation

Electrocompetent *E. coli* were prepared according to (Gonzales, Brooks et al. 2013) with modifications. An overnight culture of the *E. coli* strain was used to inoculate 100 mL of LB medium (2 % v/v). The culture was incubated at 37 °C with shaking at 200 rpm until OD_{600nm} reached mid-exponential phase (0.3-0.5). The cells were cooled down at 4 °C for 30 min before harvesting by centrifugation at 10000 rpm and 4 °C for 15 min (Sorvall RC-5, refrigerated floor centrifuge, England). The pellets were washed with 100 mL of ice-cold sterile water and centrifuged. The resulting pellet was washed three times with a decreasing volume of ice-cold 10 % glycerol (100, 50, and 20 mL). After the last wash, cells were resuspended in 1 mL of 10 % glycerol, divided into 100 µL aliquots, and kept at -80 °C.

The mixture of 100 µL electrocompetent *E. coli* and 50-100 ng construct was transferred to a prechilled 2 mm gap width electroporation cuvette (Thermo Fisher

Scientific), followed by electroporation at 2.5 kV (Electroporator 2510, Eppendorf, Germany). The mixture was transferred to 0.9 mL LB in a sterile 13 mL tube (Sarstedt; Germany) and incubated at 37 °C, or 30 °C, when needed, 200 rpm for 1 h for recovery. After 1 h, the mixture was centrifuged at 7000 rpm, 4 °C for 5 min (benchtop centrifuge Eppendorf 5430R), 700 µL supernatant were discarded, and cells were resuspended in the residual medium. One hundred µL cell suspension was spread on an appropriate selective LB agar plate and incubated at 37 °C, or 30 °C until colonies appeared.

2.3.8. Plasmid isolation

Plasmids were extracted from 3 mL overnight bacterial cultures containing the plasmid of interest using GeneJET Plasmid Miniprep Kit (Thermo Fisher Scientific), according to the manufacturer's instructions. The concentration and quality of extracted plasmid was assessed with BioDrop µLite (Lab plan, Kildare, Ireland) and by gel electrophoresis.

2.3.9. Colony PCR screening

Transformants were selected directly from the plate and screened by colony PCR. These colonies were resuspended with 10 µL of the Master Mix reaction containing 5 µL AccuStart II PCR ToughMix (VWR) and 0.5 µM of each primer. PCR conditions consisted of one initial denaturation cycle at 95 °C for 5 min, 30 cycles of denaturation at 95 °C for 30 s, 30 cycles of annealing at 59 °C for 30 s, extension at 68 °C 1min/kb, and a final extension at 68 °C for 7 min. The annealing temperature and extension time were adjusted according to primers and size of the insert. PCR products were verified on 1 % (w/v) agarose gel stained with 0.1 µg/mL SafeView Nucleic acid stain. Colonies that integrated the recombinant vector were sequenced (Eurofins, Germany).

2.4. CRISPR/Cas modified methods

2.4.1. CRISPR – 3-plasmid system

A modified Clustered regularly interspaced short palindromic repeats-associated protein 9 (CRISPR/Cas9) methodology described by Cook *et al.,* 2018 was used to

attempt to delete *eutD or pta* genes in BL21 (Table 2.1.), host used for the 3HBA production, and a simultaneous knock-in of the *tesB_RHBD* operon.

Three vectors are used: pCas9/λRed vector, which constitutively expresses Cas9 nuclease and L-arabinose inducible λRed recombinases; pKNOCK suicide vector, that was used to carry the repair template to be integrated into the genome (the construct T7_*Bch_phaA_RHBD*); and pgRNA plasmid was used to constitutively express small guide RNA (sgRNA; Table 2.3.).

To perform a knock-in of (*R*)3HBA (3461 bp) operon and simultaneous deletion of *eutD* (1017 bp) knockout and knock-in of the operon to produce the following protocol was attempted. All primers required for this experiment and the single-guide RNA (sgRNA) are listed in Table 2.2. C.

The single guide RNA (sgRNA) was designed using the Eukaryotic Pathogen CRISPR guide RNA/DNA Design Tool (grna.ctegd.uga.edu) and consisted of 20 bp sgRNA and a 98 bp region of the pgRNA vector which were synthesized, resulting in 118pgRNA. A ~700-bp region of the vector, with overlap with 118pgRNA, was amplified using the primers 700pgRNA_F/R, and by using PCR (Section 2.3.2.), 118pgRNA and 700pgRNA were assembled resulting in an 818pgRNA fragment. This step was performed due to difficulty of assembling small fragments, such as 20 bp sgRNA, though Gibson Assembly. The remaining of pgRNA (2384 kb) was obtained by using the primers pgRNA(Section 2.3.4.), and resulted in a 3202 bp construct. The construct was transformed by heat shock (Section 2.3.6.) into *E. coli* DH5α and selected on fresh LB containing Tet10. Colonies were screened by colony PCR (Section 2.3.2.) using the primers 118sgRNA_F and 500pgRNA_R. The correct assembly was confirmed by sequencing.

pKNOCK, a suicide vector, was used to introduce the repair template T7_*Bch_PhaA_RHBD* in the genome of BL21. To generate the repair template, pKNOCK was amplified by PCR using the primers pKNOCK_F/pKNOCK_R. A flanking region of ~800 bp upstream (US) and downstream (DS) the target gene (*eutD*) was amplified using the primer pair US_F/R and DS_F/R, respectively. Due to the amount and length of the fragments, sequential assembly was performed. Initially, pKNOCK (2098 kb) was assembled with US PCR product by PCR, using the primers US_F and pKNOCK_R. Another PCR was used to obtain the fragment

US_pKNOCK_DS, using the primers US_R and DS_F. For that, the resultant US_pKNOCK fragment (2889 kb) was assembled with DS PCR product using the primers DS_R and US_F (Table 2.2. C). The US_pKNOCK_DS resulted in a product of 3689 kb. Finally, the US_pknock_DS fragment was assembled with T7_Bch_phaA_RHBA as in Section 2.3.4. (Figure 2.1.) (Table 2.2. C).

To amplify the T7_*Bch_PhaA_RHBD* fragment, the construct digested with XhoI was used as template. The operon T7_*Bch_PhaA_RHBD* was amplified using the primers T7_Bch_PhaA_RHBD_F/R. pKNOCK_US_DS was assembled with T7_Bch_PhaA_RHBD using NEBuilder HiFi DNA Assembly Master Mix Kit. The pKNOCK_US_DS_T7_*Bch_PhaA_RHBD* resulted in a product of 6558 bp. (Figure 2.1.).

The assembled pKNOCK construct for deletion was transformed (Section 2.3.6.) into *E. coli* DH5a λpir competent cells by heat shock and plated in selective LB Km50. Colony PCR, with the primers pKNOCK_A and pKNOCK_B (Table 2.2. C), was used to identify clones carrying the insert (Section 2.3.9.). The positive clones were grown overnight using LB Km50. Plasmids from positive colonies were isolated and sequenced.

pKNOCK was transformed into BL21 by conjugation. In this method, three *E. coli* strains were used: *E. coli* HB101/pRK600, the “helper strain”, involved in transferring DNA into the recipient strain; *E. coli* DH5α λpir, harbouring the recombinant pKNOCK construct i.e donor strain; and BL21 (DE3), the recipient strain (Table 2.2).

Overnight cultures with the appropriate antibiotic were prepared. A mix containing 50 µL of the donor strain (DH5α λpir), 50 µL of the helper strain, and 200 µL of the recipient strain (BL21) was prepared in a 1.5 mL tube. Two hundred µL of the mixture were plated on a non-selective LB agar plate and incubated at 30 °C overnight. The conjugation mixture was washed off with 2 mL LB, that was subsequently diluted 100, 1000, 10000, and 100000-fold. Each dilution was plated on LB agar km50 and incubated at 37 °C until colonies appeared.

Identification of BL21 was confirmed using specific primer pair for T7 RNA polymerase (T7_RNApol_F/R), and pKNOCK construct was identified using primers for the km resistance gene (Km_F/R). Lastly, pKNOCK chromosomal integration was verified by

using one vector- and one genome-specific primer, like Flank_F and Target_R or Flank_R and Target_F.

Once pKNOCK integration was confirmed, 50 ng of pCas9 vector was introduced by electroporation (Section 2.3.7.), and cells plated on Km50/Gen20. Obtained colonies were grown overnight at 30 °C and electroporated with 100 ng pgRNA. These transformants were plated on LB agar Tet10/Gen25 until colonies appeared.

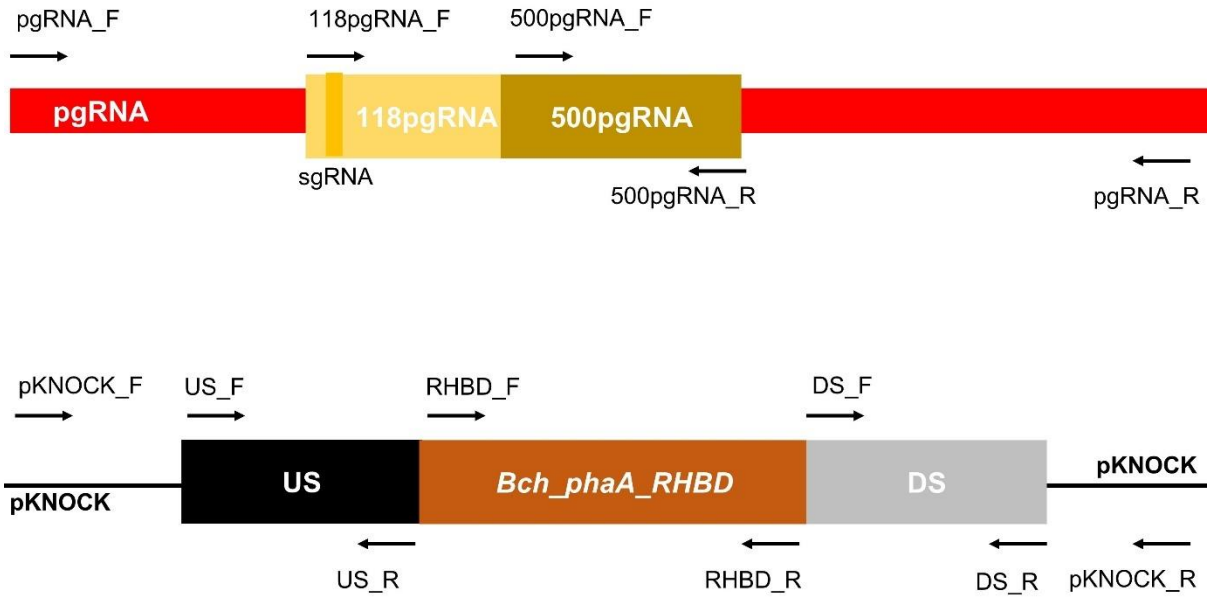

Figure 2. 1. Schematics for pgRNA (top) and pKNOCK (bottom) vectors assembly with primers used labelled with arrows. For pgRNA construct assembly a fragment of 118 bp was synthesized and assembled with 500 or 700 bp of pgRNA; while the remaining of pgRNA was PCR amplified. Gibson assembly was used to ligate the two fragments. For pKNOCK assembly the homologous US and DS regions, pKNOCK vector and the insert were PCR amplified. US and pKNOCK were assembled via PCR and US_pKNOCK was assembled with DS also by PCR. US_pKNOCK_DS and RHBD were ligated by Gibson assembly.

To only delete, an 854 bp of the gene was targeted for deletion leaving a 216 bp scar, which would be used as a site for integration. The primers used to amplify US, DS, pgRNA and pKNOCK are shown in Table 2.2. D. The three fragments were assembled

as above. However, in this case, the pgRNA fragment used to assembly the sgRNA had 500 bp instead of 700 bp as discussed above.

The pKNOCK construct used for deletion was 3697 bp, and after confirmed by sequencing it was conjugated into the BL21 strain.

2.4.2. CRISPR – 2-plasmid system

For this experiment, pCas9 is used to express the recombinases genes and pgRNA or pTarget to expresses the sgRNA, as above. However, the repair template is supplied as linear double-stranded DNA (dsDNA) (Jiang et al., 2015).

An US and DS region of the target gene comprising ~800 or ~500 bp each was assembled with the RHBD operon as mentioned above in Section 2.2.1. BL21 transformed with pCas9 by electroporation was grown overnight at 30 °C, 200 rpm, and used to inoculate 400 mL LB with 20 µg/mL gen. When OD_{600nm} reached 0.1, expression of λ-red genes was induced by adding 10 mM L-arabinose and cells continued to grow until OD_{600nm}=0.5. These cells were then used to prepare electrocompetent cells by the protocol described in Section 2.3.7. One hundred µL electrocompetent competent BL21_pCas9 were transformed with 100 ng pgRNA and 400 ng donor DNA.

To only delete 798 bp of the *eutD* gene and keep 200 bp for future integration, 801 bp US and 804 bp DS of the target region were amplified and assembled in US_DSdel. All primers used for this strategy are shown in Table 2.7. Donor dsDNA and pgRNA were electroporated into BL21_pCas9 and recovered in 0.9 mL LB for 1 h at 30 °C. This method was successful in deleting ~800 bp of *eutD* from *E. coli*'s genome.

As the deletion of *eutD* was achieved using this method, *pta* was targeted using the same methodology. Around 800 bp upstream and downstream of the *pta* gene were PCR amplified with the primer pair US800_pta_F/R and DS800_pta_F/R, respectively. The donor DNA comprised US_DS dsDNA with ~1600 bp. pgRNA was assembled as mentioned above, using the same 500bp pgRNA_F/R primer pair and using the specific gRNA for *pta* knockout (Table 2.2. E). One hundred ng pCas9 and pgRNA, and 400 ng donor DNA were transformed into BL21 and Δ*eutD* strains. The colonies

were screened using colony PCR and one genomic and one specific primer, Target_F and Flank_R, or Target_R and Flank_F

Another strategy, relying on pTarget instead of pgRNA to carry the sgRNA was used (Jiang, Chen et al. 2015). A shorter homologous region, with 500 bp upstream and downstream of *pta*, was amplified and cloned the sgRNA to pTarget (Table 2.2. F). Similar to pgRNA, 1.5 kb of pTarget were amplified with the primer pair pTarget(1.5kb)_F/R, while 0.6 kb of pTarget were amplified with the primer pair pTarget(0.6kb)_F/R to enable the assembly with the two sgRNAs tested, pTarget (118bp) pta_sgRNA1 and pTarget (118bp) pta_sgRNA2. US and DS of 500 bp each were amplified and assembled by PCR and provided as dsDNA repair template (Table 2.2. F).

One hundred ng pgRNA with sg1 or pTarget with sg1 or sg2, (Table 2.2. E) and 400 ng donor DNA were electroporated to BL21 or Δ*eutD* which were previously transformed with pCas9 that was induced with 10 mM arabinose (Section 2.4.2.). The cells were transferred to 900 µL LB in 13 mL tubes and recovered at 30 °C for 1 h, followed by centrifugation for 10 min at 4 °C and 7 000 rpm (benchtop centrifuge Eppendorf 5430R). 800 µL supernatant was discarded and cells were resuspended in the remaining 200 µL. Finally, the transformants were plated on LB km50/spec50 plates and incubated at 30 °C until colonies appeared. Transformants were screened with pTarget(0.6kb)_F/R and pta_Flank_F/R primers. All primers are available in Table 2.2. F.

The genomic integration of the *tesB_SHBD* operon in the scar left by *eutD* knockout, was also attempted using this methodology with pgRNA or pTarget to express the sgRNA. pgRNA 0.6kb and 118pgRNA were assembled by PCR and Gibson assembly as in Section 2.3.3. pTarget was also assembled as above using primers from Table 2.2. F and 2 sgRNAs, namely pTarget_int _118 bp_1, 2 and 3. BL21 and Δ*eutD* cells harbouring pCas9 with expressed recombinases, as abovementioned, were used to transform 100 ng pgRNA or pTarget and 400 ng double-stranded donor DNA.

2.5. Protein expression and purification

An overnight culture of BL21 harbouring a gene for recombinant protein expression (Table 2.3.) was used to inoculate 400 mL LB (0.2 % v/v) and cells were grown at 37

°C at 200 rpm until OD_{600nm} reached mid-exponential phase (0.3-0.5). When cells grew to the appropriate OD_{600nm}, flasks were incubated at 4 °C for 30 min and protein expression was induced by adding 0.5 mM IPTG. To optimize protein expression cells were incubated at 200 rpm and 30 °C. When protein expression under these conditions was optimal, temperature was reduced to 25 or 20 °C to maximise expression over cell growth

The protein expression was evaluated by time course expression analysis using 1 mL aliquots from protein expression mentioned above. Time zero (0 h) was considered the sample prior to induction by IPTG. At 0 h and after induction, 1 mL of sample was withdrawn every hour for four h. OD_{600nm} of samples was normalised by dilution to correspond to OD_{600nm}=0.5 and cells were pelleted and lysed with 50 µL BugBuster® Protein Extraction Reagent (Merk Millipore, USA). The mixture was incubated at 37 °C for 30 min at 200 rpm. The cell extract (CE) i.e. the lysate was centrifuged for 2 min at maximum speed (benchtop centrifuge Eppendorf 5810 R) to obtain the cell free extract (CFE). Both CE and CFE were analysed on 12 % SDS-PAGE.

When the time-course was determined, the cells expressing the protein of interest were grown in 400 mL LB at 200 rpm and for about 3 h until OD_{600nm}=0.3-0.5 was reached. As above, the flaks were incubated at 4 °C for 30 min and protein expression induced with 0.5 mM IPTG. Generally, flasks were incubated at 30 °C for 4 h induction and 200 rpm. The cell pellet obtained from protein expression (2 g wet weight) was resuspended in BugBuster®Master Mix (3 mL per g of cell) (Merk Millipore, USA) and binding buffer (2 mL/ g of cell) (50 mM Sodium Phosphate, 20 mM Imidazole, 300 mM Sodium Chloride, pH 7.4). The mixture was incubated at 37 °C 200 rpm for 30 min and the cell-free extract was obtained by centrifuging the mixture at 7000 rpm for 10 min at 4 °C (benchtop centrifuge Eppendorf 5430R). The resultant supernatant was filtered using a 0.45 µM syringe filter (Syringe filter, Filtropur S) and used for protein purification. For protein purification the CFE was loaded onto a HisTrap FF 1 mL column (Amersham Biosciences/GE Healthcare, England). The low affinity proteins were removed by washing the column with 2 mL binding buffer pH 7.4 and protein purification was carried out in ÄKTAprime chromatography system (Amersham Biosciences, GE Healthcare, England). Proteins were eluted from the column with increasing elution buffer gradient (50 mM sodium phosphate, 500 mM imidazole and 300 mM NaCl, pH 7.4). Eighteen 2 mL fractions were collected at a flow rate of 0.5

mL/min and imidazole concentration from 20 to 500 mM following the increasing gradient of elution buffer of (mL/B %): 6 mL / 0, 16 mL / 0/45, 2 mL / 45/50, 2 mL 50/60, 10 mL 60/100 %.

2.5.1. SDS-PAGE electrophoresis

Fifteen microliters of protein sample, either pure protein, CE or CFE, were resuspended in 5 µL 2x reduced SDS-PAGE sample buffer (80 mM Tris-HCl, pH 6.8, 10 % β-mercaptoethanol, 2 % sodium dodecyl sulfate (SDS), 10 % (v/v) glycerol, 0.1 % bromophenol blue). The mixture was incubated at 95 °C for 5 min. Denatured proteins were separated on an 5 % (w/v) stacking gel and 12 % (w/v) polyacrylamide SDS resolving gel. EZ-Run prestained Rec protein ladder was used (Thermo Fisher Scientific, Ireland) and the gel was run on PowerPac™ Basic Power Supply at 30 milliampers. The gel was stained using ReadyBlue Protein Gel Stain until bands could be visualized.

2.5.2. Western blot assay

Protein samples were run on SDS-PAGE gel as in Section 2.6.1. with an additional lane containing 5 µL ECL DualVue Western blotting marker. Low-fluorescence PVDF transfer membranes (ThermoFisher Scientific, USA) were activated by being immersed in 80 % methanol for 20 s and rinsed with ultrapure water for 2 min under agitation in a Fisherbrand Platform Shaker (USA). Finally, PDVF membranes were incubated in transfer buffer (25 mM trizma base, 192 mM glycine, 20 % v/v methanol) for 3 min. Blotting was carried out in a V20-SDB semi-dry western blotting device (Biophoretics, USA) maintained at 55 mA for 2 h.

After the transfer, the membrane was immersed in phosphate buffered saline-Tween (PBST) blocking buffer (137mM NaCl, 2.7mM KCl, 10mM NA_2HPO_4, 1.8mM KH_2PO_4, 0.05 % Tween-20 (v/v), 5 % (w/v) skimmed milk powder) at 4 °C under agitation overnight. Then, the membrane was placed into 10 mL PBST blocking buffer with the addition of 1 µL/mL of anti-His antibody (Sigma-Aldrich, Ireland) and 1 µL of S-protein-HRP Conjugate (Sigma-Aldrich, Ireland) and incubated for 2 h under agitation. The transfer membrane was washed again in PBST for 10 min twice on rocking platform. The membrane was then incubated with the Pierce ® ECL Western Blotting substrate

kit (ThermoFisher Scientific, USA), following the manufacturer's instructions. The signals were visualised using Fusion Fx Visualizer (Vilber).

2.6. Analytical methods/Protein activity assays

2.6.1. Dehydrogenase activity assay

Both alcohol dehydrogenases (ADHs) and lactate dehydrogenases (LDHs) used in this study are dependent of NAD^+ as a cofactor (Bonete, Ferrer et al. 2000, Mutti, Knaus et al. 2015). During the oxidation of a hydroxy group to a carbonyl group, NAD^+ is reduced to NADH, that can be measured spectrophotometrically at abs_{340nm} and it is in a 1:1 stochiometric ratio with the product of the reaction (Figure 2.2.) (Mutti, Knaus et al. 2015). Thus, NADH was used to monitor the oxidation catalysed by these enzymes. The standard reaction in 0.2 mL for ADHs consisted of 5 mM NAD^+, 1 mM of substrate, 20 mM of buffer, and 60 µg/mL purified ADH. Two buffers were tested: TRIS chloride pH 7.5, and potassium phosphate pH 7.0 at 30 °C on a SPECTROstarNano (BMG LABTECH Ltd., UK). As positive control, 2-butanol (**A** - 2but) was used as a substrate for ADHs and lactic acid (**B**) for LDHs. The target substrates tested were 2-hydroxybutyric acid (**C** - 2HBA), 2-hydroxyhexanoic acid (**D** - 2HHA), 2-hydroxyoctanoic acid (**E** - 2HOA), (*R*)-hydroxybutyric acid (**F** – (*R*)3HBA) and (*S*)-3-hydroxybutyric acid (**G** – (*S*)3HBA) (Figure 2.3.)

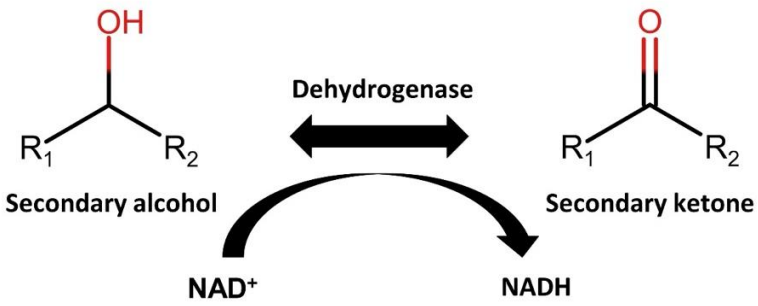

Figure 2. 2. Example of a reaction catalysed by an alcohol dehydrogenase where NADH is produced and can be measured spectrophotometrically.

Three negative controls were used: (1) protein denatured at 95 °C for 5 min, (2) no substrate added, and (3) no protein added. Detection of activity was observed by NADH formation and protein activity was measured as rate of reaction using the molar extinction coefficient of NADH (ε abs_{340nm} = 6.220 $mM^{-1}cm^{-1}$).

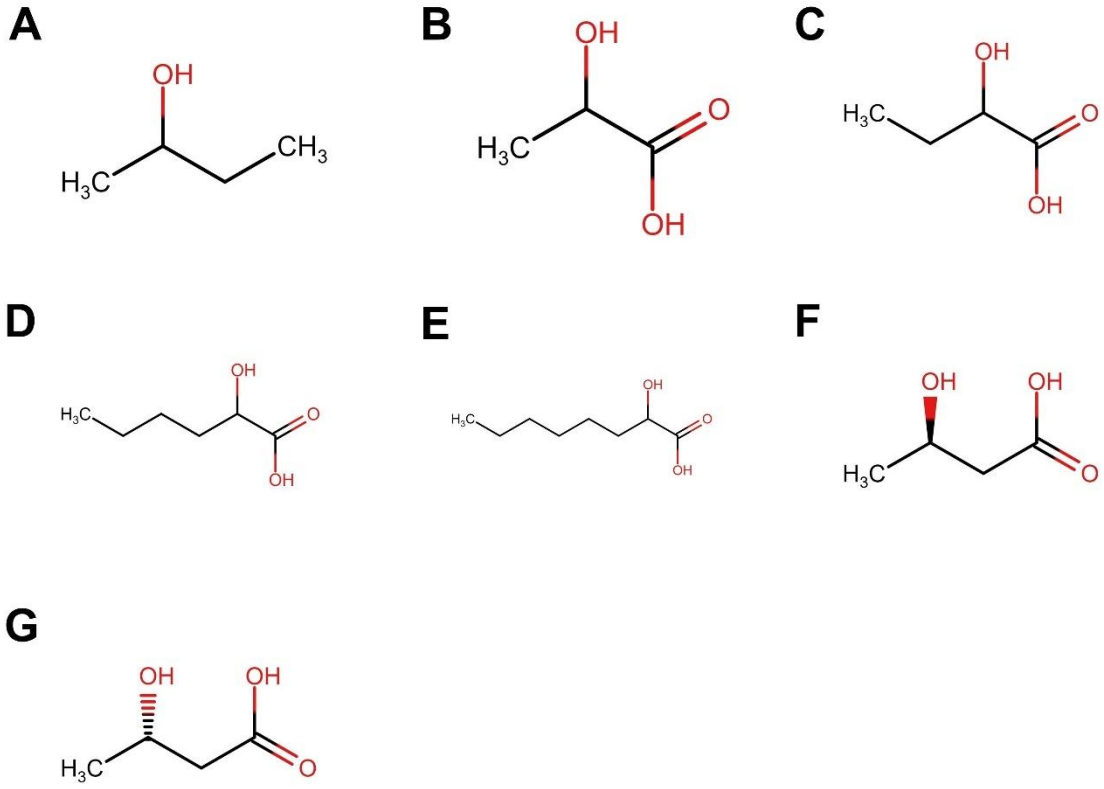

Figure 2. 3. Structures of hydroxy fatty acids used to assess the activity of ADHs, LDHs and GO. (A) 2-butanol (2but) used as positive control for AHDs, (B) lactic acid (LA) (C) 2-hydroxybutyric acid (2HBA), (D) 2-hydroxyhexanoic acid (2HHA), (E) 2-hydroxyoctanoic acid (2HOA), (F) (*R*)-3-hydroxybutyric ((*R*)3HBA)) and (G) (*S*)-3-hydroxybutyric acid ((*S*)3HBA). 2but was used positive control for AHDs and LA for GO and LDHs.

2.6.2. Glycolate oxidase activity assay

Glycolate oxidase (GO - EC 1.1.3.15) is a flavin mononucleotide (FMN) enzyme that catalyses the oxireduction of hydroxy acids (Das, Glenn Iv et al. 2010). The oxidation

of hydroxy acids by GO produces hydrogen peroxide as a by-product (Figure 2.4.), which can inhibit GO activity (Wahart, Staniland et al. 2022). Hydrogen peroxide reacts with *o*-dianisidine, resulting in the formation of *o*-dianisidine radical cation that absorbs light at abs_{440nm} and can be used to measure GO activity ($\varepsilon\ abs_{440nm}$ = 11.6 $mM^{-1}cm^{-1}$) (Macheroux 1991, Dellero, Mauve et al. 2015).

The standard reaction (0,2 mL) consisted of 20 mM phosphate buffer pH 7.0, or 20 mM Tris-HCl pH 7.5, 1 mM substrate (Figure 2.3.), 1 mM *o*-dianisidine (20 % Triton X-100), 0.2 mM FMN, and 0.1 mg/mL horseradish peroxidase (HRP - EC 1.11.1.7) and 50 µg/mL pure protein assayed from 150 min. DL-LA was used as positive control. The assay was performed in a 96-well plate (Greiner UVStar® 96 well plates, Sparks), which was incubated at 30ºC and the A_{440nm} was recorded every min for 30 min using SPECTROstar Nano (BMG LABTECH). GO activity was calculated using the molar extinction coefficient of oxidised o-dianisidine (ε = 11.3 $mM^{-1}cm^{-1}$) through Lamber-Beer equation.

2.6.3. TesB and BCH activity assay

The hydrolase activity of Bch and TesB was determined against acetoacetyl-CoA using the commercial standard reagent with the previously reported Ellman's reagent methods (Zheng *et al.*, 2004; Clomburg *et al.*, 2012) This method quantifies the free sulfhydryl group that reacts with 5,5′-dithiobis (2-nitrobenzoic acid) (DTNB) to yield a mixed disulphide and a measurable yellow product 5-thio-2-nitrobenzoic acid (TNB) quantified at 412 nm. The molar extinction coefficient of TNB is 13.6 $mM^{-1}cm^{-1}$.

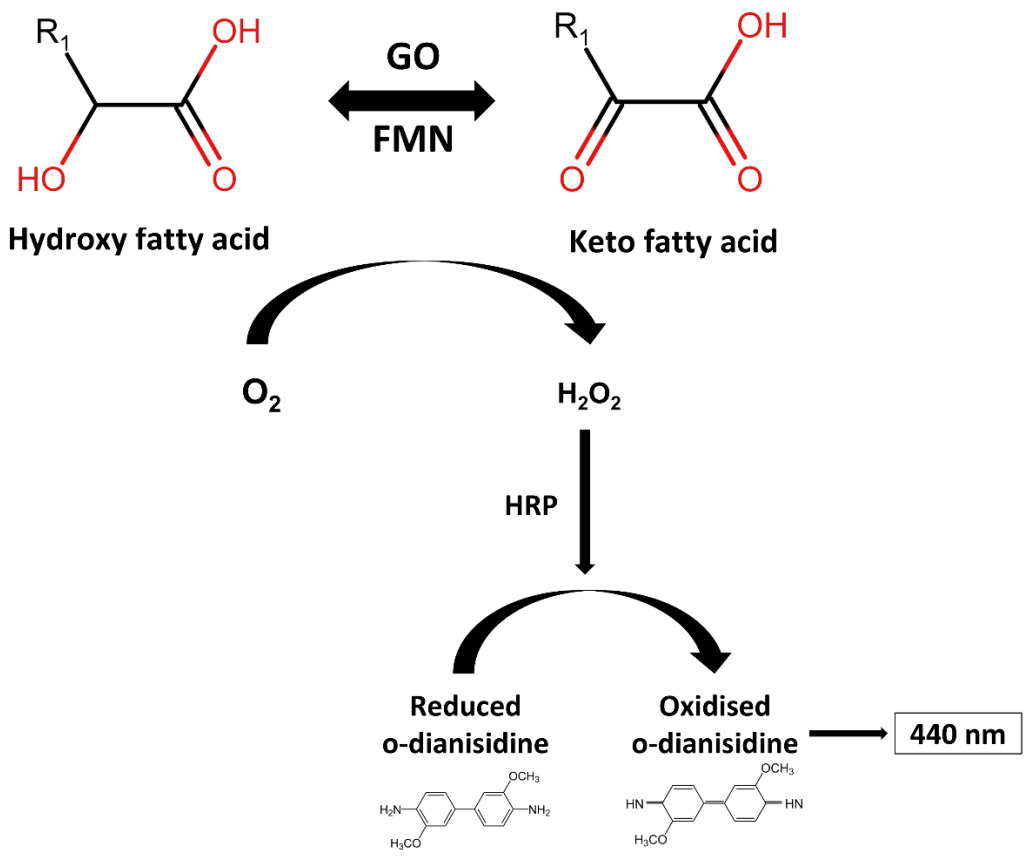

Figure 2. 4. Coupled reaction catalysed by glycolate oxidase (GO) with its cofactor flavin mononucleotide (FMN). The reaction produces hydrogen peroxide, a by-product, that is broken down by horseradish peroxidase (HRP) in the presence of *o*-dianisidine, which can be measured at abs_{440nm}.

The activity assay for TesB consisted of 100 mM Tris-HCl, 2 mM KCL, 2 mM 5,5-dithio-bis(2-nitrobenzoic acid (DNTB), 0.2 mM -CoA substrate and cell free extract of cells expressing TesB in 0,2 mL reaction volume. A_{412nm} was recorded every minute for 30 min SPECTROstar Nano (BMG LABTECH). It was previously observed (Liu, 2020) that DNTB inhibits BCH activity. Thus, reactions were prepared as for TesB, but without DNTB. The reactions had to be staggered, and the abs_{412nm} was recorded after 0, 5, 10, 15, 20, 25 and 30 min.

2.6.4. Transaminase (CV_TA) activity assay

CV_TA activity towards keto fatty acids was monitored by a spectrophotometric assay described by Schätzle and collaborators (2009). This method uses 1-phenylethylamine (1-PEA) as the amino donor, and the detection acetophenone (AP), which is formed when the amine group is transferred from 1-PEA to the amino acceptor. This reaction can be monitored at 245nm and allows the detection of protein activity using different keto substrates as it measures AP formed, rather than different amino products (Schätzle 2009).

The standard CV_TA reaction was performed at 30 °C in 96-well plate (Greiner UVStar® 96 well plates, Sparks) and consisted of 200 µL with 10 mM 1-PEA, 2.5 mM substrate (ratio donor:acceptor 4:1), 0.25 % DMSO, 0.2 mM PLP, 100 mM phosphate buffer pH 7.0 and 50 µg/mL CV_TA. Product formation was calculated based on the molar extinction coefficient of acetophenone (ε = 7.03 $mM^{-1}cm^{-1}$)

2.6.5. Transaminase screening

A screening assay using commercially available ATA-117 (*Arthrobacter* sp. KNK168), ATA-217 (*Vibrio fluvialis*), CDX043 (*V. fluvialis*), CV_TA and CV_TA Y168F (Almahboub, Narancic et al. 2018), BL21_pET45b was used as negative. For this assay, the deamination of 3-aminobutyric acid (3ABA) was tested in the presence of acetophenone or pyruvate, and the deamination of L-ala in the presence of acetophenone as amino acceptor. Whole cells or commercial enzymes were resuspended in 100 mM potassium phosphate buffer pH 7.0 to a final concentration of 5 mg/mL and mixed with 2.5 mM amino acceptor (AP or pyruvate) and 10 mM amino donor 3ABA or L-ala (ratio 4:1), 0.2 mM PLP and 0.25 % DMSO. Each reaction had two 1 mL volume, which were incubated for 1 h and 24 h at 30 °C 200 rpm for staggered analysis and analysed by HPLC (Section 2.7.2.).

2.6.6. One-pot activity assay

Purified GO and CV_TA were combined in a one-pot assay aiming for the synthesis of α-ncAAs. The assay was undertaken in the same conditions as the individual reactions. Each reaction consisted of 20 mM phosphate buffer, 0.25 % DMSO, 2.5 mM

1-PEA, 0.2 mM PLP and 50 µg/mL for CV_TA, and 1 mM *o*-dianisidine, 0.2 mM FMN, 2.5 mM DL-LA, 0.1 mg/mL HRP and 50 µg/mL of pure GO. The reaction had the final volume of 200 µL and was allowed to occur at 30 °C for 30 min with abs_{245nm} for the detection of acetophenone.

2.7. Analytical methods/HPLC

2.7.1. Organic acids and glucose quantification

Concentration of glucose, Acetate and 3HBA in the culture supernatant was assessed by a high-performance liquid chromatography (HPLC) system. The supernatant was filtered through Mini-UniPrep syringeless filter devices (Agilent) and 20 µL were injected into the system equipped with RID-10A refractive index detector (Shimatzu) at 50 °C. Aminex-87H column (Bio-Rad) at 40 °C and 0.014 N H_2SO_4 at a flow rate of 0.55 mL/min under the pressure of 4.3 MPa were used to analyse the organic acids and glucose. The standards were prepared using the commercial chemicals ran on the same programme to prepare the standard curves.

2.7.2. Derivatisation and quantification of amino acids

An automated method for amino acid derivatisation based on the use of *o*-phthalaldehyde (OPA) and 3-mercaptopropionic acid (MPA) was used here. Supernatant samples from biotransformation were analysed by HPLC 1260 Infinity II Prime LC System (Agilent) using the column AdvanceBio Amino Acid Analysis (AAA), 4.6 x 100 mm, 2.7 µm LC column.

Amino acid compounds were separated by using the following linear gradient elution (min/B %): 0/2, 0.35/2, 19/43.5, 19.10/100, 21.30/100, 21.40/2, 23/end at 40 °C. Standard curves for the target amino acids were acquired using commercially available pure amino acids diluted in 0.5 mM 2ABA as internal standard. The peak areas of the amino acids were normalised based on 2ABA peak areas. Amino acid concentration in the supernatant was then calculated based on these standard curves.

2.8. The antibacterial activity of unmodified vs modified bLFcin core peptide

2.8.1. Minimum inhibitory concentration (MIC)

The nonameric core of bLFcin ranging from residues 4 to 12 (RRWQWRMKK) (Wakabayashi, Matsumoto et al. 1999), and the nonamer N- or C-terminally modified with 2ABA, 2-aminohexanoic acid (2AHA), 2-aminooctanoic acid (2AOA), and 2-aminodecanoic acid (2ADA) were chemically synthesized (Eurogentec - Belgium) (Table 2.4.).

A dilution series of Lfcin peptides was prepared in 40 % (v/v) DMSO to result peptide concentrations of 4, 2, 1, 0.5, 0.25, and 0.125 mg/mL. Two Gram-positive bacteria, *B. subtilis* and *S. aureus*, and three Gram-negative bacteria, *E. coli*, *P. aeruginosa* and *S. typhimurium* were used to test the activity of AMPs (Table 2.2.). The standard microdilution method by the European Committee on Antimicrobial Susceptibility Testing (EUCAST) was used to determine the minimum inhibitory concentration (MIC).

Table 2. 4. Series of bLFcin core amino acid peptides tested in this study.

Sequence (N-C terminus)	Modification	ncAA chemical structure
RRWQWRMKK	Unmodified	NA
2ABA-RRWQWRMKK	2-aminobutyric acid	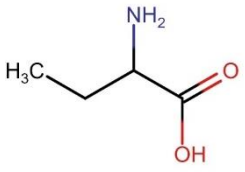
RRWQWRMKK-2ABA	2-aminobutyric acid	
2AHA-RRWQWRMKK	2-aminohexanoic acid	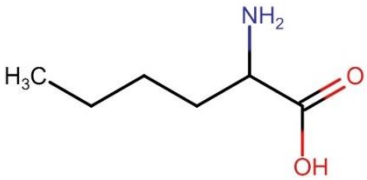
RRWQWRMKK-2AHA	2-aminohexanoic acid	
2AOA-RRWQWRMKK	2-aminooctanoic acid	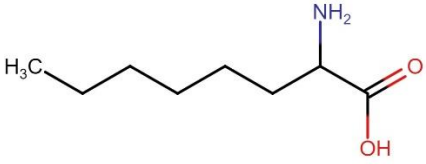
RRWQWRMKK-2AOA	2-aminooctanoic acid	

2ADA-RRWQWRMKK	2-aminodecanoic acid	
RRWQWRMKK-2ADA	2-aminodecanoic acid	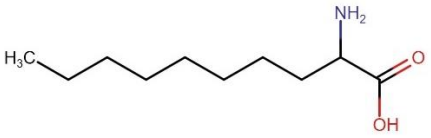

NA indicates that there is no ncAA in the peptide.

For MIC assays the mentioned bacteria strains were grown for 18 h at 35 °C 200 rpm in LB broth with decreased NaCl (0.1 %). The experiment was performed in technical triplicates in a 96-well polypropylene microtiter plates (96 well cell culture cluster, Costar) and consisted of 200 µL final volume that included 100 µL of bacterial culture ($5x10^5$ CFU/mL), 80 µL of LB (0.1 % NaCl) and 20 µL of AMP in the appropriate concentrations so the final DMSO concentration in each dilution was 4 % v/v. Plates were incubated at 35 °C 200 rpm for 18 h and the cell growth was measured as OD_{600nm}. Controls included uninoculated LB 0.1 % NaCl, uninoculated LB 0.1 % NaCl supplemented with AMP, and a positive control of growth with the strains in LB 0.1 % NaCl supplemented with 4 % (v/v) DMSO. After the 18 h incubation the OD_{600nm} was measured MIC is defined as the lowest concentration of an antimicrobial agent that prevents visible growth of a microorganism.

The half-maximal inhibitory concentration IC_{50} was calculated on Prism – GraphPad 8.0 where the Log of concentration was obtained, and the inhibition of growth was normalised so the growth without peptides was considered as 100 % and the maximum inhibition observed was considered as 0 %. Finally, a non-linear-three-parameter analysis was performed.

2.8.2. Minimum bactericidal concentration (MBC)

To determine the minimum bactericidal concentration (MBC), samples from the MIC assay were collected using a 96-well sterile metal stamp (Enzyscreen, The Netherlands) and transferred to a fresh LB 0.1 % NaCl agar plate. The plate was incubated at 30 °C overnight. The AMPs were considered as bactericidal when the growth was inhibited in the MIC assay and the bacteria did not grow on the agar, whilst the AMP was considered as bacteriostatic when bacterial growth was inhibited in the MIC assay, but not the agar plate. Furthermore, the ratio MBC/MIC was used to

evaluate the potency of the AMP. If the ratio MBC/MIC ≤ 2, the antimicrobial activity is bactericidal; if 4≤ CBM/CIM ≤ 32 the activity is considered bacteriostatic; and if the ratio MBC/MIC ≥ 32 the bacteria is considered tolerant to the AMP (Lv, Yin et al. 2018).

2.8.3. Microscopy

2.8.3.1. Scanning electron microscopy (SEM)

An antimicrobial assay was performed according to 2.81. in triplicates and using MIC and the sub-MIC concentrations MIC x 0.5 and MIC x 0.25 (Wang, Xu et al. 2022). *E. coli* NCTC9001 and *B. subtilis* ATCC6633 were chosen as a model to study the damages caused by the AMPs in a Gram-positive and a Gram-negative representative bacteria. Bacteria untreated with AMPs in 4 % DMSO were used as growth control. After the 18 h incubation period, the triplicates were combined in a 1.5 mL sterile Eppendorf, resulting in 600 µL of culture to be fixed. Cells were washed twice in phosphate buffered saline (PBS) and fixed. The fixation was carried out with 2.5 % glutaraldehyde buffered in potassium PBS pH 7.3 at room temperature. Cells were harvested and washed twice for 5 min in PBS. Finally, the dehydration consisted of resuspending cells in increasing concentration of ethanol: 30, 50, 70, 90 % ethanol for 10 min, and 100 % ethanol for 20 minutes.

Five µL of these cells were mixed with 20 µL hexamethyldisilazane and a drop of this mixture transferred to a cover slip to air dry. The samples were coated with platinum and images obtained with ZEISS Sigma 300.

2.8.3.2. Transmission electron microscopy (TEM)

For transmission electron microscopy (TEM), cells were prepared as above up to the step of dehydration with ethanol. After dehydration, samples were washed twice with 100 % propylene oxide for 15 min. Following the transfer to a solution of propylene oxide/epon resin 1:1 (v/v) overnight. Followed by 2 h incubation at 37 °C with 100 % epon for complete resin infiltration and 24 h at 60 °C for resin polymerization. Samples were centrifuged for 3 min 180 rotational centrifugal force (rcf) at room temperature between each step.

After polymerization, ultrathin (80 nm) sections were obtained using a Leica EM UC7. These sections were collected on 200 mesh thin bar copper grids, stained with uranyl

acetate for 20 min and lead citrate for 5min. Sections were examined using Tecnai G2 20 TWIN (FEI Company, Oregon, USA) transmission electron microscope at an accelerating voltage of 120kV.

2.8.4. Circular dichroism (CD)

Circular dichroism (CD) was used to investigate how whether the ncAAs cause changes in the secondary structure of the peptides. It was observed that DMSO, used to solubilize the peptides, affected CD detection. Thus, the AMPs were lyophilised and resuspended in water to yield 20 mg/mL stock concentration. One hundred µM of each peptide was prepared in 50 % 2,2,2-trifluoroethanol (TFE), PBS pH 7.3, or 12 mM sodium dodecyl sulfate (SDS). Spectra were recorded in the far UV region (190–280 nm) on an Aviv Circular Dichroism Spectrometer, model 410 (Biomedical Inc. Lakewood, NJ, USA), using a 0.4 cm quartz cuvette (Hellma, USA). The instrument was first flushed for 10 min with pure nitrogen gas to avoid strong absorption of light by oxygen at these wavelengths. CD spectra were recorded at 25 °C, using a response time of 2 s, a scanning speed of 50 nm min−1, a bandwidth of 1 nm, and data pitch of 0.2 nm. Each sample was read three times and the mean residue ellipticity calculated. The secondary structure was estimated based on the CD spectra from 190 to 250 nm on Beta Structure Selection (BeStSel) (https://bestsel.elte.hu/sexamin.php) (Micsonai, Moussong et al. 2022).

2.9. Molecular docking studies

Automated docking was carried out by GOLD, version 4.0 (Jones, Willett et al. 1997). CV_TA was downloaded from PDB (PDB 4AH3) (Sayer, Isupov et al. 2013) and two chains from the homotetrameric structure were used; the monomeric structure of GO was used (PDB 1GOX) (Lindqvist 1989), and the native (PDB 3WWH) and mutated structure of ATA-117 (PDB 3WWJ). Water molecules were removed, and the amino acids protonated using an all-atom model. The binding site was defined as a 20 Å radius in the binding pocket, which includes known catalytic amino acids and cofactors. The chosen fitness function was chemscore_kinase and the scoring function was CHEMPLP. Genetic algorithm was set for 20 runs. The simulations were ranked according to the highest chemscore_kinase and the pose used for further

evaluation was the one with the best score. CV_TA interactions were simulated against pyruvate, a positive control, acetoacetate, and methyl-acetoacetate, while GO was tested against LA, positive control, 2HBA and (*S*)-3HBA, and ATA-117 native or mutated were tested with 3OBA and 3OBA-CoA

Further investigation of molecular interactions and images assessment were performed on Discovery Studio Visualizer v24.1.0.23298 (BIOVIA 2024).

Chapter 3

Microbial synthesis of 3-hydroxybutyric acid

3. Introduction

Beta-hydroxybutyric acid (3HBA) is a chiral hydroxy fatty acid, naturally found in some bacterial species, but it can also be found in plants and animals, including humans (Mierziak, Burgberger et al. 2021). In bacteria, such as *C. necator*, 3HBA is mostly found as the monomer of poly-3-hydroxybutyrate (PHB), which is depolymerized under starvation conditions (Jendrossek and Handrick 2002). βHBA can be synthesized by microbes via two routes: (1) the native synthesis of PHB, followed by enzymatic depolymerization to 3HBA; or (2) recombinantly by a β-ketothiolase that condenses two acetyl-CoA molecules originating from the TCA cycle, resulting in one molecule of acetoacetyl-CoA; acetoacetyl-CoA is then reduced to 3-hydroxybutyryl-CoA by an acetoacetyl-CoA reductase, and finally, the CoA group is removed by a thioesterase (Liu 2020).

Industrial synthesis of fine chemicals often requires chiral molecules, and this is the case for 3HBA. It can be used directly or converted to its derivative, ethyl-3-hydroxybutyrate, for the synthesis of vitamins, perfumes, and antibiotics (Yun, Kwak et al. 2015). The biological synthesis of 3HBA offers advantages over chemical synthesis, such as enantioselectivity, green chemistry, and mild reaction conditions (Biernacki, Riechen et al. 2017).

Our group previously designed two synthetic operons combining the genes of a thioesterase from *E. coli* K12 (*tesB*), an acetoacetyl-CoA thiolase (*phaA*), and an (*R*)-3-hydroxybutyryl-CoA dehydrogenase (*phaB* – RHBD) from *C. necator* to allow for the synthesis of (*R*)3HBA (Liu 2020). For the synthesis of the (*S*)3HBA enantiomer, we used an (*S*)-3-hydroxybutyryl-CoA dehydrogenase gene (*paaH1* - SHBD) from *C. necator* (Liu 2020). Additionally, we tested the 3-hydroxyisobutyryl-CoA hydrolase (Bch) from *B. cereus* ATCC6630 as a candidate for the CoA-removing enzyme instead of TesB. It was observed that constructs expressing *bch_RHBD* showed higher synthesis of the (*R*)3HBA monomer with the titter of 1.70 ± 0.08 g/L, while the construct *tesB_SHBD* had higher production of the (*S*)3HBA monomer with the concentration reaching 1.40± 0.15 g/L. Analysis of the activity of BCH vs. TesB ruled out that this was the contributing factor to the different titre. The activity of SHBD was also compared to the activity of RHBD, and in vitro assay showed that SHBD has higher activity. Furthermore, acetic acid was detected in the supernatant, 1.5 to 3.5-fold

higher in the case of (S)3HBA synthesis, suggesting that some of the glucose was converted into this side, undesired product.

The work presented in this chapter aimed to address these issues. Firstly, acetate production was addressed via deletion of genes whose products are involved in acetate production. To create a more stable production strains, integration of the *tesB_RHBD* mini-synthetic pathway was attempted also.

3.1. Genetic engineering of *E. coli*

The production of 3HBA was established in BL21 strain. The high expression of the target enzymes is facilitated via T7 promoter, and BL21 strain is engineered to express high level of T7 polymerase (Liu 2020). Therefore, to maintain the high expression of the relevant enzymes, while reducing the by-product formation, Pta and EutD, two phosphate acetyltransferases which reversely converts acetyl-CoA into acetyl-P, were chosen as a target for deletion (Figure 3.1.). The strategy also included the attempt to simultaneously insert the production module into the genome. Initially, the simultaneous knock-in of the *tesB_RHBD* operon (Table 2.3.) and knockout of *eutD* was attempted using a well-stablished method in our research group that uses 3 plasmids (Table 2.3.) based on Cook, Rand et al. (2018). This methodology was firstly designed for *Pseudomonas putida,* and it is based on a complex formed by Cas9 nuclease and a single guide RNA (sgRNA). sgRNA is composed of a trans-activating (tracrRNA) and crisprRNA (crRNA), that together indicate where the Cas9 should remove or add DNA. The recombineering occurs after a double-stranded chromosomal break and the recombination with the repair DNA provided is assisted by λRed recombinases. In *P. putida* this method resulted in gene deletions with efficiency varying from 85 to 100 % (Cook, Rand et al. 2018). The recombination occurs in two steps: first the repair DNA is integrated to the chromosome and second, after introduction of pgRNA and pCas vector, the double-stranded break allows for the homologous recombination.

Upstream (785 bp) and downstream (801 bp) regions of the *eutD* gene (1017 bp) were PCR amplified (Section 2.3.2.), using primers presented in Table 2.4., and Gibson assembled (Section 2.3.4.) with pKNOCK suicidal plasmid and the RHBD PCR products. Construct and vector transformations were performed as in Section 2.4.1.

However, while integration did occur, colony screening showed that a fragment smaller than the donor DNA was integrated in several attempts in which the induction time was altered to overnight, the concentration of tet was reduced up to 5 µg/mL and the plates were incubated up to 1 week at 30 °C. BL21 and transformants were screened using one genome- and one vector-specific primer (ie. Flank_F and pKNOCK_B or Flank_R and pKNOCK_A – Table 2.4). The screening is taken this way because in the first round of recombination two fragments are observed, one with the gene to be deleted flanked by US and DS (3494 bp), and the other with the insert also flanked by US and DS (5938 bp). As observed in Figure 3.1., the fragment of 3.5 bp was detected. However, the larger fragment does not have the expected size (~4.5 kb). Upon DNA purification a sequencing of the ~4.5 kb fragment it was noted that only part of the larger fragment integrated.

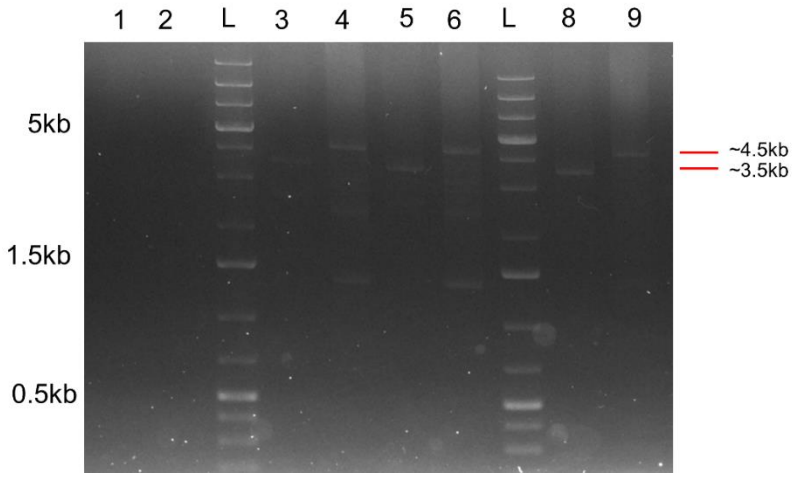

Figure 3. 1. Colony screening for integration of pKNOCK for the simultaneous knock-in/knock out. Colonies were screened with one vector- and one genome-specific primer. BL21, lanes 1 and 2 was used as negative control, where signals were not expected. Three transformants were also screened, for correct pKNOCK integration using the same primer combination and should yield 5938 bp for the fragment containing US_RHBD_DS and 3494 bp for the fragment containing US_*eutD*_DS. Lanes 3, 5, and 8 are the reactions for flank_F and pKNOCK_B and lanes 4, 6 and 9 for flank_R and pKNOCK_A, for colonies 1, 2 and 3, respectively.

The simultaneous knock-in/out process might be overwhelming for the cells. Thus, only the knockout of the *eutD* gene was attempted using the same three plasmid methodology. The primers used to assemble pKNOCK and pgRNA constructs are described in Table 2.2. D and the conditions for transformation described in 2.4.1., such as, recovery time after transformation, electroporation or heat-shock, concentration of L-arabinose (Cas9 and λRed induction), concentration of antibiotics was changed aiming to facilitate the deletion, which could not be observed.

The above paragraphs describe the simultaneous knock-in of the RHBD operon and knock out of *eutD*, followed by the sole *eutD* knock out, both using the 3-plasmid methodology. As the use of the 3-plasmid methodology did not yield the aimed gene deletions/integration, a modified methodology designed by Jiang et al. (2015) was attempted. The 2-plasmid methodology is based on pCas9 to provide the constitutive expression of recombinases and pgRNA for the expression of sgRNA. However, this method supplies the repair DNA as dsDNA, instead of using a suicide vector, as pKNOCK. The methodology was observed to have up to 97 ± 4 % efficiency for double deletions in *E. coli* MG1655 (Jiang, Chen et al. 2015).

Initially, the entire *eutD* gene (1017 bp) was targeted for deletion using now the 2-plasmid system. Yet, knock out of *eutD* was not achieved. Thus, a portion of the gene with approximate length as the homologous regions was targeted. The hypothesis is that it would be easier to knock out a smaller portion and still disrupt the gene by deleting 78 % of its sequence. Where pCas9 and pgRNA were used and the repair donor DNA was provided as double-stranded PCR product comprising of US (801 bp) and DS (804 bp) Figure 3.2. A and B, respectively). Followed by US and DS ligation by PCR (Figure 3.2. C). The pgRNA construct and ds repair DNA were prepared using primers shown in Table 2.2. C and transformed as described in Section 2.4.2. Besides the use of two plasmids and repair DNA provided without a vector, this method has only one step of recombineering and transformants can be screened using Target_del_F/R primers in Table 2.2.

Only after an extended incubation for three days at 30 °C two colonies with large size appeared on the gentamycin/tetracycline selective plate, suggesting that the deletion of *eutD* has occurred. The colonies were screened by colony PCR first (Section 2.3.9), using Flank_del_F/R and Target_del_F/R (Table 2.2. C). The signals of ~800 bp for

BL21 and no signals should be present when using the target primers, while 2496 bp for BL21 and 1698 bp corresponds to Δ*eutD* using primers flanking the gene. It was observed to be a mixed colony DNA fragments expected for the BL21 and Δ*eutD* (Figure 3.2. D).

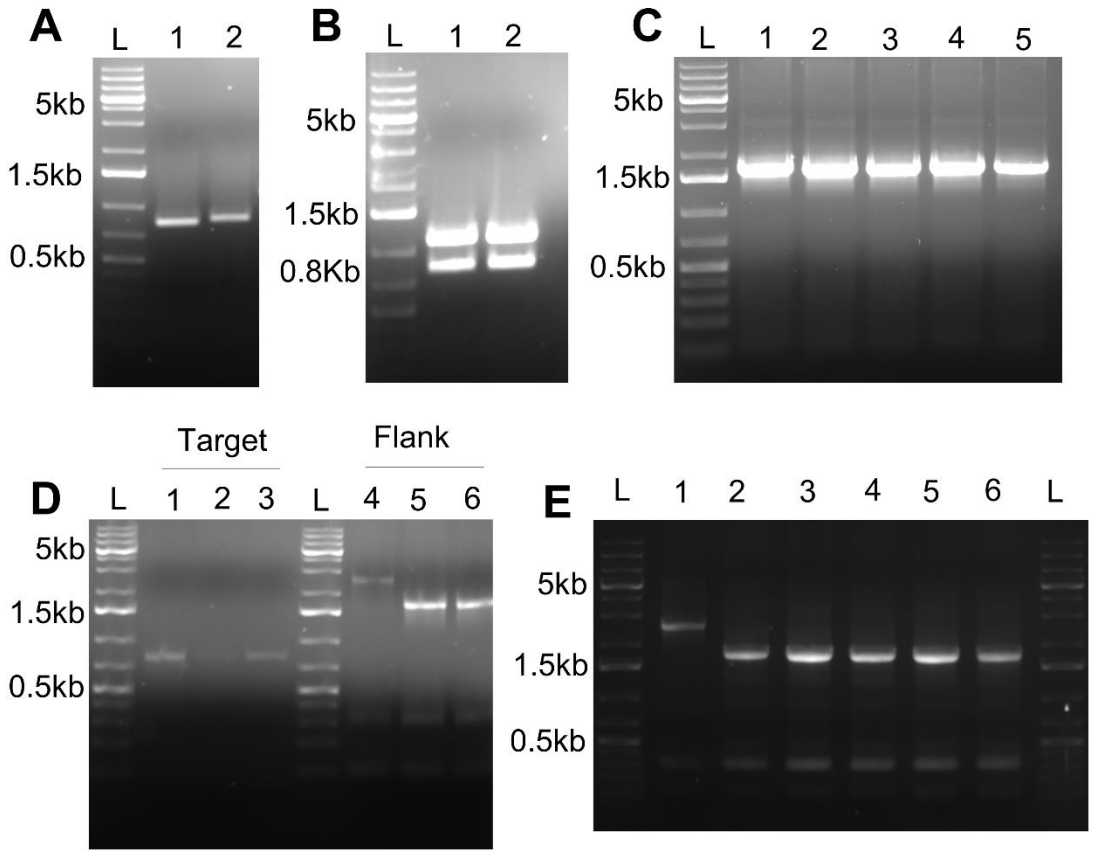

Figure 3. 2. Generation of *ΔeutD* strain. (A) amplification of 801 bp upstream (US – lanes 1-2) and (B) 804 bp downstream (DS lanes 1-2) from the *eutD* gene; (C) lanes 1-5 overlap PCR to generate the US_DS repair template of 1605 bp; (D) colony screening of BL21, lanes 1 and 4, and two mixed colonies showing bands for the BL21 and Δ*eutD*; colony 1 in lanes 2 and 5, and colony 2 in lanes 3 and 6 for BL21. All colonies were screened with primers targeting (798 bp for BL21) and primers flanking the *eutD* gene (2496 bp for BL21). For target (E) screening of the subculture, lanes 1-6, for the identification of *eutD* deletion. BL21 was used as a negative control. Gene ruler 1 kb plus DNA ladder used (L).

To amend that and obtain pure Δ*eutD* colonies, cells were grown in 3 mL LB overnight 30 °C and 200 rpm and streaked in LB tet10/Gen20 plate overnight at 30 °C. Colonies in this plate were screened as before and the deletion was confirmed by sequencing. Although in low efficiency in producing colonies to be screened and long incubation period, this method was successful for the deletion of ~800 bp of the *eutD* gene (Figure 3.2. D)

This deletion left a 216 bp scar for further engineering i.e. to be used as an integration site. pCas9_gen and pgRNA were curated by growing the knockouts overnight in 3 mL LB at 37 °C 200 rpm without antibiotics and cells were prepared for electroporation.

The *pta* gene also encodes a phosphate acetyltransferase and was therefore selected as a target for deletion. The deletion was attempted in BL21 strain, as well as in BL21 Δ*eutD.* Constructs and repair DNA were (801 bp US and 804 bp DS) obtained as before and 798 bp were targeted for deletion (Table 2.2. E). However, while the above-described strategy was the only successful strategy in case of *eutD* deletion, it did not yield either a single or a double mutant. Therefore, the pTarget was used to express the sgRNA and kanamycin or gentamycin were tested as resistance markers for pCas9 aiming to verify if varying it would improve the efficiency. The length of the homology regions was also altered to 497 bp US and 500 bp DS, both were PCR amplified using the primer pair US_pta_F/R and DS_pta_F/R (Figure 3.3. A) The length of the homology regions was reduced from 800 to 500 bp because it was previously observed to be efficient using the two-plasmid system (Jiang, Chen et al. 2015). Amplification of US and DS was followed by an overlap PCR to with US_pta_F and DS_pta_R to obtain US_DS repair template to be used in the deletion of *pta* (Figure 3.3. B). Electroporation was carried out as mentioned (Section 2.3.6) using BL21 or Δ*eutD* previously transformed with pCas9_gen or pCas9_km. Overall, *pta* deletion was observed in both BL21 (Figure 3.3. C; strain designed is Δ*pta*) and Δ*eutD* (Figure 3.3. D, strain designed is Δ*eutD*Δ*pta*) regardless of the pCas9 version used Table 2.1.). However, when pCas9_km resistance was used, 48 out of 76 (63 %) BL21 colonies lacked the *pta* gene. Using gen^r marker resulted in fewer BL21 colonies. However, 6 out of 8 (75 %) colonies, 1 out of 1 (100 %) was positive when using pta_sg1 and pta_sg2 primers, respectively. For Δ*eutD* strain, the number of transformants observed was even lower. When pta_sg1 was used in Δ*eutD* and pCas9_gen only 1 colony out of 7 (14 %) was a knock out, while the same pta_sg1

tested with pCas9_km resulted in one positive knock out of 10 (10 %) colonies. Three colonies were observed when pts_sg2 was transformed with pCas9_gen (0 %), but none were positive and 4 out of 16 (25 %) colonies were knock outs when pCas9_km was used. These results suggest pCas9_km may be more suitable for future attempts.

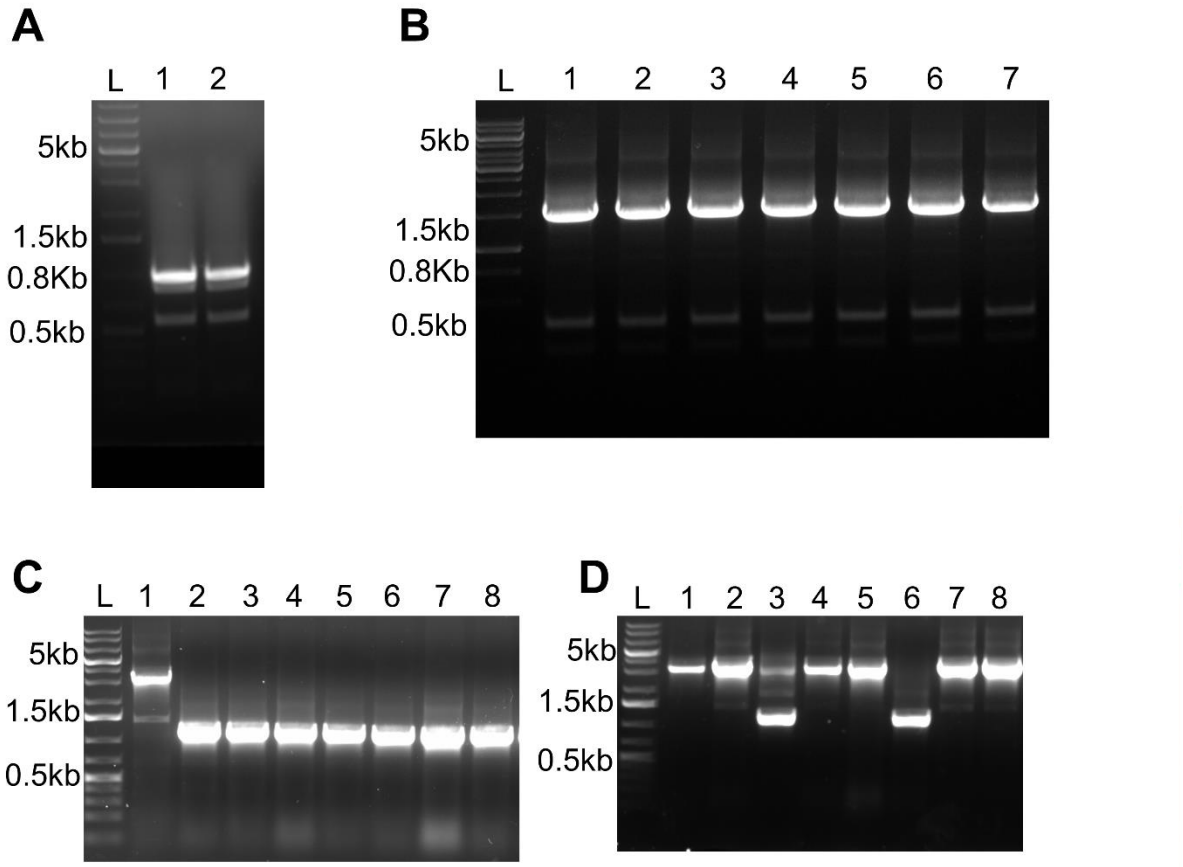

Figure 3. 3. Generation of Δ*pta* and Δ*eutD*Δ*pta* strains. (A) PCR amplification of upstream (US, 497 bp – lane 1) and downstream (DS, 500 bp – lane 2); (B) overlap PCR to design the US_DS repair template of 997 bp (lanes 1-7); (C) colony PCR of BL21 transformed with pTarget_sg1 with km resistance (lanes 2 -8) and BL21 (lane 1); and (D) Δ*eutD* cells transformed with pTarget_sg2 with km resistance (lanes 2-8) and BL21 (lane 1). BL21 was used as a control and yields a signal of 3158 bp, while Δ*pta* shows a signal of 1013 bp. Gene ruler 1 kb plus DNA ladder was used (L).

Next, as the strategy with pCas9_km and pTarget worked well when *pta* deletion was created, the same was applied with the aim to integrate the SHBD operon in the site where scars corresponding to 1 bp of 3' and 216 bp of 5" end of *eutD* were left (Section

2.4.2) US (501 bp), DS (495 bp) and SHBD (3380 bp) were amplified (Figure 3.4 A and B). A PCR to assemble US and SHBD and SHBD and DS was attempted using US_int_F and SHBD_int_R, or SHBDint_R and DSint_R. The PCR product for both reactions should result in 4.3 kb fragment. However, it was not possible to obtain the US_SHBDint fragment, while SHBD_DSint was observed in low concentration (Figure 3.4. C). It was hypothesized, based on sequencing of the fragment, that the variation in GC content in US and DS and the two RBS fragments in the SHBD operon was a limiting factor in PCR. We then designed primers annealing in the middle of the *phaA* gene in the operon. The primers, called phaA_F/R, were used in two PCR reactions: (1) the primers USint_F and phaA_R (2363 bp) and (2) using phaA_F and DSint_R (2199 bp) (Figure 3.4. D lanes 1 and 2, respectively). These PCRs resulted in the expected PCR products, which were then used in another PCR to combine US_pha and pha_DS using the primer pair USint_F and DSint_R. This PCR result in the product with the expected size, with 4562 bp. However, several PCR conditions were tested to obtain a single PCR product, but the unspecific binding of the primers were still present (Figure 3.4. E). Thus, several PCR reactions were needed to achieve the high concentration (400 ng/transformation) required. Once the PCR products from different reactions were pooled and vacuum concentrated, however the ratio A260/A280 = 2.5 was observed, indicating DNA degradation (not shown).

Due to difficulties in assembling the donor DNA for integration (Figure 3.5. A), a repair donor DNA comprising of T7_US_SHBD_DS_T7 terminal was purchased from GeneWiz (Figure 3.5. B) in pUC-GW vector flanked by NheI restriction sites (Figure 3.5. C). Electroporation was used to transform BL21 or Δ*eutD* with 400 ng donor DNA and 100 ng pTarget_Km with one of the three sgRNA generated.

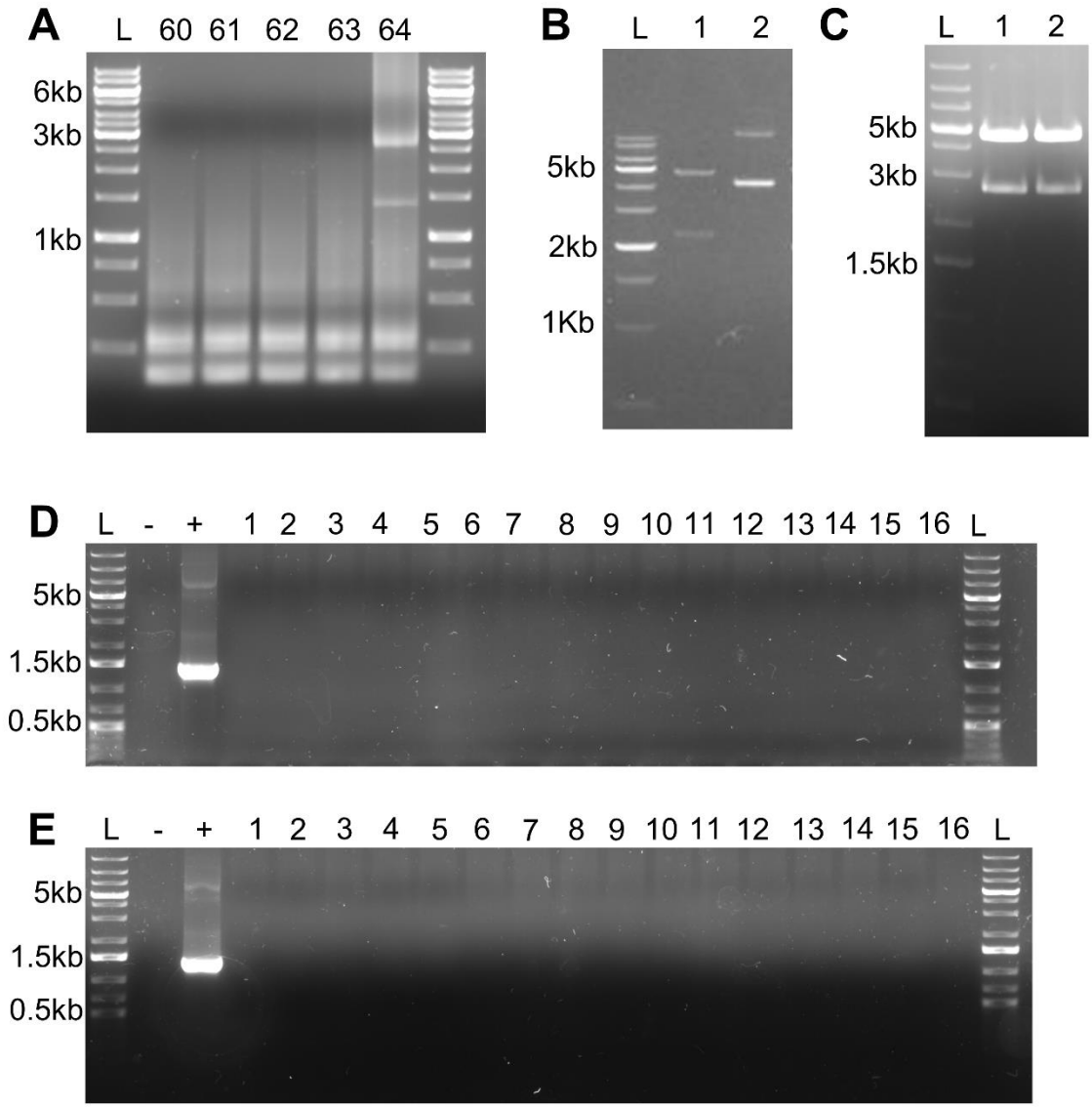

Figure 3. 4. Design of the repair template for SHBD integration into BL21, *Δpta* and *ΔeutDΔpta* strains. (A) US (lanes 1-2) and DS (lanes 3-4) with 501 bp and 495 bp, respectively; (B) 3380 bp SHBD operon amplified to be used in overlap PCR; (C) overlap PCR to amplify US_SHBDint or SHBD_DSint using different temperatures (shown above the corresponding lanes); (D) amplification of US_phaA (lane 1) and phaA_DS (lane 2); and (E) PCR for amplification of US_SHBD_DS using US_phaA and phaA_DS as templates. Gene ruler 1 kb plus DNA ladder was used (L).

Transformation was undertaken as before (Section 2.4.2.), and cells streaked on LB Km50/spec50 agar plates. As it was not possible to PCR amplify the donor DNA, it would be difficult to screen the transformants with one genomic and target primer.

Thus, colony screening with a primer pair (SHBD_usds_2_F and phaA_R – Table 2.2. G) that can only amplify a ~1.3 kb region of the donor DNA was used. Figure 3.5. shows only 16 colonies, but around fifty colonies of BL21 (Figure 3.5. D) and Δ*eutD* (Figure 3.5. E) were screened using BL21 as negative control (-) and pUC-GW_donor as positive control (+). No colonies with the corresponding fragment were identified.

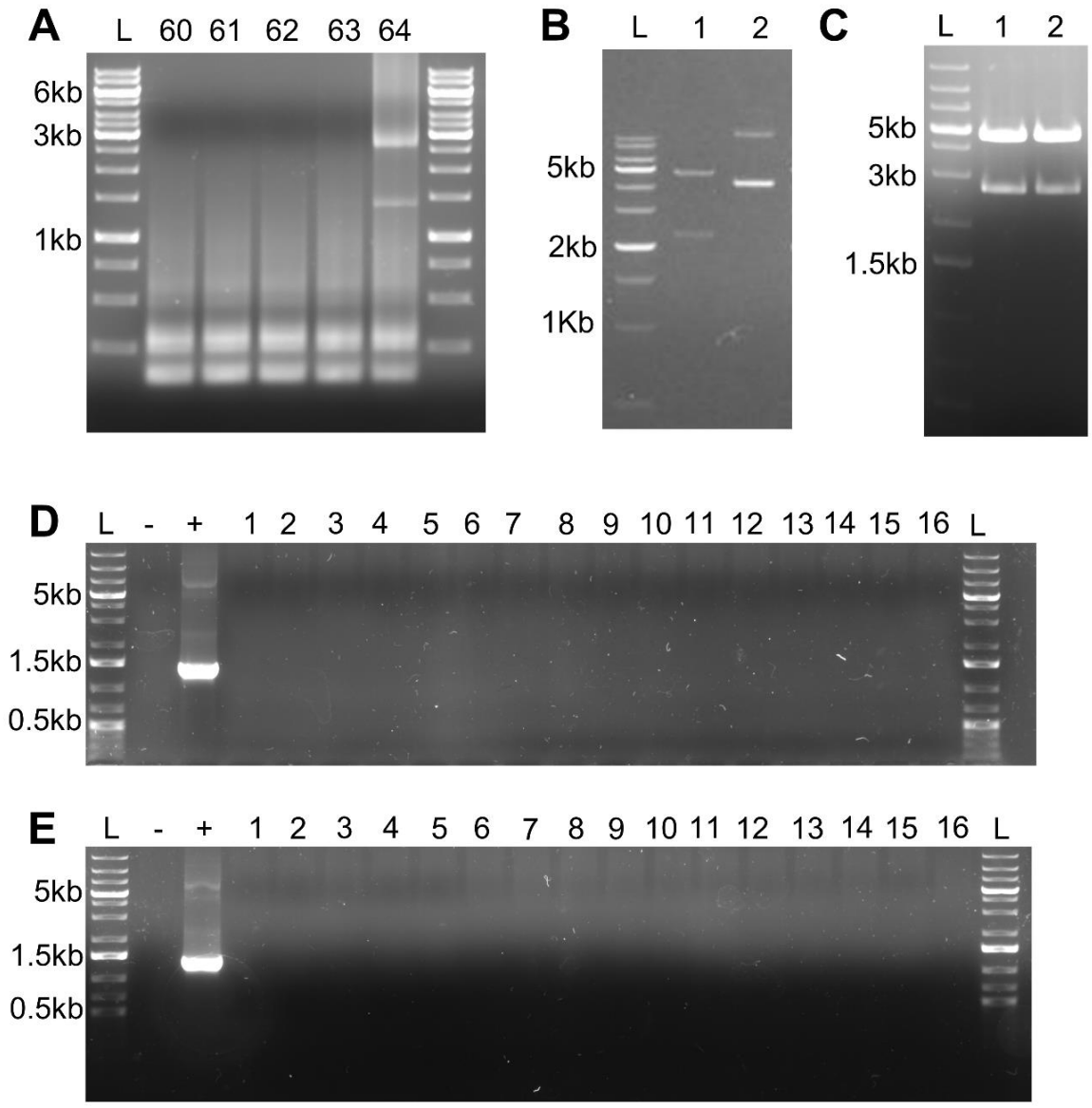

Figure 3. 5. Generation of BL21 and Δ*eutD* strains for the knock-in of the SHBD operon. (A) amplification of the donor DNA with different temperatures tested shown in each lane; (B) donor DNA purchased from GeneWiz and digested with PvuII (line 1) and undigested (line 2) (1kb ladder used); (C) donor DNA digested with NheI from pUC-WG with the donor DNA insert; colony PCR for (D) BL21 or (E) Δ*eutD*

transformed with donor DNA and pTarget. Positive colonies for integration would yield a ~1.3 kb signal as it observed in the positive control (+). Gene ruler 1 kb plus DNA ladder was used (L).

3.2. Synthesis of 3HBA by BL21, *pta* and *eutD* deletion strains

Firstly, previously designed constructs for the production of (*R*)3HBA were analysed in BL21, Δ*eutD,* Δ*pta,* and Δ*eutD*Δ*pta* strains. The production was tested in LB medium supplemented with glucose (Section 2.2.2.). Glucose is supplemented as a substrate that will be broken down to acetyl-CoA, the intermediate used in the mini synthetic pathway encoded in the construct. (Table 2.3.) (Liu 2020). BL21_pET45b was used as a negative control.

The genetic context of the production host i.e. the presence or absence of *eutD* and *pta*, had an effect on both (*R*)3HBA and acetate production (Table 3.1.). Surprisingly, no (*R*)3HBA was detected in Δ*pta_tesb_RHBD* cultures (Table 3.1.). A 0.45-fold lower (*R*)3HBA (0.45 ± 0.012 g/L) was observed for the double mutant in comparison to the control BL21_*tesB_RHBD* (1.066 ± 0.010 g/L). On the other hand, Δ*eutD_tesB_RHBD* produced 1.48 ± 0.029 g/L (*R*)3HBA, which represents 1.4-fold increase in comparison to the control BL21_*tesB_RHBD* (1.06 ± 0.01 g/L).

Table 3. 1. Acetic acid and 3-hydroxybutyric acid concentration observed for BL21 Δ*eutD*, Δ*pta*, and Δ*eut*DΔ*pta* mutants harbouring *tesB_RHBD*.

Strain	**Acetic acid (g/L)**	**(*R*)3HBA (g/L)**
BL21_pET45b	1.74 ± 0.45	0
BL21_*tesB_RHBD*	1.29 ± 0.018	1.066 ± 0.010
Δ*eutD_tesB_RHBD*	1.43 ± 0.026	1.485 ± 0.029
Δ*pta_tesB_RHBD*	0.95 ± 0.016	0
Δ*eutD*Δ*pta_tesB_RHBD*	1.07 ± 0.016	0.454 ± 0.012

The highest acetate concentration of 1.43 ± 0.026 g/L was observed in Δ*eutD_tesB_RHBD*, representing 1.4-fold increase over the control BL21_*tesB_RHBD* followed by the BL21_*tesB_RHBD*, the double mutant and lastly Δ*pta_tesB_RHBD*, where the lowest acetic acid concentration was observed, 0.95 ± 0.016 g/L.

As Δ*pta* and Δ*eutD*Δ*pta* did not produced 3HBA or produced less when compared to BL21, only Δ*eutD* was selected for the following experiments.

3.2.3. Effect of BCH and TesB in (*R*)3HBA concentration in Δ*eutD* strain

Previous analysis and comparisons of (*S*)3HBA and (*R*)3HBA production constructs have shown that BCH exhibits the same activity with both (*R*)- and (*S*)3HB-CoA, while TesB has a 2-fold higher activity to (*S*)3HB-CoA compared to (*R*)3HB-CoA. Also, TesB has 20-50-fold higher activity compared to BCH in this context (Liu, 2020). βHBA was not detected in Δ*pta* strain and Δ*eutD*Δ*pta* produced less of the product. Thus, Δ*eutD* was further investigated. To test if the rate of CoA cleavage and release of the product in the context of the deleted *eutD* have an effect, BL21 or ∆*eutD* with *tesB_RHBD*, *tesB_SHBD*, *bch_RHBD* or *bch_SHBD* were analysed. Total of 9 strains were tested, using 100 mL LB supplemented with 10 g/L glucose (Section 2.2.2.). Unfortunately, none of the combinations showed higher level of the product formation at 24 h or 48 h compared to the control i.e. BL21 carrying the constructs. Secondly, no effect of having TesB or BCH as a -CoA cleaving enzyme was observed (Figure 3.6.).

The highest product concentration observed was 3.33 ± 0.06 g/L for BL21_*bch_RHBD*, which is in agreement with the previous study (Liu 2020). As shown before, replacing BCH with TesB shows higher level of (*S*)3HBA production, with the highest level of 2.90 ± 0.29 g/L produced by ∆*eutD tesB_SHBD* at 48 h (Table 3.2.). However, this was similar to the production by BL21 carrying the same construct and EutD still present (2.866 ± 0.26 g/L), indicating that the deletion did not have a positive impact on diverting the carbon from acetate to 3HBA synthesis.

The highest production of 3HBA did not necessarily coincide with the lowest acetate formation (Table 3.2.). At 48 h of incubation, Δ*eutD_tesB_RHBD* showed the highest acetate levels which were comparable to the control BL21_pET45b, where no 3HBA

was synthesized and all carbon available for the 3HBA synthesis could have been spilled as acetate. However, Δ*eutD_tesB_RHBD* showed a decent (*R*)3HBA production, with the majority of the product accumulated within the first 24 h (1.79 g/L), which then increased by only 0.08 g/L in the following 24 h (Figure 3.6.). However, the acetate increase between these two analysed time points was 0.75 g/L. While this trend suggests some shift between the desired product formation and acetate secretion, the same trend was not observed in all analysed strains. The change in how much glucose was consumed at these two time points also could not be accurately correlated to how much 3HBA or acetate were produced.

Incomplete glucose consumption was observed in all cases, with the highest consumption seen in the control strain BL21_pET45b (Figure 3.6.), where only 0.36 g/L was detected in the supernatant after 48 h (Table 3.2.). All 8 production strains consumed up to 70 % of supplemented glucose, with a varying degree. The (*S*)3HBA producing strains BL21_*tesB_SHBD* and Δ*eutD_tesB_SHBD* showed the lowest glucose consumption (only about 40 %), while simultaneously showing the highest (*S*)3HBA level (2.87 and 2.91 g/L, respectively; Table 3.2.).

BL21 and Δ*eutD_tesB_SHBD* showed the poorest growth (OD_{600nm}=5.28 ± 0.62 and 4.32 ± 0.17, respectively) when compared to the other producing strains (Table 3.1.) and 1.8- and 2.2-fold lower than BL21_pET45b control at 24 h. BL21 and Δ*eutD* cells carrying *tesB_RHBD* had similar growth trends, where growth plateaued at 24h, with very little increment at 48h after induction. While BL21_pET45b had the highest growth at 24 h (OD_{600nm}=9.43 ± 0.18) and 48 h (OD_{600nm}=13.37 ± 1.20), which is expected as these cells can use glucose for growth instead of 3HBA synthesis. Overall, lower growth was observed when comparing the BL21 to the knockout. However, a 1.7-fold lower growth was only observed in Δ*eutD_bch_SHBD* (at 48 h after induction OD_{600nm}=6.04 ± 0.29) in comparison to the parent strain carrying the same construct (at 48 h after induction OD_{600nm}=10.39 ± 0.37) (Figure 3.6.).

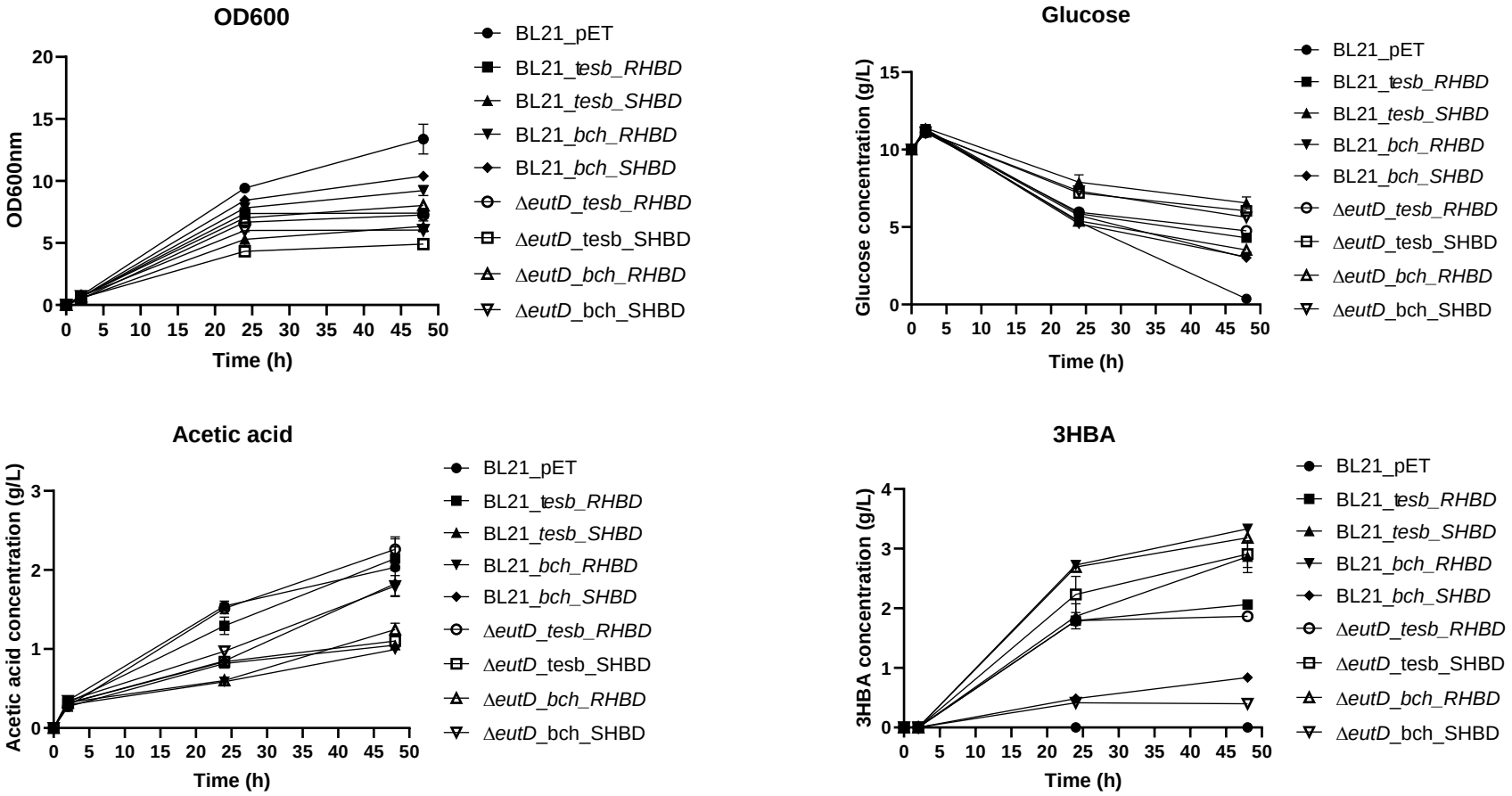

Figure 3. 6. (*R*)HBA synthesis in flask experiments under different CoA removing enzymes. BL21 and Δ*eutD* synthesizing 3HBA from 100 mL LB and 10 g/L glucose. Acetic acid, 3HBA, glucose and OD_{600nm} were measured at 24 and 48 h of experiment.

Table 3. 2. Production of (*S*)- or (*R*)-3-hydroxybutyric acid (3HBA) from glucose (10 g/L) by recombinant BL21 or Δ*eutD* at 24 and 48 h of induction of protein expression.

Producing strain	3HBA (g/L)		Acetic acid (g/L)		Glucose remaining (g/L)	
	24 h	48 h	24 h	48 h	24 h	48 h
BL21_pET45b	NA	NA	1.544 ± 0.06	2.034 ± 0.36	5.315 ± 0.07	0.364 ± 0.29
BL21_*bch_RHBD*	2.72 ± 0.06	3.33 ± 0.06	0.586 ± 0.05	0.994 ± 0.03	5.205 ± 0.04	3.067 ± 0.07
BL21_*bch_SHBD*	0.4848 ± 0.31	0.839 ± 0.01	0.849 ± 0.03	1.825 ± 0.02	5.737 ± 0.12	3.017 ± 0.17
BL21_*tesB_RHBD*	1.792 ± 0.03	2.062 ± 0.05	1.294 ± 0.10	2.144 ± 0.14	5.854 ± 0.15	4.303 ± 0.20
BL21_*tesB_SHBD*	1.865 ± 0.21	2.866 ± 0.26	0.816 ± 0.02	1.049 ± 0.03	7.895 ± 0.47	6.552 ± 0.39
Δ*eutD_bch_RHBD*	2.691 ± 0.06	3.182 ± 0.06	0.60 ± 0.005	1.245 ± 0.08	5.388 ± 0.11	3.517 ± 0.04
Δ*eutD _bch_SHBD*	0.414 ± 0.005	0.399 ± 0.002	0.970 ± 0.01	1.796 ± 0.132	7.319 ± 0.16	5.631 ± 0.16
Δ*eutD _tesB_RHBD*	1.791 ± 0.05	1.865 ± 0.05	1.513 ± 0.06	2.261 ± 0.15	5.954 ± 0.09	4.757 ± 0.09
Δ*eutD _tesB_SHBD*	2.230 ± 0.30	2.906 ± 0.22	0.839 ± 0.02	1.10 ± 0.08	7.190 ± 0.16	6.043 ± 0.11

3.3. Bioprocess for improved (*R*)3HBA synthesis

The production medium contains LB supplemented with 10 g/L glucose. This excess of carbon should drive the product formation (Guevara-Martínez, Sjöberg Gällnö et al. 2015). However, as seen from Figure 3.6., in this case, between 40 and 70 % glucose supplied was consumed, Secondly, we hypothesized that perhaps the rate of glucose utilization could be controlled to decrease the carbon spillage in the form of acetate. Therefore, the next step was to develop a bioprocess for 3HBA synthesis.

It was previously observed by Phue et al., (2005) that 30 % pO_2 concentration resulted in negligible acetic acid concentration, while 6 or 1 % pO_2 yield high acetic acid in *E. coli*. It was also noted that by increasing pO_2 from 20 to 40 %, the synthesis of recombinant proteins can be improved (Qoronfleh 1999). These results were attributed to alterations in the expression of genes involved in glucose and acetate metabolism, as the expression of around 200 genes are dependent on oxygen concentration in *E. coli* (Unden, Becker et al. 1995, Phue and Shiloach 2005). This led to the investigation of aeration effect in the microbial synthesis of 3HBA.

3.3.1. Batch fermentations for (*R*)3HBA synthesis using BL21_*tesB_RHBD*

3.3.1.1. Effect of partial dissolved oxygen concentration

As the *tesB_RHBD* operon was selected for knock-in, BL21_*tesB_RHBD* was chosen for bioprocess as in Section 2.2.3. The behaviour of the strain was studied under fermentation conditions and the effect of two pO_2 concentrations, 5 % and 20 %, was investigated using batch fermentations. These fermentations were performed in duplicates and consisted of 1 L LB supplemented with 0.2 g/L $MgSO_4$, 20 g/L glucose. The cells were grown to OD_{600nm}=5-8 at 37 °C, and then the temperature was reduced to 30 °C, to maximise protein expression over growth. Protein expression was induced by adding IPTG.

The cells grew quicker at 5 % pO_2, and this was accompanied by higher glucose consumption, with the highest consumption between 3 and 5 h (4.1 g/h) (Figure 3.7. A). Glucose is fully consumed between 7 and 9 h. It was expected to develop a process to increase product, while reducing acetic acid concentration. However, acetic acid reaches a high concentration of 5.83 ± 2.7 g/L at 9h. 3HBA concentration also peaks at 9 h and a concentration of 1.63 ± 0.125 g/L is achieved. Nonetheless, 3HBA

concentration is 3.6-fold lower than acetic acid in this condition (Figure 3.7. A).
In contrast, at 20 % pO_2 glucose was consumed at a much slower rate and at the end of the experiment an average of 9.69 ± 0.68 g/L glucose was still observed, which is similar to results observed in flask experiments where about only 50 % of glucose was consumed. Glucose consumption also occurs at a lower rate when compared to 5 % pO_2, with 1.99 g/h being the maximum observed between 8 and 9h. At 9 h of experiment OD_{600nm}=14.54 ± 4.4. As in 5 % pO_2, 3HBA concentration peaked at 9 h and yield an average concentration of 1.63 ± 0.2 g/L, which is again similar. Nonetheless, acetic acid concentration when cells were grown at 20 % pO_2 was kept low through the experiment, reaching its highest concentration of 1.13 ± 0.32 g/L at 6 h (Figure 3.7. B). Supplementing 20 % pO_2 resulted in 0.7-fold acetic acid compared to 3HBA.These results indicate that the microaerobic conditions in flask experiments were likely directing the carbon flux towards acetic acid. However, 3HBA concentration appears not to be affected by pO_2 levels (Figure 3.7.).

3.3.1.2. Inducing protein expression at higher OD_{600nm} using BL21_*tesB_RHBD*

Next, a higher cell density (OD_{600nm}) at induction was tested. In the above experiments, the cells were grown to OD_{600nm}=5-8 before being induced. Here, the induction was done at OD_{600nm}=15. As observed in the previous Section, acetate production was lower at pO_2 20 %, this condition was also applied here (Section 2.2.3.).
It took about 5 h incubation at 37 °C to reach OD_{600nm}=15. Similarly to what was observed for cells induced at lower OD_{600nm}, glucose consumption is not as fast as 5 % pO_2 and at 9 h 5.8 ± 2.5 g/L glucose is still observed in the supernatant (Figure 3.8.). Product formation peaked at 9 h with the averaged concentration of 1.63 ± 0.20 g/L, which represents a similar result to the obtained inducing protein expression at OD_{600nm}=5. Furthermore, acetic acid levels were also low, the highest concentration observed being 0.54 ± 0.135 g/L at 9 h (Figure 3.8.).
The rate of glucose consumption was calculated (Section 2.2.3.) and the highest observed was 2.8 g/h between 2 and 3 h of incubation, but at the end of the 9 h glucose was still detected in the supernatant. Although 9.69 ± 0.68 g/L (48 %) glucose remained in the supernatant when protein expression was induced at lower OD_{600nm} and 5.8 ± 2.5 g/L (29 %) was observed here, the extra consumed glucose seemed to be diverted to biomass.

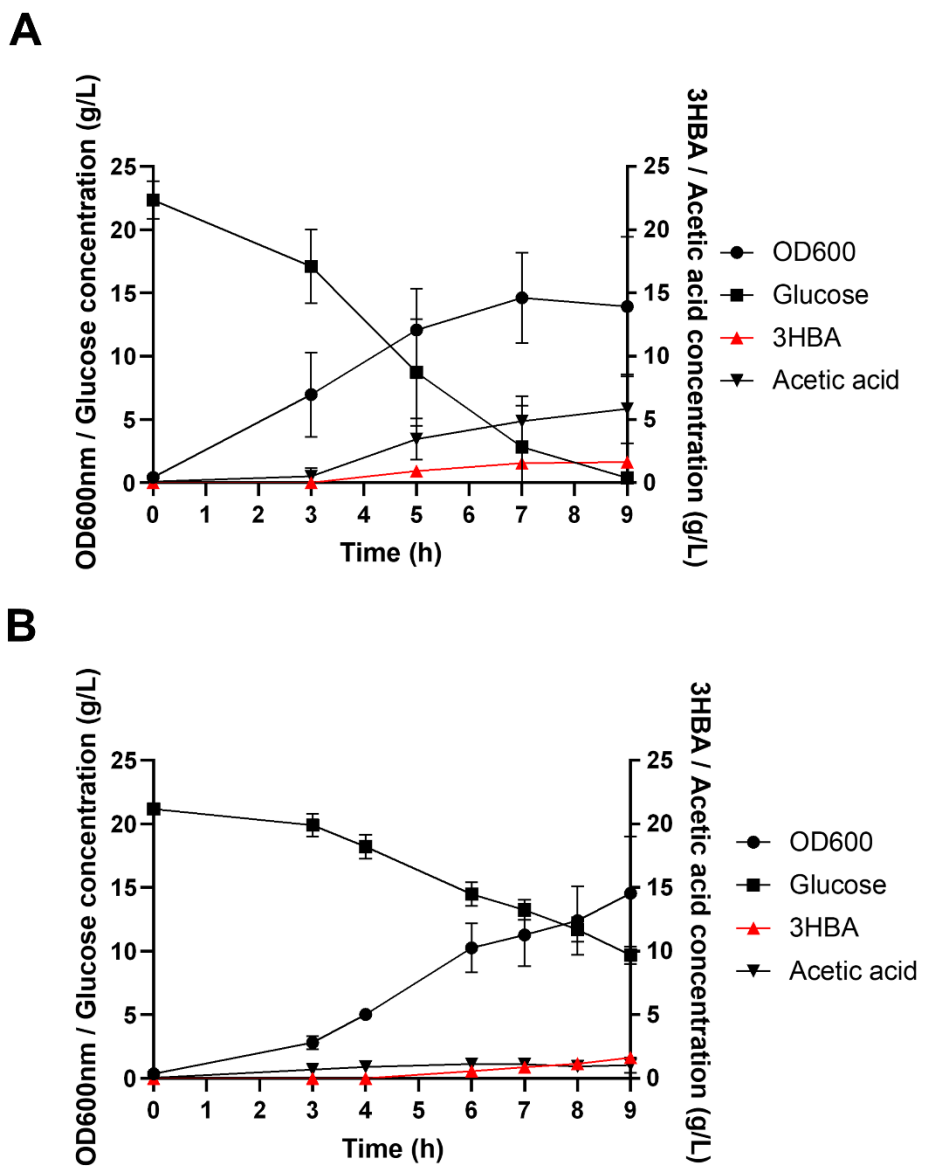

Figure 3. 8. Synthesis of (*R*)3HBA by BL21 with induction of protein expression at high cell density. OD_{600nm} (●), glucose (■), acetic acid (▼) and (*R*)3HBA (▲) concentration for batch using BL21_*tesB*_*RHBD* to synthesize 3HBA from 20 g/L glucose at 20 % pO_2 and protein expression induced at OD_{600nm}=15.

3.3.2. Fed-batch fermentations

According to the literature, glucose concentration must be in excess for optimal 3HBA synthesis (Guevara-Martínez, Sjöberg Gällnö et al. 2015, Perez-Zabaleta, Sjöberg et al. 2016). However, we aim to keep carbon in excess, but as low as possible to avoid high costs and carbon spillage as acetate. The rate of glucose consumption in the batch experiments above was around 2 g/L/h. Thus, this concentration was chosen for fed-batch reactions. To test how much glucose was needed, two experiments were conducted in 1 L LB (Section 2.2.3). In Condition 1, a batch of 20 g/L glucose in 1 L

LB and a constant feed with 2 g/L/h glucose were started at 0 h to keep glucose in excess at 20 g/L. Protein expression was induced at OD_{600nm}=5 in this condition (Figure 3.9. A). In Condition 2, 20 g/L glucose was supplied to LB medium, and after glucose concentration in the bioreactor reached 10 g/L the constant glucose feed (2 g/L/h with $MgSO_4$; Section 2.2.3.) was started. At this point, the OD_{600nm}=15 was reached, and protein expression was induced (Figure 3.9. B).

In general, the OD_{600nm} values are similar between the two conditions tested, 32.36 ± 2.80 and 30.92 ± 1.15 for Condition 1 and 2, respectively. However, for cells induced at OD_{600nm}=5 (Condition 1), grew faster in the first hours of incubation, while cells induced at OD_{600nm}=15 (Condition 2), had faster growth between 6 and 23 h (Figure 3.9.). It was observed that it was not possible to maintain glucose concentration at 20 g/L in Condition 1. Glucose accumulates in Condition 1, but it is consumed at Condition 2. As glucose is provided at 2 g/L/h and it is consumed at an approximate rate for Condition 2, but Condition 1 requires less glucose concentration per hour. It is possible to keep glucose levels within the desired range (~10 g/L) for Condition 2.

Similarly to OD_{600nm}, 3HBA concentration after 24 h incubation was 6.8 ± 2.4 g/L for Condition 1 and 6.89 ± 1.2 g/L for Condition 2, indicating that the induction at different cell densities or glucose concentration in the supernatant did not affect 3HBA concentration.

Moreover, acetate concentration was within the values observed for the other experiments using 20 % pO_2. In both conditions acetic acid can be detected as early as 0 h, due to acetate being present in the seed culture. For Condition 1, acetic acid concentration fluctuates around 1 g/L and the highest concentration observed was 1.2 ± 0.67 g/L at 21 h, while for Condition 2, the acetic acid detected was lower though the process, with the highest concentration observed of 0.8 ± 0.04 g/L, which is 66 % less compared to the maximum in Condition 1. Altogether, inducing at higher OD_{600nm} was successful in keeping glucose levels constant though the process and acetic acid concentration slightly lower compared to Condition 1.

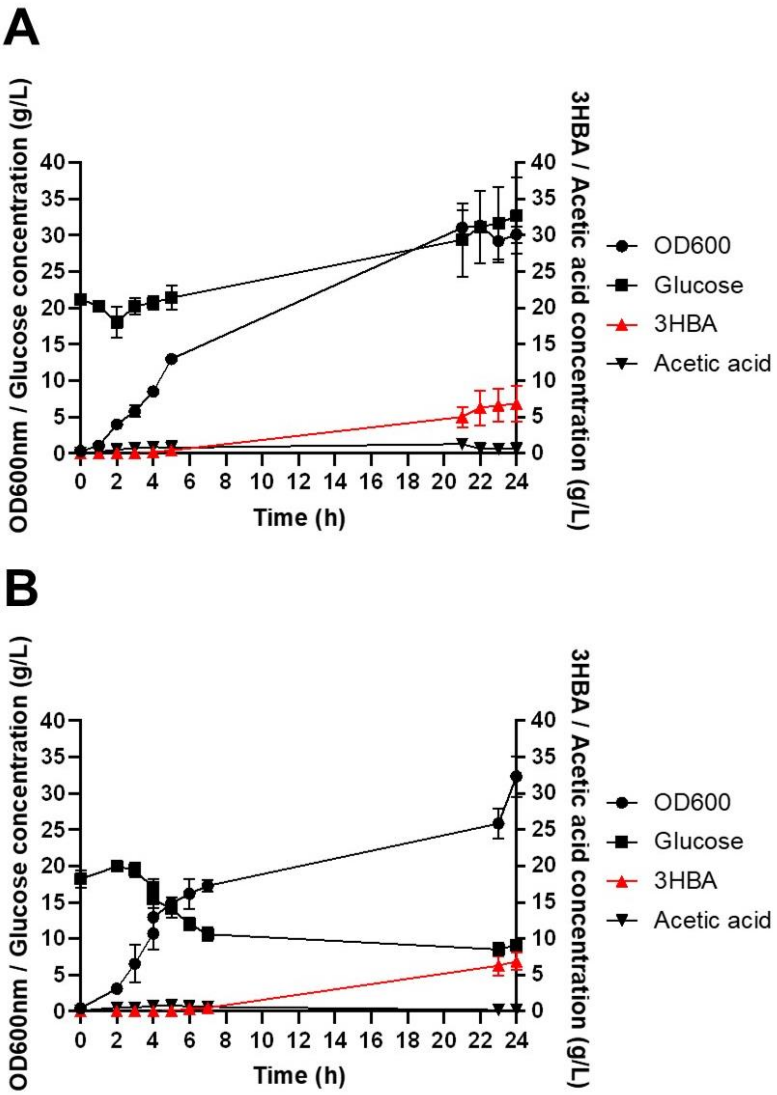

Figure 3. 9. Synthesis of (*R*)3HBA by BL21 under varying glucose concentrations and cell densities for induction of protein expression. OD_{600nm} (●), glucose (■), acetic acid (▼) and (*R*)3HBA (▲) concentration in fed-batch fermentation using BL21_*tesB_RHBD* and constant glucose feed to keep glucose at (**A**) 20 g/L and induce cells at OD_{600nm}=5 (Condition 1) (**B**) or 10 g/L glucose and OD_{600nm}=15 (Condition 2).

3.3.2.1. Aerobic fermentation for the synthesis of (R)3HBA in ΔeutD mutants

The Δ*eutD* knockout did not perform substantially better than BL21 in flask experiments regarding 3HBA synthesis and control of acetate spillage, but the bioprocess improved 3HBA synthesis in the BL21. Thus, we aimed to test Δ*eutD_tesB_RHBD* in bioreactor. The experiment was performed as in Section 2.2.3.

with 20 g/L glucose provided in 0 h with $MgSO_4$, protein expression was induced when OD_{600nm} reached 15 and a constant glucose feed was started to keep glucose constant around 10 g/L.

The highest OD_{600nm} for Δ*eutD* was observed at 24 h and it was 37.45 ± 3.37 (Figure 3.10.). BL21_*tesB_RHBD* achieved OD_{600nm}=30.92 ± 1.15 at the same time of cultivation. That represents 1.2-fold increase in biomass for the mutant strain.

Acetic acid, like in the BL21, was kept low through the process, but slightly higher than in BL21. The highest acetic acid concentration was observed was 1.61 ± 2.18 g/L at 6 h incubation, but overall, the acetic acid concentration fluctuated around 1 g/L.

Contrary to what was observed for fermentation with BL21_*tesB_RHBD*, 3HBA concentration was improved 1.6-fold in the Δ*eutD* strain when compared to Condition 2 in Section 3.3.1.2. At 24 h of incubation, 11.2 ± 2.08 g/L of 3HBA were detected in the supernatant, while for Condition 2, 6.89 ± 1.2 g/L. The increase in product concentration can be attributed to higher biomass achieved in bioreactor by the mutant.

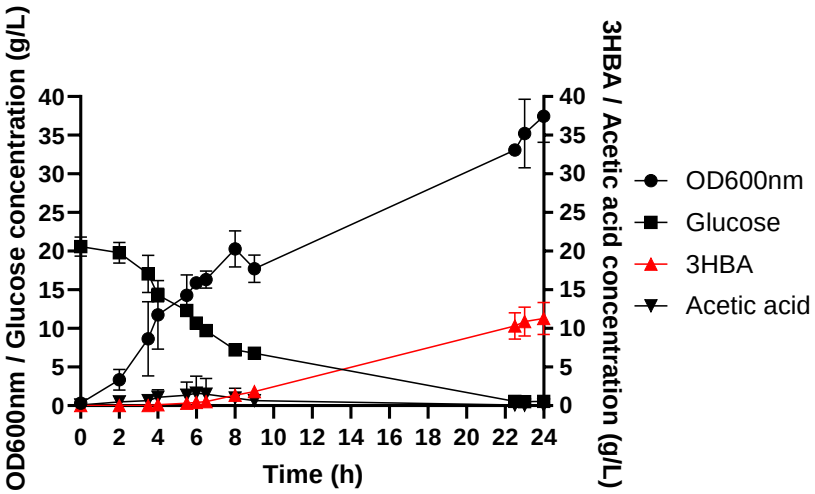

Figure 3. 10. Synthesis of 3HBA by Δ*eutD_tesB_RHBD* strain. OD_{600nm} (●), glucose (■), acetic acid (▼) and (*R*)3HBA (▲) concentration of fed-batch fermentation using Δ*eutD_tesB_RHBD* at 20 % pO_2, using 20 g/L glucose as carbon source and constant 2 g/h/L glucose feed over 24 h.

This improvement can be attributed to better conditions provided in the bioreactor, such as, aeration, pH control, etc. On the other hand, it was not possible to keep

glucose levels constant. Between 9 and 22 h of incubation there was a sharp decrease in glucose concentration (Figure 3.10.), indicating that glucose provided at a rate of 2 g/L/h was not sufficient to maintain it constant at 10 g/L, as it was achieved in Condition 2. It may have been caused by some of the glucose being directed to cell growth.

3.3.3. Aerobic fermentation for (*S*)3HBA synthesis

As the process was optimized for the synthesis of (*R*)3HBA, the synthesis of the (*S*)3HBA isomer was also attempted with Δ*eutD_tesB_SHBD*. The same conditions forementioned were used. This strain grew slower than its (*R*) counterpart. Thus, induction of protein expression was done at OD_{600nm}=10, which was observed after 7 h of incubation. Assuming the glucose consumption occurs similarly to Δ*eutD_tesB_RHBD*, and a constant feed with 2 g/L/h of glucose and $MgSO_4$ was started at the moment of induction.

The growth rate shows the Δ*eutD* knockout synthesizing (*S*)3HBA grows slower than cells synthesizing the (*R*) isomer (Figure 3.11.). The highest increment cell growth was observed between 5 and 4 h of incubation where OD_{600nm} increased by 2.26 ± 0.86 per hour. This can be observed comparing the biomass at 9 h: for Δ*eutD_tesB_RHBD* OD_{600nm}=17.72 ± 1.7, while for Δ*eutD_tesB_RHBD* OD_{600nm}=9.91 ± 1.1. Regarding glucose consumption, it did not vary massively compared to the process for (*R*)3HBA and it was not possible to keep glucose constant ~10 g/L. At the end of the process, 24 h, 2.57 ± 3.6 g/L remained in the supernatant (Figure 3.11.).

While acetic acid concentration fluctuated around 1 g/L for ΔeutD_*tesB_RHBD*, acetic acid concentration was much higher for Δ*eutD_tesB_SHBD*. In the (*S*)3HBA producing strain, acetic acid increased in all time-points and reached 4.55 ± 2.25 g/L at 24 h.

As mentioned, protein expression was induced at 7 h of incubation and it is possible to observe 3HBA 2 h after induction. The highest product concentration was 3.75 ± 1.51 g/L, which observed at 24 h. (*S*)3HBA concentration was 2.9-fold lower than the concentration for (*R*)3HBA and that can be attributed to the shorter time for protein expression. While 4 h were required for Δ*eutD_tesB_RHBD* to reach OD_{600nm}=15, 7 h were necessary for Δ*eutD_tesB_SHBD* reach OD_{600nm}=10. Flask experiments showed that SHBD constructs perform better when combined with *tesB* and BL21 and Δ*eutD* performed similarly in terms of 3HBA yield (Section 3.2.3). Nonetheless, (*S*)3HBA

synthesis by Δ*eutD_tesB_SHBD* in bioreactor did not follow this tren. It was previously observed that the SHBD dehydrogenase has 29-fold higher catalytic efficiency when compared to the RHBD dehydrogenase (Liu 2020). Lower catalytic efficiency of SHBD may have resulted in carbons being diverted to acetic acid.

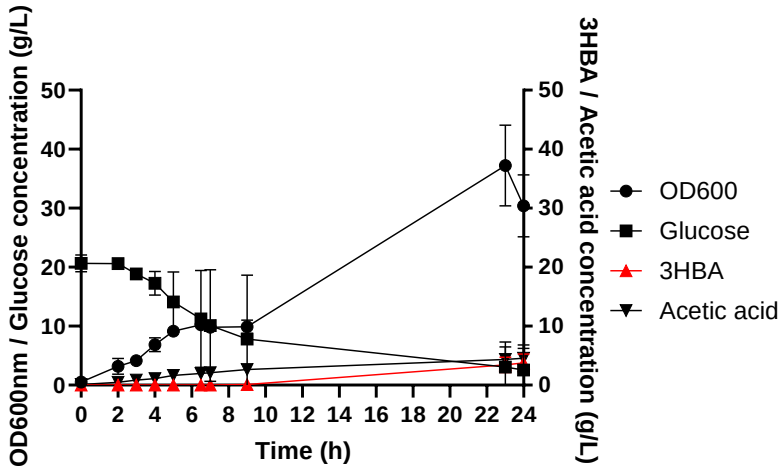

Figure 3. 11. Synthesis of 3HBA by Δ*eutD_tesB_SHBD* strain. OD_{600nm} (●), glucose (▄), acetic acid (▼) and (*R*)3HBA (▲) concentration of Δ*eutD_tesb_SHBD* using 20 g/L glucose as carbon source and 20 % pO_2 over 24 h.

Chapter 4

Synthesis of α and β-non-coded amino acids

Introduction

Amino acids are the monomers which make up proteins. There are 22 coded amino acids, including selenocysteine, which make up selenoproteins in all kingdoms of life, and pyrrolysine, mostly found in archaea and some bacteria (Castro, Melle-Franco et al. 2023, Zhang, Zhao et al. 2024). There are several amino acids for which the cell does not have the machinery, or a blueprint to add them to proteins. Thus, these amino acids are called non-coded amino acids (ncAAs) (Chen, Xin et al. 2023). Although ncAAs do not have specific tRNA-aminoacyl synthetase pairs, they can be naturally charged by aminoacyl-tRNA synthetases/tRNA pairs for analogue coded amino acids and be found in proteins, for example, azaleucine and leucine, tryptophan and 5-hydroxytryptophan can be charged by the same aminoacyl-tRNA synthetases/tRNA pair (Kohrer 2013, Grishin, Zhdanov et al. 2020). ncAAs can also be the product of post translational modification, which increases the number of these molecules to 140 ncAAs derived from coded amino acids reported in proteins (Ambrogelly, Palioura et al. 2007).

The chemical synthesis of ncAAs often rely on transition-metal catalysis (Ypsilantis, Garypidou et al. 2023), asymmetric phase-transfer catalysis (Yang, Freas et al. 2021), and Strecker reaction (Zuend, Coughlin et al. 2009). In addition to expensive and rare chemical catalysts, these methods usually involve multiple steps making them non-trivial and frequently polluting (Liu, Zhou et al. 2024). Biocatalysts, such as transaminases, offer an alternative for the chemical synthesis. However, there are certain challenges, such as the substrate range, that pose difficulties in wider adoption of these enzymes.

As it was demonstrated in Chapter 3 that 3HBA can be produced from glucose, it was hypothesized that this pathway could be used and further developed to produce a 3-aminobutyric acid (3ABA). Furthermore, as previous work has shown the utility of fatty amino acids, this chapter explored the possibility to build cascade reactions to produce these valuable molecules

4.2. Metabolic engineering for the synthesis of 3-aminobutyric acid

4.2.1. Synthetic operon for 3-aminobutyric acid

A strategy that involves genes from the synthetic pathway for the production of 3HBA described in Chapter 3 was developed with the aim to convert glucose to 3-aminobutyric acid (3ABA). Similarly to what was described previously, the aim here was to obtain a pool of acetyl-CoA from glucose using the native machinery from *E. coli*. Acetoacetyl-CoA would be obtained by overexpressing PhaA, and TesB removes the CoA from acetoacetyl-CoA, releasing acetoacetate. We hypothesize that by replacing the 3-hydroxybutyril-CoA dehydrogenase catalysed step with a transaminase, it would be possible to synthesize the respective β-amino acid (Figure 4.1.). The said transaminase from *Chromobacterium violaceum* (CV_TA) was observed to be active towards methyl-acetoacetate (Almahboub, Narancic et al. 2018).

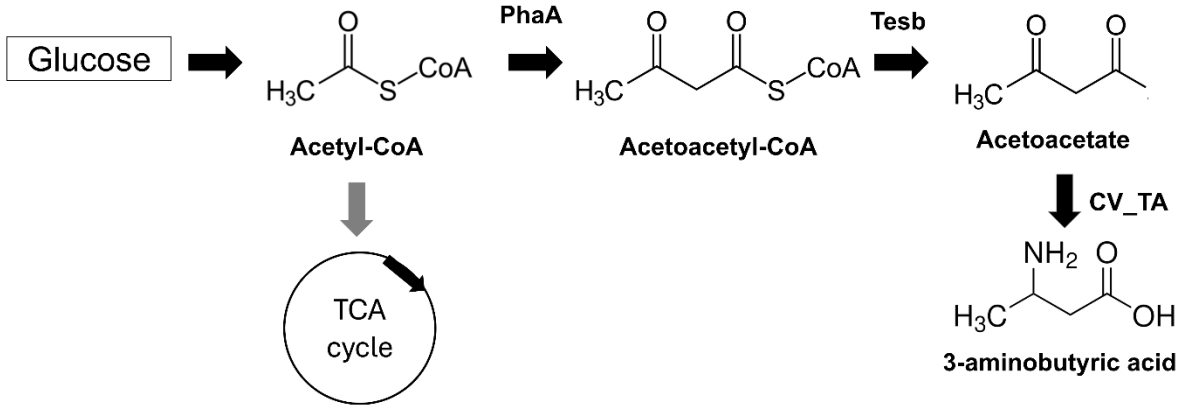

Figure 4. 1. Proposed metabolic engineering for the synthesis of 3-aminobutyric acid from glucose. The proposed synthetic mini-pathway aimed to use glucose as substrate and the native machinery to obtain acetyl-CoA. Acetoacetyl-CoA would be formed by the condensation of two acetyl-CoA by PhaA, and TesB cleaves the CoA. Finally, transaminase would aminate acetoacetate and synthesize 3-aminobutyric acid.

CV_TA was previously tested with methyl-3-oxobutyric acid as an amino acceptor with a catalytic efficiency 0.5 mM/min, which is 29-fold lower when compared to the catalytic efficiency with pyruvate (Almahboub, Narancic et al. 2018). In the case

presented here, the amino acceptor would be acetoacetate, or acetoacetyl-CoA. In the 3HBA operon, TesB or BCH were used to remove the CoA from 3-hydroxybutyryl-CoA (Section 2.6.3). Then, the question was asked if BCH or TesB could cleave CoA from acetoacetyl-CoA made by the PhaA catalysed condensation of two acetyl-CoA molecules (Figure 4.1.).

Thus, the cell-free extract (CFE) of *E. coli* BL21 overexpressing TesB or BCH were tested regarding their activity towards acetoacetyl-CoA, a reaction that would result in free acetoacetate (3-oxobutyric acid). Both enzymes showed activity towards acetoacetyl-CoA, measured as abs_{412nm} (Figure 4.2. A-B). This assay uses 5,5′-dithiobis (2-nitrobenzoic acid – DNTB) to interact with free CoA to produce 5-thio-2-nitrobenzoic acid (TNB), which can be detected at abs_{412nm} (Liu 2020). As it is easier to test the activity of TesB, due to DNTB inhibiting BCH activity (Liu, 2020), TesB was chosen for the next steps.

Since TesB was chosen as the enzyme to release acetoacetate, the next step was to replace the RHBD in the construct with CV_TA. Two constructs were targeted to be designed namely ABA (*tesB_phaA_CV_2025*) and 3ABA operon (*CV_2025_tesB_phaA*) (Table 2.3; Figure 4.2. C). Two versions of CV_TA were also tested, native and the variant Y168F shown to be more active towards methyl ester-3OBA (Almahboub, Narancic et al. 2018). The DNA fragments for 3ABA operon with either versions of CV_TA were successfully amplified, but several Gibson assembly attempts using the gene for CV_TA Y168F did not result in colonies, which is surprising as there is only one codon difference in between the two CV_TA variants. ABA operon with native CV_TA was transformed into DH5α (Section 2.3.6.) and sequence verified,

followed by introduction in *E. coli* BL21 for the synthesis of 3ABA.

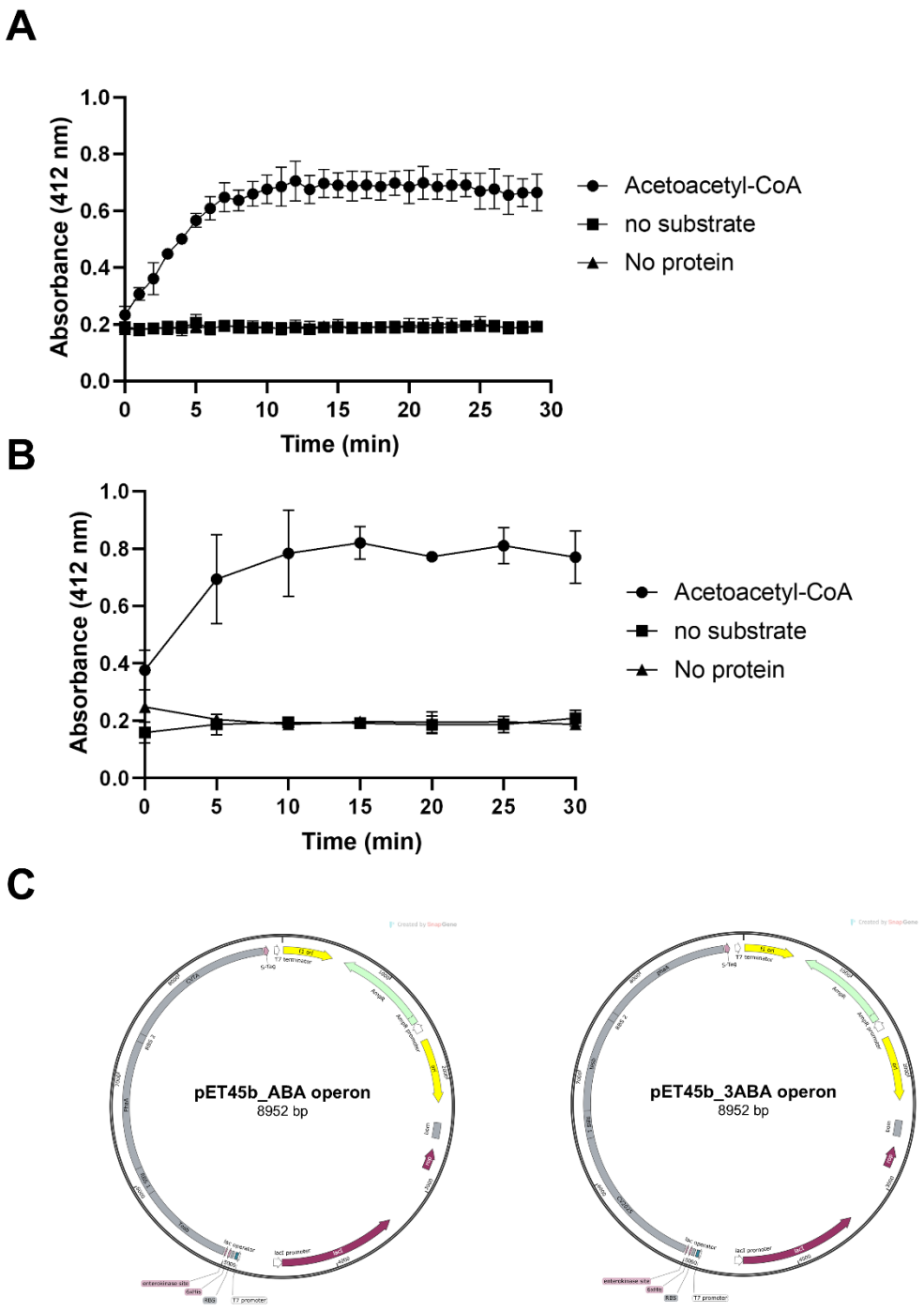

Figure 4. 2. Design of the operon for 3-aminobutyric acid synthesis. (A) TesB and (B) BCH thioesterase activity towards acetoacetyl-CoA. Activity measured as change of the absorbance abs_{412nm}; (C) diagram of the operon for the production of 3-aminobutyric acid including the genes *tesB*, *phaA* and *CV_2025* in the following orders: *tesB*_RBS1_*phaA*_RBS2_*CV2025* (ABA operon) or

*CV2025*_RBS1_*tesB*_RBS2_*phaA* (3ABA operon) cloned in pET45b for protein expression

The synthesis of 3ABA was carried out in 100 mL LB supplemented with 10 g/L glucose with BL21_ABA and BL21_pET45b as negative control (Section 2.2.2.). Following the induction of protein expression, samples were collected at 0, 2, 4, 7, 10 and 12 h, centrifuged, and the supernatant was analysed by HPLC Section 2.71, for organic acids and Section 2.7.2. for 3ABA. No 3ABA was detected in the samples regardless of the time point (Figure 4.3. B). Glucose concentration, however, was noted to be little affected over 12 h of experiment, which suggests carbons are not being directed to the desired amino product.

LB is a rich media with several amines present that could be masking the detection of 3ABA or would have an inhibitory effect on the synthesis of ABA. Therefore, an alternative defined medium M9 was tested (Section 2.2.2.). Glucose (10 g/L) was supplied; however, no product was detected.

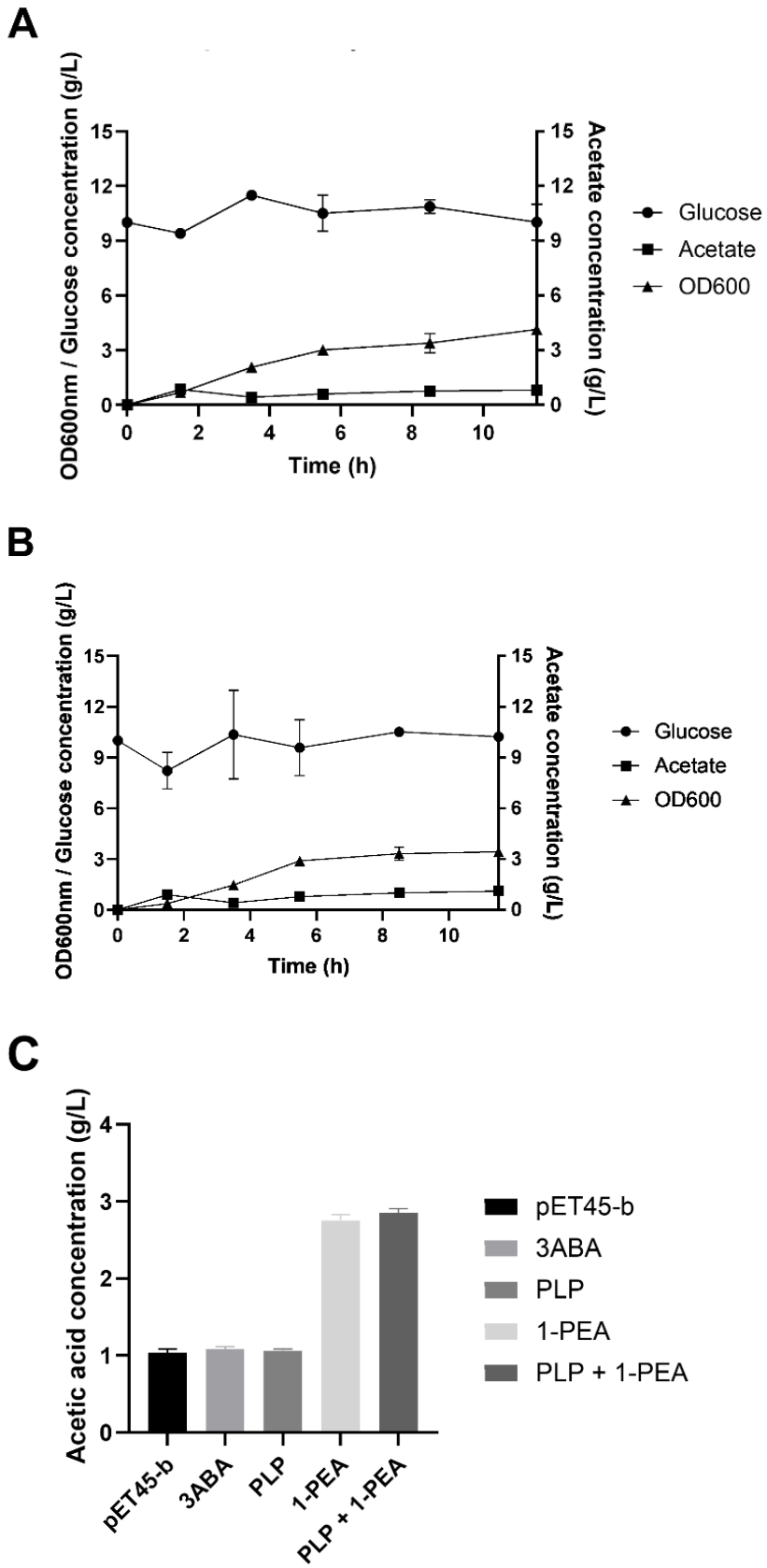

Figure 4. 3. Synthesis of 3-aminobutyric acid from glucose in BL21. Quantification of glucose, acetate and OD_{600nm} in (A) the negative control BL21_pET45b (B) and BL21_ABA operon subjected to 3ABA synthesis in LB 10 g/L glucose; (C) acetate

concentration for BL21_pET45b and BL21_ABA supplemented with 1-phenylethilamine (1-PEA), pyridoxal 5'-phosphate (PLP) or both combined.

As mentioned, CV_TA activity was demonstrated with a methyl-ester of 3-oxobutyric acid (Almahboub, Narancic et al. 2018). Since the substrate produced by the ABA operon would be a free acetoacetate, the activity of CV_TA towards acetoacetate was investigated. Also, as a variant of this transaminase, CV_TA Y168F showed better activity towards methyl-3OBA, this variant was also tested as in Section 2.6.4. (Almahboub, Narancic et al. 2018).

While the reaction with 3-OBA methyl ester did occur, no activity was observed with 3-oxobutyryc acid (Figure 4.4.).

The homodimeric structure of CV_TA (EC 2.6.1.18), previously resolved by X-ray crystallography, (Humble, Cassimjee et al. 2012) was used to analyse the interaction of the enzyme with the methyl-ester of 3-oxobutyryc acid vs. 3-oxobutyric acid. Pyruvate, as a native substrate, was also used in the docking studies. The homodimer has two active sites, each formed by both subunits, and with one PLP molecule covalently bound to K288. This interaction is further stabilised by D259, Y153 and V261. Additionally, R416 forms a salt bridge with the carboxylic group in the substrate and it can alter its conformation in the active site depending on the presence of a substrate (Humble, Cassimjee et al. 2012).

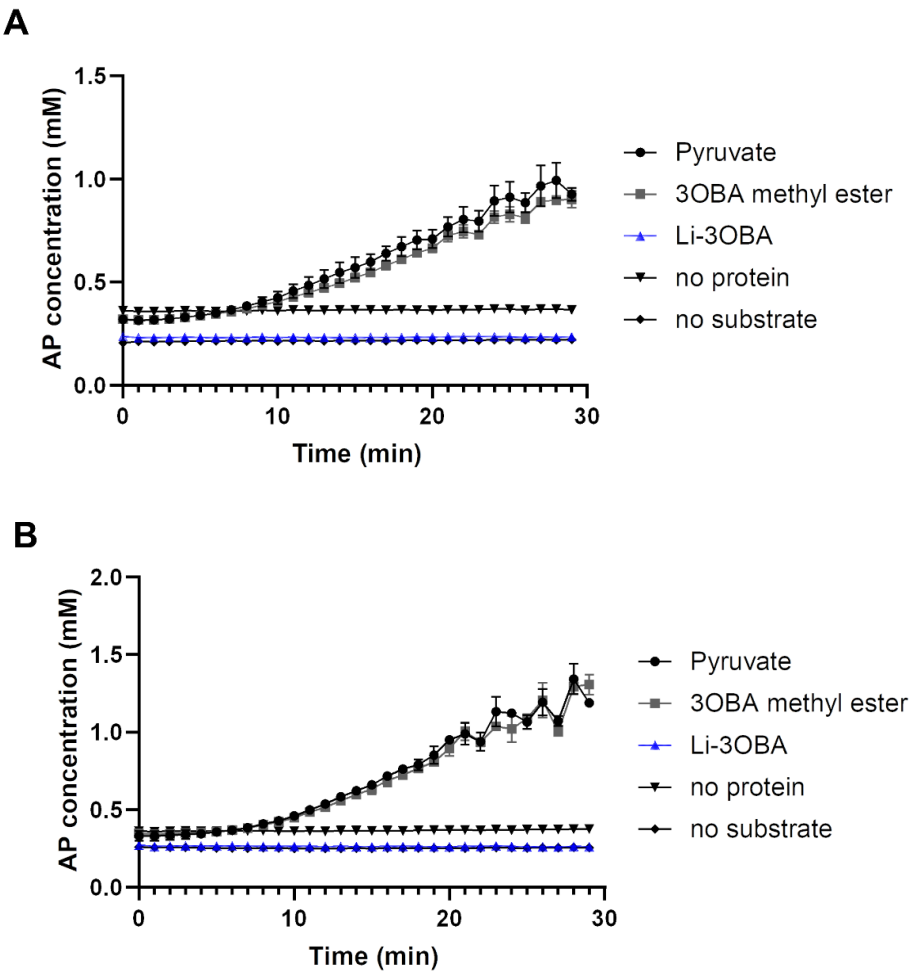

Figure 4. 4. CV_TA activity assay with 3-oxobutyric acid substrates. CV_TA Y168F activity assay testing methyl-3-oxobutyric acid and 3-oxobutyrate a substrate tested in potassium phosphate buffer pH 6.6, 2.5 mM substrate and (A) 0.022 mg/mL or (B) 0.044 mg/mL pure protein. Activity assay performed for 30 min for detection of acetophenone at abs_{245nm}.

Docking simulations performed by GOLD, as in Section 2.9., show that although the three simulations were performed independently, the tested ligands are docked closely in the active site, suggesting they interact with CV_TA in a similar way (Figure 4.5.), which does not explain the lack of activity towards 3-oxobutyric acid.

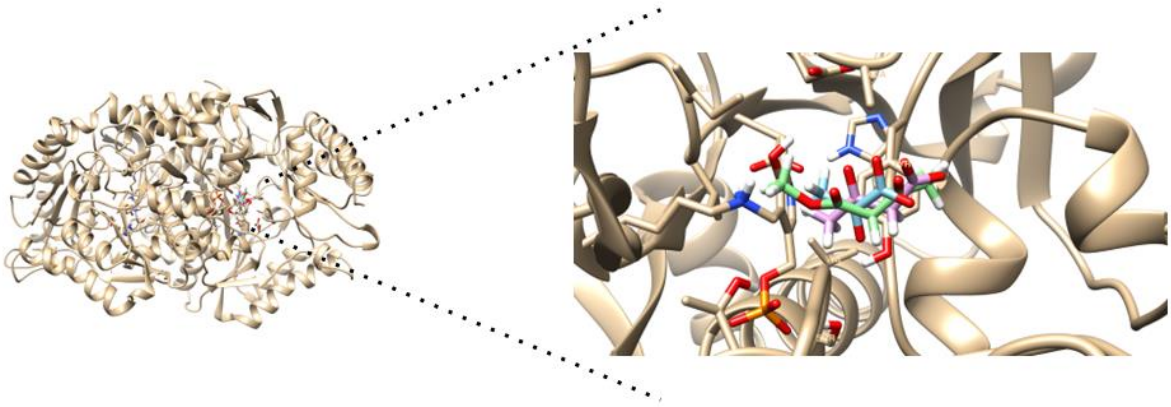

Figure 4. 5. Molecular docking simulation of CV_TA interaction with the target substrates performed by GOLD. On the left: a zoom in of pyruvate (blue), 3-oxobutyric acid (purple) and methyl-3-oxobutyric acid (green) positioned closely in the active site.

By further looking at details of the interactions it was observed that R416 forms a hydrogen bond with an oxygen from the carboxylic group of pyruvate, while Y153 creates a hydrogen bond with the other oxygen. A231, PLP and F88 interact with pyruvate via alkyl or P-alkyl bonds, and K288 and T60 form van der Waals interactions, while L59 and F22 create Pi-donor hydrogen bonds, which are stronger than conventional H interactions (Figure 4.6. A).

On the other hand, weaker interactions were observed between CV_TA and 3-oxobutyric acid. Firstly, R416 seems to interact with an oxygen from the carboxylic group via a salt bridge and F22 binds to the same oxygen by electrostatic interaction. Y168 interacts with the other oxygen in the carboxylic group by hydrogen bond. Finally, A231, W60, K288, L59, T321, Y153, F88 and PLP interact with 3OBA via van der Waals interactions (Figure 4.6. B).

Lastly, simulations with methyl-3OBA reveals that PLP, W60 and L59 interact with the methyl present in the molecule via alkyl or Pi-alkyl interaction, while R416 creates a hydrogen bond with the two carbonyl groups present in the molecule. Further, van der Waals interactions were observed with M169, Y168, F22, M166, Y153, A231, F88, K288 and T321 (Figure 4.6. C).

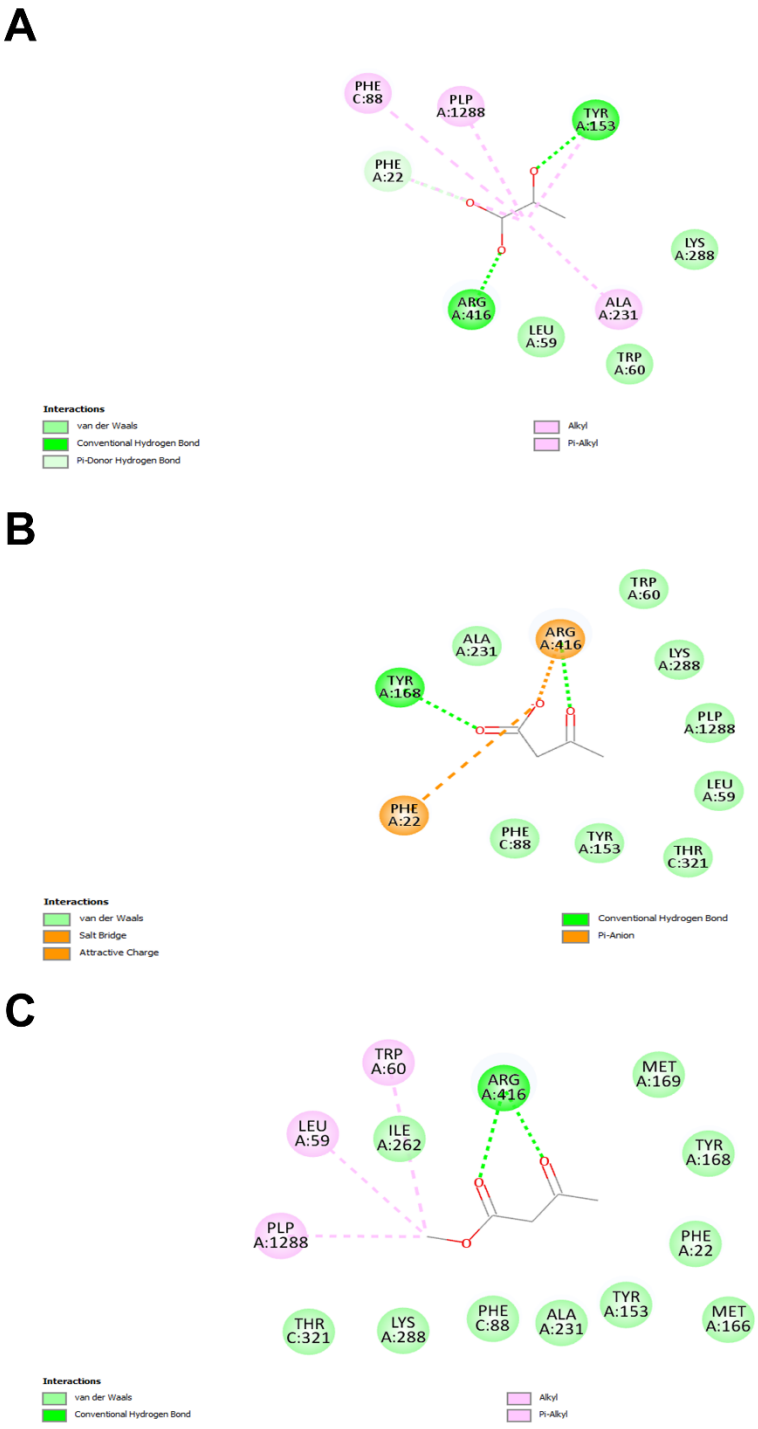

Figure 4. 6. Molecular docking analysis of CV_TA and 3-oxobutyric acid substrates. CV_TA was tested with (A) Pyruvate, as a positive control, (B) 3OBA, and (C) methyl-3OBA. Docking simulations were performed on GOLD and intermolecular interactions analysed on Discovery studio. The interactions between amino acids and the ligands are shown as dotted lines colour-coded according to the interaction type: dark green for hydrogen bonds, light green for van der Waals interaction, orange for

salt bridge and orange for Pi-anion, light orange for attractive charge, pink for alkyl and Pi-alkyl interactions.

The absence of strong interactions between PLP and 3OBA can help to explain why transaminase has no detectable activity towards this ligand even though the salt bridge interaction between 3OBA and R416 is present. Furthermore, the presence of the methyl group in methyl-3OBA seems to favour substrate's interaction with amino acids in the active site.

4.2.2. Transaminase screening for the synthesis of 3-aminobutyric acid

CV_TA seems to be a good candidate for the synthesis of α-ncAAs, but no activity was observed for free 3-oxobutyric acid. Thus, a screening assay using commercially available ATA-117 (*Arthrobacter* sp. KNK168), ATA-217 (*Vibrio fluvialis*), CDX043 (*V. fluvialis*) was carried out as in Section 2.6.5. CV_TA and CV_TA Y168F, as well as BL21_pET45b were used as a control. For this assay, the deamination of 3ABA was tested in the presence of acetophenone or pyruvate and the deamination of L-alanine (L-ala) in the presence of acetophenone (AP) as amino acceptors.

Acetophenone and 1-PEA were not detected using either of the HPLC systems mentioned in Sections 2.7.1. and 2.7.2. Pyruvate was not detected in any of the reactions either. This is surprising because the deamination of L-ala results in pyruvate and the decreasing L-ala concentration should be proportional to the increasing pyruvate concentration. It is possible that the concentration of pyruvate, 1-PEA and AP were out of the range of detection and the signal was not detected. The other conditions, using L-ala as donor and AP as acceptor or 3ABA as donor and AP as acceptor, did not yield consistent results. For instance, when ATA-117 was tested using 3ABA as amino donor and AP as acceptor, 0.40 mM 3OBA (byproduct) and 1.4 mM 3ABA (donor) were detected, but no L-ala, which would be the amino acid produced (Table S. 1. and Table S. 2.).

Furthermore, there was no detectable conversion for samples incubated for 1 h. On the other hand, after 24 h incubation, it was possible to detect the conversion in reactions using ATA-117, ATA-113, and ATA-217 with 3ABA as amino donor and pyruvate as amino acceptor, with ATA-117 performing best (Table 4.1.). To observe if

ATA-117 could be used to produce 3ABA, the reaction towards 3ABA synthesis was carried out using L-ala as amino donor and 3OBA as amino acceptor, this reaction would result in 3ABA and pyruvate as product and by-product, respectively.

Table 4. 1. Transaminase screening for the synthesis of 3-aminobutyric acid. Quantification of amino and keto fatty acids used to screen the activity of commercial transaminases in deaminating 3-aminobutyric acid and using pyruvate as amino acceptor.

Transaminase	Concentration (mM)			
	Amino donor (3ABA)	Amino acceptor (Pyr)	Amino product (L-ala)	Keto by-product (3OBA)
ATA-117	12.78	NA	2.39	13.57
ATA-217	15.94	NA	0.59	1.13
ATA-113	16.18	NA	0.60	NA
CV_TA	13.88	NA	1.83	NA
BL21_pET45b	14.58	NA	NA	NA

NA indicates that the compound could not be detected in the samples.

4.2.3. Molecular docking with ATA-177

To verify whether ATA-117 can be used in the 3ABA operon, molecular docking was carried out as before. The structure of ATA-117 (PDB 3WWH) and ATA-117-Rd11 (PDB 3WWJ), which is the same protein with 28 mutations, were obtained from the Protein Data Bank (Guan, Ohtsuka et al. 2015). Interaction of the two variants of ATA-117 was simulated with 3OBA and 3OBA-CoA. 3OBA-CoA was tested to verify if the enzyme can aminate the -CoA substrate and dispense the overexpression of TesB, counting only in the native expression of TesB from BL21.

It was observed that 3OBA interacts with several amino acids known to be important for catalysis in the native ATA-117 (Figure 4.7. A). For instance, a salt bridge with K188. Hydrogen bonds were observed with Y67, A284, T283 and T282, while van der Waals interactions were observed with V69, G224 and W192. On the other hand, ATA-117-Rd11 interacts weakly with 3OBA. Putative van der Waals interactions were predicted

with G245, R86, P244, I246, L264, and K249. Nonetheless, a salt bridge was predicted between R248 and the ligand (Figure 4.7. B).

The simulation between ATA-117 and 3OBA-CoA shows several interactions, likely because the substrate is bulkier. However, two unfavourable bonds were predicted between W1952, N189 and the ligand. ATA-117-Rd11 was mutated to have a larger active site and catalyse bigger substrates, ie. prositagliptin ketone (Savile 2010). However, unfavourable bumps or unfavourable donor-donor interactions, interaction between two donor groups, were observed between 3OBA-CoA and K181, T62, T276, S275, and PLP (Figure 4.7. C).

These results show that native ATA-117 is likely to catalyse 3OBA, but not 3OBA-CoA. Also, ATA-117-Rd11 only has weaker interactions with 3OBA, which makes the catalysis unlikely to happen for this substrate. Lastly, 3OBA-CoA is a large substrate and clashes even in the larger engineered active site of ATA-117-Rd11. Based on these results, ATA-177 is then a suitable candidate for the 3ABA operon.

Constructs for 3ABA synthesis with ATA-117 were designed and ordered, but they were not received in time to be tested. The constructs with genes in various orders included: *tesB*_RBS1_*phaA*_RBS2_ATA117, ATA117_RBS1_*phaA* and *tesB*__RBS1_ATA117__RBS2_*phaA* which were cloned in pET45b. The RBS sequences are shown in Table 2.2. B. The synthesis of ATA117_RBS1_*tesB*_RBS2_*phaA* was not possible due to impossibility of cloning the operon in pET45b. The cloning was attempted and failed in *E. coli* DH5a/TOP10F'/DBQ/EPI400.

4.2. Cascade reaction for the synthesis of ncAAs

The second strategy for the synthesis of α and β-ncAAs employed a two-enzyme reaction presented in Figure 4.8. The proposed cascade reaction was investigated as hydroxy acids can be produced via hydrolysis of plant sources (Patel, Dumancas et al. 2016), while keto fatty acids, especially β-acids, can be thermodynamically unstable and are not as easily available (Rudat, Brucher et al. 2012). Ideally, the enzyme to complement (Figure 4.8. E1) the cascade with CV_TA (Figure 4.8. E2) would be able to oxidise 2- and 3-hydroxy fatty acids.

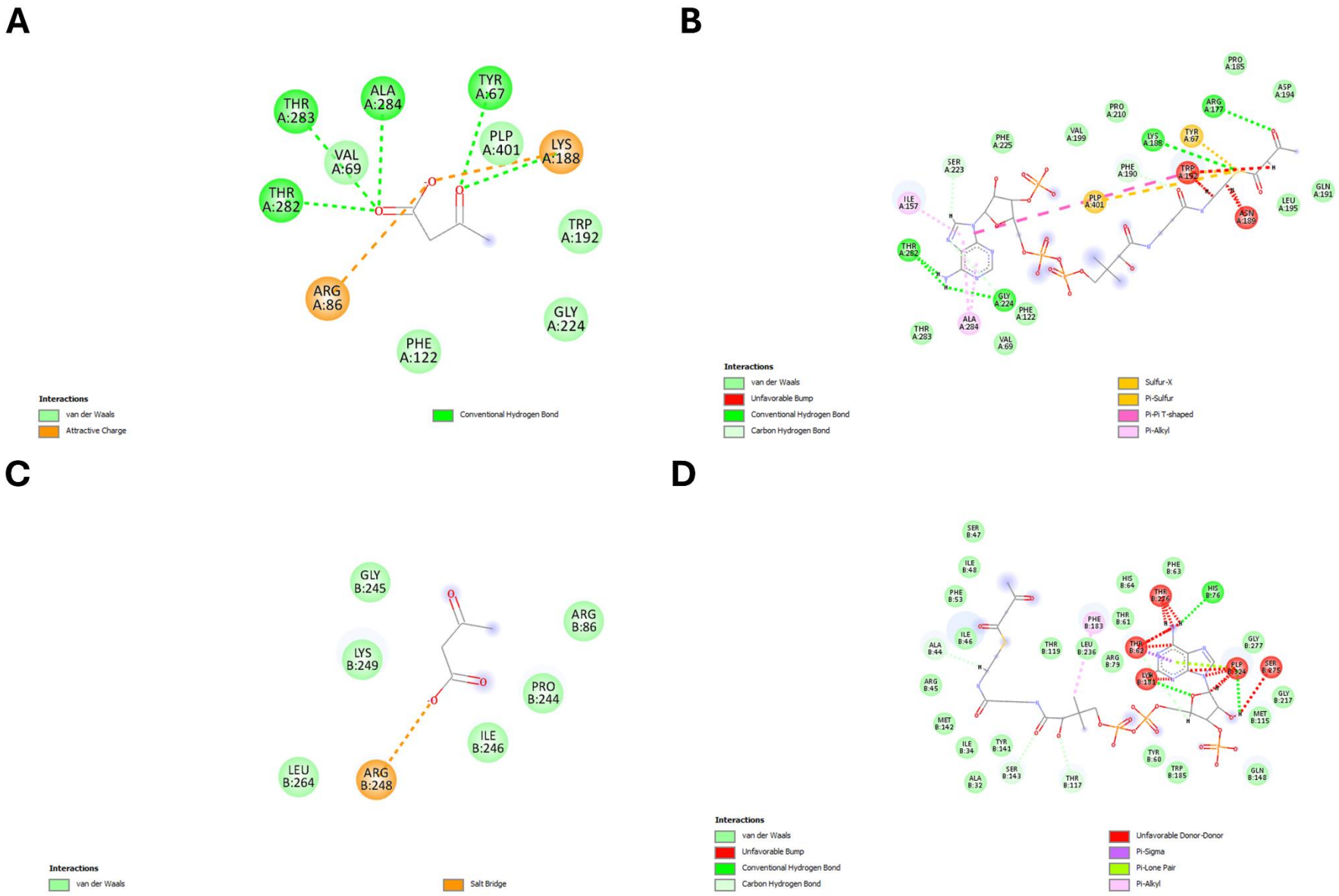
A
THR A:283
ALA A:284
TYR A:67
PLP A:401
LYS A:188
VAL A:69
THR A:282
TRP A:192
ARG A:86
GLY A:224
PHE A:122
Interactions
van der Waals
Attractive Charge
Conventional Hydrogen Bond
B
PRO A:185
ASP A:194
ARG A:177
PRO A:210
VAL A:199
PHE A:225
LYS A:188
TYR A:67
SER A:223
PHE A:190
TRP A:192
GLN A:191
ILE A:157
PLP A:401
LEU A:195
ASN A:189
THR A:282
GLY A:224
PHE A:122
ALA A:284
THR A:283
VAL A:69
Interactions
van der Waals
Unfavorable Bump
Conventional Hydrogen Bond
Carbon Hydrogen Bond
Sulfur-X
Pi-Sulfur
Pi-Pi T-shaped
Pi-Alkyl
C
GLY B:245
ARG B:86
LYS B:249
PRO B:244
ILE B:246
LEU B:264
ARG B:248
Interactions
van der Waals
Salt Bridge
D
SER B:47
ILE B:48
PHE B:63
HIS B:64
PHE B:53
THR B:276
HIS B:76
PHE B:183
THR B:61
ILE B:46
ALA B:44
THR B:119
LEU B:236
ARG B:79
THR B:62
GLY B:277
LYS B:191
PLP B:324
SER B:275
ARG B:45
GLY B:217
MET B:142
MET B:115
ILE B:34
TYR B:141
TYR B:60
SER B:143
TRP B:185
ALA B:32
THR B:117
GLN B:148
Interactions
van der Waals
Unfavorable Bump
Conventional Hydrogen Bond
Carbon Hydrogen Bond
Unfavorable Donor-Donor
Pi-Sigma
Pi-Lone Pair
Pi-Alkyl

Figure 4. 7. Molecular docking simulation of transaminase ATA-117 with acetoacetate substrates. (A) the native structure of ATA-117 tested 3-oxobutyric acid or (B) acetoacetyl-CoA, and the mutated ATA-117_Rd11 was also tested with (C) 3-oxobutyric acid and (D) acetoacetyl-CoA. The interactions between amino acids and the ligands are shown as dotted lines colour-coded according to the interaction type: dark green for hydrogen bonds, light green for van der Waals interaction, orange for salt bridge and orange for Pi-anion, light orange for attractive charge, yellow for sulphur and Pi-sulfur interactions, pink for alkyl, Pi-alkyl interactions, and red for unfavourable interactions. The molecular docking simulations were performed on Gold and detailed molecular interactions studied on Discovery Studio.

Two alcohol dehydrogenases (ADHs) were chosen as they were previously reported to be active towards aliphatic and aromatic α and β-alcohols (Mutti, Knaus et al. 2015). Glycolate oxidase (GO) was reported to be active towards aromatic and aliphatic α- and β-hydroxy fatty acids (Das, Glenn Iv et al. 2010).

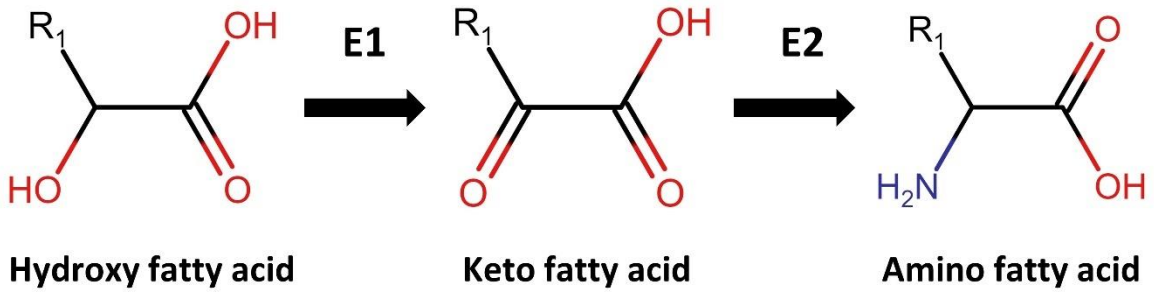

Figure 4. 8. Proposed cascade reaction for the synthesis of non-coded α and β-amino fatty acids from α-hydroxy fatty acids. The scheme shows as example the conversion of a generic α-hydroxy fatty acid to its respective keto and amino fatty acid in a linear cascade catalysed by two different enzymes represented by E1 and E2. In the scheme, the oxidation of hydroxy fatty acids is performed by E1, and the amination step is performed by E2.

Two lactate dehydrogenases were also selected, a D-specific 2-hydroxyacid dehydrogenase from *Haloferax mediterranei* (named L-DDH) active towards 2-

ketobutyrate, ketoisocaproate, and pyruvate (PDB 5MH6, GenBank: DQ223970.1) (Bonete, Ferrer et al. 2000), and a 2-hydroxy acid dehydrogenase (PDB 3WX0 GenBank: AM946981.2) from *E. coli,* named L-DDH, was chosen due to its reported activity towards glyoxylate, oxaloacetate, and hydroxypyruvate (Furukawa, Miyanaga et al. 2014).

4.2.1. Design of constructs for the expression of target enzymes

The constructs for the candidate genes were designed in SnapGene v. 7.2.1. (SnapGene) and then the coding sequences of the two AHDs, GO and LDHs with the homology regions required for the assembly of the expression constructs were purchased from Twist Biosciences. The coding fragments and were cloned in the expression vector pET45b using Gibson assembly (Section 2.3.4).

Figure 4.9. A shows the PCR products of (*R*)-specific alcohol dehydrogenase originating from *L. brevis* (RADH - GenBank: LS483405) with 759 bp and (*S*)-specific alcohol dehydrogenase from *Aromatoleum aromaticum* (SADH - GenBank: CR555306) with 750 bp. These two enzymes were chosen as they were shown to have activity towards 1-octanol, 1,3-butanediol, 3-phenyl-1-propanol, and other aliphatic and aromatic alcohols (Mutti, Knaus et al. 2015). It was therefore hypothesised that they could be used as the first step in the oxidation of a hydroxyl group to the carbonyl group and therefore produce the substrate for the transaminase. As in the previous chapter the pathways for two products were designed i.e. (*R*)-3-hydroxybutyric acid (RHBA) and (*S*)-3-hydroxybutyric acid (SHBA), both (*R*)- and (*S*)-specific enzymes were required. RADH and SADH were amplified using specific primers shown in Table 2.2. A. For instance, RADH_F/R were used to amplify the coding sequence, while pET was amplified with pET_RADH_F/R. PCR fragments for SADH were obtained similarly. The products were then assembled into pET45b vector to yield the following constructs: pET45b_RADH and pET45b_SADH (Table 2.3.). The constructs were verified by sequencing and transformed to BL21.

Similar procedure was followed to generate the (*S*)-specific glycolate oxidase (GO) expression construct, namely pET45b_GO. This enzyme was shown to specifically oxidase 2-hydroxyisobutyric acid, 2-hydroxy-4-pentoxybutyric acid, 2-

hydroxyhexanoic acid, 2-hydroxydecanoic acid, and the β substrates 3-phenyllactic acid and 3-indolelactic acid (Adam, Lazarus et al. 1997, Das, Glenn Iv et al. 2010). The coding sequence of GO (GenBank XM_022011288.1) with 1114 bp was PCR amplified using GO_F and GO_R primers (Figure 4.9.) and pET45b amplified with pET_GO_F and pET_GO_R primers. Both fragments had homologous nucleotides to facilitate Gibson assembly. Primers are shown in Table 2.2. A. The pET45b_GO construct was cloned to DH5α, sequence verified and transformed to BL21 for protein expression.

One D-specific 2-hydroxyacid dehydrogenase from *H. mediterranei* (named L-DDH) is active towards 2-ketobutyrate, ketoisocaproate, and pyruvate (PDB 5MH6, GenBank: DQ223970.1) (Bonete, Ferrer et al. 2000), and an L-2-hydroxy acid dehydrogenase from *E. coli* (PDB 3WX0 GenBank: AM946981.2) named L-LDH observed to be active towards glyoxylate, oxaloacetate, and hydroxypyruvate (Furukawa, Miyanaga et al. 2014) were chosen for screening. L-DDH with 927 bp and L-LDH with 990 bp were PCR amplified (Figure 4.9.) as the previous genes along with pET45b complementary for each gene (Table 2.2. A). Gibson assembly was used to obtain pET45b-LLDH, for L-LDH, and pET45b-LDDH, for L-DDH (Table 2.3.).

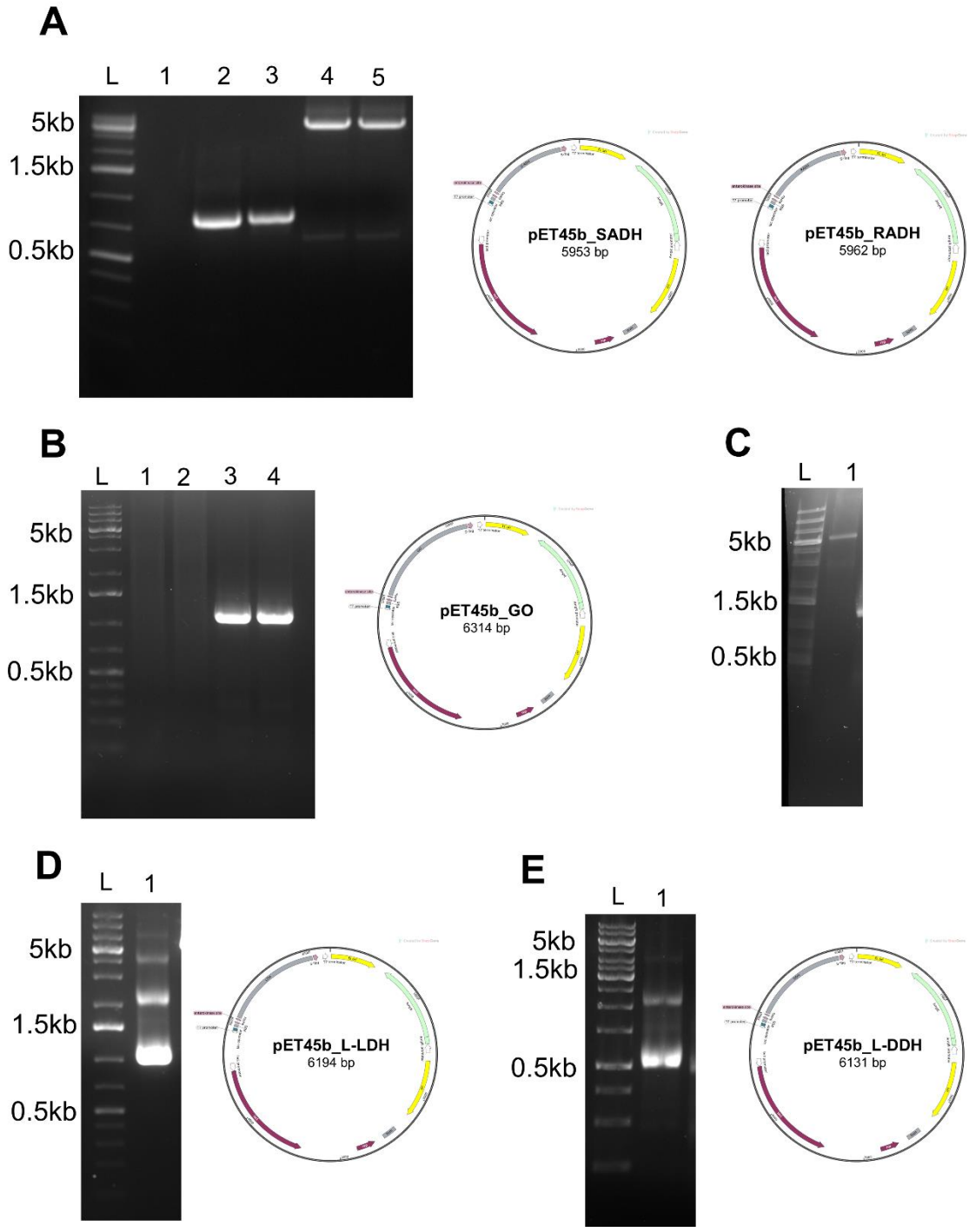

Figure 4. 9. The expression constructs design. (A) the pET_SADH construct and the corresponding PCR products used to assemble it. SADH (lane 2; 750 bp) and RADH (lane 3; 759 bp) and pET45b complementary to (lane 4) SADH and (lane 5) RADH; (B) GO amplification (lanes 3-4; 1114 bp); (C) pET45b amplification (5191 bp); (D) amplification of L-LDH (990 bp); (E) and L-DDH (927 bp). The PCR products were resolved on 1 % (w/w) agarose gel and1 kb Plus DNA ladder (L) was used.

4.2.2. Alcohol dehydrogenases: Expression, purification and activity assay Protein expression and purification

Firstly, a time-course expression was used to assess the optimal expression time for the RADH and SADH. BL21_RADH and BL21_SADH were cultivated as described in Section 2.5. After the induction of expression with IPTG (T0), 1 mL samples were collected after 1, 2, 3 and 4 h of induction and analysed by SDS-PAGE. The expected size of a his-tagged RADH is 27.57 kDa, while 27.49 kD band was expected for his-tagged SADH (Figure 4.10.). It appears that the maximum protein is produced 4 h after the induction, and this time was used in the further experiments.

Next, the recombinant BL21 strains were grown in 400 mL medium, and the cell pellet obtained after 4 h from the induction of protein expression was used for protein purification by affinity chromatography in a nickel-chelating column and increasing concentration of imidazole as a competing agent (Section 2.5.). The fractions collected during chromatography were run on a 12 % SDS-PAGE to determine which fractions contained purified enzymes. Fractions 5 to 7 contain pure RADH where around 5-15 % elution buffer 500 mM imidazole is used (Figure 4.10. A), while SADH elutes between fractions 10 and 18, with elution buffer 500 mM imidazole varying from 45-100 % (Figure 4.10. B). Fractions 5 and 6 for RADH were pooled and resulted in 670 µg/mL.

4.2.2.1. Alcohol dehydrogenase activity assay

Both alcohol dehydrogenases tested here were previously used in a cascade reaction for the synthesis of aliphatic and aromatic primary and secondary amines starting from alcohols, such as, 1-octanol, 1,3-butanediol, 3-phenyl-1-propanol, among others (Mutti, Knaus et al. 2015). We hypothesized that these ADHs could reduce hydroxy

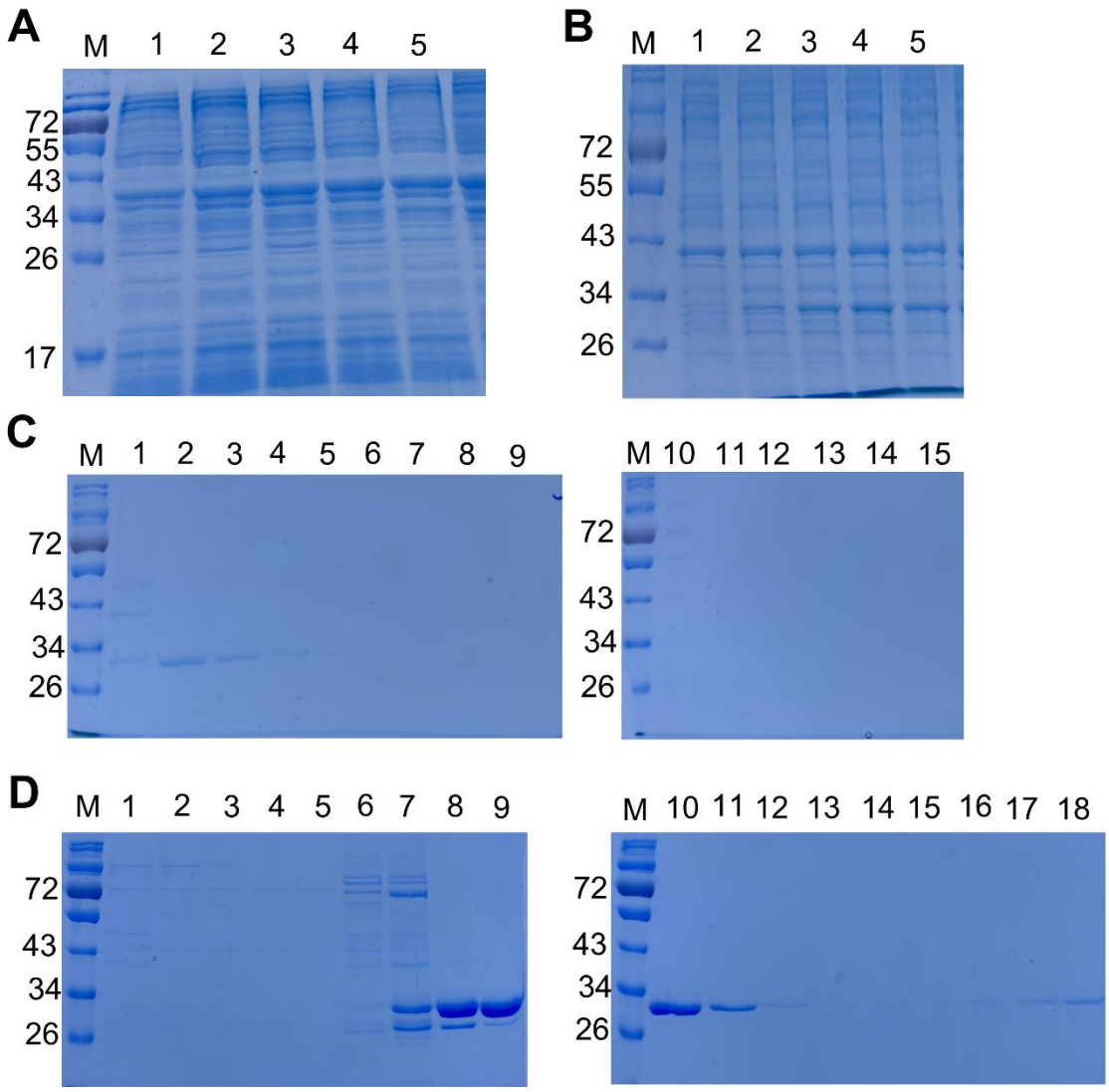

Figure 4. 10. SDS-polyacrylamide gel electrophoresis of expressed and purified (*S*)- (SADH) and (*R*)-alcohol dehydrogenases (RADH). Time-course expression profile for (A) RADH with ~27 kDa and (B) SADH also with ~27 kDa accounting with the his-tag. Affinity chromatography purification showing fractions 4 to 18, labelled from 1 to 15, eluted with 500 mM elution buffer and imidazole gradient increasing from 0-100 %. Gels for (C) RADH and (D) SADH purification. EZ-Run prestained Rec protein ladder (M) was used.

fatty acids to keto fatty acids. The two alcohol dehydrogenases selected for this study rely on the use of NAD^+ as a cofactor in the oxidation reaction. Therefore, during the oxidation of the hydroxyl group of the substrate NADH will be produced. The increase in NADH can be monitored spectrophotometrically by measuring the absorbance abs_{340nm} (Section 2.6.1.). The assay for both RADH and SADH, in addition to the

protein (60 µg/mL), contained the cofactor 5 mM NAD^+ and the 1 mM substrate. The target substrates were 2-hydroxybutyric acid (2ABA), 2-hydroxyhexanoic acid (2AHA), 2-hydrooctanoic acid (2AOA), (*R*)-hydroxybutyric acid (R3HBA) and (*S*)-3-hydroxybutyric acid (S3HBA) (Figure 2.3.). RADH and SADH can natively catalyse the reversible conversion of acetophenone to phenylethanol, but as 2-butanol (2-but) is a simple and small alcohol observed to be reduced by the organisms related to the source organisms racemic 2-but was therefore used as a positive control for both enzymes (Russmayer, Marx et al. 2019, Becker, Wünsch et al. 2024). Since the previous analyses of the transaminase CV_TA activity, the second enzyme in the foreseen cascade reaction, have shown that phosphate buffer pH 7.0 and phosphate buffer pH 6.4 are the optimal buffers for 2AOA and 3OBA, respectively (Almahboub, Narancic et al. 2018), the activity of both RADH and SADH were analysed in phosphate buffer pH 7.0, as well as Tris-HCl 7.5 as it was demonstrated these enzymes work well in buffers from pH 7.0 to 8.7 (Mutti, Knaus et al. 2015).Thus, Tris-HCl was chosen because its range is more appropriate than phosphate buffer. The activity assay was performed as in Section 2.6.1.

Both RADH and SADH showed activity in Tris-HCl pH 7.5 and phosphate buffer pH 7.0 when racemic 2-but was used as substrate (Figure 4.11.). RADH produced approximately 300 mM NADH over 30 min (Figure 4.11. A-B), while SADH showed up to 2-fold higher activity when compared to RADH. The activity of both enzymes towards 2-but was slightly higher when tested in Tris-HCl pH 7.5. Neither RADH nor SADH showed a detectable activity with the tested target substrates (Figure 4.11.). While some activity appeared in the case of SADH with the 2-hydroxy target substrates, especially RADH in Tris-HCl pH 7.5 (Figure 4.11. D), by calculating the rate of reaction it was observed it was comparable to the negative controls. This indicates that SADH and RADH are not active to the target hydroxy substrates.

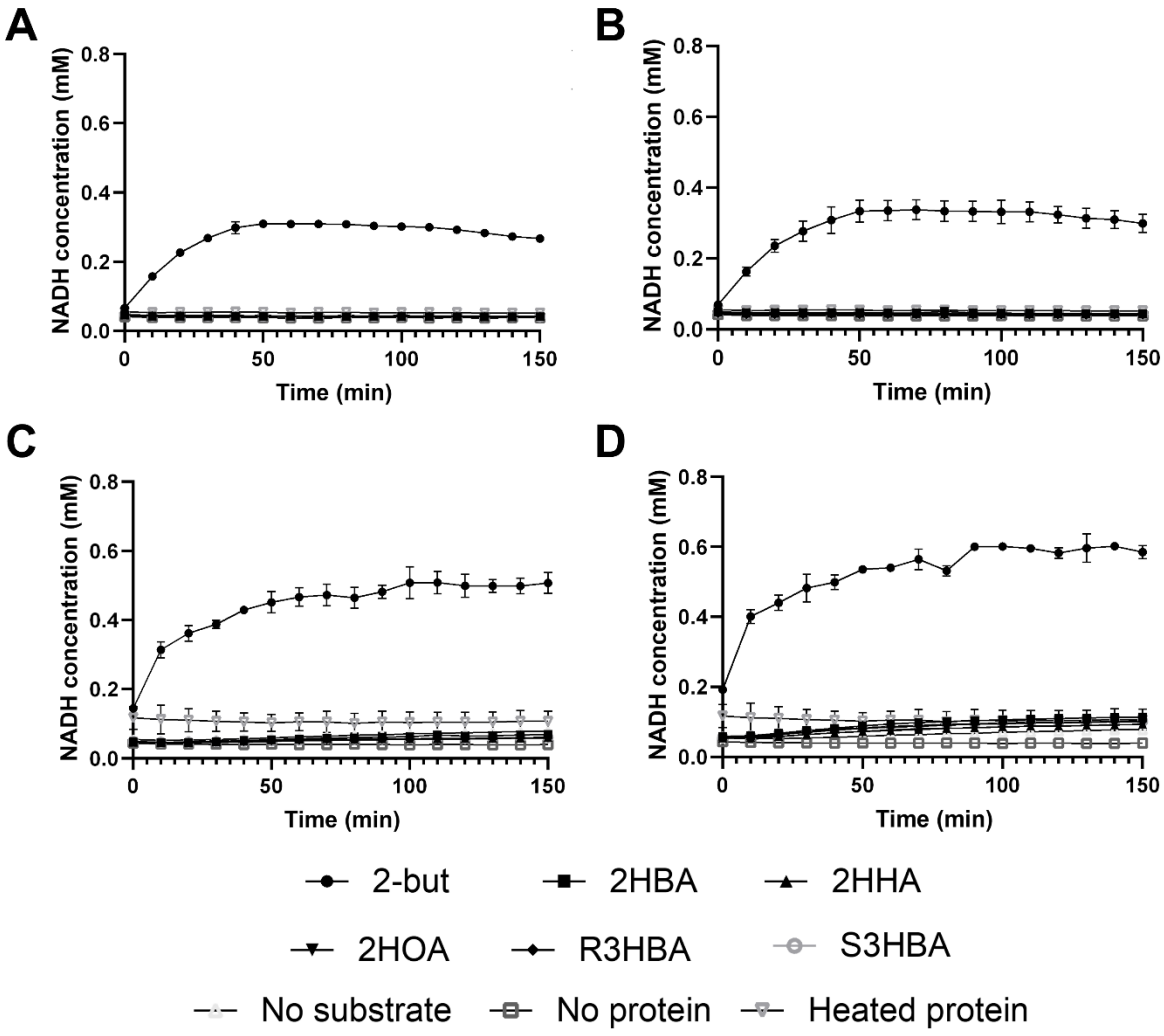

Figure 4. 11. The activity of (*R*)- (RADH) and (*S*)-specific alcohol dehydrogenase (SADH) activity. The spectrophotometric assay is based on the reduction of NAD^+ to NADH (abs_{340nm}). The activity of RADH in (A) 20 mM phosphate buffer, or (B) 20 mM Tris-HCl pH 7.5, and the activity of SADH in (C) 20 mM phosphate buffer, or (D) 20 mM Tris-HCl pH 7.5 are shown. The reaction was monitored over 150 min at 30°C consisted of 5 mM NAD^+ and 60 µg/mL pure protein The positive control included 2-butanol (2-but) and the target substrates were 2-hydroxybutyric acid (2HBA), 2-hydroxyhexanoic acid (2HHA), 2-hydroxyoctanoic acid (2HOA), (*R*)-hydroxybutyric acid (R3HBA) and (*S*)-3-hydroxybutyric acid (S3HBA). The negative controls had all components, but protein or 2-but, and heated protein at 95 °C for 5 min.

4.2.3. Lactate dehydrogenases: Expression and purification

Following the same expression and purification strategy as described above, the two lactate dehydrogenases, L-LDH and L-DDH, were purified and analysed via SDS-PAGE and western blot (Figure 12.). The expression of L-LDH starts before IPTG induction (T0), as a band was observed at ~39 kDa, which corresponds to the His-tagged L-LDH (Figure 12 A), while it was not possible to clearly distinguish L-DDH time-course expression by SDS-PAGE (Figure 12 B). Expressing systems using T7 promoter, as pET45b vectors, are known to have basal levels of T7 RNA polymerase, which can start the expression of the target gene before induction (Spehr, Frahm et al. 2000). To verify if pET45b_LLDH had leaked expression and clearly observe the expression pattern of L-DDH, western blot analysis was carried out (Section 2.5.2.). Western blot analysis indicates the expression of L-LDH really starts before induction and increases up to 2h after induction (Figure 12. C). The expression of L-DDH was observed 1 h after induction, however two bands were consistently detected in the time course samples (Figure 12. D). The higher band corresponds to ~34 kDa and therefore to the expected size of the His-tagged L-DDH. The lower band of ~ 30 kDa could be a truncated L-DDH as it also appears to be his-tagged However, the reason for this truncation is not clear.

After the affinity chromatography purification two bands were consistently observed in the fractions 7 to 15 for L-DDH (Figure 12. E). L-LDH elutes when imidazole concentration reached around 50 mM imidazole, and even with the further increase in the imidazole concentration the two bands were still visible up to ~400 mM imidazole. In the case of nonspecific proteins, they elute in the first 5 fractions, and no pure L-DDH was observed in later fractions (Figure 12 E).

L-DDH was used for affinity chromatography as well. Nonetheless, pure bands were not observed for this protein over various attempts. However, fraction 14 L-DDH (Figure 12. F) was used for activity assay as in Section 2.6.1. but no activity could be detected. It seemed that protein purification also promoted loss of activity for L-LDH, but the reason is not clear. These fractions were pooled, and the resulting mixture had 870 µg/mL.

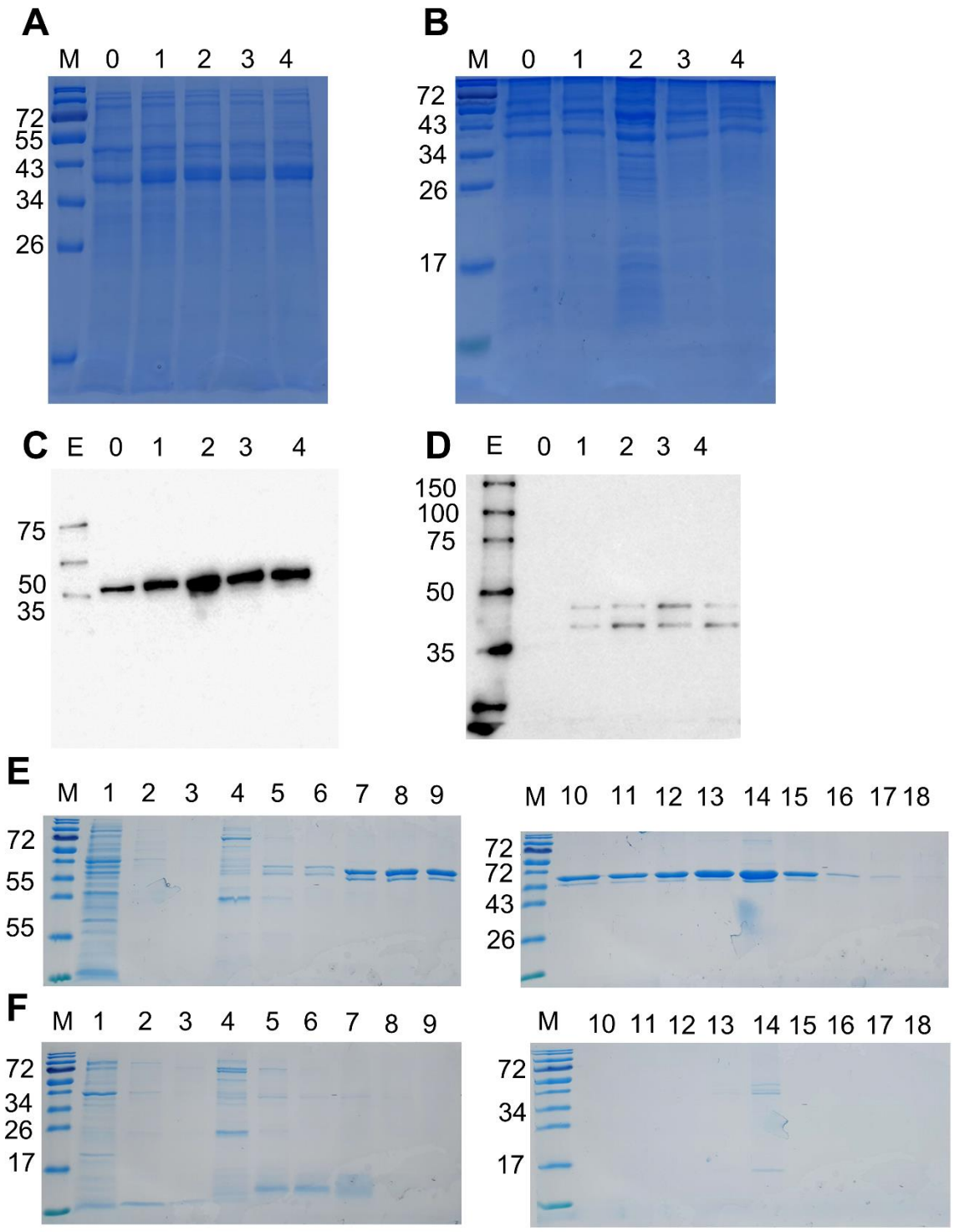

Figure 4. 12. Lactate dehydrogenases expression and purification profiles. SDS-PAGE of time-course expression for (A) L-LDH and (B) L-DDH; western blot analysis of time-course samples for (C) L-LDH and L-DDH; SDS-PAGE of nickel affinity chromatography purification of (E) L-LDH and (F) L-DDH. The expected size of his-tagged L-LDH was ~39.37 kDa and ~34 kDa for L-DDH. For time-course samples (A-D) lane 1 shows CFE before induction of protein expression and the other lanes show

every hour after induction. For purification gels (E-F), lanes 1 to 15 represent fractions 4 to 18 eluted with increasing gradient concentration of elution buffer 500 mM imidazole. EZ-Run ladder prestained Rec protein (M) was used for SDS-PAGE, while ECL DualVue Western Blotting markers (E) was used for western-blot.

4.2.4. Glycolate oxidase: Expression, purification and activity

The expected size of His-tagged GO is ~41 kDa. During the time course inspection of GO expression, a signal at around 40 kDa was observed (Figure 4.13 A). However, to make sure this signal corresponds to GO, a western blot was carried out with the sample from time-course expression. Western blot analysis however showed GO expression 1 h after the induction, while no signal was observed in the T0 sample (Figure 4.13. B). It appears that the highest intensity band occurs in the sample 3 h and 4 h post induction, and 4 h expression time was used next. GO was purified using the same procedure as described for RADH and SADH. However, unlike RADH and SADH, GO was eluted with much higher ~500 mM concentration of imidazole (97-100 % elution buffer), fractions 16 and 17. The concentration of pure protein in these fractions was 750 and 520 µg/mL, respectively.

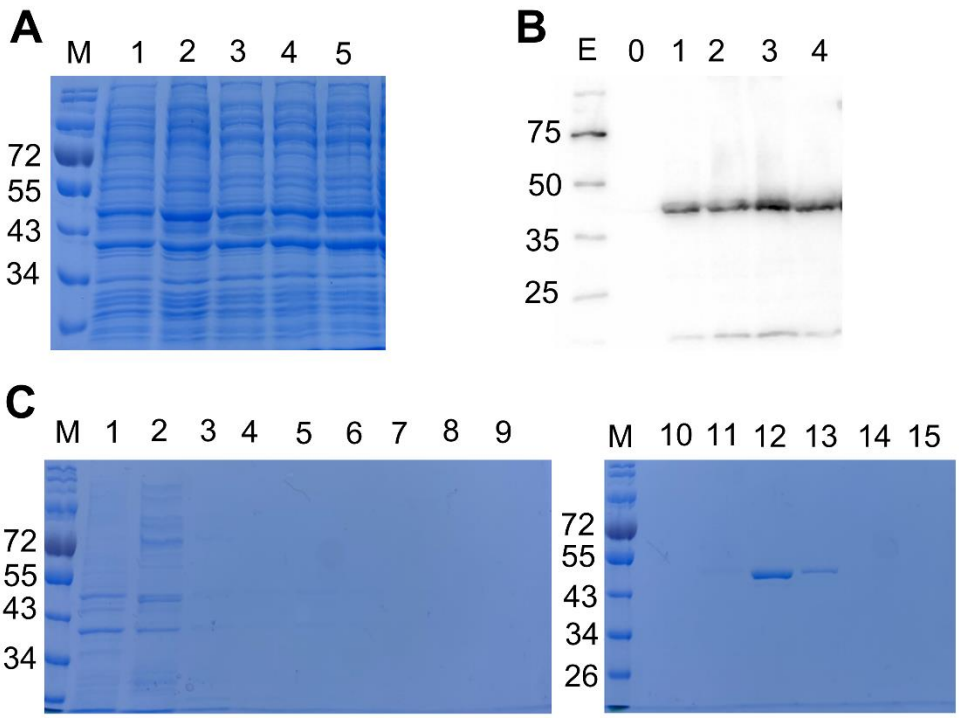

Figure 4. 13. Glycolate oxidase time-course expression and purification profiles. (A) SDS-PAGE and (B) western blot of GO using time-course expression samples labelled from lanes 1 to 5 where lane 1 shows 0 h (before induction) and lanes 2-5 every h after induction; (C) purification of histidine-tagged GO with 18 fractions collected with increasing gradient of imidazole. EZ-Run ladder prestained Rec protein (M) was used for SDS-PAGE, while ECL DualVue Western Blotting markers (E) was used for western-blot.

4.2.4.1. Glycolate oxidase activity

Although GO is an (*S*)-specific oxidase, racemic substrates were used to test its activity (Lindqvist 1989). This was done so the substrates were compatible with the other candidate enzymes. As a mixture of enantiomers is being used, it is expected that GO oxidises 50 % of the available substrate. The byproduct of a GO catalysed oxidation reaction is hydrogen peroxide. As this byproduct can inhibit the GO activity (Wahart, Staniland et al. 2022), horseradish peroxidase (HRP) was used to remove the peroxide. The free oxygen from H_2O_2 produced by HRP activity interacts with *o*-dianisidine producing the oxidised *o*-dianisidine, which absorbs light at abs_{440nm} and can be measured spectrophotometrically (Dellero, Mauve et al. 2015, Duminil, Oury et al. 2024). Similarly to the ADHs, GO was tested in phosphate buffer pH 7.0 and Tris-HCl pH 7.5 (Section 2.6.2.).

4.2.4.1.1. Cofactor concentration

The assay was first optimised by using the control substrate, DL-lactic acid (DL-LA). Despite of the name, GO has higher activity towards LA than it has to glycolate, hence, LA was used as positive control (Wang, Xu et al. 2016). The assay includes 0.2 mM or 0.02 mM FMN, 20 mM potassium phosphate buffer pH 7.0 or Tris-HCl pH 7.5, 1 mM o-dianisidine, 0.1 mg/mL peroxidase (HRP), 50 µg/mL GO and 2.5 mM substrate. The reaction was allowed to run for 150 in case GO required more time to oxidise the target hydroxy acids (Section 2.6.2.). The control reaction to which no substrate was added, as well as the control reaction with the inactivated or in the absence of protein showed high background absorbance (Figure 4.14. B and D). To try and reduce this background, a 10-fold lower concentration with 0.02 mM FMN was tested. Compared

to the activity detected with 0.2 mM FMN, a 6.2-fold decrease in activity was observed with LA as substrate in phosphate buffer pH 7.0 (Figure 4.14. A and B). In Tris-HCl pH 7.5 no reaction was detected with 0.02 mM FMN, but the activity was comparable to the same reaction in potassium phosphate pH 7.5. for 0.2 mM FMN. Thus, the following reactions were performed in potassium phosphate buffer, the medium compatible with CV_TA (Almahboub, Narancic et al. 2018).

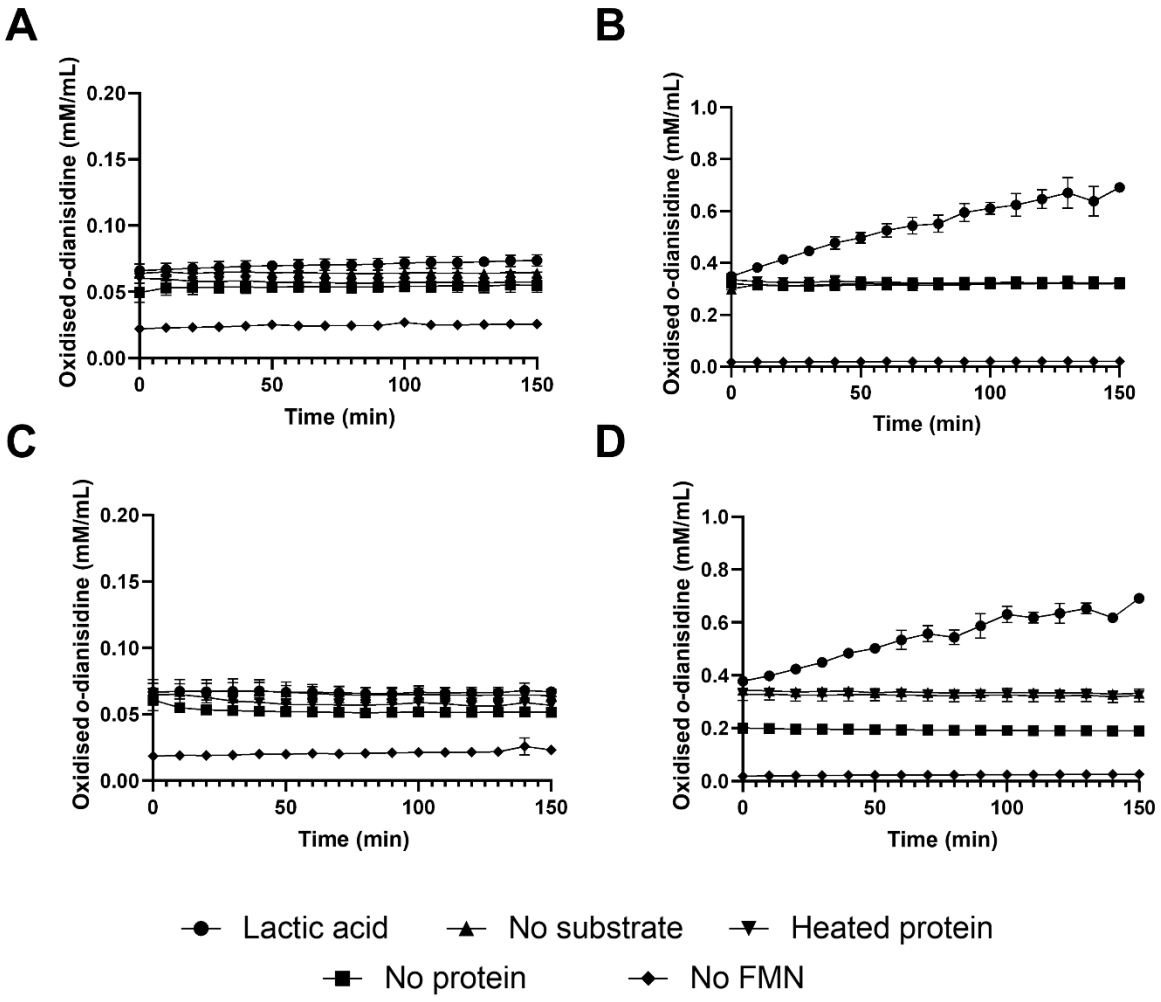

Figure 4. 14. Glycolate oxidase activity tested with varying cofactor concentration. GO activity tested with 2.5 mM DL-lactic acid and (A) 0.02 or (B) 0.2 mM FMN in 20 mM phosphate buffer pH 7.0 or (C) 0.02 or (D) 0.2 mM FMN in 20 mM Tris-HCl pH 7.5 at 30 °C. The negative controls included no GO, no DL-lactic acid (substrate), no FMN and GO inactivated at 95 °C for 5 min.

4.2.4.1.2. GO activity with the target substrates

As no difference was observed between the activity in phosphate and Tris-HCl buffer, the target substrates were tested in phosphate buffer as it is the optimum buffer and pH for CV_TA (Almahboub, Narancic et al. 2018). The target hydroxy fatty acids included the same compounds that ADHs were tested for GO. GO has catalytic activity towards all 2-hydroxy fatty acids tested and, in all cases, the activity was higher for the target substrates than for the positive control, LA. However, no activity was detected for (*S*) or (*R*)3HBA. GO is an α-hydroxy acid oxidase, which are specific for 2-hydroxy fatty acids (Diêp Lê and Lederer 1991). Therefore, the lack of activity towards 3HBA is not surprising.

The highest reaction rate was observed for 2HBA which was 1.4-fold higher than for LA, followed by 2HOA (1.2-fold higher) and 1.1-fold higher for 2HHA (Figure 4.15.). These results indicated that GO can potentially be used in the cascade for the synthesis of α-ncAAs as E1 (Figure 4.15.).

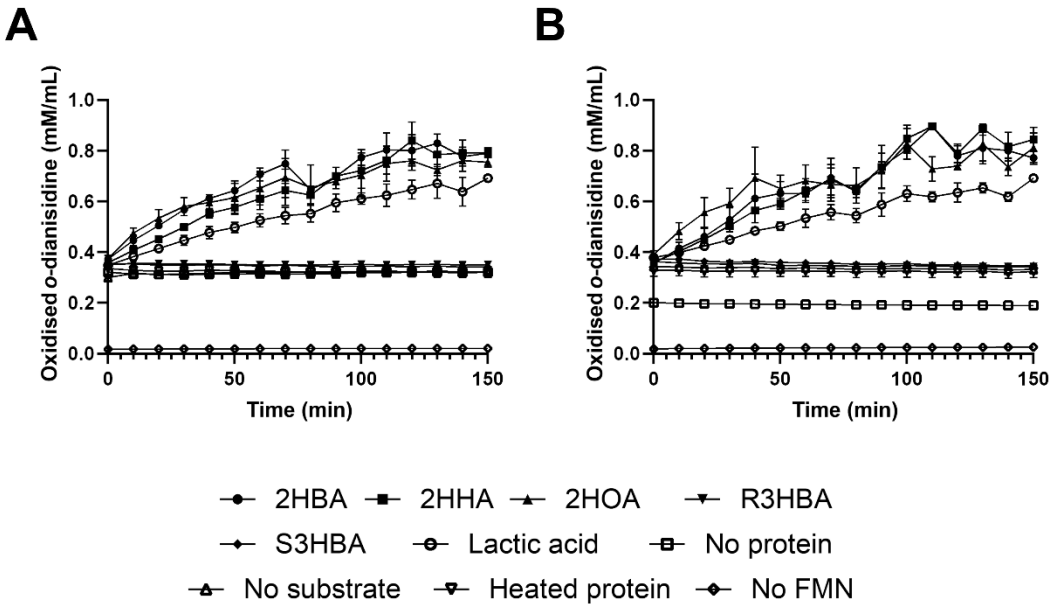

Figure 4. 15. **Glycolate oxidase activity tested with DL-LA and target 2-hydroxy fatty acids**. GO activity assay regarding the oxidation of lactic acid, 2-hydroxybutic acid (2HBA), 2-hydroxyhexanoic acid (2HHA), 2-hydroxyoctanoic acid (2AOA), (*R*)-3-hydroxybutyric acid (R3HBA) and (*S*)-3-hydroxybutyric acid (S3HBA) to their respective keto acids. The assay was performed at 30 °C with 0.2 mM FMN and 50

µg/mL pure protein in (A) 20 mM phosphate buffer pH 7.0 or (B) 20 mM Tris-HCl pH 7.5.

4.2.4.1.3. GO storage stability

As GO has shown activity towards some of the target substrates, and was therefore targeted for the cascade reaction, the stability of purified enzyme stored for 7 days at 4 °C in elution buffer was tested and compared to the activity of the freshly purified GO, also in elution buffer, with DL-LA as the substrate for the reaction. The activity of the stored enzyme is comparable to the freshly purified one (Figure 4.16).

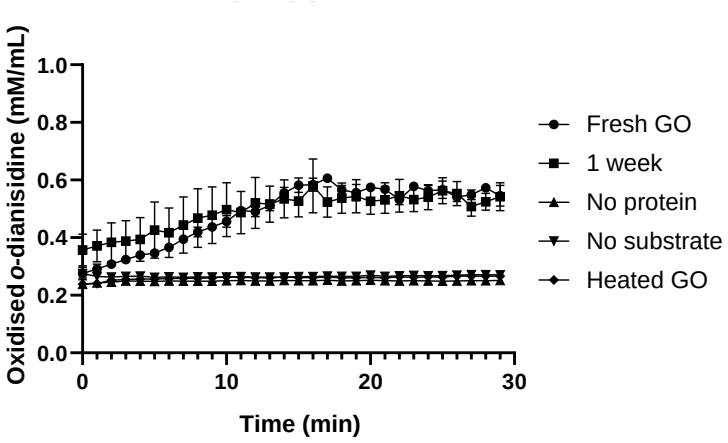

Figure 4. 16. The stability of stored glycolate oxidase. Comparison of GO activity freshly purified and stored at 4 °C for 7 days tested at 30 °C with 0.2 mM FMN, 50 µg/mL GO and 2.5 mM DL-lactic acid in phosphate buffer pH 7.0.

4.2.4.2. GO molecular docking

To understand why GO only has catalytic activity towards 2-hydroxy fatty acids, but not to 3HBA, and allow for future protein engineering, the GO-substrate interaction was analysed as described before (Section 2.9.). It was postulated that Y24, Y129, and R257 appear to be involved in substrate binding, while H254 is directly involved in catalysis (Lindqvist 1989). Furthermore, S106, Y129, T155, and K230 are important for FMN stabilization (Lindqvist 1989). The hydride transfer mechanism seems to be the most likely mechanism of action for GO (Dellero, Mauve et al. 2015). H254

abstracts the proton from the hydroxyl group in the substrate, concomitantly transferring the said proton to the N5 atom of FMN. The proton abstraction step by FMN was observed to be a rate limiting factor in catalysis (Macheroux 1991, Dellero, Mauve et al. 2015).

GO was docked with LA, a positive control, 2HBA and (*S*)3HBA, two target substrates, the first known to be catalysed by GO and the second known not to be catalysed (Section 2.15). It can be observed in Figure 4.17. that LA and 2HBA seem to bind in the same position as both ligands are superimposed. (*S*)3HBA, on the other hand, docked in the opposite direction, with the carboxylic group facing away from FMN.

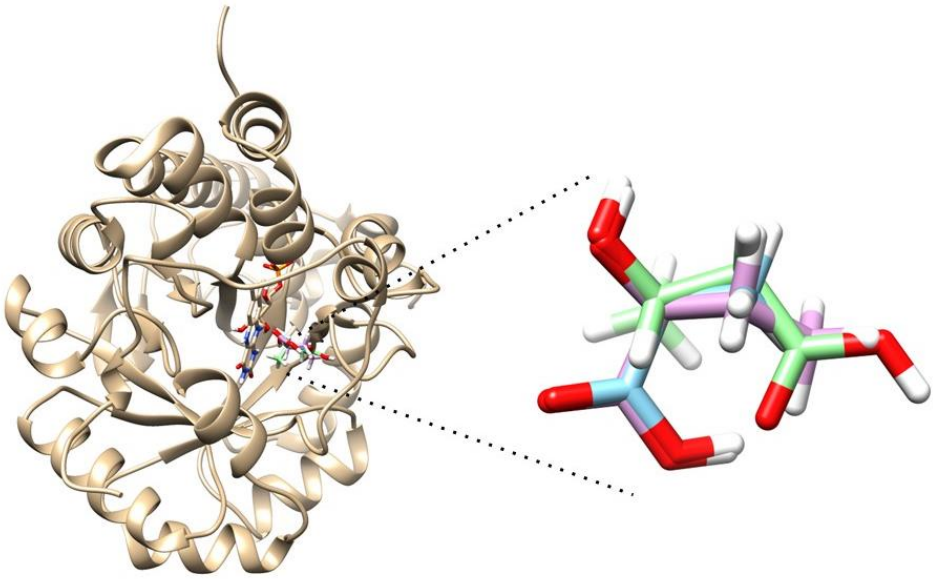

Figure 4. 17. Molecular docking simulation of glycolate oxidase and hydroxy fatty acids. Details show LA (blue), 2HBA (purple) and (S)-3HBA (green) positioned in the active site.

Further investigation on the intermolecular interactions reveals the oxygen in the carboxylic group with the double bond of LA and 2HBA interacts with R249 and Y25 via hydrogen bond, while the oxygen with a single bond in the carboxylic group interacts with R165. The other oxygen present in both ligands interact with His246 and, in the case of 2HBA, R249 also interacts with this oxygen (Figure 4.18. A and B). LA and 2HBA are further stabilized in the active site by alkyl interactions with Leu162. LA interacts with Gln250 and Gly163 via van der Waals interactions. On the other

hand, an additional van der Waals bond is observed between 2HBA and T159 (Figure 4.18. B).

As mentioned above, (*S*)3HBA docked in the opposite direction in the active site, which affects the interactions observed. The carbonyl oxygen of (*S*)3HBA binds to R165, while the other oxygen binds to R249 and G163, opposed to what is observed in the previous ligand described above. H246 and L162 bind to (*S*)3HBA via alkyl interaction. Furthermore, an unfavourable acceptor-acceptor interaction, which is an interaction between two acceptor molecules, is observed between an oxygen in the carbonyl group and R249. (*S*)3HBA, due to its inverse orientation, interacts with differently with amino acids in the active site and likely due to that, the unfavourable interaction prevents catalysis with (*S*)3HBA (Figure 4.18. C).

lines colour-coded according to the interaction type: dark green for hydrogen bonds, light green for van der Waals interaction, pink for alkyl, Pi-alkyl interactions, and red for unfavourable interactions.

4.2.1. Transaminase (CV_TA): Expression, purification and activity

Among the proteins tested, only GO appears to be suitable for the oxidation of hydroxy substrates in the first step of the two-enzyme cascade reaction. Before the cascade was tested, the CV_TA was expressed and purified as above. CV_TA was previous cloned by (Almahboub, Narancic et al. 2018), where the optimum time for induction of protein expression was determined as 4 h. CV_TA was expressed as the other proteins and purified using the same affinity chromatography system. Purification SDS gels indicate that CV_TA has higher expression compared to the previous tested proteins and it elutes as pure protein between fractions 8 to 16 where concentration of elution buffer 500 mM imidazole varies from 40 to 90 % (Figure 4.19.).

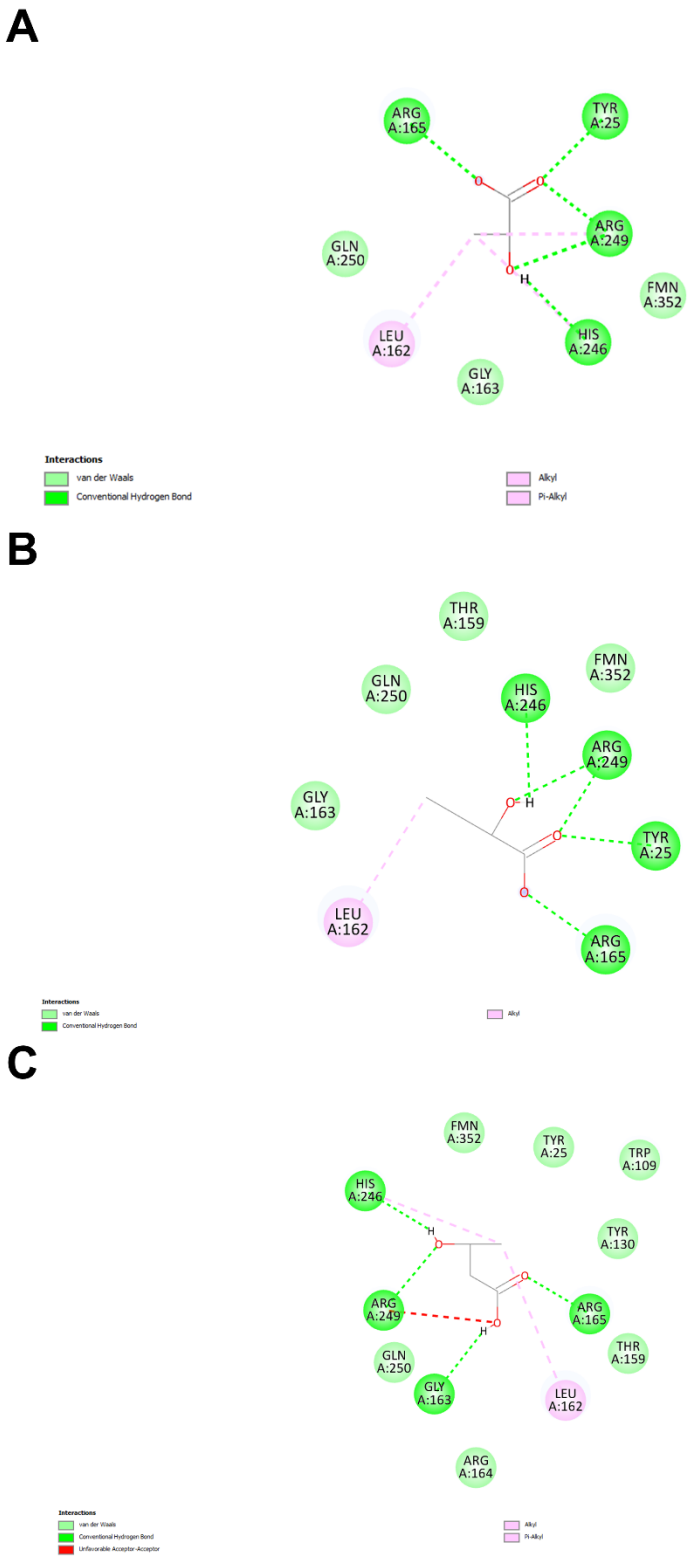

Figure 4. 18. Molecular docking of glycolate oxidase with hydroxy fatty acids. Details of molecular interactions, predicted by molecular docking, between GO and (A) lactic acid; (B) 2-hydroxybutyric acid (2HBA); and (C) (*S*)-3-hydroxybutyric acid

(S3HBA). The interactions between amino acids and the ligands are shown as dotted lines.

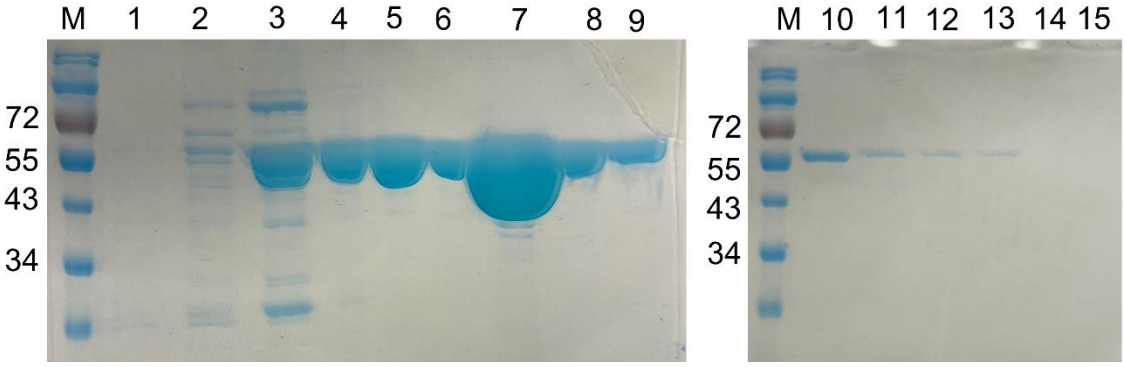

Figure 4. 19. Transaminase (CV_TA) purification. Purification of histidine tagged CV_TA ~55 kDa in a nickel-chelating column with increasing gradient of imidazole concentration. Lanes 1 to 15 represent fractions 4 to 18. EZ-Run ladder prestained Rec protein (M) was used.

Following purification, the activity was analysed as in Section 2.6.4. Its native substrate, pyruvate, was used as an acceptor (2.5 mM) and 4-fold excess of amino group donor 1-phenylethylamine (1-PEA) (Almahboub, Narancic et al. 2018). Upon the transfer of the amino group from 1-PEA, acetophenone (AP) is formed, which can be measured at abs_{245nm}. Various CV_TA concentrations were used, namely 12.5, 25 and 50 µg/mL. A linear-like relationship between protein concentration and CV_TA activity can be observed with R^2 of 0.92. CV_TA activity increased 1.3-fold between 12.5 and 25 µg/mL, while it increased 1.2-fold between 25 and 50 µg/mL (Table 4.2.). As protein activity with 50 µg/mL yield the highest product formation (Figure 4.20. A), it was chosen for the following assays.

Table 4. 2. CV_TA activity tested with pyruvate and several protein concentrations. Protein activity is expressed as the rate of reaction (mM/min/mg).

CV_TA concentration (µg/mL)	Rate of AP production (mM/min/mg)
12.5	1.63 ± 0.29
25	2.27 ± 0.10
50	2.87 ± 0.08

As with GO, the stability of CV_TA activity was tested upon storage at 4 °C and compared to the activity of freshly purified enzyme. CV_TA stored at 4 °C for 10 days maintained similar activity levels (Figure 4.20. B). Figure 4.20. B shows the rate of reaction for all samples under different storage conditions, and these are comparable. These results indicate that CV_TA can be stored for 10 days without losing efficiency.

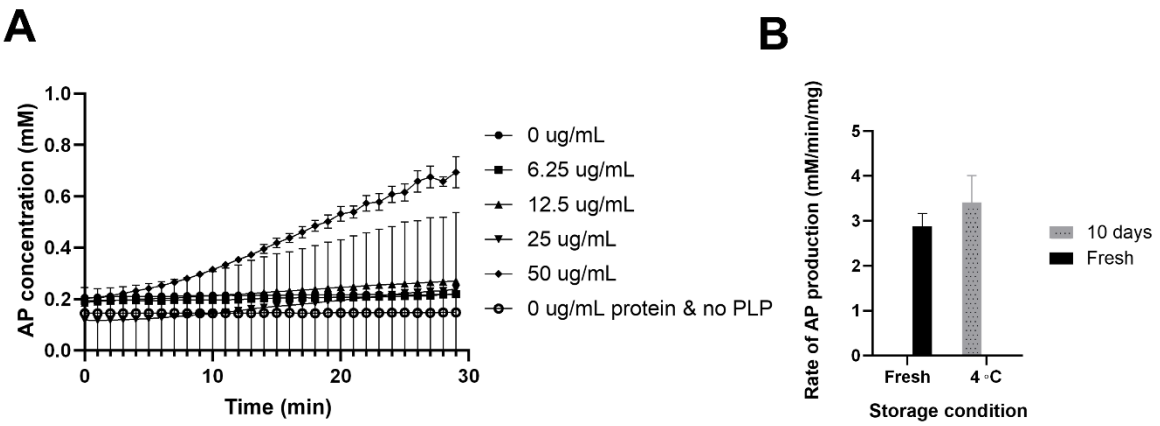

Figure 4. 20. Transaminase (CV_TA) activity. CV_TA activity assay for determination of (A) optimum protein concentration and (B) stability to storage for 10 at 4 °C. Both assays were performed at 30 °C in 20 mM phosphate buffer pH 7.0 with 0.2 mM pyridoxal 5'phosphate (PLP), 2.5 mM pyruvate (substrate) for the detection of acetophenone (AP).

4.2.2. One-pot reaction for the synthesis of α-ncAAs

As GO activity could be detected towards the target substrates, a one-pot reaction combining GO and CV_TA was used aiming to produce α-ncAAs (Section 2.6.6.). The

assay consisted of CV_TA reaction components (0.25 % DMSO, 2.5 mM 1-PEA, 0.2 mM PLP) and GO reaction components (1 mM *o*-dianisidine, 0.2 mM FMN, 2.5 mM DL-LA, 0.1 mg/mL HRP) including 50 µg/mL of both purified proteins. As with the individual assays, the reaction was carried out for 30 min in 200 µL in potassium phosphate buffer pH 7.0. The reaction was monitored by abs_{245nm} for AP formation.

Firstly, the absorbance of all reaction components was scanned from 230 to 500 nm to analyse whether the reaction components of GO reaction did not overlap with AP absorption spectrum around 245nm promoting an additive effect that could overestimate the combined reaction. All components of CV_TA reaction were previously tested and there is no interference around the AP absorbance at abs_{245nm} (Almahboub, Narancic et al. 2018). While *o*-dianisidine seems to have a peak at abs_{230nm}, the detected absorbance decreases from abs_{240nm} to abs_{260nm}, from where the absorbance increases again until around abs_{330nm} (Figure 4.21). None of the other components from GO reaction are likely to interfere with AP's detection. As the interference of *o*-dianisidine in AP detection is unlikely, it was concluded that for the initial screening AP assay may be suitable.

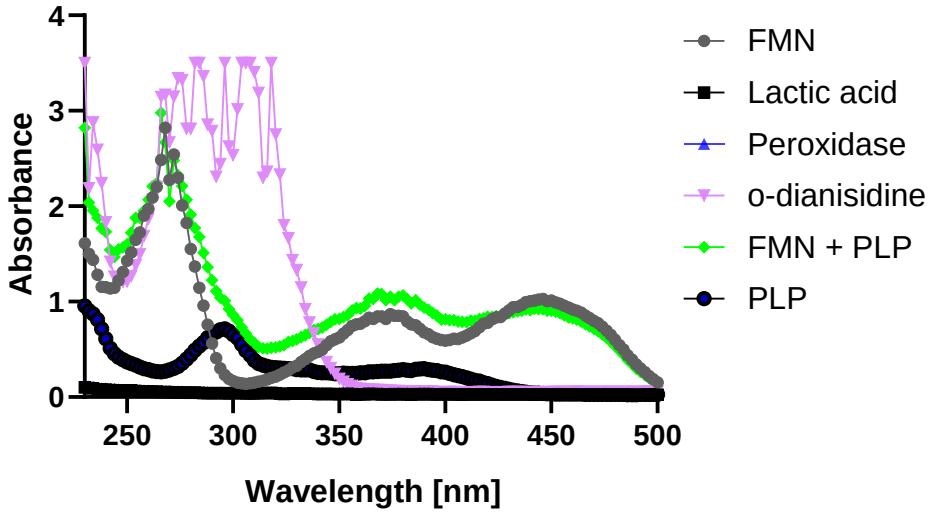

Figure 4. 21. Wavelength scanning of the components present in the two-enzyme assay. Transaminase cofactor, namely pyridoxal 5'phosphate (PLP), and glycolate oxidase reaction components, lactic acid, horseradish peroxidase, *o*-dianisidine, the

cofactor flavin mononucleotide (FMN) and the combined cofactors FMN and PLP were scanned for absorbance abs_{230nm} to abs_{500nm}.

As shown in Figure 4.8., this cascade aimed to produce amino acids from hydroxy acids. For instance, GO performs the conversion of LA to pyruvate, and CV_TA would finally produce L-ala using pyruvate as substrate. 2HBA, 2HHA, and 2HOA were also used in the cascade reaction (Figure 2.3.). Under these conditions no reaction was observed for any of the substrates tested. It was previously observed that the optimum temperature for CV_TA is 45 °C. However, CV_TA shows good activity at 30 °C, which was used in the above assays. To test if the change of temperature may improve the likelihood of the cascade. Unfortunately, GO was not active at 45 °C and no oxidation of the 2-hydroxy substrates was observed.

To verify what is the cause for the lack of reaction, the following parameters were analysed. GO and CV_TA activity assays were carried out independently in the same reaction volume (0.2 mL) and one component from the reaction catalysed by the other enzyme would be included in the same concentration used in the standard reaction (Sections 2.6.2. and 2.6.4.) to assess if any of the assay components have an inhibitory effect. To make it easier to analyse the reaction rate was calculated by measuring the detectable product (mM) per min per of protein added. While DMSO, 1-PEA, or pyruvate had no negative effect on the GO catalysed reaction, in fact the reaction rate in the presence of DMSO and 1-PEA improved 1.15-fold and was similar in the presence of pyruvate (1.3 mM/min/mg). The addition of PLP caused a 4.8-fold lower reaction rate (Figure 4.22 A.). The addition of FMN or *o*-dianisidine to CV_TA reaction caused an increment of 3.3-fold and 2.5-fold in absorbance, respectively. It was observed that FMN, GO's cofactor, completely inhibits the activity of CV_TA, while *o*-dianisidine reduces it (Figure 4.22. B). These results demonstrate that GO and CV_TA reactions are incompatible. Compartmentalization of the reactions, similar to what occurs in cells, can be used to overcome this issue (Oh, Jeong et al. 2023).

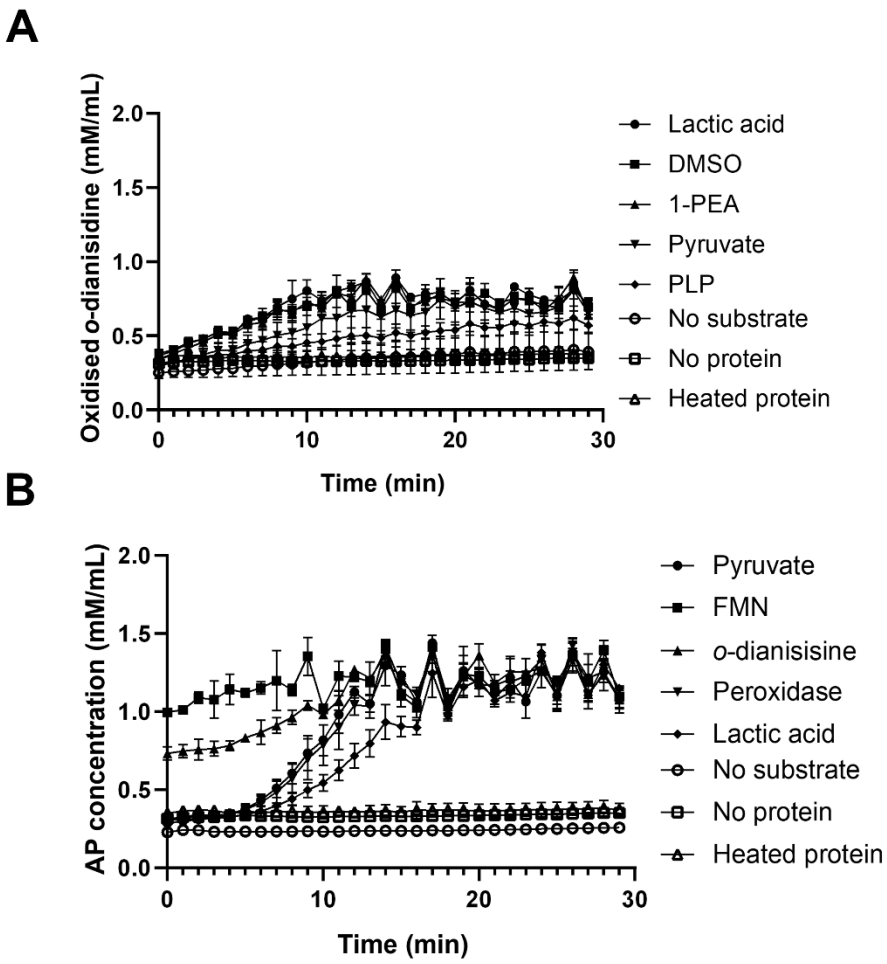

Figure 4. 22. Inhibitory effect in the one-pot reaction. (A) The effect of the transaminase (CV_TA) assay components on the glycolate oxidase (GO) catalysed reaction and (B) GO assay components on the CV_TA catalysed reaction. The reactions were carried out in triplicates adding one component of the other enzymatic assay in the same concentrations used. Pyridoxal 5'-phosphate (PLP) and flavin mononucleotide (FMN) were added at 0.2 mM, 10 mM 1-phenylethylamine (1-PEA), 0.25 % dimethylsulfoxide (DMSO), 2.5 mM pyruvate, 1 mM *o*-dianisidine and 0.1 mg/mL peroxidase.

Therefore, GO activity was tested with decreasing concentration of FMN. As the cofactor concentration used in standard reactions was 0.2 mM, the concentration was reduced to 0.15, 0.1, and 0.05 mM. While reducing FMN to 0.15 mM had no effect in reaction rate, decreasing it to 0.1 and 0.05 mM in improved the reaction rate 1.4-fold (Figure 4.23.). Similarly, PLP concentration was lowered CV_TA reaction to 0.15, 0.1,

and 0.05 mM. No major change in CV_TA activity was observed varying cofactor concentrations (Figure 4.23. B). The one-pot activity reaction combining GO and CV_TA was then tested with 0.05 mM FMN and 0.05 mM PLP at 30 °C, while maintaining the other components as abovementioned. Nonetheless, the activity could still not be detected.

Reports that riboflavin (FMN) dependent enzymes can be inhibited by PLP could not be found, nor that transaminases can be inhibited by FMN. It is known that pyridoxine 5′-phosphate (PNP) and pyridoxamine phosphate (PMP), the aminated version of PLP, can be converted to PLP by a pyridoxine 5′-phosphate oxidase. This enzyme is dependent on FMN, converting the cofactor in $FMNH_2$ (Barile, Nogués et al. 2020).

A leucine dehydrogenase (LeuDH) from *Bacillus thuringiensis* (PDB 8HR6) was previously used to aminate 2-oxobutyric acid and produce 2-aminobutyric acid (Li, Gao et al. 2023). As this dehydrogenase is NAD+/NADH dependent, we hypothesize that NAD(H) would not inhibit GO or the dehydrogenase be inhibited by FMN. The coding sequence of this protein was purchased from Twist Biosciences in pET28a, an expression vector like pET45b, but there was not due time to overexpress and test LeuDH activity.

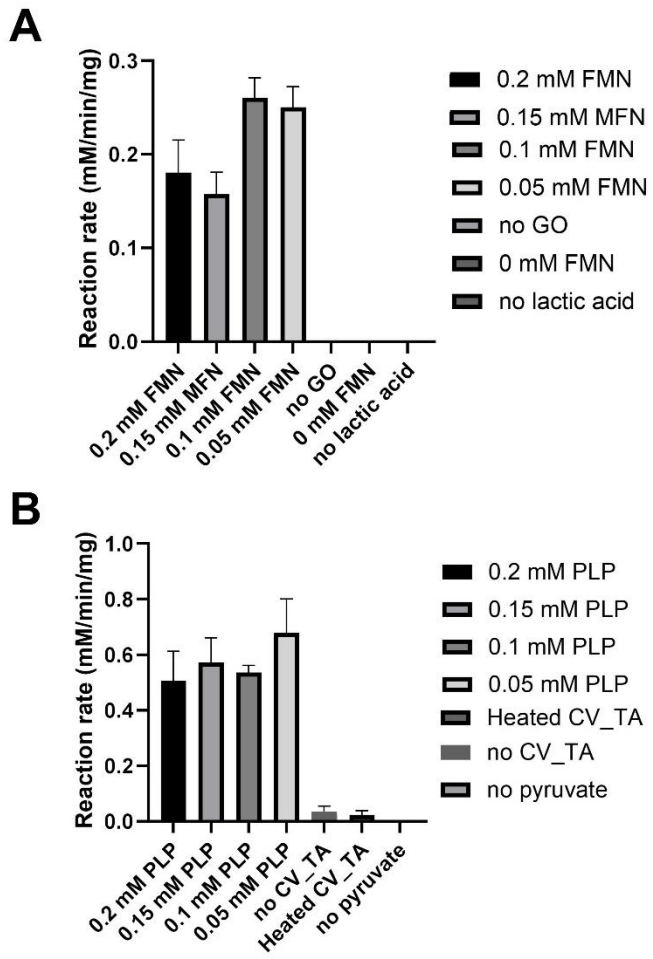

Figure 4. 23. Investigation various cofactor concentration in GO and CV_TA activity. (A) GO tested in various FMN concentrations and (B) CV_TA tested in various PLP concentrations. The assay was carried out at 30 °C for 30 min with 50 µg/mL pure protein, pyridoxal 5'-phosphate (PLP) and flavin mononucleotide (FMN) were added at concentrations varying from 0.2-0.05 mM, for CV_TA activity 10 mM 1-phenylethylamine (1-PEA), 0.25 % DMSO and 2.5 mM pyruvate, while for GO 1 mM *o*-dianisidine and 0.1 mg/mL peroxidase, and 2.5 mM lactic acid were used.

Chapter 5

The effect of the modification of core LFcin peptide with ncAAs

5. Introduction

Antimicrobial peptides (AMPs) are a diverse class of molecules ubiquitous in nature (Tossi, Sandri et al. 2000). AMPs can exert antibacterial, antifungal and anticancer activity (Wang, Li et al. 2016). The activity of AMPs relies on physicochemical characteristics, such as, hydrophobicity, cationicity, amphipathicity, etc (Powers and Hancock 2003). It has been reported that by modulating the said physicochemical properties it is possible to potentialize the antimicrobial activity (Almahboub, Narancic et al. 2018), resistance to proteolytic degradation and even reduce the cytotoxic activity against host cells (Powers and Hancock 2003). The latter is one of the drawbacks for the widespread use of AMPs in clinical treatment.

Our research group previously tested the activity of the bovine lactoferricin (bLFcin) core peptide, 9-mer modified C- or N-terminally, with 2-aminooctanoic acid (2AOA) and compared it to the activity of the unmodified peptide. The results showed that both modifications increase antimicrobial activity against Gram-positive and Gram-negative bacteria, with C-terminal addition of 2AOA being the most potent (Almahboub, Narancic et al. 2018). The present chapter aimed to use a range of α-ncAAs that could be produced using the strategies developed in Chapter 4 to modify bLFcin core peptide and investigate how the size of the hydrophobic chain, and the site of modification (N-terminus vs. C-terminus) affects the structure and activity of LFcin. Thus, the peptide was acylated and aminated with amino fatty acids: 2-aminobutyric (2ABA), 2-aminohexanoic (2AHA), 2AOA and 2-aminodecanoic acid (2ADA).

Furthermore, scanning and transmission electron microscopy were used to study whether membrane is the primary target for the AMP and if the damage could be observed, while circular dichroism was used to analyse whether the ncAAs cause structural changes in LFcin.

5.1. Antimicrobial activity of LFcin modified with ncAAs

With an aim to demonstrate the application potential of the ncAAs produced by the transaminases in Chapter 4, the nonameric (RRWQWRMKK) core peptide of bLFcin was modified with amino fatty acids ranging from 2 to 10 carbons in the acyl chain, C- or N-terminally (Table 2.4.). Modification with these ncAAs increases hydrophobicity,

which is known to play an important role in antimicrobial activity as discussed in section 1.3.2.

It was previously observed that amination of LFcin with 2AOA resulted in improved antimicrobial activity with the tested bacterial strains. The unmodified AMP showed antimicrobial activity to *E. coli* at 400 µg/mL. However, for the other strains tested, this AMP did not exhibit antimicrobial effect in the applied concentrations. However, N-terminally modified LFcin (AOA-LFcin) promoted antimicrobial activity towards *B. subtilis* (400 µg/mL) and *S. typhymurium* (200 µg/mL) and improved the activity towards *E. coli* (100 µg/mL). Furthermore, C-terminal modification (LFcin-AOA) made the AMP more potent to all tested strains and reduced the MIC (Almahboub, Narancic et al. 2018).

The next question was if this effect could be attributed only to the increased hydrophobicity. Therefore, the amino fatty acids shorter than 2AOA (2ABA, 2AHA), and a longer fatty amino acid, 2ADA, were used to modify LFcin core peptide. Secondly, as the effect observed with C-terminally modified LFcin was more profound, the comparison of the activity of the range of amino fatty acids used for N- or C-terminal modification should provide an indication into the type of changes that occur to the modified peptide. For example, if no difference is observed in the activity between the N-terminal or C-terminal modification, and an increased activity is observed with the increase in the chain length, the effect of modification could be attributed to increased hydrophobicity. If the effect differs, this could indicate that the C-terminal or N-terminal modification may induce some structural changes in LFcin as well.

When the antimicrobial activity of the modified LFcin was tested with Lfcin peptide series against the same bacteria, it was observed that the unmodified LFcin had antimicrobial activity against *B. subtilis* and *S. typhimurium*, at 200 and 400 µg/mL, respectively. The MIC for the three other strains, *E. coli*, *P. aeruginosa* and *S. aureus*, was above 400 µg/mL (Table 5.1).

For the modified peptides, based on the MIC assay, it appears that the length of the hydrophobic chain in the ncAAs affects the antimicrobial activity. This trend was observed in the case of *E. coli, B. subtilis*, *P. aeruginosa* and *S. typhimirium*, where the MIC decreased with the increase in the chain length for the amino fatty acid used

for the modification (Table 5.1.). On the other hand, *S. aureus* was not sensitive to LFcin peptide series, excepting 2AOA-LFcin where growth was inhibited at 400 μg/mL peptide (Table 5.1). It is possible that the concentrations higher than 400 μg/mL for the other peptides in the series are needed to have an effect on *S. aureus* as a dose-dependent reduction in OD_{600nm} can be observed for *S. aureus* treated with 2ABA-LFcin, LFcin-2AOA, 2ADA-LFcin and LFcin-2ADA (Figure 5.1.).

C- or N-terminal addition of 2ABA had a varying effect compared to the unmodified LFcin for the tested strains (Table 5.1.). *B. subtilis* was inhibited by LFcin or the modified peptide in either terminal positions by 2ABA at 200 μg/mL while the other strains were not sensitive to LFcin and the modifications with 2ABA. N-terminal modification with 2AHA (2AHA-LFcin) inhibits growth of *E. coli* at 400 μg/mL and *B. subtilis* at 100 μg/mL, while the MIC for the unmodified peptide was 2-fold higher for both strains (Figure 5.1. D). The effect of C-terminal modification with 2AHA was even more pronounced as it has inhibited the growth of *E. coli* at a 2-fold lower concentration compared to the N-terminal modification, while the same MICs were recorded for *S. typhimurium* and *B. subtilis* as with N-terminal modification (Figure 5.1. D and E; Table 5.1.).

When 2AOA was used to modify the LFcin core peptide, the growth of *P. aeruginosa* and *S. typhimurium* was inhibited at 200 μg/mL, regardless of the position of the modification (Figure 5.1. F and G). However, the position of the modification did have an effect when it comes to the three other strains tested. Only N-terminal modification inhibited growth of *S. aureus* at 400 μg/mL (Figure 5.1. F), which is in disagreement with the previous results where only the modification of the C-terminus had an effect (Almahboub, Narancic et al. 2018). The N-terminal modification was also more efficient in the case of *B. subtilis*, where a 2-fold lower concentration was needed to inhibit the growth compared to the C-terminal modification and 8-fold lower concentration compared to LFcin (Figure 5.1. F and G). In the case of *E. coli*, the C-terminal modification was 2-fold more efficient. The other observed MIC values also differed from the previously reported. MIC values can be affected by factors such as density of the starting culture, induction of resistance, and intra or interlaboratory variation (Schuurmans, Nuri Hayali et al. 2009). MIC is also a range between two tested concentrations, not an exact value, and this range can vary depending on technical and biological variations (Mouton, Meletiadis et al. 2018). Therefore, multiple

factors could have contributed to the discrepancy in the results of this study and the previous one. However, overall, it can be noted that 2AOA modified peptides were more efficient than the peptides modified with 2ABA and 2AHA (Table 5.1).

The addition of 2ADA to the N-terminus decreased MIC 2-fold only in the case of *E. coli*, compared to the N- and C-terminal modification by 2AOA respectively (Figure 5.1. F-H). 2ADA-LFcin showed the same MICs as 2AOA-LFcin with *P. aeruginosa* and *S. typhimurium*, while 2-fold higher concentration was needed to inhibit the growth of *B. subtilis*, and the growth of *S. aureus* was not inhibited. C-terminally modified peptide LFcin-2ADA however exhibited a more profound effect, requiring lower concentration to inhibit the growth of *B. subtilis*, *P. aeruginosa*, *S. typhimurium*, and *E. coli* compared to all other variants of LFcin core peptide tested (Table 5.1). Only *S. aureus* was not sensitive in the tested concentrations (Figure 5.1. H and I). It is worth mentioning that some growth of the tested strains was observed at 400 μg/mL (Figure 5.1. I). This could be attributed to the longer lipidic portion of 2ADA oligomerizing or interacting with the polystyrene in the microtiter plate, reducing the potency of the peptide.

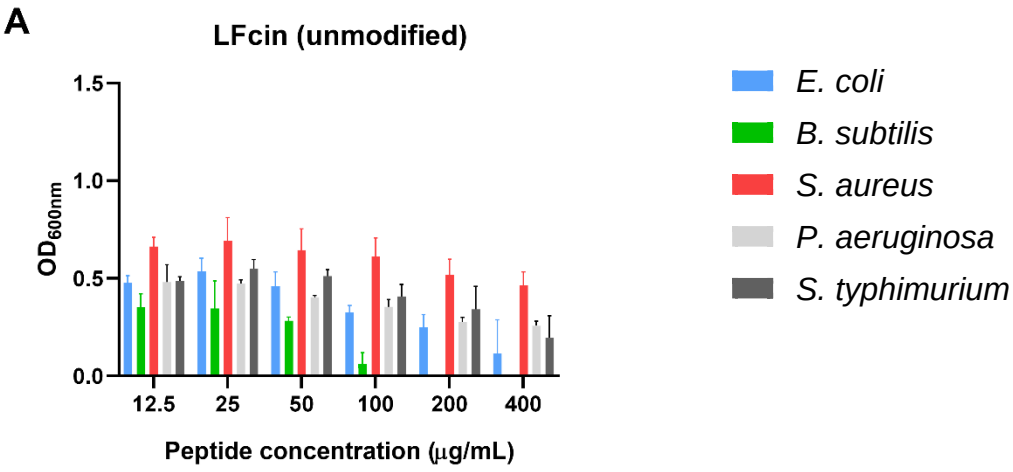

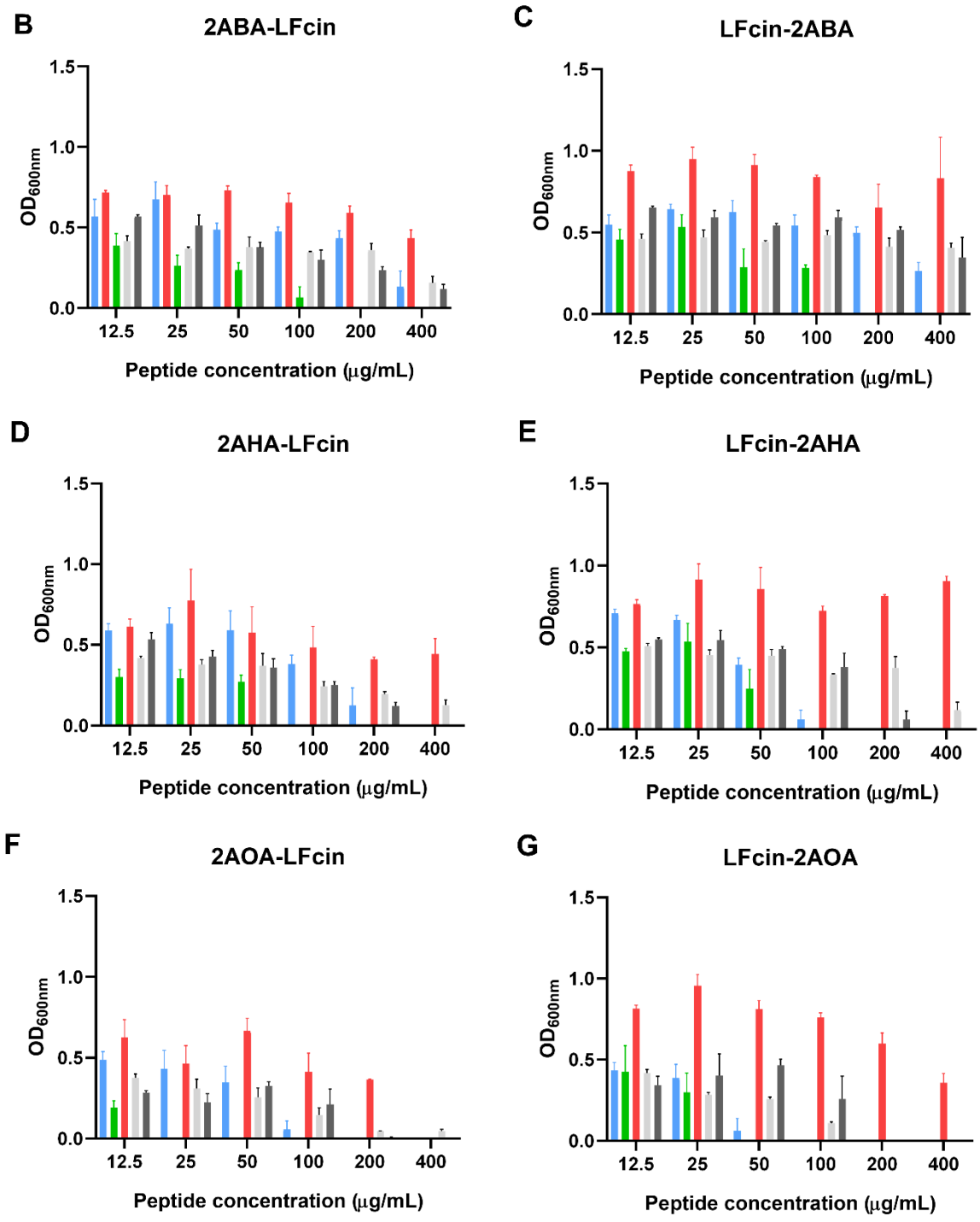
B
2ABA-LFcin
C
LFcin-2ABA
D
2AHA-LFcin
E
LFcin-2AHA
F
2AOA-LFcin
G
LFcin-2AOA
OD600nm
1.5
1.0
0.5
0.0
12.5
25
50
100
200
400
Peptide concentration (μg/mL)

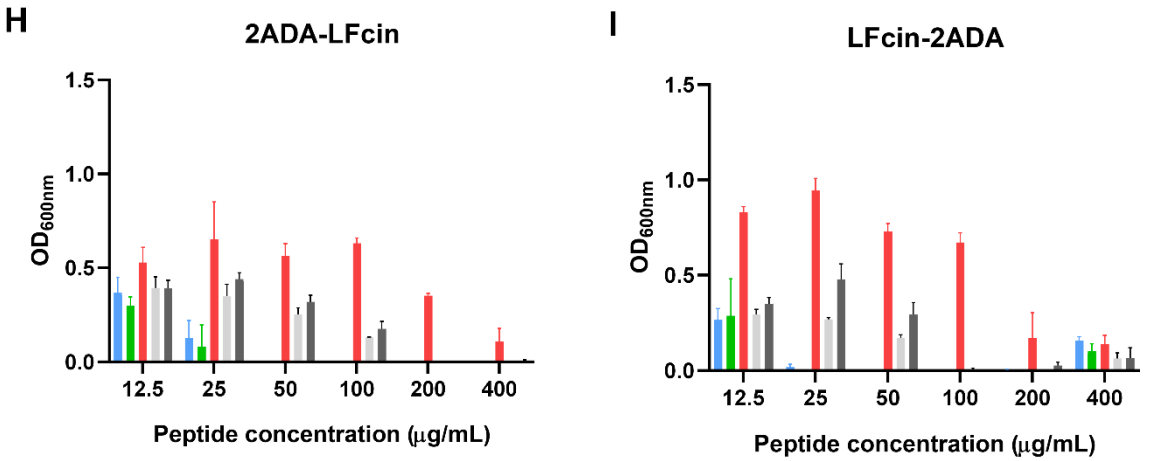

Figure 5. 1. Growth of tested bacterial strains in the presence of a range of concentrations of LFcin and its modified variants. (A) The core amino acid residues of LFcin (RRWQWRMKK), or the variants modified with the following amino fatty acids: 2-aminobutyric acid (B-C - 2ABA), 2-aminohexanoic acid (D-E - 2AHA), 2-aminooctanoic acid (F-G - 2AOA), and 2-aminodecanoic acid (H-I - 2ADA). When the core peptide was modified on N-terminus the following designation was used: 2ABA-LFcin, while LFcin-2ABA was used in the case of a C-terminal modification. The peptides were solubilised in diH2O with 4 % (v/v) DMSO. The assay included the negative controls with LB 4 % (v/v) DMSO, LB and the appropriate peptide concentration, and only LB. As a positive control, each strain was grown in LB and 4 % DMSO.

It seems like the improvement of antimicrobial activity depends on the type of the ncAA used, and the position of the ncAA i.e. C- or N-terminus, as well as the bacterial strain used. Only the N-terminal addition of 2AOA made the LFcin core peptide active towards *S. aureus*, while it was not possible to determine the MIC for *S. aureus* for the other AMPs in the tested concentrations (Table 5.1.). The addition of 2ADA to the C-terminus of LFcin core peptide had the most profound effect on all tested strains, bar *S. aureus*. The C-terminally modified peptide was more efficient in the case of *E. coli* when 2AHA and 2AOA were used too, while N-terminal modification with 2AOA was more efficient in the case of *B. subtilis* and *S. aureus* (Table 5.1). The position of the modification had no effect on the MIC in the case of 2AHA and *B. subtilis* and *S. typhimurium*, and 2AOA and *S. typhimurium* and *P. aeruginosa*.

The common trend appears to be that with the increase in the length of the acyl chain of the fatty amino acids more bacterial strains become susceptible to it. Therefore, an increase in hydrophobicity may be the contributing factor. However, the effect of the position of the modification is also observed, suggesting that the observed behaviour was not only due to the increased hydrophobicity. This would indicate that the modification could also affect the structure of the peptide, or the way it interacts with the bacterial membrane

Table 5. 1. Minimum inhibitory concentration (MIC) of LFcin nonameric antimicrobial peptide unmodified and modified at the C- or N-terminal region with 2-aminobutyric (2ABA), 2-aminohexanoic (2AHA), 2-aminooctanoic (2AOA) and 2-aminodecanoic acids (2ADA).

	MIC (µg/mL)				
AMP	***E. coli***	***B. subtilis***	***S. aureus***	***P. aeruginosa***	***S. typhimurium***
LFcin	>400	200	>400	>400	400
2ABA-LFcin	>400	200	>400	>400	>400
LFcin-2ABA	>400	200	>400	>400	>400
2AHA-LFcin	400	100	>400	>400	400
LFcin-2AHA	200	100	>400	>400	400
2AOA-LFcin	200	25	400	>400	400
LFcin-2AOA	100	50	>400	200	200
2ADA-LFcin	50	50	>400	200	200
LFcin-2ADA	50	25	>400	100	100

5.2. Minimal bactericidal concentration (MBC)

While MIC determines the lowest concentration to inhibit the growth in the liquid medium, the minimal bactericidal concentration (MBC) refers to the lowest concentration to inhibit growth on the agar plate inoculated from the liquid culture used to measure MIC (Bury-Moné 2014). The MBC is usually equal or higher than MIC, but an agent is considered antimicrobial if the MBC is up to four times higher the MIC

(Rodríguez-Melcón, Alonso-Calleja et al. 2021). The MBC was determined by inoculating samples directly from the plate used for the MIC assay in LB 0.1 % NaCl agar plates (section 2.8.2.). If the growth was inhibited by the certain concentration in the MIC assay and bacteria from that well did not grow on the agar, it meant the AMP has a bactericidal effect at that concentration. If the growth was inhibited in the MIC assay, but visual growth was observed on the agar, the effect is said bacteriostatic. In all cases, the MBC/MIC ratio was calculated. If the ratio MBC/MIC ≤ 2, the antimicrobial activity is bactericidal, if 4≤CBM/CIM≤32 the activity is bacteriostatic. For ratios MBC/MIC≥32 the bacteria were considered as tolerant (Lv, Yin et al. 2018). The visual growth inspection on the agar plate was performed after overnight incubation.

Values for MBC/MIC ratios are presented in Table 5.3. Due to the MIC not being detected in several cases, 4≥MBC/MIC≥32 was not observed, which does not mean that the effect is bacteriostatic, only that the bacteria is tolerant for the concentrations tested.

E. coli, S. aureus, P. aeruginosa and *S. typhimurium* were not inhibited by LFcin (Table 5.1.), thus the MBC could not be determined (Table 5.2). No growth on the agar plate was observed for LFcin at 200 µg/mL meaning LFcin appears to have a bactericidal effect for *B. subtilis*. 2ABA-LFcin, 2AHA-LFcin, LFcin-2AHA, LFcin-2AOA and 2ADA-LFcin also exhibit a bactericidal effect on *B. subtilis* (Table 5.3). In this test, LFcin-2AOA and LFcin-2ADA appear to exhibit a bacteriostatic effect on *B. subtilis*. It is hard to explain these differences, and perhaps more biological replicates are needed to get a more accurate analysis. 2AOA-LFcin inhibited the growth of *S. aureus* at 400 µg/mL, but there was visual growth in the agar plate indicating the AMP exerts bacteriostatic activity at this concentrations.

The MIC for *S. aureus* and *P. aeruginosa* was not determined for the tested concentrations when using LFcin modified with 2AHA, thus the MBC was not determined either (Table 5.1.). C- or N-terminal addition of 2AHA inhibited *S. typhimurium* at 400 µg/mL, but the MBC is out of the tested range (Table 5.2.).

There appears to be no clear trend in terms of hydrophobicity and bactericidal/bacteriostatic effect link, nor the position of the modification and bactericidal/bacteriostatic effect link (Table 5.3.). 2AOA-LFcin had bacteriostatic activity for *S, aureus*, and bactericidal effect for *E. coli, B. subtilis* and *S. typhimurium*,

while the (Table 5.3.). LFcin N-terminally modified with 2ADA had bacteriostatic effect for *E. coli* and bactericidal for *B. subtilis, P. aeruginosa* and *S. typhimurium*. However, the C-terminal addition of 2ADA showed bacteriostatic for *E. coli, B. subtilis* and *S. typhimurium*, while it was bactericidal only for *P. aeruginosa* (Table 5.3.).

Table 5. 2. Minimal bactericidal concentration (MBC) of LFcin nonameric antimicrobial peptide unmodified and modified at the C- or N-terminal region with 2-aminobutyric (2ABA), 2-aminohexanoic (2AHA), 2-aminooctanoic (2AOA) and 2-aminodecanoic acids (2ADA).

	MBC (µg/mL)				
AMP	***E. coli***	***B. subtilis***	***S. aureus***	***P. aeruginosa***	***S. typhimurium***
LFcin	>400	200	>400	>400	>400
2ABA-Lfcin	>400	400	>400	>400	>400
LFcin-2ABA	>400	>400	>400	>400	>400
2AHA-LFcin	400	200	>400	>400	>400
LFcin-2AHA	>400	100	>400	>400	>400
2AOA-LFcin	200	100	>400	>400	400
LFcin-2AOA	200	100	>400	400	>400
2ADA-LFcin	200	50	>400	200	200
LFcin-2ADA	400	100	>400	200	400

NA indicates that the MBC and the MIC were higher than the tested concentration and the ratio could not be determined.

The trend observed for improved MIC for *E. coli*, *P. aeruginosa* and *S. typhimurium* regarding increased size of the acyl chain in the ncAA and the position of the modification does not seem to extend to MBC. For *E. coli*, only the addition of 2AHA and 2AOA had bactericidal effect, with the longest ncAA used, 2ADA causing the bacteriostatic effect.

As already mentioned, lipopeptides can oligomerize and this can affect the antimicrobial potency, especially with longer acyl chains. Conversely, addition of long acyl chains, ie. palmitoyl C16, promote peptide micellization, which in the case of short

arginine-rich peptides, peptides micelles are not involved in antimicrobial activity, it is rather the peptide itself (Sikorska, Stachurski et al. 2018). It could also be that the addition of 2ADA somehow changes the mechanism of action of LFcin. This would potentially offer an explanation why 2ADA modifications had bacteriostatic when compared to the other fatty amino acids used, and why there is growth at higher LFcin-2ADA concentration, but bacteria are inhibited when the concentration decreases (Figure 5.1. I).

Table 5. 3. Minimum bactericidal concentration (MBC)/minimum inhibitory concentration (MIC) ratio (MBC/MIC) of LFcin nonameric antimicrobial peptide unmodified and modified at the C- or N-terminal region with 2-aminobutyric (2ABA), 2-aminohexanoic (2AHA), 2-aminooctanoic (2AOA) and 2-aminodecanoic acids (2ADA). If MBC/MIC ratio ≤ 2, the antimicrobial activity is bactericidal; if it is 4≤ CBM/CIM ≤ 32 the activity is considered bacteriostatic; and if the ratio CBM/CIM ≥ 32 the bacteria is considered tolerant to the AMP.

	RATIO MBC/MIC				
AMP	***E. coli***	***B. subtilis***	***S. aureus***	***P. aeruginosa***	***S. typhimurium***
LFcin	ND	1	ND	ND	>1
2ABA-LFcin	ND	2	ND	ND	ND
LFcin-2ABA	ND	>2	ND	ND	ND
2AHA-LFcin	1	2	ND	ND	>1
LFcin-2AHA	>2	1	ND	ND	>1
2AOA-LFcin	1	4	>1	ND	1
LFcin-2AOA	2	2	ND	2	>2
2ADA-LFcin	4	1	ND	1	1
LFcin-2ADA	8	4	ND	2	4

ND – not determined. The MBC and/or MIC was out of the range of tested concentrations.

5.3. Half-maximal inhibitory concentration (IC_{50})

The half-maximal inhibitory concentration (IC_{50}) is a metric which indicates how much of a compound is necessary to inhibit a biological process by half, thus compounds with lower IC_{50} are more potent (Aykul and Martinez-Hackert 2016). It is a more precise measurement than MIC, and it allows the comparison of efficiency of different drugs (Berrouet, Dorilas et al. 2020). The IC_{50} was calculated for the AMPs and bacteria where complete lack of growth was observed in the MIC and MBC assays (Table 5.1).

Widely, the IC_{50} values agree with the observed MICs. The increase in potency with the increase in acyl chain length may be observed (Figure 5.2.). For *B. subtilis* the trend in reduced IC_{50} can be observed when comparing N- and C-terminal modifications separately. The IC_{50} for *B. subtilis* treated with LFcin was 57.66 µg/ mL and it progressively decreases for the C-terminal modification, excepting the IC_{50} for LFcin-2ABA. The IC_{50} for the C-terminal modifications of treated *B. subtilis* was 132.4, 66.7, 25.07, and 6.26 for this strain treated with LFcin-2ABA, LFcin-2AHA, LFcin-2AOA and LFcin-2ADA, respectively. For this modification a 9-fold decrease was observed between LFcin and the modification with 2ADA. Similar results were observed for *B. subtilis* treated with LFcin modified in the N-terminus. Where the IC_{50} for B. subtilis tested with 2ABA, 2AHA, 2AOA and 2ADA was 39.9, 37.7, 2.29 and 2.53, respectively. The effect of N-terminal modification was more pronounced as 22-fold lower IC_{50} is observed between LFcin and the modification with 2ADA (Figure 5.2. A-I). Yet, the reduction in IC_{50} with increased size of the acyl chain was observed to depend on the terminal position of the modification, with C-terminal addition of the ncAAs showing an R^2 of 0.808 and the N-terminal modification showing an R^2 of 0.935 for *B. subtilis*. (Figure S. 1.).

This is not the case for *E. coli*, where C-terminal modification showed lower IC_{50} value when compared to C-terminal modification (Figure J-N). The MIC for *E. coli* tested with LFcin was above. The growth of *B. subtilis* was inhibited by all AMPs tested, and this agrees with the MIC assay, where all of the peptides at MIC ≤ 200 µg/mL showed the growth inhibition. In the case of *B. subtilis*, it can be observed that the IC_{50} decreases as the size of the hydrophobic amino fatty acid increases (Figure 5.2. A-I). For instance, the IC_{50} for *B. subtilis* tested with unmodified LFcin was 57.66 µg/mL,

E. coli was inhibited by LFcin-2AHA, 2AOA-LFcin, LFcin-2AOA, 2ADA-LFcin and LFcin-2ADA (Table 5.1.). The IC_{50} for *E. coli* N-terminally modified with 2AOA and 2ADA was 35.5 and 7.94 µg/mL, respectively. While the C-terminal modification with 2AHA, 2AOA and 2ADA resulted in IC_{50} of 231.6, 17.83 and 2.40 µg/mL, respectively (Figure 5.2. J-N). Like for *B. subtilis*, the IC_{50} values for the modified peptides calculated *E. coli* show there is a linear relationship between longer acyl chains in the ncAAs and lower IC_{50}. The R^2 for *E. coli* treated with LFcin C-terminally modified showed correlation of R^2 = 0.71, while the IC_{50} for E. coli treated with N-terminally modified peptides was R^2 = 0.94 (Figure S. 1.).

These results show that for *B. subtilis* the N-terminal modification with all tested ncAAs is better at improving the IC_{50}, so increasing size of the acyl chain results in lower IC_{50}. For *E. coli* the IC_{50} of only five peptides were calculated, namely LFcin-2AHA, LFcin-2AOA, 2AOA-LFcin, LFcin-2ADA and 2ADA-LFcin. Opposed to what was observed for *B. subtilis*, the C-terminal modification with the said ncAAs was better at reducing the IC_{50} for *E. coli* and the same reduction in IC_{50} with increased length of acyl chain was noted (Figure S. 1.). Although N-terminal modification with 2ADA was 2.3-fold lower when compared to the C-terminal addition of 2ADA for *P. aeruginosa*, it is hard to discuss trends for *P. aeruginosa* or *S. typhimurium*, as only 2ADA modified peptides were used in the IC_{50} calculations.

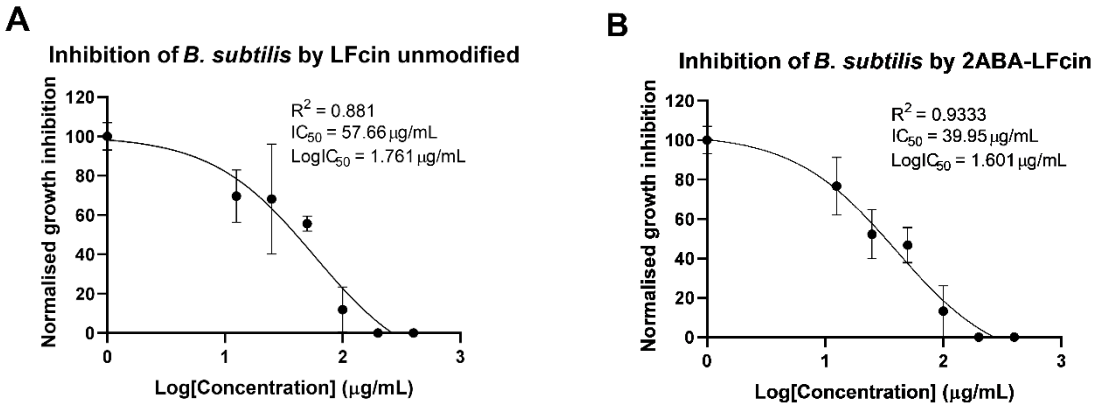

C

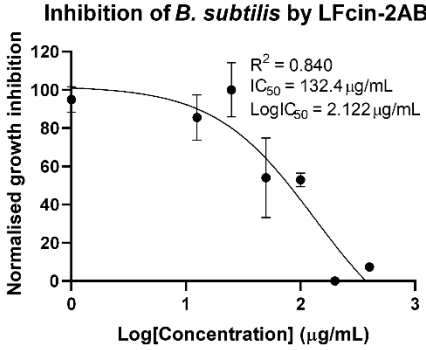
Inhibition of B. subtilis by LFcin-2ABA
R2 = 0.840
IC50 = 132.4 µg/mL
LogIC50 = 2.122 µg/mL
Normalised growth inhibition
Log[Concentration] (µg/mL)

D

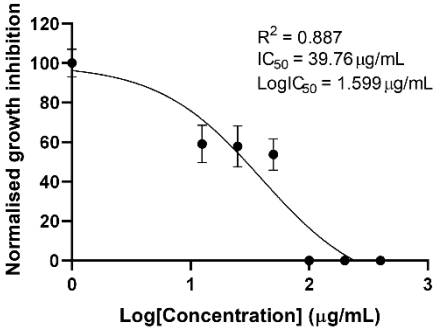
Inhibition of B. subtilis by 2AHA-LFcin
R2 = 0.887
IC50 = 39.76 µg/mL
LogIC50 = 1.599 µg/mL
Normalised growth inhibition
Log[Concentration] (µg/mL)

E

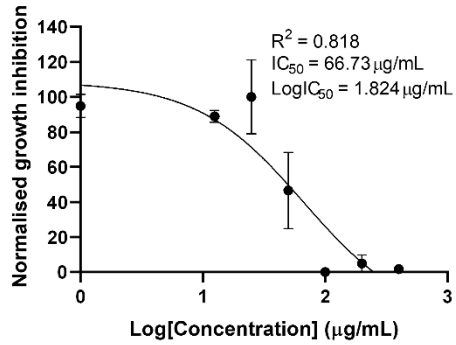
Inhibition of B. subtilis by LFcin-2AHA
R2 = 0.818
IC50 = 66.73 µg/mL
LogIC50 = 1.824 µg/mL
Normalised growth inhibition
Log[Concentration] (µg/mL)

F

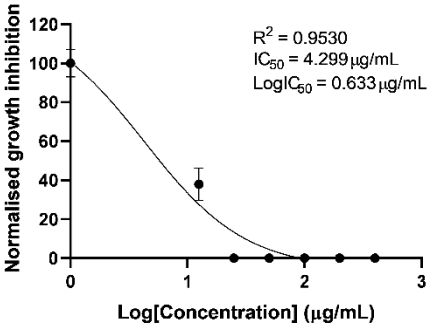
Inhibition of B. subtilis by 2AOA-LFcin
R2 = 0.9530
IC50 = 4.299 µg/mL
LogIC50 = 0.633 µg/mL
Normalised growth inhibition
Log[Concentration] (µg/mL)

G

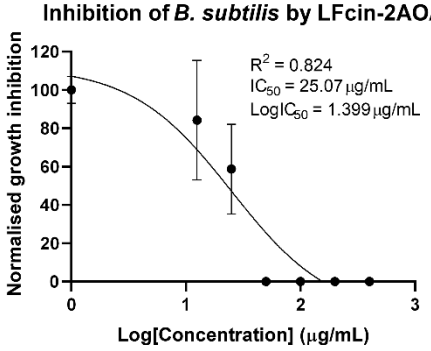
Inhibition of B. subtilis by LFcin-2AOA
R2 = 0.824
IC50 = 25.07 µg/mL
LogIC50 = 1.399 µg/mL
Normalised growth inhibition
Log[Concentration] (µg/mL)

H

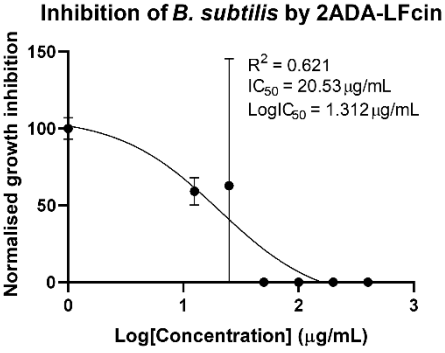
Inhibition of B. subtilis by 2ADA-LFcin
R2 = 0.621
IC50 = 20.53 µg/mL
LogIC50 = 1.312 µg/mL
Normalised growth inhibition
Log[Concentration] (µg/mL)

I

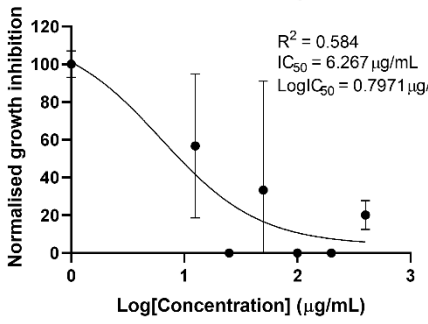
Inhibition of B. subtilis by LFcin-2ADA
R2 = 0.584
IC50 = 6.267 µg/mL
LogIC50 = 0.7971 µg/mL
Normalised growth inhibition
Log[Concentration] (µg/mL)

J

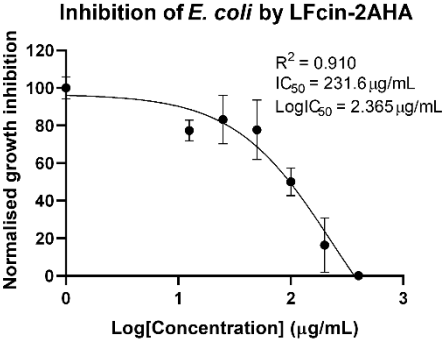
Inhibition of E. coli by LFcin-2AHA
R2 = 0.910
IC50 = 231.6 µg/mL
LogIC50 = 2.365 µg/mL
Normalised growth inhibition
Log[Concentration] (µg/mL)

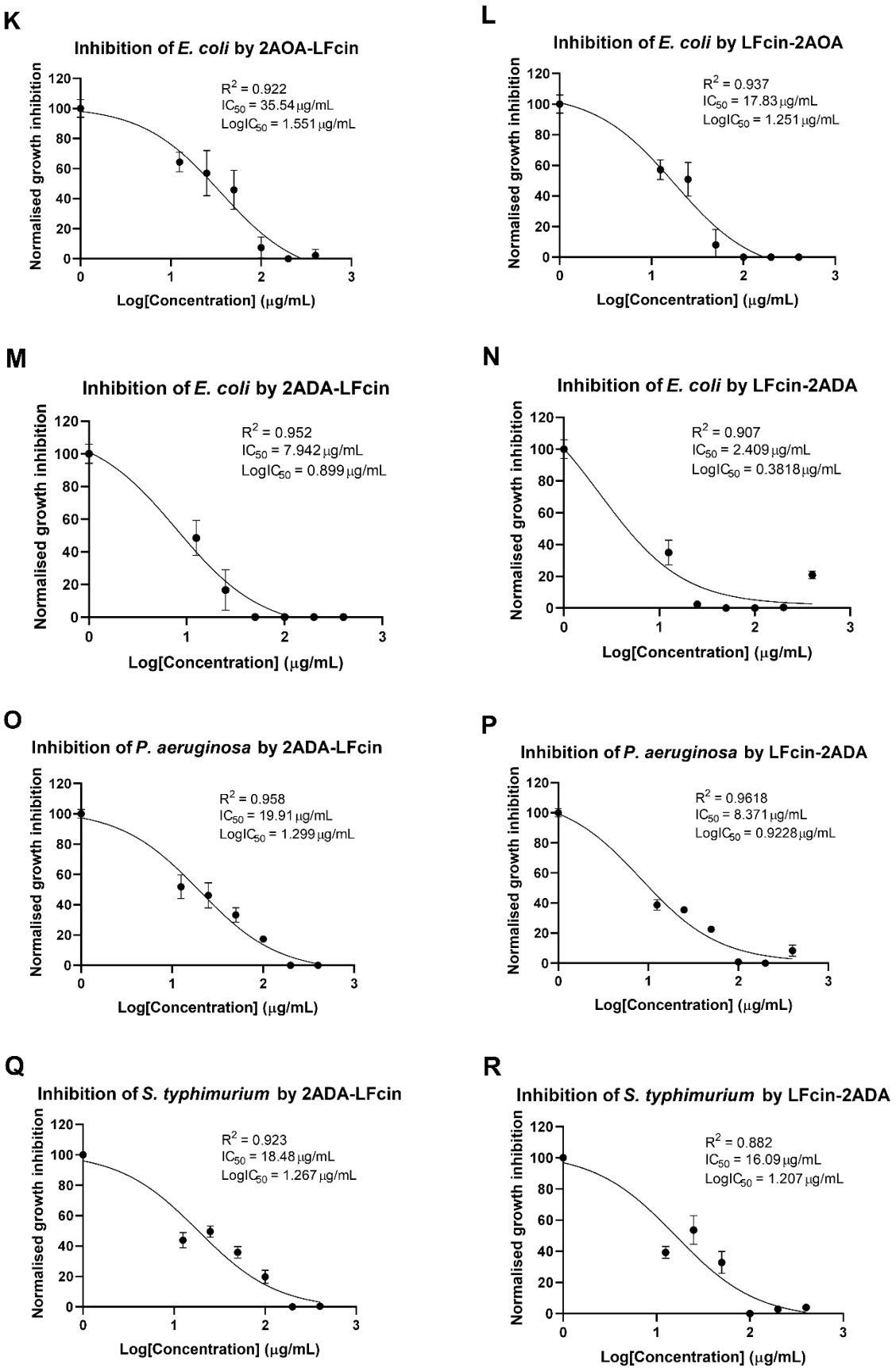

Figure 5. 2. Half maximum inhibitory concentration (IC_{50}) of LFcin peptide series.

IC_{50} for bacteria strains where the growth was completely inhibited in at least one of

the tested concentrations. The IC_{50} was calculated using the Log of the AMP concentration versus the MIC values normalised, followed by a non-linear-three-parameter analysis in Prism – GraphPad 8.0.

5.4. Morphological alterations in *E. coli* and *B. subtilis* caused by LFcin peptide series

Scanning (SEM) (section 2.8.3.1.) and transmission electron microscopy (TEM) (Section 2.8.3.2) were used to investigate if any morphological changes are caused by LFcin core peptide modified with 2AHA, 2AOA or 2ADA. These were selected as a clear effect was observed in MIC assay for *E. coli* or *B. subtilis*, as representatives of a Gram-negative and a Gram-positive strain, respectively. SEM creates images by detecting reflected electrons from a sample that has to be coated by an electroconductive material, ie. platinum, and generates information on the shape and morphology of the sample (John Owonubi, Malima et al. 2020). TEM uses the transmitted electrons through of a biological sample fixed in a plastic resin to generates more detailed images of the membrane and intracellular milieu (Lam, Katti et al. 2021).

The untreated *B. subtilis* cells display a rugged surface under SEM (Figure 5.3.). This could have been caused by DMSO added to the positive control (LB 0.1 % NaCl + 4 % DMSO), or the dehydration process with ethanol (section 2.8.3.1.). However, no pores or other unusual structures that would indicate a membrane damage are observed. When *B. subtilis* was treated with LFcin, on some of the cells it was possible to observe the membrane damage in the form of pore-like structures (Figure 5.3.). However, these structures were not observed in the case of *B. subtilis* treated with C- or N-terminally modified LFcin with 2AHA, which did show lower IC_{50} values compared to the unmodified peptide (Figure 5.3. red arrows). It is worth noting that a lower than MIC concentration was used in these experiments i.e. MIC x 0.5 or MIC x 0.25 to facilitate the growth, while still causing an effect. The pore-like membrane damage can again be observed for 2AOA-LFcin. The effect was more pronounced with LFcin-2AOA. These membrane pore-like structures cannot be observed on *B. subtilis* cells treated with 2ADA-LFcin, while small pore-like structures can be seen on cells treated with LFcin-2ADA. Both MIC and IC_{50} values appeared improved in the case of LFcin modified either N- or C-terminally with 2ADA, however, the membrane damage is not

of the extent observed for the peptide modified with 2AOA (Figure 5.3) As already mentioned, it appears that 2ADA modified LFcin has a bacteriostatic activity for *E. coli* and *B. subtilis*, in the case of Lfcin-2ADA (Table 5.3.). The antimicrobials that exhibit a bacteriostatic effect usually inhibit protein translation via different mechanisms (Lartey, Nellans et al. 1994). This would perhaps mean that the peptide modified with 2ADA would be taken up by the cell, and do not necessarily cause a membrane damage. However, further experiments such as labelling the AMPs with fluorescent tags for cellular localization and cell free translation (Sneideris, Erkamp et al. 2023), would be required to clarify the nature of 2ADA-LFcin and LFcin-2ADA with the target cell.

2AHA-LFcin and both modifications using 2ADA caused membrane damage when *E coli* was incubated in their presence (Figure 5.3.). The unmodified LFcin did not seem to affect the growth of *E. coli*, and this is in the agreement with the lack of inhibitory effect in the tested concentrations (Table 5.1.). The clearest effect was observed when 2AHA-LFcin was used (Figure 5.3., orange arrow). Here, pore-like structures are visible as well as a mass that could be a leaked intracellular content. Differently to what was observed for *B. subtilis*, LFcin C- or N-terminally modified with 2AOA did not result in a visible membrane damage, which is surprising. The MIC for these peptides were lower, and the MBC/MIC ratio indicates they are bactericidal. Addition of 2ADA to LFcin had bacteriostatic activity *E. coli* membranes look undamaged. For bacteriostatic activity and cases where there is no membrane damage, another MOA other than the pore-forming mechanisms can be in place or the membrane lytic mechanism occurs quickly and could not be visualised by SEM.

The control *B. subtilis* sample under TEM shows integrity of cellular membranes and high electron density in the cytoplasm (Figure 5.4.). The samples of *B. subtilis* treated with the unmodified LFcin show the presence of lysed cells, evidenced by ruptured membrane (Figure 5.4. blue arrow), while it could also be noted that the cell wall appears thinner on the non-lysed cells (Figure 5.4. red arrow). Treatment with all the peptide series resulted in similar observations. For instance, *B. subtilis* treated with 2AHA-LFcin shows cells with high electron density, but the peptidoglycan and membrane are not as defined as in control cells. Lysed cells have broken membranes, where cytoplasmic content leaked. This can be observed by lower electron density and heterogeneity in the cytoplasm (Figure 5.4.).

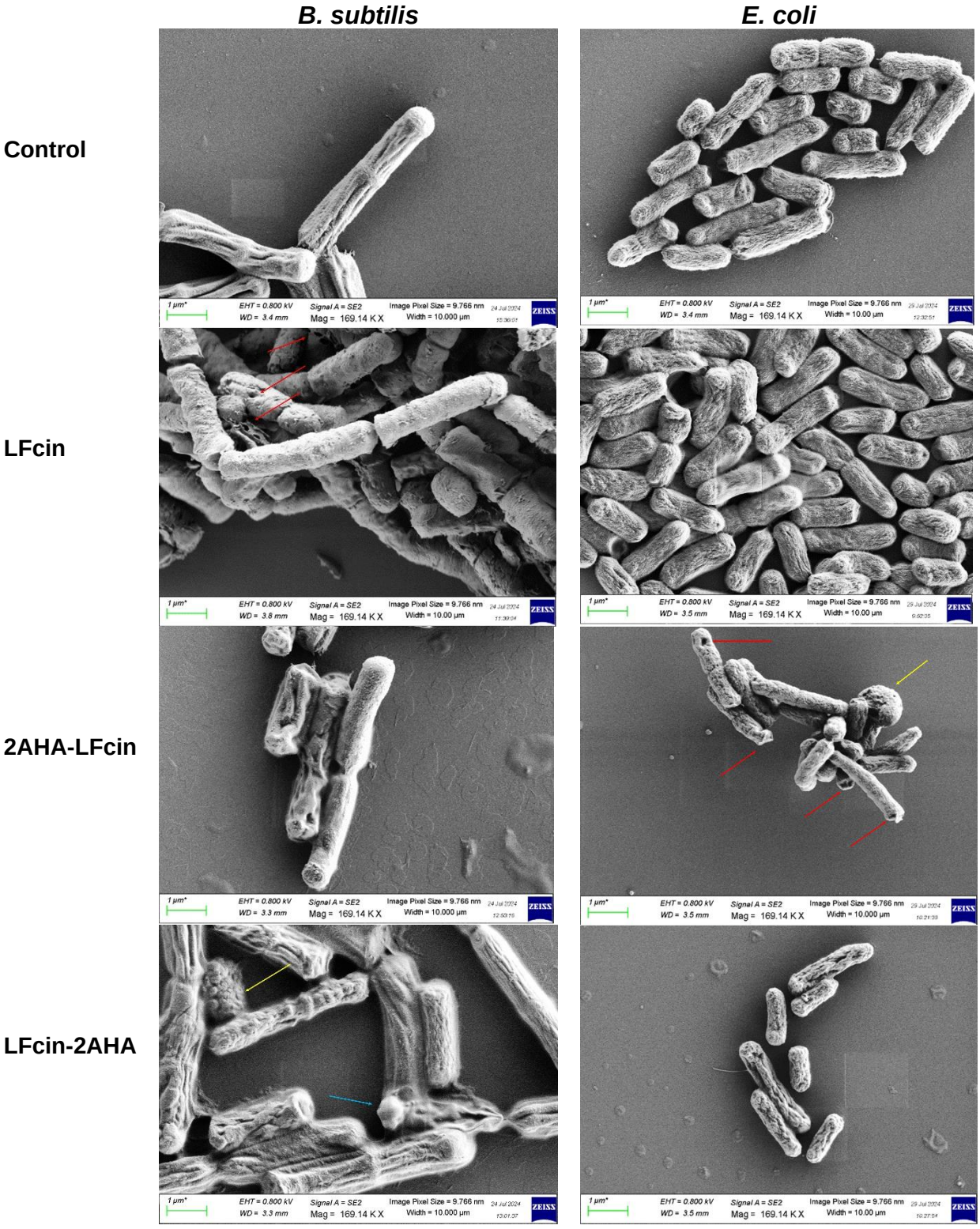
B. subtilis
E. coli
Control
LFcin
2AHA-LFcin
LFcin-2AHA

2AOA-LFcin

LFcin-2AOA

2ADA-LFcin

LFcin-2ADA

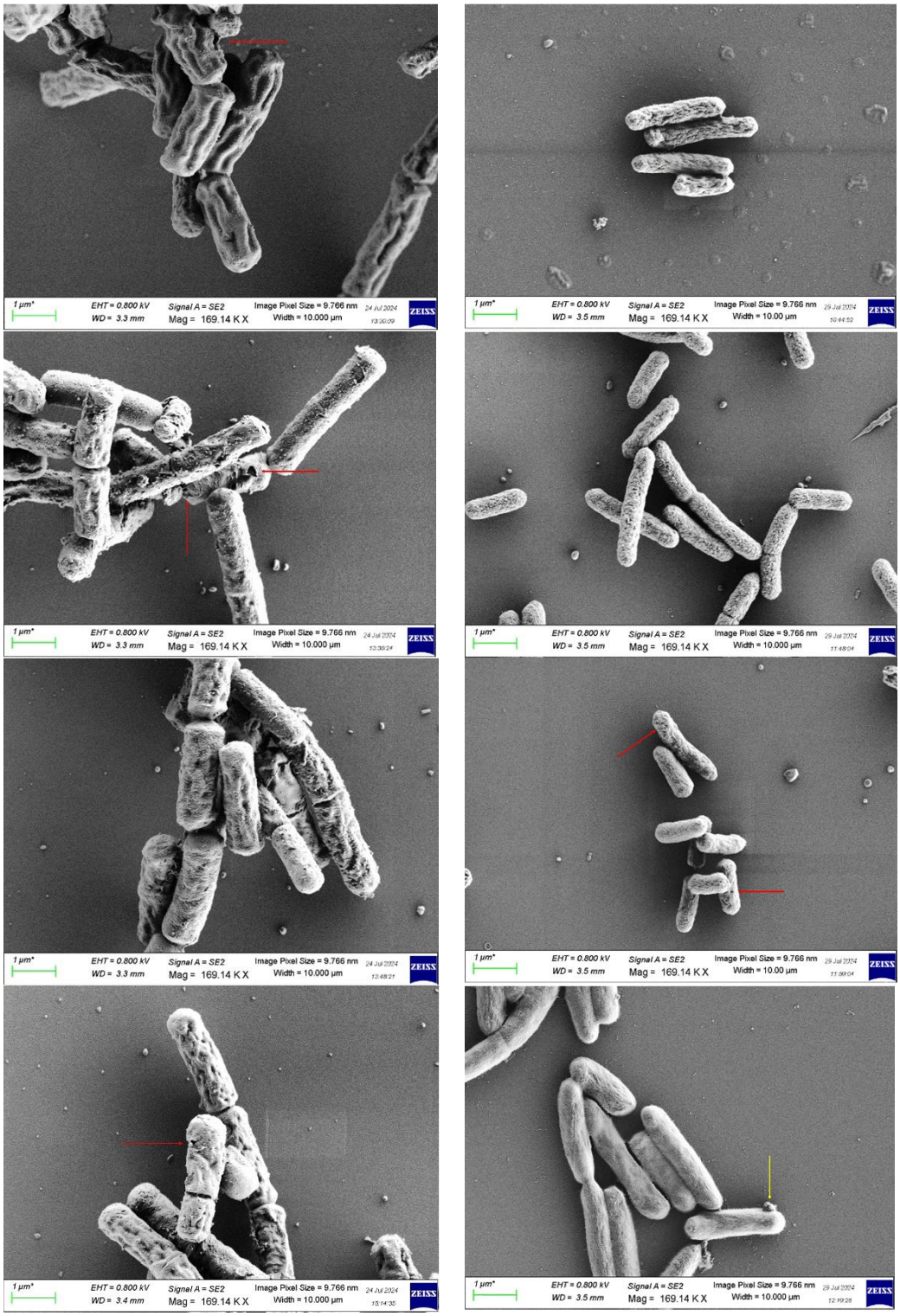

Figure 5. 3. Scanning electron microscopy (SEM) of *B. subtilis* and *E. coli* treated with unmodified LFcin core amino acids and modified C- or N-terminally with 2-aminohexanoic acid (2AHA), 2-aminooctanoic acid (2AOA) or 2-aminodecanoic acid (2ADA). Cells were grown in LB 0.1 % NaCl for 18 h in the presence of the peptides. Red arrows point to membrane alterations, while orange arrows point to putative

cellular content extravasated by treatment with the peptides. It was applied a 67.66 K X magnification, and the scale is 2 μm, shown at the right bottom corner.

Similarly to *B. subtilis* control, *E. coli* control shows membrane integrity with space between the peptidoglycan and cell membrane (Figure 5.4.). In general, treatment with LFcin peptide series on *E. coli* did not appear to have as damaging effect as was observed for *B. subtilis*. Treatment with the unmodified LFcin thins the peptidoglycan layer and the membrane cannot be visualised in the polar region of some cells. *E. coli* treated with LFcin modified with 2AHA, either C- or N-terminally, have lighter density in the cytoplasm, cells with deformed shape and thin membrane. Same can be seen for treatment with 2AOA-LFcin. Treatment with 2AOA-LFcin reveal dead and deformed cells, while cells treated with LFcin-2AOA have structures projecting out on the membrane surface (Figure 5.4.). Most cells treated with 2ADA-LFcin or LFcin-2ADA have the peptidoglycan and membrane undamaged and the space between it and the cellular membrane well-defined. However, the presence of structures protruding from the peptidoglycan are visible for cells treated with all AMPs. As an example, Figure 5.5. (red arrows) show details of these structures in *E. coli* treated with 2ADA-LFcin. These alterations observed are similar to APOL3, which is a host-defence protein that interacts with lipids in the inner membrane of bacteria and forms a lipoprotein with these lipids resulting in a detergent-like cell lysis (Gaudet, Zhu et al. 2021).

	B. subtilis	***E. coli***
Control	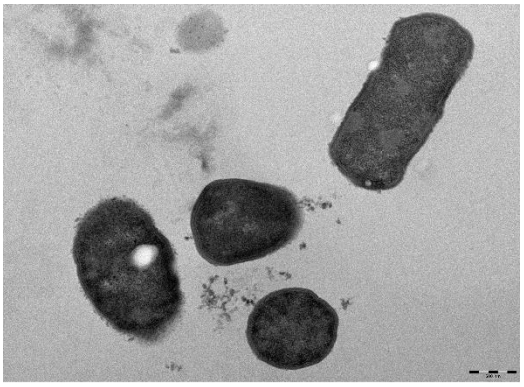	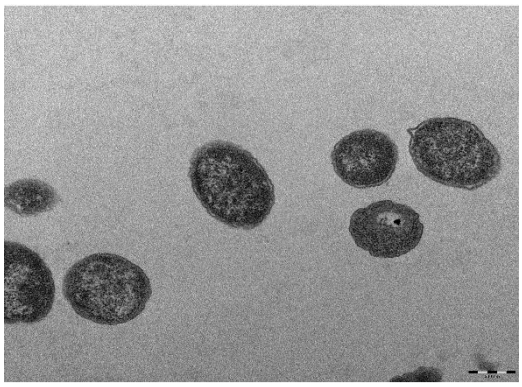

LFcin

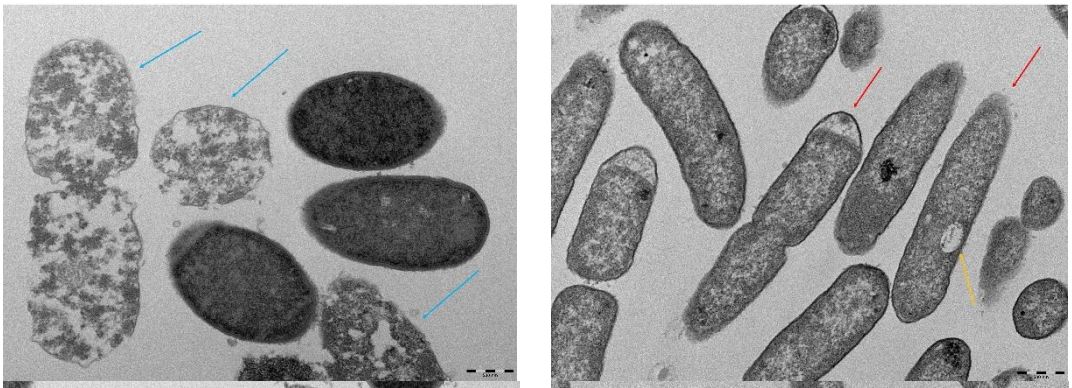

2AHA-LFcin

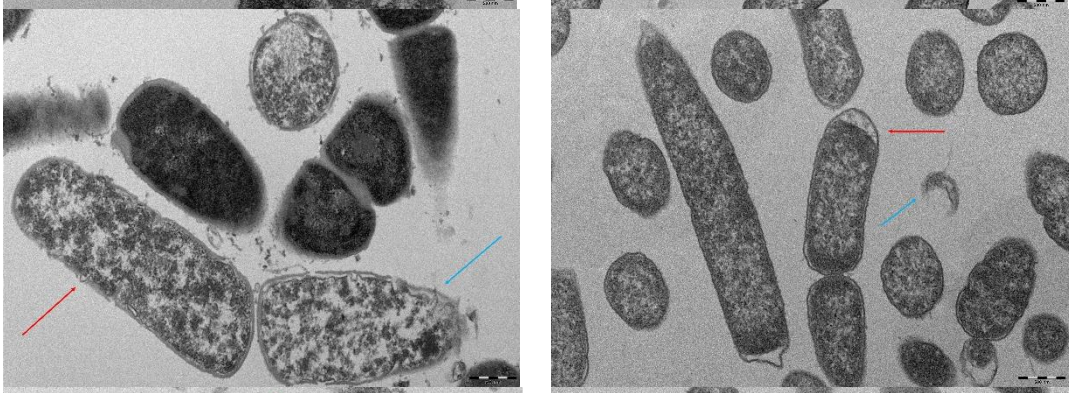

LFcin-2AHA

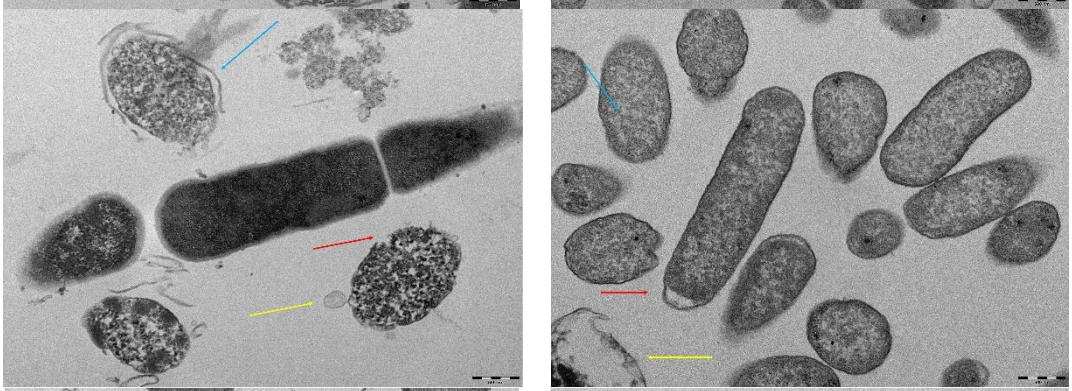

2AOA-LFcin

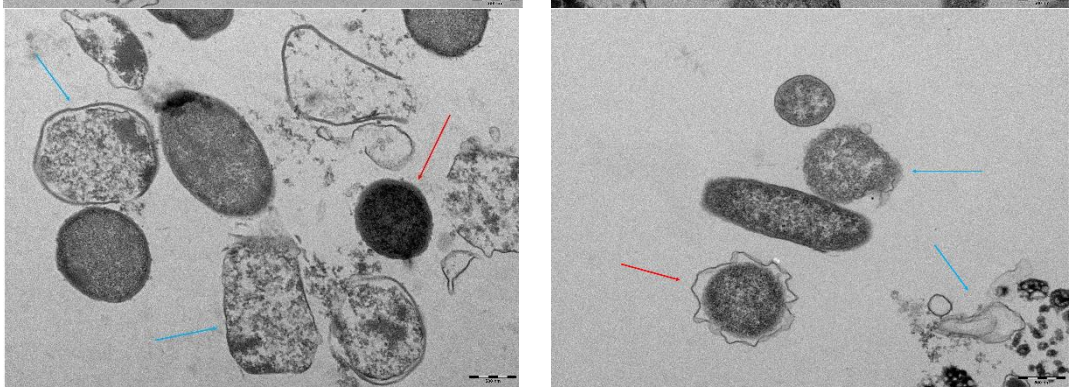

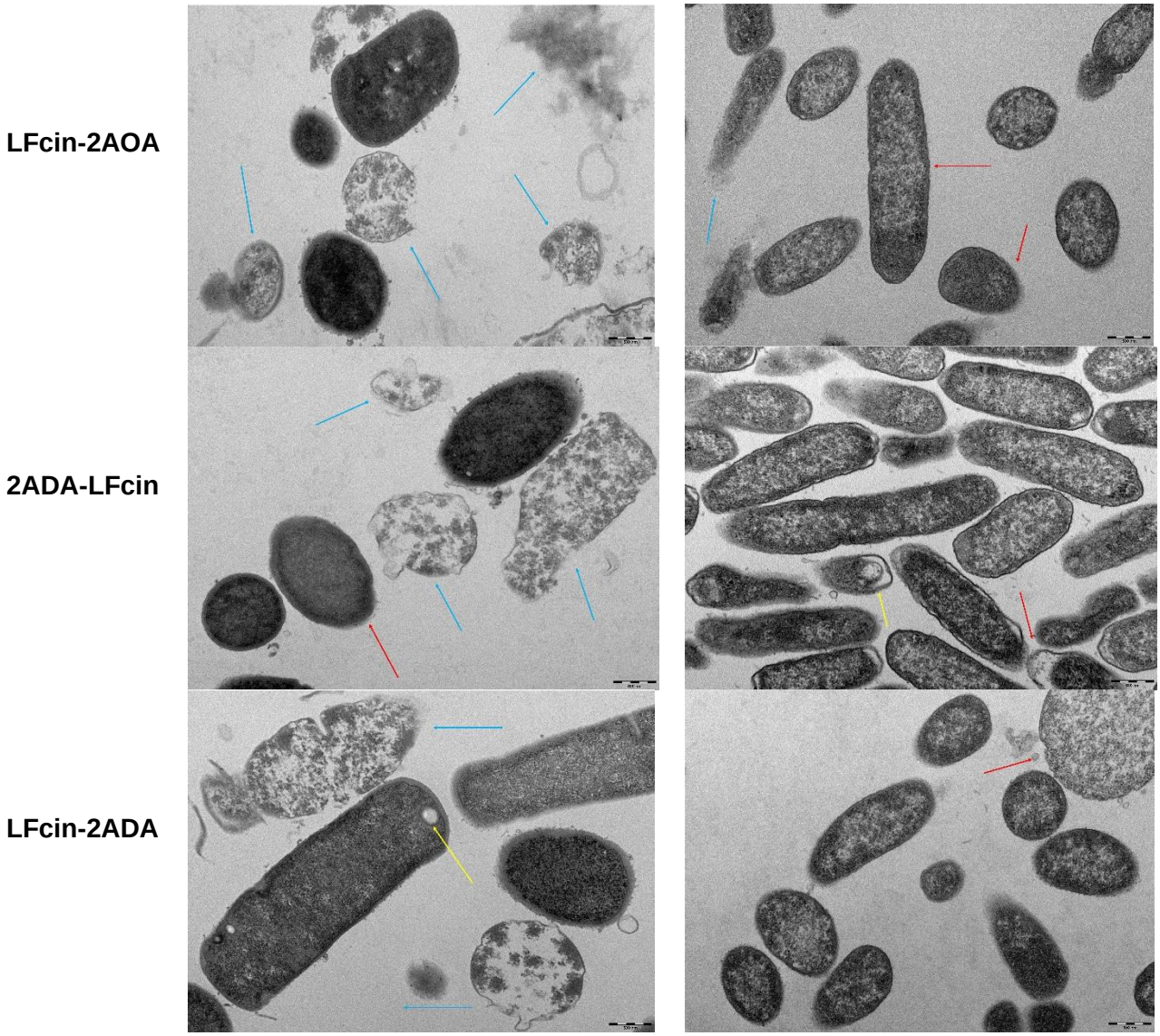

Figure 5. 4. Transmission electron microscopy (TEM) of *B. subtilis*, and *E. coli*. Cells were treated with unmodified LFcin core amino acids and LFcin modified C- or N-terminally with 2-aminohexanoic acid (2AHA), 2-aminooctanoic acid (2AOA) or 2-aminodecanoic acid (2ADA). Cells were grown in LB 0.1 % NaCl for 18 h in the presence of the peptides. Red arrows point to membrane alterations, yellow arrows indicate intracellular alterations, while orange arrows point to putative cellular content extravasated by treatment with the peptides. It was applied a 67.66 K X magnification, and the scale is 2 µm, shown at the right bottom corner with 2 µm.

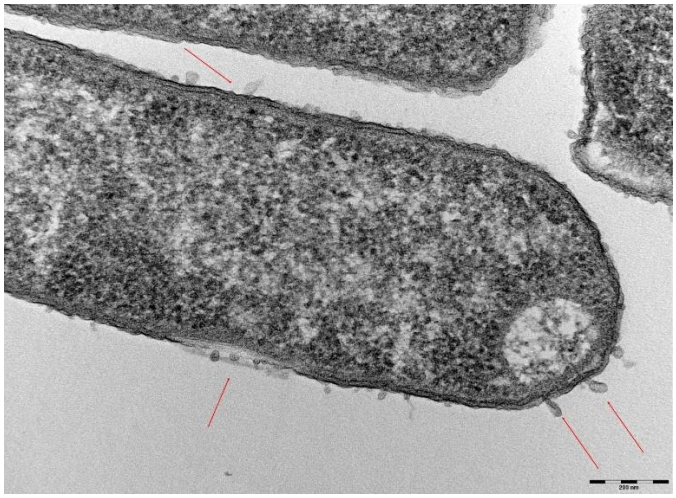

Figure 5. 5. Transmission electron microscopy of *E. coli* treated with 2ADA-LFcin. Magnification of 62000x to show the details of structures protruding out of the cell surface. Scale of 200 nm.

5.5. Analysis of the effect of ncAAs on the structure of LFcin

It was observed that addition of longer amino fatty acids reduced the required AMP concentration for antimicrobial activity of the nonameric LFcin, especially addition to the C-terminus for *E. coli* and N-terminus for *B. subtilis* (Figure S.1.). We aimed to study how the structure of LFcin is affected by addition of the ncAAs. However, modelling tools available like SwissModel (Waterhouse, Bertoni et al. 2018) and Alphafold (Jumper, Evans et al. 2021), require sequences with longer length, 30 and 16 amino acids, respectively, while the modified peptides are only 10 amino acids long. Furthermore, most designing tools only support the use of coded amino acids, and do not support the ncAAs used here.

By using the “Build Structure” tool in UCSF Chimera 1.15. the secondary structure of LFcin was modelled based on ψ and Φ angles between the amino acids of LFcin. Φ angles are found between the nitrogen in the amine group of one amino group and the α-carbon in the next AA, while Ψ angles are observed between the α-carbon and the carbonyl carbon of the same amino acid. Based on this modelling strategy, the LFcin structure an α-helix stabilized by hydrogen bonds (Figure 5.6.)

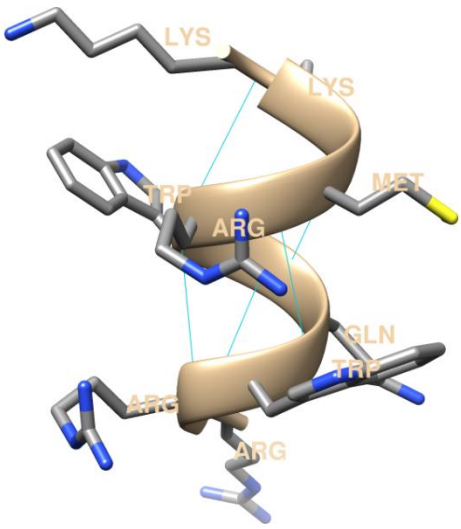

Figure 5. 6. Predicted structure of LFcin. Structure of unmodified LFcin predicted based on ψ and Φ dihedral angles. Hydrogen bonds stabilizing the helix are shown in blue lines. Structure designed on UCSF Chimera 1.15.

Next, circular dichroism (CD) was used to analyse the structure of LFcin core peptide and the modified variants (Section 2.8.4.). The peptide series were tested in physiological conditions using phosphate buffered saline (PBS) and membrane mimicking environments by using SDS and TFE. SDS is known to promote secondary structure, as it mimics negatively charged membranes, while 2,2,2-trifluoroethanol (TFE) appears to stabilize secondary structures (Fort and Spray 2009). In aqueous, or physiological conditions, AMPs can be unstructured, but when in contact with membrane mimicking agents, the same AMPs assume a secondary structure that can be different in SDS and TFE (Sun, Gu et al. 2019).

A similar pattern was observed for all peptides in the three environments tested, with little variation in the secondary structure content. Based on the model (Figure 5.6.), it was expected that LFcin folded as an α-helix. However, the double negative bands at 208 and 222 nm characteristic for α-helical structures were not readily distinguishable in the spectra (Figure 5.7.). When observing all AMPs in three different environments, it can be noted that none of the modifications massively altered the secondary structure, and in particular, no structural differences can be observed between the C- or N-terminal modifications (Figure 5.7.). Moreover, by studying the behaviour of each

AMP it can be seen that the CD spectra of the same peptide is also similar in the three solvents tested (Figure S. 2.).

Based on deconvolution of CD spectra, it appears that an antiparallel β-sheet (anti-β) is the predominant structure in LFcin (Table 5.4.). None of the AMPs showed any percentage of α-helix in PBS, while the % anti-β ranged from 21.2 % in LFcin-2ADA to 32.9 % in LFcin-2AOA. The model designed based on the amino acid sequence does not agree with the experimental data obtained by CD.

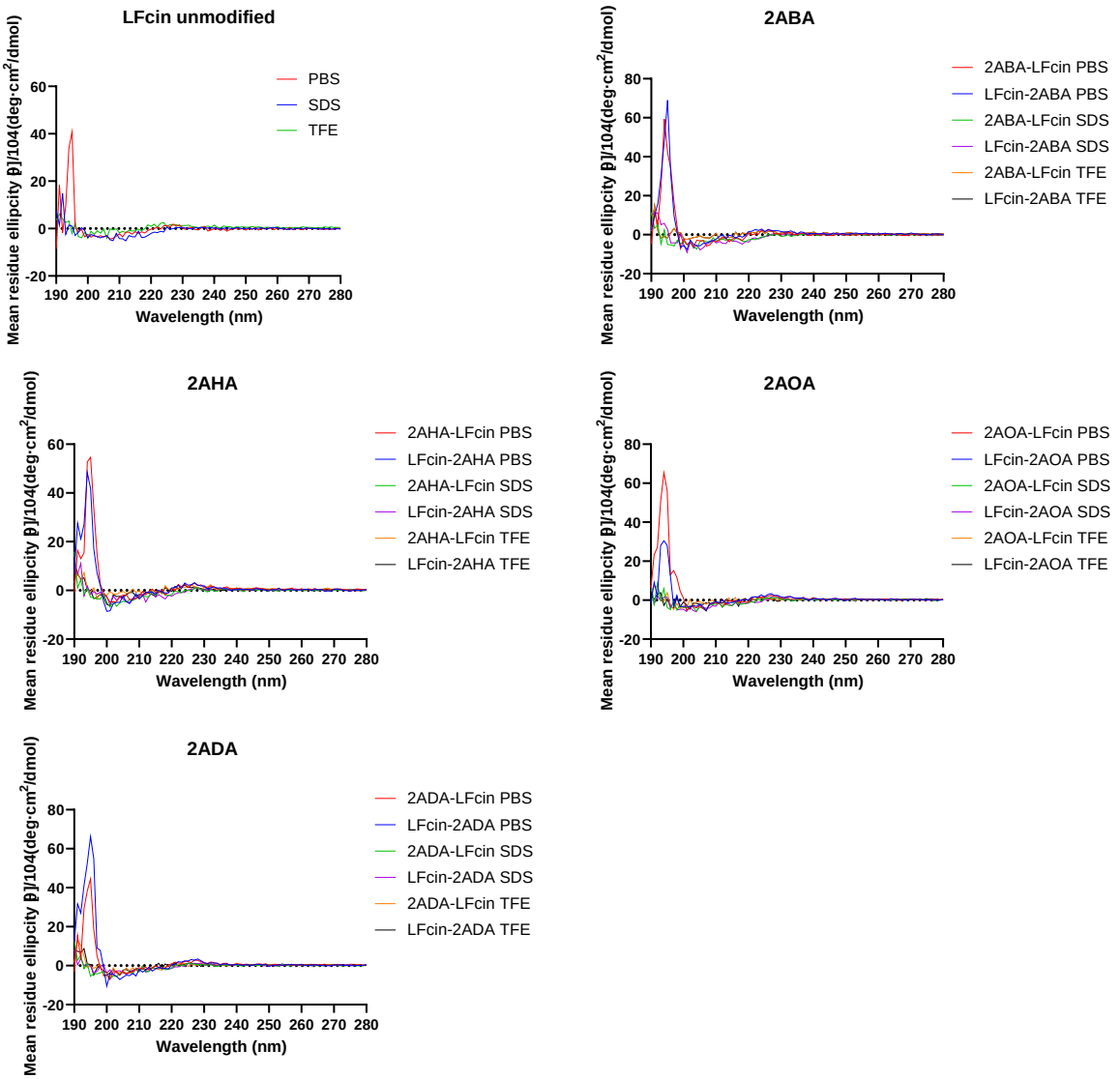

Figure 5. 7. Evaluation of C- versus N-terminal modification of LFcin. Comparison of LFcin peptides series modified with ncAAs either C- or N-terminal. Peptides were tested in physiological environment (PBS) and membrane mimicking environments (SDS or TFE).

Additionally, when the peptides are in a hydrophobic environment i.e. in the presence of SDS and TEF, the % of anti-β increases when compared to PBS, indicating these molecules are more structured in the presence of a bacterial membrane. The minimum % of anti-β was 26.6 % for LFcin-2ABA and the highest was 41.8 % for LFcin-2AOA. α-helix was not observed when the peptides were analysed in the presence of TFE, indicating that the anti-β pattern is more structured in this environment. Similarly, when in SDS, the peptides' structures showed at least 34.2 % anti-β. For the unmodified LFcin and LFcin-2AHA a low percentage of helical structure was observed (Table 5.4.).

As some differences were observed in the activity of the peptides with respect to the position of the modification i.e. C-terminus or N-terminus addition, it was hypothesized that the addition of ncAAs could affect the structure. However, CD spectra for all peptide series is similar for N- or C-terminal addition of the ncAAs regardless of the environment tested (Figure 5.8.).

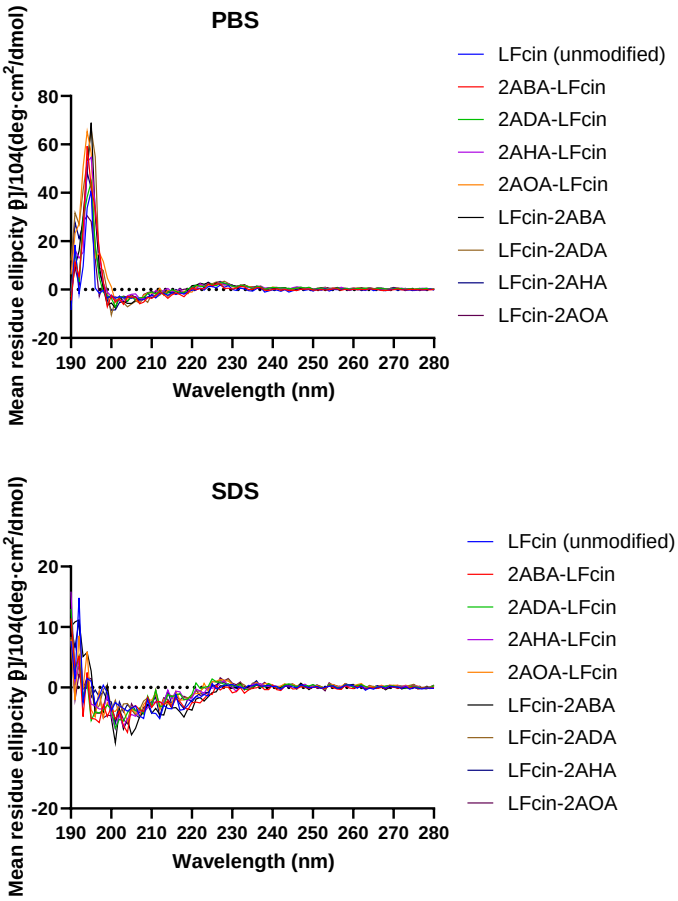

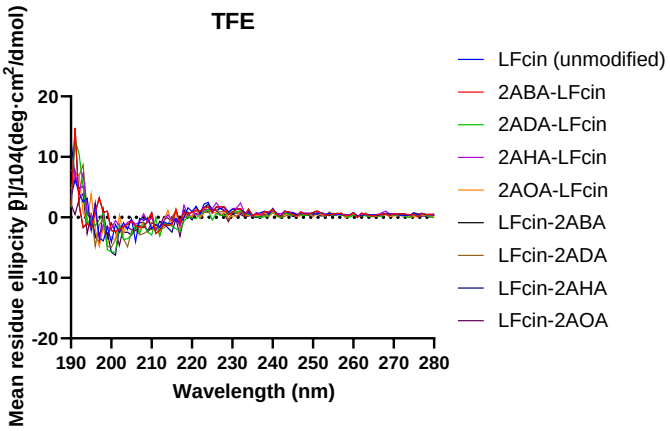

Figure 5. 8. LFcin peptides series comparison in different environments. CD spectra of LFcin peptides unmodified and modified with ncAAs in PBS, SDS and TFE. Results indicate that addition of any of the tested ncAAs did not cause structural alteration in LFcin.

The percentage of anti-β was observed to be higher in SDS and, especially, in TFE. The CD spectra for all peptides were similar when in the three tested environments. Overall, there is no clear correlation between secondary structure alteration and improved activity. Going back to the two hypothesis raised in the beginning of this Chapter, the MIC for *E. coli*, *B. subtilis*, *P. aeruginosa* and *S. typhimurium* is reduced by increasing the hydrophobicity of LFcin using longer ncAAs, rather than altering the secondary structure, as it was observed in CD. As for the second hypothesis, the ncAAs are flanking LFcin and interaction/repulsion with the amino acids in the vicinity may affect the freedom of the acyl chain in interacting with the membrane, which would explain the variation between C- and N-terminal addition of ncAAs. In the first case, membrane permeabilization experiments would shed light on how the AMPs directly affect the lipids in the membrane, while for the latter, 2D or 3D Nuclear Magnetic Resonance (NMR) could be used to elucidate the structure of the peptides in solution and reveal how the ncAAs are interacting with the environment and amino acid side chains.

Table 5. 4. Percentage of secondary structures formed by LFcin peptide series. Deconvolution of Circular Dichroism (CD) data calculated on BestSel of LFcin peptide series tested in PBS, TFE and SDS.

	Secondary structure content (%)								
	PBS			TFE			SDS		
	A	Anti-β	Turn	α	Anti-β	Turn	α	Anti-β	Turn
LFcin (unmodified)	0	32.2	10	0	35.4	17.1	1.6	40.9	12.8
2ABA-LFcin	0	23.3	6.3	0	35.2	15.4	0	38	14.1
LFcin-2ABA	0	21.6	6.8	0	26.6	20.4	0	38.7	13.5
2AHA-LFcin	0	24.4	6.9	0	41	15.8	0	37	14.5
LFcin-2AHA	0	23.7	8.9	0	36.6	16.7	1.2	34.8	14.6
2AOA-LFcin	0	23.6	4.6	0	41.5	17.3	0	36.2	14.6
LFcin-2AOA	0	32.9	9.2	0	41.8	14.6	0	37.8	14.7
2ADA-LFcin	0	27.7	8.3	0	36.1	17.3	0	38.2	14.7
LFcin-2ADA	0	21.2	3.5	0	37.3	16.8	0	38.5	13.5

Chapter 6

Discussion

The present work aimed to develop biotechnological approaches to synthesize hydroxy and amino fatty acids. Advances in science allowed the discovery of genes with new functions and novel proteins with higher catalytic efficiency (Bauman, Butler et al. 2021). That, aligned with the advances in laboratory techniques, such as, molecular assembly (Gibson, Young et al. 2009) and CRISPR/Cas9 (Cook, Rand et al. 2018), enabled the development of tailored organisms or reactions to produce a target molecule.

In the scenario of biotechnology, whole-cells or cell-free systems, using cell lysates or purified enzymes, can be used to perform a reaction, each has its advantages and disadvantages (Hughes and Lewis 2018). In whole-cells, native cellular pathways can be used as one of the steps in a synthetic pathway, for example, a recombinant system can make use of the metabolites generated from the hydrolysis of glucose in the TCA cycle, as it was demonstrated in Chapter 3. This makes whole-cell process less costly. However, the number of components in the cell may interact with byproducts and inhibit the process, in this regard, cell-free system is more tolerant to inhibition by by-products, products or metabolites (Claassens, Burgener et al. 2019).

Catalysts, chemical, organo- or biocatalysts, are an essential part of industry, as they are used to reduce the energy necessary for a reaction to occur, thus reducing the time (Ney, Jawad Nasim et al. 2018). The catalysis market is valued in about $15 billion worldwide and around 95 % of industrial processes require a catalyst (Hedayati Marzbali, Hakeem et al. 2024). In the past decades there was a shift from chemical to biocatalysis and more recently the concept of circular bioeconomy has been implemented aimed to align economic development with sustainable practices (Mesa, Sierra-Fontalvo et al. 2024).

The distancing from chemical catalysis is promoted by higher conversion rate, stereoselectivity, non-toxic solvents and operation under milder conditions in biocatalysis (Biernacki, Riechen et al. 2017, Gezae Daful, Loridon et al. 2024). Additionally, the United Nations launched in 2015 the Sustainable Development Goals, which are 17 Goals to promote a more sustainable society model (UnitedNations 2015). These goals are directly related to the 12 Principles of Green chemistry, which aim to make use of safer solvents and biocatalysts, when possible, to reduce the generation of toxic waste or byproducts, and to improve the energy efficiency

(Ivanković 2017). Furthermore, the European Commission developed the Safe and Sustainable by Design frameworks that, similarly to the other two cited, creates an holistic approach to develop greener processes for manufacturing and to deal with the end-of-life materials, and at the same time, study how these innovations affect society and health to implement policies (Apel, Sudheshwar et al. 2024, EuropeanCommission 2024).

6.1. Microbial synthesis of 3-hydroxybutyric acid

Biocatalytic approaches have been applied for the synthesis of various molecules, including 3-hydroxybutyric or β-hydroxybutyric acid (3HBA, βHBA). βHBA is a hydroxycarboxylic fatty acid naturally found in animals, plants and bacteria (Mierziak, Burgberger et al. 2021). Species of bacteria, like *Cupriavidus necator*, naturally produce 3HBA which is quickly polymerised into poly-3-hydroxybutyric acid (PHB) (Bellini, Tommasi et al. 2022). In these organisms, PHB is produced as a carbon and energy storage polymer when excess of carbon and a limitation of an inorganic element, such as phosphorus or nitrogen is present (Mohanrasu, Guru Raj Rao et al. 2022). The depolymerization of PHB by a depolymerase PhaZ occurs naturally and results in the crotonic acid that can be utilized to produce more PHB or readily used for energy (Eggers and Steinbuchel 2013)

βHBA is a commodity chemical used as a scaffold for the synthesis of fine chemicals. For example, the derivative of (*S*)3HBA, ethyl (*S*)3HBA, was used as substrate for the chemical synthesis of a carbapenem antibiotic in a 6-step method (Chiba and Nakai 1987). βHBA is also a precursor of the short-chain ester named butyl butyrate, which is used in industry as fragrance and flavour additive (Noh, Lee et al. 2019).

Recombinantly, 3HBA can also be obtained by producing PHB followed by its depolymerization. This can be achieved by overexpressing PhaA, 3-hydroxybutyryl-CoA dehydrogenase, and PHB polymerase, which will result in PHB, and further overexpressing a PHB depolymerase PhaZ. However, the two-step synthesis of 3HBA requires the initial production of PHB and its depolymerization by the methods mentioned in Section 1.1.2. The extraction and separation steps required solvents, such as acetonitrile and controlled temperature and pressure, which increases costs and makes this approach less desirable (Ruth, Grubelnik et al. 2007).

Our group has previously designed a 3-gene synthetic pathway for the microbial synthesis of 3HBA (Liu 2020). This pathway includes an acetoacetyl-CoA β-thiolase PhaA from *C. necator*, which condenses two molecules of acetyl-CoA into acetoacetyl-CoA (Figure 1.2.). An (*R*)-3-hydroxybutyryl-CoA dehydrogenase (RHBD), or (*S*)-3-hydroxybutyryl-CoA dehydrogenase (SHBD) were used to reduce acetoacetyl-CoA into (*R*)-3-HB-CoA or (*S*)-3-HB-CoA. The corresponding genes which encode the two enzymes are *phaB* or *paaH1,* respectively, both from *C. necator*. Finally, the cleavage of -CoA has to take place to allow for the product to be secreted, and two thioesterases were analysed for this role: TesB from *E. coli* K12 or BCH from *Bacillus cereus* ATCC6630. The combination *bch_phaA_RHBD* yield the highest synthesis of RHBA, while *tesB_phaA_SHBD* resulted in high SHBA synthesis. All genes were placed under the T7 promoter, yielding a polycistronic transcript in *E. coli* BL21. Strong ribosome binding sites (RBSs) were placed between the genes to ensure the expression of individual enzymes. In flasks, using the corresponding pathways, 2.13 g/L (*S*)3HBA, and 2.11 g/L (*R*)3HBA were produced (Liu 2020). As LB supplemented with 10 g/L glucose was used as a production medium, acetate production was detected in both cases, with 0.7 g/L acetate accumulated in the supernatant. The excess glucose in *E. coli* usually converts to acetate that is secreted in the medium (Harden 1901).

Similar results were observed during (*R*)3HBA production in *E. coli* JM105, DH5α and BW25113 (Liu, Ouyang et al. 2007). The genes were supplied on different, or same plasmid, and 1.5 and 3.98 g/L of (*R*)3HBA were produced. This was also accompanied by acetate production (Liu, Ouyang et al. 2007).

Among other reasons, it is believed that *E. coli* secretes acetate to acidify the environment and inhibit the growth of competing bacteria (Sengupta, Ekka et al. 2017). However, for biotechnological applications, carbon spillage is undesirable because it diverts carbon from the target product. In addition, as acetate is the product of glucose catabolism, it will inhibit the glycolysis. Two potential routes to address acetate byproduct are metabolic engineering to remove the key players in acetate production, and bioprocess development. Both routes were explored in this work.

The acetate metabolism in *E. coli* includes the malate synthase (AceB), isocitrate lyase (AceA) and isocitrate dehydrogenase kinase/phosphatase (AceK), with genes encoding these proteins clustered in the genome (Cortay, Nègre et al. 1991). Several

other proteins, such as, acetyl-CoA synthetase (ACS), acetate kinase (AckA), phosphotransacetylase (Pta), pyruvate oxidase (PoxB), pyruvate dehydrogenase (AceE) and the phosphotransacetylase EutD are also involved in acetate metabolism and its regulation, and can be linked to the production of acetate under high glucose concentration, and its consumption as energy source (Bologna, Campos-Bermudez et al. 2010, El-Mansi, Phue et al. 2021). The phosphotransacetylases EutD and Pta convert acetyl-CoA to acetyl-P, which is dephosphorylated to acetate by acetate kinase (Figure 1.3.).

The balance between acetate kinase (AckA) and phosphotransacetylase (Pta) has been reported to be the major regulator of the acetate balance as it is a reversible reaction and can support acetate production and consumption in *E. coli* K12 (Enjalbert, Millard et al. 2017, Millard, Enjalbert et al. 2021). The genes encoding these key proteins, *eutD*, *pta* and others are often deleted aiming to increase productivity. For example, Dittrich et al., (2015) deleted *ackA-pta* pathway and *poxB* aiming to improve the synthesis of isoamyl acetate. Deleting *ackA-pta* reduced acetate by 4 %, while deleting *poxB* reduced acetate by 10 % (Dittrich 2005). Deletion of *pta* or double deletion Δ*pta*Δ*poxB* resulted in about 70 % less acetate produced by *E. coli* AF1000 used for the synthesis of 3HBA (Perez-Zabaleta, Guevara-Martínez et al. 2019).

Therefore, *eutD* and *pta* were targeted for deletion using two CRISPR-Cas9 methodologies, with the idea of removing these key enzymes involved in acetate production. Simultaneously, we wanted to integrate the production gene cluster in the chromosome of *E. coli*, as this would generate a more stable production strain. Cook, Rand et al. (2018) developed a methodology for gene deletion and integration for *Pseudomonas putida* (Cook, Rand et al. 2018). Although this method, named here 3-plasmid system, showed from 85-100 % efficiency in *P. putida*, it was incompatible with *E. coli*, no troubleshooting efforts expected to increase the efficiency, such as the inducer concentration, cultivation and recovery time, temperature at which the single cross-over strains were grown resulted in the generation of an *eutD* deletion, or insertion of the production cluster (Chapter 3). This may be due to a difference in the plasmid copy number between a *Pseudomonas* strain and *E. coli* (Cook, Rand et al. 2018).

As the above strategy was unsuccessful, a different CRISPR/Cas9 strategy described by (Jiang, Chen et al. 2015) was attempted. This methodology was developed for engineering of *E. coli* MG1655 and provided Cas9 in a similar pCas vector, while pgRNA was provided in pTarget and the repair template was provided as double-stranded DNA (dsDNA). The repair DNA can be provided as single-stranded DNA, double-stranded DNA or in a vector, as it was the case of pKNOCK (Widney, Yang et al. 2024). This methodology was successful in creating deletion and insertion mutants (Jiang, Chen et al. 2015).

While both Pta and EutD are the enzymes that perform the same function i.e. the reversible conversion of acetyl-CoA into acetyl-P (Bologna, Campos-Bermudez et al. 2010, Campos-Bermudez, Bologna et al. 2010). Under similar conditions, ∆*eutD_tesb_RHBD* and ∆*pta_tesb_RHBD* strains showed a different behaviour when grown in flasks, using LB supplemented with 10 g/L glucose as the production medium (Section 3.2.). Firstly, the product (*R*)3HBA was not detected when ∆*pta_tesb_RHBD* was used (Table 3.1.). The reason for this is unclear. While 1.4-fold less acetate was found in the supernatant of the ∆*pta_tesb_RHBD* compared to the parent strain BL21_*tesb_RHBD,* there was still acetate in the supernatant, suggesting other enzyme(s) are contributing to acetate synthesis. Secondly, as these cells lost the ability to produce the targeted product (3HBA), even though they contained the production module, they obviously would not be of interest. Also, the pool of acetate created by the balance of these genes is used in non-enzymatic acetylation. *E. coli* Δ*pta* strains are shown to have poorer growth and lower lysine acetylation compared to the parent strain (Fatema and Fan 2023). This is explained by lower availability of ATP in *pta* mutants, which is also produced during the conversion of acetyl-CoA to acetyl-P and lower acetate available for non-enzymatic protein acetylation (Schütze, Benndorf et al. 2020). Δ*pta_tesb_RHBD* did not exhibit the poorest growth and the lack of 3HBA synthesis is yet unclear.

∆*eutD_tesb_RHBD* showed levels of acetate in the supernatant comparable to the parent strain (Table 3.1.). However, 1.4-fold increase in (*R*)3HBA concentration was observed. Since the same amount of acetate was detected, and more product is observed, it is not clear why this increase in carbon flow towards the product has occurred in ∆*eutD_tesb_RHBS* cells. Deletion of *eutD* and *pta* can improve pyruvate

supply by decreasing the flux of carbons towards acetyl-CoA (Wang, Meng et al. 2014), however, more research is needed to understand the differences observed between Δ*eutD* and Δ*pta*. The ∆*eutD*∆*pta_tesb_RHBD* also showed a 1.2-fold decrease in acetate, however, 3HBA synthesis decreased by 2.3-fold. Again, it is not clear how pta deletion is affecting recombinant protein expression, quantitative PCR with genes in the RHBD operon can further elucidate this problem.

Overall, it can be concluded that acetate metabolism is complex and other pathways, such as, the citrate lyase (Kakuda, Shiroishi et al. 1994) and N-acetylornithine deacetylase (Javid-Majd and Blanchard 2000), also contribute to acetate levels in the cell. Therefore, more of the streamlining would be required to divert the carbon flow from acetate to 3HBA synthesis.

One of the crucial steps in the mini-pathway is the removal of CoA as it is known that high acetyl-CoA concentrations, for instance, can inhibit thiolase activity. The removal of the CoA from 3-hydroxybutyril-CoA has been observed to be more important than its synthesis in regard to the synthesis of 3HBA (Gao, Wu et al. 2002). Studies achieved recombinant 3HBA synthesis in *E. coli* using only natively expressed thiolases (Guevara-Martínez, Sjöberg Gällnö et al. 2015, Jarmander, Belotserkovsky et al. 2015). The genome of *E. coli* is known to encode for several thioesterases, including TesA, TesB, FadM and YciA. The catalytic efficient of these enzymes have been tested with regards to 3HBA synthesis and Ycia showed the best results (Guevara-Martínez, Perez-Zabaleta et al. 2019). The activity of TesB and BHC were previously investigated for (*S*) and (*R*)3HBA synthesis, where it was observed that when BCH was used 4.2-fold less (*S*)3HBA was produced compared to when TesB was used, while 1.3-fold higher (*R*)3HBA was observed when TesB was used when comparing to BCH (Liu 2020). Initially, the synthesis of (*R*)3HBA in mutants was assayed, we then aimed to test de efficiency of TesB and BCH in Δ*eutD*, which was the best producer knock out strain, at 24 and 48h of induction of protein expression. The final 24 h did not increase 3HBA concentration substantially, but resulted in 3.33 g/L (*R*)3HBA for BL21_*bch_RHBD* and 3.90 g/L (*S*)3HBA for BL21_*tesb_SHBD,* which is in line with the results observed by (Liu 2020). *ΔeutD* mutants showed similar 3HBA concentrations (Table 3.2.).

The excess of glucose, reported to be needed in the production medium (Lee, Park et al. 2008) surely contributes to the spillage of carbon as acetate. It was observed that in all cases tested in this work between 22 and 48 % glucose was consumed (Table 3.2.), leaving a good portion of supplied carbon non utilised. This was observed in other works as well. For example, Liu and coworkers observed 40-70 % of the glucose consumed in 48 h of cultivation (Liu, Ouyang et al. 2007). Δ*eutD_tesb_SHBD* had the highest 3HBA concentration (2.91 g/L) and only 40 % of the glucose provided was consumed. For this strain, the acetate concentration was also one of the lowest observed (Table 3.2.).

This led us to think that perhaps the rate of glucose consumption may be linked with acetate spillage, and therefore, a bioprocess was designed to test how different glucose feeding regimes affect the product and byproduct formation. Fermentation permits to control conditions, such as, pH, temperature and partial dissolved oxygen (pO_2), the latter known to be the key contributing factor for the efficiency of a bioprocess (Stanbury 2013). Fermentations can be conducted in a batch, where all the nutrients are supplied at the start, in a continuous process where there is a feed with nutrients and the removal of byproducts and spent media, or fed-batch process with addition of nutrients to make the bioprocess longer (Bolmanis, Dubencovs et al. 2023).

Furthermore, reduced acetate accumulation was observed in *E. coli* when an online feedback control of increased acetate concentration regulated pO_2 was used, indicating that bioprocess could be applied to improve 3HBA productivity (Åkesson, Hagander et al. 2001). The bioprocess was analysed using BL21. Firstly, a batch process using 20 g/L of glucose added to LB and two different pO_2 concentrations 5 or 20 % were analysed. Five % was chosen as it was expected that this would slow down the glucose consumption rate. The biomass accumulated within the cultivation period and the product formed are the same for the two processes (Figure 3.7). However, acetate was 3.6-fold higher when 5 % pO_2 was used (Figure 3.7.). This was in agreement with previously reported work, where *E. coli* grown at 1 or 6 % pO_2 produced more acetate than when grown at 30 % (Phue and Shiloach 2005). The flasks used in the above-mentioned experiments would present a microaerophilic environment, which likely contributed to higher acetate formation observed there.

Another factor that may contribute to the acetate vs. (*R*)3HBA production is the cell density at which the production gene cluster is induced. If the recombinant protein expression is induced earlier i.e. at a lower cell density, perhaps the carbon may be redirected towards the desired product. The induction later may provide a larger number of cells expressing the required proteins, and therefore increase the product formation. For example, the induction at high cell density has been used to obtain high recombinant protein concentrations in *E. coli* (Zhao, Wang et al. 2021, Ganjave, Dodia et al. 2022). However, the induction at OD_{600nm}=15 did not lead to the increased product concentration in the supernatant (Figure 3.8). The acetate concentration secreted into the medium was at similar levels for both conditions, 1.63 g/L inducing cells at OD_{600nm}=5 and 0.54 g/L for OD_{600nm}=15, which is 3-fold lower for protein induction at higher cell density (Figure 3.8.). More glucose was consumed however, which seems to have been used for the biomass formation, as the biomass in this case was 1.5-fold higher than when the cells were induced at OD_{600nm}=5 (Figure 3.8.). Even though (*R*)3HBA concentration was similar between the two cell densities experiments, the (*R*)3HBA/acetate ratio for the higher cell density condition was 3.01, boosted by 2-fold lower acetate in cells induced at higher OD_{600nm}.

It is known that glucose concentrations from 20 to 70 g/L do not affect (*R*)3HBA or acetate concentration using *E. coli* DH5α (Gao, Wu et al. 2002), but glucose is also required in excess (Lee, Park et al. 2008). The excess of glucose was evaluated and aimed to be maintained at 20 g/L and cells induced at lower OD_{600nm} or to be kept at 10 g/L for cells induced at higher OD_{600nm}. It was not possible to keep glucose levels at 20 g/L as carbons accumulated indicating that glucose consumption was reduced when this substrate was in high concentration. On the other hand, keeping glucose at 10 g/L was successful, even though (*R*)3HBA, acetate and the final biomass were similar across both experiments. The (*R*)3HBA/acetate ratio was 5.6 and 8.6 for lower and higher cell density experiments, respectively.

Next, the Δ*eutD_tesB_RHBD* strain was assessed as the production host. Starting from a batch with 20 g/L glucose and constant feed with 2 g/L/h glucose provided, induction of the production cluster when cells reached OD600=15, this strain produced 11.2 g/L 3HBA, which was a 1.6-fold improvement compared to the best bioprocess with BL21_*tesB_RHBD*. While this process also showed a relatively high acetate formation 1.61 g/L, that resulted in a 3HBA/acetate ratio of 6.95. To test if the same

bioprocess can be employed for (*S*)3HBA synthesis, the strain Δ*eutD_tesB_SHBD* was used under the same bioprocess conditions used for the synthesis of (*R*)3HBA. However, high acetate 4.55 g/L acetate and only 3.75 g/L (*S*)3HBA were detected, which represents a 3HBA/acetate ratio of 0.82, well below the observed for (*R*)3HBA. While the two strains differ only in two genes used in the production cluster, namely the gene encoding the SHBD and the gene *tesB* encoding the thioesterase, it appears that the host context can affect how different recombinant genes are expressed and therefore contribute to the product formation. The expression of a green fluorescent protein (GFP) was used to measure the impact of deleting the genes involved in acetate metabolism (*pta, acs* and *ackA*) or lysine acetylation (*patZ* and *cobB*), in recombinant protein synthesis. *patZ* encodes a peptidyl-lysine N-acetyltransferase acetyltransferase, while *cobB* encodes a protein deacetylase. Higher GFP expression was observed in the Δ*ackA* (5-fold) and Δ*pta* (1.6-fold) background strains (Lozano Terol, Gallego-Jara et al. 2019). Additionally, it was previously observed that (*S*)3HBA was recombinantly produced at lower concentration when compared to (*R*)3HBA under the same conditions. The authors suggest these results are caused by (*S*)3HBA-CoA is an intermediate in the pathway for β-oxidation (Gao, Wu et al. 2002, Lee, Park et al. 2008).

The basis of 3HBA production here through the deletion of *eutD* and *pta* and overexpression of the production module combined with the bioprocess development, could be further streamlined. Other alternatives for improvement include the overexpression an enzyme to increase cofactor regeneration and further gene deletion (Jarmander, Belotserkovsky et al. 2015). Knock outs of *poxB,* a pyruvate dehydrogenase that converts pyruvate in acetate and CO_2, *pta*, and *iclR* (transcriptional repressor IclR), which is part of a family of transcription regulators, were generated and evaluated in *E. coli* AF1000 (MC4100, relA1+) (Perez-Zabaleta, Guevara-Martínez et al. 2019). *pta* and *pta-poxB* deletion resulted in 77 and 85 % reduction in acetate concentration, respectively, but it did not affect (*R*)3HBA. Δ*iclR* sole knock out had little impact in acetate concentration (18 %). Following that, seven *E. coli* strains (B, BL21, W, MG1655, W3110, BW25113, and AF1000) were screened for the lowest acetate production and identified *E. coli* BL21. BL21 expressing the three genes and without deletion of the genes involved in acetate was used in fermentations where glucose concentration was kept >10 g/L in minimal medium. The

fermentation had an initial repeated batch phase that lasted 12 h where $(NH_4)_2SO_4$ was manually added, followed by a nitrogen-limited fed-batch phase and resulted in 16.3 g/L 3HBA over 24 h in a 24-hour fermentation (Table 6.1.). The acetate concentration reached 5.5 g/L in the N-limited phase, which is a 3HBA/acetate ratio equals 2.96, which is low compared to the ratio observed for our best BL21 producing strain (8.6) at OD_{600nm}=15 and keeping glucose at 10 g/L.

Table 6. 1. List of recombinant *E. coli* strains used to synthesize 3-hydroxybutyric acid and their respective concentrations.

Strain	Highest 3HBA (g/L)	Incubation period (h)	Reference
E. coli DH5α	12	48	(Gao, Wu et al. 2002)
E. coli AF1000	6.8	13	(Guevara-Martínez, Sjöberg Gällnö et al. 2015)
E. coli BL21 (DE3)	10.3	38	(Lee, Park et al. 2008)
E. coli AF1000	12.7	30	(Perez-Zabaleta, Sjöberg et al. 2016)
E. coli AF1000	14.3	24	(Guevara-Martínez, Perez-Zabaleta et al. 2019)
E. coli BW25113	1.02	47	(Fei, Luo et al. 2021)
E. coli BW25113	12	24	(Liu, Ouyang et al. 2007)
E. coli BL21 (DE3)	16.3	24	(Perez-Zabaleta, Guevara-Martínez et al. 2019)

As PhaB, the β-ketothiolase used here is NADPH dependent, the increased NADPH supply could contribute to more 3HBA synthesised. The overexpression of glucose-6-phosphate dehydrogenase, which generated NADPH had a beneficial effect on *E. coli* DH5α. This enzyme catalyses the first step in the pentose phosphate pathway and generates NADPH. By doing that, the specific production rate of 3HBA was increased by 50 % (0.06 gg^{-1} h^{-1}) compared to the reference cultivation, without overexpressing

glucose-6-phosphate dehydrogenase (Perez-Zabaleta, Sjöberg et al. 2016). In *P. putida* the balance between CoA and NAD^+/NADH balance the synthesis of PHB (Prieto, Escapa et al. 2016). It can be hypothesized that the activity of (*S*) or (*R*)-3-hydroxybutyryl-CoA dehydrogenases can be improved by increasing the cellular levels of NADH/NAD^+ or simply by maximizing glucose consumption by overexpressing a gene such as for formate dehydrogenase.

To stimulate the PHA accumulation, in native producers, such as *Pseudomonas* or *C. necator* strain, from which the genes for the production cluster were used, an inorganic nutrient limitation is often employed (Guevara-Martínez, Sjöberg Gällnö et al. 2015). Under the nutrient imbalanced condition, when carbon is present in excess, and nitrogen or phosphorous in limited amount, after the limited substrate is used, the carbon is converted to PHA. While the genes used here are under the control of T7 promoter, rather than σ^{54} i.e. stress-induced promoter, it is possible that the limitation would shift the available acetyl-CoA towards 3HBA production. This strategy was employed by Guevara-Martinez and coworkers, who expressed a β-ketoacyl-CoA thiolase and acetoacetyl-CoA reductase from *H. boliviensis* into *E. coli* AF1000. Minimal salt medium supplemented with 15 g/L glucose was used, under separately testing ammonium or phosphate depletion/limitation. Phosphate depletion resulted in higher 3HBA productivity compared to ammonium depletion. The highest productivity was observed in the exponential feed phase in phosphate-limited fed-batch, with 3HBA accumulating to 1.5 g/L/h, correlating with higher cell density (Guevara-Martínez, Sjöberg Gällnö et al. 2015, Perez-Zabaleta, Sjöberg et al. 2016).

6.2. Synthesis of α and β-non-coded amino acids

While the previous section focused on 3HBA, either (*R*) or (*S*), as a relevant product, the route of glucose conversion to 3HBA was also seen as a potential route that could be diverted to another valuable product, an amino acid. Amino acids, which are chiral amines, are ubiquitous in nature as they make up the structure of proteins and participate in range of biological processes, as enzymes, hormones and neurotransmitters (Alberts 2002). Although several amino acids have been described in the L- or D-configuration, generally speaking, all proteins are made up of 22 L-amino acids (Martínez-Rodríguez, Torres et al. 2020). Coded, or natural, amino acids have a

primary NH_2, an α-carboxyl group and a variable side-chain that grants different characteristics to these molecules. Coded amino acids need the pair tRNA/tRNA synthetase so they can be added to a nascent peptide chain (Alberts 2002). In addition to these, there are non-coded amino acids (ncAAs) for which the cell lacks the machinery to add them to a proteins (Zou, Li et al. 2018). They can have numerous roles, such as precursor molecules in neuroprotective and antidiabetic molecules (Harris, Tallon et al. 2006). Yet, ncAAs can naturally be found in proteins, for example, collagen has a high content of the ncAA hydroxyproline, which are formed via post translational modification and help to stabilize the collagen structure (Gauza-Włodarczyk, Kubisz et al. 2017).

As already mentioned in the Introduction, various routes exist for the synthesis of ncAAs. Here, the biocatalytic synthesis of ncAAs was explored by developing cascade reactions. As mentioned above, an intermediate produced in the 3HBA synthesis route is acetoacetyl-CoA (Figure 1.2.). This was seen as a potential substrate for a transaminase catalysed reaction to produce 3-aminobutyric acid (3ABA). The amination step in artificial cascades is often performed by transaminases (TAs) or amine/amino acid dehydrogenases (AADH). TAs are pyridoxal 5'phosphate dependent enzymes that require an amino donor (usually an amino acid) and amino acceptor, that can be a keto acid, ketone or aldehydes (Guo and Berglund 2017). On the other hand, AADHs are $NADP^+$/NADPH dependent enzymes that catalyse the amination of ketones and aldehydes (Knaus, Böhmer et al. 2017).

An ω-TA from *Chromobacterium violaceum* (CV_TA) is shown to be active towards a methyl ester of acetoacetate i.e. 3-oxobutyric acid methyl ester (3OBA) (Almahboub, Narancic et al. 2018), and it was therefore hypothesised that it could be used for the transamination of acetoacetate However, as acetoacetyl-CoA was produced in the pathway, it was not clear if the transaminase would show an activity towards such a bulky substrate. Therefore, TesB thioesterase, already part of the production cluster, was expressed and its activity towards acetoacetyl-CoA was demonstrated (Figure 4.2. A-B). Therefore, the gene encoding CV_TA was used to replace the RHBD in the production cluster (Figure 4.2. C). The new construct was transformed in the BL21 and the production of 3ABA from glucose was attempted. Unfortunately, no product was observed. The activity of the thioesterases TesB and BCH, used for CoA removal of 3-hydroxybutyril-CoA in the artificial pathway for the synthesis of 3HBA, was tested

against acetoacetyl-CoA and both enzymes had similar levels of activity. BCH activity is inhibited by DNTB used to measure the release of CoA (Liu 2020), thus TesB was chosen for the next step.

Like in the 3HBA operon, the genes for the thioesterase (*tesB*), acetoacetyl-CoA thiolase (*phaA*) and CV_TA (*CV_2025*) were cloned to BL21 as the ABA operon (*tesb_phaA_CV_2025*). However, the synthesis of 3ABA was not detected.-One of the potential explanations was that the CV_TA has poor activity towards acetoacetate. To test this, the enzyme was expressed, and the activity was tested in an in vitro assay, and it was confirmed that while the reaction happens when the methyl ester is used, CV_TA has no detectable activity towards the free 3OBA (Figure 4.4.). Molecular docking revealed that R416 interacts with the methyl group in the methyl ester from of the substrate, likely stabilising the enzyme substrate interaction. This residue proved to be essential for the activity of CV_TA (Almahboub, Narancic et al. 2018). Its role in the substrate coordination was shown via a conservative amino acid substitution to K The CV_TA variant with R416K substitution completely lost activity towards all tested substrates (Almahboub, Narancic et al. 2018), thereby emphasising the importance of the R416 interaction with the substrate. This is the likely explanation for the lack of CV_TA activity towards free 3OBA. In addition, when CV_TA wildtype, or variants were tested with a range of substrates, the poorest activity was observed with the methyl ester of 3OBA (Almahboub, Narancic et al. 2018).

There are other transaminases that may have better activity towards β-keto substrates. The (*R*)-specific TA from *Arthrobacter* sp. KNK168 had activity towards small cyclic ketones, methyl ketones and primary amines (Koszelewski, Clay et al. 2009). This enzyme was subjected to several rounds of mutagenesis that resulted in 28 mutations to allow catalysis for the bulky prositagliptin ketone (Savile 2010). However, an ω-TA from *Vibrio fluvialis* JS17 was shown to convert β-amino-n-butyric acid to the corresponding keto acid (Shin and Kim 2002).

Three TAs, namely ATA-117, ATA-217 and CDX043 were screened for the activity towards 3OBA. These TAs ware previously used for the amination of bulky substrates (Savile 2010, Novick, Dellas et al. 2021, Haarr, Sriwong et al. 2024). Among the three, only ATA-117 showed the activity towards 3OBA (Table 4.1.). Due to time constraint, it was not possible to investigate placing the gene for ATA-117 in the production cluster

as part of this work, but the potential to use ATA-117 along with PhaA and TesB for the conversion of glucose into 3ABA will be investigated in the future.

As already mentioned, TAs are highly interesting enzymes, that can afford the synthesis of novel chiral amines via reductive amination (John 1995). In particular, ω-TAs usually show a wide substrate range, being able to accept both various amino group donors or acceptors (Kelly, Pohle et al. 2018). One of the best examples of the TA application is sitagliptin production (Savile 2010). Here, both the enzyme and the bioprocess were engineered simultaneously, which has resulted in the real industrial application.

Even though TAs have been seen as enzymes with potentially a wide substrate range, keto substrates may be unstable, or expensive (Rudat, Brucher et al. 2012). Therefore, this part of work focused on identifying enzymes that could be employed in a cascade, where a hydroxy-fatty acid could be oxidised to a keto substrate suitable for a TA catalysed reaction. Fatty acids are abundant substrates, and a range of enzymes have been investigated for their hydroxylation(Kim and Oh 2013). A deletion of an acyl-CoA synthetase and an overexpression of an acetyl-CoA carboxylase and an acyl-CoA thioesterase in *E. coli* allowed for the synthesis of 58.7 mg/L of hydroxy fatty acids namely 9-hydroxydecanoic acid methyl ester, 11-hydroxydodecanoic acid, 10-hydroxyhexadecanoic acid and 12-hydroxyoctadecanoic acid, using glucose as substrate (Cao, Cheng et al. 2016). Other approaches available make use of esterases, hydratases and monoxygenases to achieve the production of hydroxy fatty acids (Kim and Park 2019). Therefore, it could be envisaged that a pathway for the conversion of fatty acids into amino fatty ncAAs could be designed. The utilisation of the amino fatty ncAAs has been reported, including our previous work where 2-aminooctanoic acid was used to modify an antimicrobial peptide (Almahboub, Narancic et al. 2018).

Amongst the ncAAs targeted to be synthesised in Chapter 4, 2-aminobutyric acid (2ABA or L-homoalanine) is the precursor of three drugs available in the market: ethambutol, levetiracetam, and brivaracetam (El-Sayed, Yassin et al. 2015). The chemical synthesis of levetiracetam was accomplished *via* Evans type asymmetric synthesis and involved 5 steps that resulted in only 33 % yield (Chandra Babu, Buchi Reddy et al. 2013). Several biocatalytic approaches were employed to address the

low yield and process cost. The high cost of 2-oxobutyric acid (2OBA) substrate has been reduced by employing L-threonine deaminases to produce 2OBA from L-threonine (Park, Kim et al. 2010). The transamination in this process can be performed either by a TA or an amino acid dehydrogenase (AADH).

A whole-cell cascade reaction was developed an L-threonine deaminase to obtain 2OBA from L-threonine and an ω-TA from *Paracoccus pantotrophus* to perform asymmetric synthesis of L-2ABA. The system was tested using 1-phenylmethylamine or L-alanine as amino donors and expressing enzymes to remove the byproducts when each amino donor is used. When 1-phenylmethylamine was used as donor an aldehyde reductase and a glucose dehydrogenase to convert the benzaldehyde, produced by deamination of benzylamine, to benzyl alcohol, and the glucose dehydrogenase was used to recirculate NAD+/NADP. When L-ala was used as amino donor, an alanine dehydrogenase was used to recirculate the amino donor, L-ala, and a formate dehydrogenase to convert formate produced by alanine dehydrogenase activity to CO_2. The cascade using benzylamine as donor produced 71.6 % yield L-2ABA with >99 % enantiomeric excess (Luo, Hu et al. 2021). D-2ABA synthesis was also achieved by obtaining 2OBA from L-threonine, as above, and using and D-amino acid dehydrogenase to convert 2OBA to D-2ABA (Chen, Cui et al. 2017). This system also has a formate dehydrogenase to recycle NAD^+/NADH and yield > 95 % product with enantiomeric excess ≥ 99 % for cell-free extract or purified enzymes. Using whole-cells to produce D-isomers may be an issue as L-specific enzymes can compete for the intermediates (Chen, Cui et al. 2017).

2-Aminohexanoic acid (2AHA, 2-aminocaproic acid or norleucine) is an analogue of methionine observed to increase resistance to chemical degradation when used to replace a methionine in a bovine pancreatic ribonuclease sequence (Anfinsen and Corley 1969). The biocatalytic synthesis of 2AHA was previously achieved starting with hexanoic acid, P450 oxigenase to hydroxylate hexanoic acid, a hydroxyisocaproate dehydrogenase to obtain the keto intermediate, and a leucine dehydrogenase for the amination with >97 % enantiomeric excess (Dennig, Gandomkar et al. 2018).

As there is a potential for the use of fatty ncAAs, we aimed to design a one-pot catalytic cascade that could convert 2-hydroxy fatty acids to 2-amino fatty acids with various length in the acyl chain. As CV_TA was shown to be active with2OBA, 2-oxopentanoic

acid, 2-oxohexanoic acid (2OHA), 2-AOA (Almahboub, Narancic et al. 2018), we relied on the use of CV_TA in the second step. Five candidate enzymes were investigated for the first reaction step, in which a 3-hydroxy fatty acid would be oxidised to a corresponding compound with a carbonyl group, susceptible to amination (Figure 4.1.).

Two alcohol dehydrogenases (ADH), (*R*)- and (*S*)-specific, from *Lactobacillus brevis* and *Aromatoleum aromaticum*, respectively, were used in a hydrogen borrowing with an amine dehydrogenase from *B. stearothermophilus* (Mutti, Knaus et al. 2015). This two-enzyme cascade produced a range of aliphatic and aromatic amines from their respective alcohols with high conversion and enantiomeric excess > 96 %. This system dispensed a cofactor regeneration system because the alcohol dehydrogenase produced the NADH used by the amine dehydrogenase (Mutti, Knaus et al. 2015). These ADHs were chosen due to the broad substrate specificity reported. However, no activity was found towards the target substrates here (Figure 4.6.). Two lactate dehydrogenases (LDH), one L-DDH from *H. mediterranei* reported to be active towards 2-ketobutyrate, ketoisocaproate, and pyruvate (Bonete, Ferrer et al. 2000), and a L-LDH from *E. coli* with activity to glyoxylate, oxaloacetate, and hydroxypyruvate, which are hydroxy or keto acids (Furukawa, Miyanaga et al. 2014). These enzymes were cloned and expressed, but due to time constraints the activity of these two lactate dehydrogenases could not be tested. If one of these enzymes show catalytic activity towards the target substrates LDH and CV_TA can be combined with a formate dehydrogenase in a tri-enzymatic cascade with cofactor recycling system to produce α-ncAAs.

Glycolate oxidase (GO) from *S. oleracea* was previously reported to be active in oxidising 2-hydroxyisobutyric acid, 2-hydroxy-4-pentoxybutyric acid, 2-hydroxyhexanoic acid, 2-hydroxydecanoic acid, and the β substrates 3-phenyllactic acid and 3-indolelactic acid to their respective keto acids (Adam, Lazarus et al. 1997, Das, Glenn Iv et al. 2010). GO showed activity towards all 2-hydroxy fatty acids tested (Figure 4.15.).

Unfortunately, it appeared that the one pot reaction using GO and CV_TA was not viable. It appears that FMN, the cofactor for GO, inhibits the activity of CV_TA, and PLP, the cofactor for CV_TA, inhibits the activity of GO (Figure 4.22). Lowering the

concentration of the cofactors did not result in a detectable activity either. Reports were not found in the literature about either enzymes being inhibited by these cofactors even in low concentrations. However, the last step for the synthesis of PLP in *E. coli* requires a PNP oxidase, which is FMN dependent. The activity of PNP oxidase can be inhibited by high concentration of the product (PLP), where it binds in the active site (Barile, Tramonti et al. 2019). More experiments are needed to evaluate the mechanism of inhibition. Molecular docking studies with both cofactors could shed light in the matter. Although less desirable, a two-pot reaction could be done aiming to separate the cofactor in the first reaction from the keto product to be used by CV_TA. Additionally, using perhaps a different class of enzyme for the amination, such as an AADH instead of CV_TA could allow GO to compose the cascade, but the inhibitory activity of NAD^+/NADH on GO activity must be tested before.

6.3. The effect of the modification of core LFcin peptide with ncAAs

In the past decades, the increasing rates of microbial resistance have alarmed the antimicrobial research field and competent organisations worldwide (Murray, Ikuta et al. 2022). The Centers for Disease Control and Prevention (CDC) published in 2024 that antimicrobial resistance increased 20 % after the COVID-19 pandemic, bringing even more attention to the matter (CDC 2024). New molecules are needed to fight the increasing rate of resistant and multidrug-resistant pathogens. Antimicrobial peptides (AMPs) offer an alternative for the development of such drugs. ncAAs can increase proteolytic resistance as they are not recognized by proteases (Enninful, Kuppusamy et al. 2024) and can be used as protein inhibitors, photoaffinity reactions, among other applications (Goettig, Koch et al. 2023).

AMPs are a diverse class of molecules aften called multifunctional peptides as the same AMP can have antimicrobial, antifungal, anticancer and antiviral activity (Scavello, Amiche et al. 2022). Bovine lactoferricin (bLfcin) is a widely studied AMP derived from natural proteolysis of lactoferrin and has shown antibacterial (Wakabayashi, Hiratani et al. 1996, Hoek, Milne et al. 1997), anticancer (Eliassen, Berge et al. 2006) and antifungal activities. bLfcin comprises 25 amino acids from the N-terminal lobe of lactoferrin with a disulfide bridge between a cysteine in the C-terminus and another cysteine in the N-terminal (Bellamy 1992). The N-terminal

portion of bLfcin is more important to antimicrobial activity than the whole peptide, thus shorter fragments with different lengths have been designed with varying potencies against Gram-positive and Gram-negative strains (Hoek, Milne et al. 1997).

The nonameric core of bovine LFcin (LFcin) was observed to have higher antimicrobial activity than the entire peptide (Wakabayashi, Matsumoto et al. 1999).

Acylation or lipidation of peptides is often used to modify AMPs in order to increase their potency (Malina and Shai 2005, Kamysz, Sikorska et al. 2020). It was noted that addition of C10, C12 or C14 makes a helical peptide to self-assembly, unlike the same peptide modified with shorter acyl chains (Kamysz, Sikorska et al. 2020). However, acylation can only occur where a primary amino group is present, such as N-terminus, or at a lysine residue, or if an adapter is used (Albada 2012). For example, the peptide $(RW)_3$ was C- or N-terminally acylated with C2-C14 using acylating lysine residues as adapters. Generally speaking, lipidation improved antimicrobial activity, especially with C8, but the terminal position of the lipidation did not affect the activity (Albada 2012). N-terminal acylation of Lfcin with the aliphatic hydrophobic chains with aliphatic fatty acids with 6, 10, 11, 14, 16 or 18 carbons improved the activity compared to the parent peptide (Wakabayashi, Matsumoto et al. 1999). The previous work in our group has shown that the use of an amino fatty acid, such as the ncAA 2AOA could be easily used to acylate C- or N-terminus (Almahboub, Narancic et al. 2018). The modified nonameric core of LFcin showed improved antimicrobial activity, especially the C-terminal modification that had increased potency when tested with *E. coli, S. aureus, B. subtilis, P. aeruginosa* and *S. typhimurium* (Almahboub, Narancic et al. 2018).

To further investigate how the size of the acyl chain, and therefore the hydrophobicity added by the incorporation of a series of amino fatty acids would affect the activity, we modified LFcin with the ncAAs targeted to be produced in Chapter 4, 2ABA, 2AHA, 2AOA or 2ADA. In the case of *E. coli, P. aeruginosa* and *S. typhimurium* the minimal inhibitory concentration (MIC) decreased with the increase in the length of the acyl chain (Table 5.1.). All three species are Gram-negative strains, which are known to be not as affected by AMPs (Barreto-Santamaría, Arévalo-Pinzón et al. 2021). However, the increase in hydrophobicity will likely result in cytotoxicity and/or haemolytic activity (Chen, Guarnieri et al. 2007). It is therefore important to establish the cytotoxic effect of the modified peptides analysed here.

While a clear effect was observed when C- vs N-terminal modification was used in the previous research (Almahboub, Narancic et al. 2018), this trend was not clear here. Some peptides exhibited lower MIC when modified N-terminally, while in the case of others C-terminal modification appeared more potent (Section 5.1). Kamysz et al., (2019) acylated the KR12 peptide with C2-C14 and observed that longer acyl chains do not always correlate to improved activity. In fact, it depends on the size of the acyl chain and bacteria tested (Kamysz, Sikorska et al. 2020). The antimicrobial activity has been reported to not be affected by terminal position of lipidation (Albada 2012). On the other hand, our results indicate that the position of modification will be more or less beneficial depending on the bacteria tested.

There are some models used to explain the mode of action (MOA) of AMPs, and they include pore forming and non-pore forming models (Wimley 2010). Human lactoferricin (hLfcin) derived peptides were noted to interact with lipopolysaccharides (LPS) in *E. coli* (Elass-Rochard, Roseanu et al. 1995). MOA for bLfcin was reported to be through membrane destabilization in *E. coli, S. aureus* (Bellamy 1993) and *Candida albicans* (Wakabayashi, Hiratani et al. 1996). The membrane damaging activity of Lfcin and death of *E. coli* cells as a consequence were recently demonstrated (Islam, Hossain et al. 2023). To try and elucidate how the modified LFcin core series analysed here interact with the cells, the target organisms were incubated with sub-MIC and analysed by microscopy (Figures 5.3 and 5.4.). *B. subtilis* and *E. coli* were chosen as model of Gram-positive and Gram-negative strains, respectively, to study Lfcin effect However, alterations in Lfcin sequence can lead to a different mode of action and different inhibition time. The MOA of Lfcin was also suggested to be explained by the all-or-none model (Hilde Ulvatne 2001). This model is well elucidated for Cecropin A and states that bacteria will be killed when the concentration of AMP is high enough, but when the concentration is lower than the required to destabilizes the membrane, cells remain alive (Hilde Ulvatne 2001, Gregory, Cavenaugh et al. 2008). This model could explain our results for *E. coli*, where the sub-inhibitory concentrations were used and reduced cell count, but membrane or intracellular alterations not as evident as they were for *B. subtilis* (Figure 5.4.).

For both strains subjected to microscopy, *E. coli* and *B. subtilis*, alterations consistent with the carpet model, non-pore forming mechanism, can be observed. Cryogenic electron microscopy (cryo-EM) showed melittin forms lipid clusters in the membrane

of *E. coli*, which are similar to the ones observed in Figure 5.5. (Chen, Wang et al. 2023). To investigate the kinetics of LFcin a time-to-kill kinetic assay be used to shed light (Greco, Emborg et al. 2019). By also understanding the peptide-to-lipid ratio required to kill the tested bacteria, it will be possible to observe how LFcin peptide series interact differently depending on the peptide concentration on the cell surface and get more detailed information on different MOA for Gram-positive and Gram-negative bacteria (Rai and Qian 2017). Still about the peptide-to-lipid ratio, the 6-mer LFcin at low peptide concentration (<2 μM) was observed to translocate through the membrane without creating pores, while when in concentrations higher than 3 μM the 6-mer induces pore formation (Hossain, Dohra et al. 2021). Another report shows that Lfcin peptide translocates the membrane without creating pores and binds to DNA possibly inhibiting metabolic processes (Moniruzzaman, Islam et al. 2017). This study suggests that the 6-mer Lfcin targets either the outer membrane or the peptidoglycan and can have intracellular targets (Hossain, Dohra et al. 2021). Perhaps it would be beneficial to analyse the response of *E. coli* and *B. subtilis* to the peptides present in various concentrations. As the samples here were prepared after the cells were incubated with three different concentrations (MIC, MIC x 0.5 and MIC x 0.25) and mixed before mounting. It is possible that the range of effects, rather than a clear affect was observed due to the applied strategy.

One of the questions posed was also if the addition of the ncAA had an effect on the peptide structure or whether the effect exhibited was cause by increased hydrophobicity. Circular dichroism spectra revealed that LFcin peptide series behave similarly regardless of the ncAA used (Figure 5.7.). This result is in line to what was observed for lipidation with C10, C12, C14 or C16, of an inactive peptide (LKKLLKKLLKKL) results in gained activity, but no structural change between active and inactive peptides (Malina and Shai 2005). The 25-mer bLfcin was observed to fold as an antiparallel β-sheet, differently from the same amino acids in the intact lactoferrin, which folds as an α-helix (Hwang, Zhou et al. 1998). This agrees with the experimental findings obtained here that identified antiparallel β-sheet as the predominant secondary structure in LFcin-derived peptides.

There was no difference of the CD spectra when the peptides were in different environments (physiological or hydrophobic). This also agrees with previous findings where LFcin CD spectra was similar in water and SDS (Daidone, Magliano et al. 2011).

This may indicate stability in the peptide structure that can be altered depending on the lipid concentration, thus by testing different peptide-to-lipid ratios it would be possible to observe alterations, ie. oligomerization. Furthermore, nuclear magnetic resonance spectroscopy (NMR) can shed light on how the amino fatty acids interfere with the membrane (Hwang, Zhou et al. 1998). There are two tryptophan residues in the 9-mer Lfcin (RRWQWRMKK) known to be important for interaction with bacterial membrane (Vogel, Schibli et al. 2002). It can be hypothesized that the difference in activity between N- and C-terminal addition of ncAAs occurs due to interaction between the ncAA amino acid added the tryptophan and arginine residues near the N-terminal position (Vogel, Schibli et al. 2002, Daidone, Magliano et al. 2011). Molecular dynamics simulation analysis of Lfcin (25-mer) showed that the side chains of two tryptophan, namely W6 and W8, alter when in the presence of hydrophobic environment and may facilitate anchoring with the membrane (Daidone, Magliano et al. 2011). By obtaining NMR LFcin series it will be possible to verify repulsion/attraction between the ncAAs used to modify LFcin tryptophan and arginine residues known to be important for membrane interaction (Vogel, Schibli et al. 2002).

Although cytotoxicity towards human cells is reported to be low for Lfcin analogues (Kang, Lee et al. 1996), longer size, such as C10 to C14, of the acyl chains attached to AMPs have been associated to increased toxicity. For example, the AMP KR12 was N-terminally modified with n-alkyl acids with carbons varying from C2-C14. It was observed that for C2 and C4, not haemolysis detected. Nonetheless, it increased with the size of the acyl chain to concentrations higher than the MIC, which is undesirable (Kamysz, Sikorska et al. 2020). A comprehensive study using Lfcin hexamer (RRWQWR) showed that N-terminal acylation with C6 reduced 3-fold the MIC and MBC and it was bactericidal for *S. aureus*, but the modified hexamer did not reduce the needed concentration and remained bacteriostatic for *E. coli* (Hossain, Dohra et al. 2021). The lack of an outer membrane in Gram-positive bacteria might be the reason *B. subtilis* was more susceptible to LFcin peptide series (Table 5.1.). The other Gram-positive strain tested was *S. aureus*, notoriously resistant to antimicrobials. We found, however, that *S. aureus* was sensitive to N-acylation with 2ABA and 2AOA. *Staphylococcus* sp. has a system to detect AMPs called antimicrobial peptide sensor comprising of a sensor histidine kinase (ApsS), a DNA-binding response regulator (ApsR) and ApsX, the latter is present only in *Staphylococcus* sp. and its function is

not clear yet (Joo and Otto 2015). Altogether they can upregulate genes involved in resistance, and cause *S. aureus* to evade AMPs action. Almahboub (2018) observed *S. aureus* was only sensitive to LFcin-2AOA (Almahboub, Narancic et al. 2018). Conversely, it was observed here that *S. aureus* was inhibited by 2AOA-LFcin. Variations in MIC may be caused by technical, biological, intra and interlaboratory variations (Schuurmans, Nuri Hayali et al. 2009). In any case, 2AOA modification may present an interesting basis for further research on how these AMPs affect *S. aureus* and why are they able to exert a different response to what is observed with other LFcin modifications.

N-terminal lipidation on the peptide KR12, a peptide derived from LL-37 (KRIVQRIKDFLR-NH_2), with C4-C14 increased antimicrobial activity against species of the ESKAPE group, namely *Enterococcus faecium*, *S. aureus*, *Klebsiella pneumoniae*, *Acinetobacter baumannii*, *Pseudomonas aeruginosa*, and *Enterobacter* spp., and reduced *S. aureus* biofilms, while presented low toxicity against human red blood cells (RBCs). On the other hand, the same peptide modified with longer acyl chains (C6-C14) presented higher toxicity, especially C10 to C14 that resulted in 100 % haemolysis (Kamysz, Sikorska et al. 2020). The results for KR12 align with the correlation we observed in Figure 5.1. I, where all bacteria, but *S. aureus*, tested with LFcin-2ADA were inhibited at 100 and 200 µg/mL, but growth was observed at 400 µg/mL. The reason for that may be that the acyl chain oligomerizes and inactivates the peptide. Oligomerization has been observed in other peptides (Adak, Castelletto et al. 2024). Additionally, KR12 modification with C6 resulted in MIC equal 8 µg/mL for *P. aeruginosa*, while modification with C12 resulted in MIC of 32 µg/mL for the same strain (Kamysz, Sikorska et al. 2020). This is in line to what was observed for LFcin peptides (Table 5.1.). At this time the cytotoxic effect of LFcin peptide series was not assayed. It is necessary to evaluate the optimum balance of increased antimicrobial activity and low toxicity of LFcin peptide series so tests can move to *in vivo* assays.

Moreover, the activity of LFcin peptides can be associated with commercial antibiotics. The synergistic use of two drugs results in a more efficient clearance of microbes and reduces the rate of acquired antimicrobial resistance. For example, by combining the AMP melimine and ciprofloxacin in the assay named checkerboard the MIC of the antibiotic was reduced from 4 to 8 times for *P.s aeruginosa* resistant to ciprofloxacin (Kampshoff, Willcox et al. 2019).

There is a plethora of investigations and applications for LFcin antimicrobial peptides. These investigations include the analysis of toxicity of the LFcin peptide series to human cells, as modification with 2ABA and 2AHA did not promote the highest levels of inhibition they can be dispensed. As LFcin peptides were lyophilised for CD and successfully resuspended in water, it would be interesting to test the antimicrobial activity and obtain new microscopy images without the cosolvent. CD provided a basic understanding of the secondary structure of the peptides, however NMR can be used to get detailed information on atom position of each amino acid in various solvents to understand the behaviour in environments mimicking different membranes (Sani, Rajput et al. 2024). It is known that ncAAs increase stability to proteolysis (Lu, Xu et al. 2020), but the stability of these LFcin peptides in the presence of human proteolytic enzymes is yet to be evaluated. Regarding the production of these peptides, chemical synthesis of proteins is very efficient, but it is costly (Andersson, Blomberg et al. 2000). A model bacteria or fungi, for which the peptides do not have antimicrobial activity, can screened and used to express LFcin. The expansion of the genetic code allows the ncAAs to be produced and incorporated to a nascent peptide chain *in vivo* (Wang, Parrish et al. 2009). With that in mind, the LFcin peptide with higher antimicrobial potency and lower toxicity towards human cells can be synthesized by an organism.

6.4. Concluding remarks and future directions

This study investigated the biosynthesis of 3-hydroxybutyric acid (3HBA) and non-coded amino fatty acids (ncAAs), the latter added to an antimicrobial peptide, bovine lactoferricin (bLFcin), aiming to increase its potency. Our results greatly improved the synthesis of 3HBA by using a combination of genetic engineering and bioprocess and observed that longer ncAAs result in higher antimicrobial potency.

3HBA is a valuable compound used for the synthesis of fine chemicals. Here, the deletion of two genes involved in acetate metabolism was used aiming to increase the carbon flux towards 3HBA. Molecular engineering is a useful tool in improving product yields. 3HBA synthesis was improved for Δ*eutD* deletion mutants, but not for Δ*pta* mutants or the double deletion strain. Further investigation is needed to shed light on how these genes can affect the synthesis of recombinant genes. The process was scaled up to a bioreactor where more reaction parameters (oxygen, pH, etc.) can be

controlled. Results indicate that oxygen plays a major role in regulating the carbon flux to acetate, at 5 % pO_2, or towards 3HBA, at 20 % pO_2. By plugging the Δ*eutD* strain in bioprocess conditions, 3HBA synthesis was nearly 2-fold improved with no increment in acetate. Further adjusting or limiting the supply of nutrients (ie. phosphorus and nitrogen), switching to a continuous process and investigating 3HBA purification methods, can create a blueprint for the large-scale biosynthesis of 3HBA.

3HBA can be used to produce its respective amino acid, named 3-aminobutyric acid (3ABA), a ncAA. ncAAs have a variety of applications, ranging from labelling molecules to new biological activities when added to peptides or proteins. The synthesis of ncAAs is highly relevant for pharmaceutical industry. We attempted to synthesise 3ABA by modifying the genes involved in the synthesis of 3HBA, but 3ABA was not detected. The synthesis of α-amino fatty acids (C2-C8), from hydroxy fatty acids, was not achieved by testing 3 candidate enzymes. Nonetheless, our results narrow the path to find a solution. Transaminases can be combined in a cascade reaction with alcohol/hydroxy acid dehydrogenases, but not oxidases, due to cofactor inhibition. Similarly, the oxidase studied can be combined with an amino acid dehydrogenase. With that in mind, the search for candidate enzymes to compose a cascade reaction.

By modifying bLFcin with ncAAs ranging from C4-C10 it was observed that the potency of this antimicrobial peptide increases with the size of the acyl chain in the ncAA for most bacteria tested. However, bLFcin modified with 2-aminodecanoic acid seem to exert more bacteriostatic than bactericidal activity. The antimicrobial activity seems to depend on the ncAA used to modify the peptide, the terminal position (ie. C- or N-terminal) and the bacteria tested. Treatment with the peptides caused pore-like structures in the membrane and consequently cell death. Leakage of intracellular content can be observed in the future by measuring NAD^+/NADH and ions levels, and by membrane integrity studies. Spectroscopic studies showed modification with all ncAAs did not affect the secondary structure. Nuclear magnetic resonance is a more sensitive tool and can allow detailed observation of atom position and explain the results observed here.

Overall, the results obtained here pave the road for the bioproduction of valuable molecules and its application in modifying an antimicrobial peptide, which is one of the alternatives to address the issue of emerging antimicrobial resistant strains.

Chapter 7

Acknowledgements

Acknowledgements

I Would like to thank my supervisor, Prof Dr. Tanja Narancic for her guidance and support during this project and in the informal chats, especially for not letting me give up. Thank you not insisting in me. Thank you also to Prof. Dr. Kevin O'Conor for the shared space, equipment and always demonstrating interest during the Lab meetings. I would like to thank Dr. Si Liu for her help and passing her research experience to me through this research, her support in the laboratory made all this possible. I would also like to thank Dr. Meg Walsh who patiently trained me in the bioprocess experiments.

I would also like to thank Prof. Dr. Marc Devocelle and John Connolly from the Royal College of Surgeons in Ireland for the support in CD analysis and Prof. Dr. Elaine O'Reilly and Dr. Marianne Haar for helping us to find another transaminase. Thank you for being available in cooperating with us.

I would like to thank all my lab mates James, Manuel, Jia-Lynn, Karthika, Jounghyun, Rhys, Yixin, Mauricio, Bryan, Jesus, Conor, Fede, Pauric, Meg, Will, Reeta, Sneha, Ciara, Katie, Reyhaneh, Meha, Binbin, and Si for the friendship and for creating a relaxed environment at and outside work.

Thank my family for the unconditional love and support in all decisions I take. I will not make a huge list, but I want to thank my friends, in Dublin and back in Brazil, for listening to me constantly talking about my PhD. Special thanks to Jessika, Bruno and Danillo for helping to solve some problems.

I would like to thank myself for getting this far and not giving up during this hard journey.

I thank the University College Dublin for all facilities and support during these four years.

Chapter 8

References

Abdel-Hamid, A. M., M. M. Attwood and J. R. Guest (2001). "Pyruvate oxidase contributes to the aerobic growth efficiency of Escherichia coli." Microbiology **147**(6): 1483-1498.
Acar, J. and B. Röstel (2001). "Antimicrobial resistance: an overview." Revue Scientifique et Technique de l'OIE **20**(3): 797-810.
Adak, A., V. Castelletto, A. De Sousa, K.-A. Karatzas, C. Wilkinson, N. Khunti, J. Seitsonen and I. W. Hamley (2024). "Self-Assembly and Antimicrobial Activity of Lipopeptides Containing Lysine-Rich Tripeptides." Biomacromolecules **25**(2): 1205-1213.
Adam, W., M. Lazarus, B. Boss, C. R. Saha-Möller, H.-U. Humpf and P. Schreier (1997). "Enzymatic Resolution of Chiral 2-Hydroxy Carboxylic Acids by Enantioselective Oxidation with Molecular Oxygen Catalyzed by the Glycolate Oxidase from Spinach (Spinacia oleracea)." The Journal of Organic Chemistry **62**(22): 7841-7843.
Åkesson, M., P. Hagander and J. P. Axelsson (2001). "Avoiding acetate accumulation in Escherichia coli cultures using feedback control of glucose feeding." Biotechnology and Bioengineering **73**(3): 223-230.
Al-Sabagh, A. M., Yehia, F. Z., Eshaq, G., Rabie, A. M., & ElMetwally, A. E. (2016). , 25(1), 53-64. (2016). "Greener routes for recycling of polyethylene terephthalate." Egyptian Journal of Petroleum **25**(1): 53-64.
Albada, H. B., Prochnow, P., Bobersky, S., Langklotz, S., Schriek, P., Bandow, J. E., & Metzler-Nolte, N. (2012). "Tuning the activity of a short Arg-Trp antimicrobial peptide by lipidation of a C-or N-terminal lysine side-chain " ACS medicinal chemistry letters **3**(12): 980-984.
Alberts, B. J., A.; Lewis, J.; Raff, M.; Roberts, K.; Walter, P. (2002). Protein Function. . Molecular Biology of the Cell. New York, Garland Science.
Ali, M., H. M. Ishqi and Q. Husain (2020). "Enzyme engineering: Reshaping the biocatalytic functions." Biotechnol Bioeng **117**(6): 1877-1894.
Almahboub, S. A., T. Narancic, M. Devocelle, S. T. Kenny, W. Palmer-Brown, C. Murphy, J. Nikodinovic-Runic and K. E. O'Connor (2018). "Biosynthesis of 2-aminooctanoic acid and its use to terminally modify a lactoferricin B peptide derivative for improved antimicrobial activity." Applied Microbiology and Biotechnology **102**(2): 789-799.
Almahboub, S. A., T. Narancic, D. Fayne and K. E. O'Connor (2018). "Single point mutations reveal amino acid residues important for Chromobacterium violaceum transaminase activity in the production of unnatural amino acids." Scientific Reports **8**(1).
Ambrogelly, A., S. Palioura and D. Söll (2007). "Natural expansion of the genetic code." Nature Chemical Biology **3**(1): 29-35.
Anderhuber, N., P. Fladischer, M. Gruber-Khadjawi, J. Mairhofer, G. Striedner and B. Wiltschi (2016). "High-level biosynthesis of norleucine in E. coli for the economic labeling of proteins." Journal of Biotechnology **235**: 100-111.
Andersen, J. H., H. V. Jenssen, K. Sandvik and T. J. Gutteberg (2004). "Anti-HSV activity of lactoferrin and lactoferricin is dependent on the presence of heparan sulphate at the cell surface." Journal of Medical Virology **74**(2): 262-271.
Andersson, L., L. Blomberg, M. Flegel, L. Lepsa, B. Nilsson and M. Verlander (2000). "Large-scale synthesis of peptides." Biopolymers **55**(3): 227-250.

Anfinsen, C. B. and L. G. Corley (1969). "An Active Variant of Staphylococcal Nuclease Containing Norleucine in Place of Methionine." Journal of Biological Chemistry **244**(19): 5149-5152.
Apel, C., A. Sudheshwar, K. Kümmerer, B. Nowack, K. Midander, E. Strömberg and L. G. Soeteman-Hernandez (2024). "Safe-and-Sustainable-by-Design Roadmap: Identifying Research, Competencies, and Knowledge Sharing Needs." RSC Sustainability.
Aslam, M. Z., S. Firdos, Z. Li, X. Wang, Y. Liu, X. Qin, S. Yang, Y. Ma, X. Xia, B. Zhang and Q. Dong (2022). "Detecting the Mechanism of Action of Antimicrobial Peptides by Using Microscopic Detection Techniques." Foods **11**(18): 2809.
Aykul, S. and E. Martinez-Hackert (2016). "Determination of half-maximal inhibitory concentration using biosensor-based protein interaction analysis." Analytical Biochemistry **508**: 97-103.
Azofra, L. M., M. A. Tran, V. Zubar, L. Cavallo, M. Rueping and O. El-Sepelgy (2020). "Conversion of racemic alcohols to optically pure amine precursors enabled by catalyst dynamic kinetic resolution: experiment and computation." Chemical Communications **56**(64): 9094-9097.
Bachosz, K., J. Zdarta, M. Bilal, A. S. Meyer and T. Jesionowski (2023). "Enzymatic cofactor regeneration systems: A new perspective on efficiency assessment." Science of The Total Environment **868**: 161630.
Baidin, V., T. W. Owens, M. B. Lazarus and D. Kahne (2021). "Simple Secondary Amines Inhibit Growth of Gram-Negative Bacteria through Highly Selective Binding to Phenylalanyl-tRNA Synthetase." Journal of the American Chemical Society **143**(2): 623-627.
Barile, A., I. Nogués, M. L. Di Salvo, V. Bunik, R. Contestabile and A. Tramonti (2020). "Molecular characterization of pyridoxine 5'-phosphate oxidase and its pathogenic forms associated with neonatal epileptic encephalopathy." Scientific Reports **10**(1).
Barile, A., A. Tramonti, M. L. Di Salvo, I. Nogués, C. Nardella, F. Malatesta and R. Contestabile (2019). "Allosteric feedback inhibition of pyridoxine 5'-phosphate oxidase from Escherichia coli." Journal of Biological Chemistry **294**(43): 15593-15603.
Barreto-Santamaría, A., G. Arévalo-Pinzón, M. A. Patarroyo and M. E. Patarroyo (2021). "How to Combat Gram-Negative Bacteria Using Antimicrobial Peptides: A Challenge or an Unattainable Goal?" Antibiotics **10**(12): 1499.
Bartlett, J. G., D. N. Gilbert and B. Spellberg (2013). "Seven ways to preserve the miracle of antibiotics." Clin Infect Dis **56**(10): 1445-1450.
Bauman, K. D., K. S. Butler, B. S. Moore and J. R. Chekan (2021). "Genome mining methods to discover bioactive natural products." Natural Product Reports **38**(11): 2100-2129.
Becker, P., D. Wünsch, L. Wöhlbrand, M. Neumann-Schaal, D. Schomburg and R. Rabus (2024). "The Catabolic Network of Aromatoleum aromaticum EbN1<sup>T</sup&gt." Microbial Physiology **34**(1): 1-77.
Bellamy, W., Takase, M., Wakabayashi, H., Kawase, K., & Tomita, M. (1992). "Antibacterial spectrum of lactoferricin B, a potent bactericidal peptide derived from the N-terminal region of bovine lactoferrin." Journal of Applied Bacteriology **73**(6): 472-479.
Bellamy, W. R., Wakabayashi, H., Takase, M., Kawase, K., Shimamura, S., & Tomita, M. (1993). "Role of cell-binding in the antibacterial mechanism of lactoferricin B." The Journal of Applied Bacteriology **75**(5): 478-484.

Bellini, S., T. Tommasi and D. Fino (2022). "Poly(3-hydroxybutyrate) biosynthesis by Cupriavidus necator: A review on waste substrates utilization for a circular economy approach." Bioresource Technology Reports **17**: 100985.
Benkovic, S. J., & Hammes-Schiffer, S. (2003). "A perspective on enzyme catalysis." Science **301**(5637): 1196-1202.
Bernal, V., S. Castaño-Cerezo and M. Cánovas (2016). "Acetate metabolism regulation in Escherichia coli: carbon overflow, pathogenicity, and beyond." Applied Microbiology and Biotechnology **100**(21): 8985-9001.
Berrouet, C., N. Dorilas, K. A. Rejniak and N. Tuncer (2020). "Comparison of Drug Inhibitory Effects ($$\hbox {IC}_{50}$$) in Monolayer and Spheroid Cultures." Bulletin of Mathematical Biology **82**(6).
Besse, A., J. Peduzzi, S. Rebuffat and A. Carré-Mlouka (2015). "Antimicrobial peptides and proteins in the face of extremes: Lessons from archaeocins." Biochimie **118**: 344-355.
Bhonsle, J. B., Clark, T., Bartolotti, L., & Hicks, R. P. (2013). "A brief overview of antimicrobial peptides containing unnatural amino acids and ligand-based approaches for peptide ligands." Current topics in medicinal chemistry **12**(24): 3205-3224.
Biernacki, M., J. Riechen, U. Hähnel, T. Roick, K. Baronian, R. Bode and G. Kunze (2017). "Production of (R)-3-hydroxybutyric acid by Arxula adeninivorans." AMB Express **7**(1).
BIOVIA (2024). "Discovery Studio." San Diego: Dassault Systèmes.
Blaskovich, M. A. T. (2016). "Unusual Amino Acids in Medicinal Chemistry." Journal of Medicinal Chemistry **59**(24): 10807-10836.
Bolmanis, E., K. Dubencovs, A. Suleiko and J. Vanags (2023). "Model Predictive Control—A Stand Out among Competitors for Fed-Batch Fermentation Improvement." Fermentation **9**(3): 206.
Bologna, F. P., C. S. Andreo and M. A. F. Drincovich (2007). "Escherichia coliMalic Enzymes: Two Isoforms with Substantial Differences in Kinetic Properties, Metabolic Regulation, and Structure." Journal of Bacteriology **189**(16): 5937-5946.
Bologna, F. P., V. A. Campos-Bermudez, D. D. Saavedra, C. S. Andreo and M. F. Drincovich (2010). "Characterization of Escherichia coli EutD: a phosphotransacetylase of the ethanolamine operon." The Journal of Microbiology **48**(5): 629-636.
Bonartsev, A. P., V. V. Voinova and G. A. Bonartseva (2018). "Poly(3-hydroxybutyrate) and Human Microbiota (Review)." Applied Biochemistry and Microbiology **54**(6): 547-568.
Bonete, M.-J., J. Ferrer, C. Pire, M. Penades and J. L. Ruiz (2000). "2-Hydroxyacid dehydrogenase from Haloferax mediterranei, a D-isomer-specific member of the 2-hydroxyacid dehydrogenase family." Biochimie **82**(12): 1143-1150.
Bornscheuer, U. T. (2018). "The fourth wave of biocatalysis is approaching." Philosophical Transactions of the Royal Society A: Mathematical, Physical and Engineering Sciences **376**(2110): 20170063.
Bourboula, A., D. Limnios, M. G. Kokotou, O. G. Mountanea and G. Kokotos (2019). "Enantioselective Organocatalysis-Based Synthesis of 3-Hydroxy Fatty Acids and Fatty γ-Lactones." Molecules **24**(11): 2081.
Bruni, N., M. Capucchio, E. Biasibetti, E. Pessione, S. Cirrincione, L. Giraudo, A. Corona and F. Dosio (2016). "Antimicrobial Activity of Lactoferrin-Related Peptides and Applications in Human and Veterinary Medicine." Molecules **21**(6): 752.
Bury-Moné, S. (2014). Antibacterial Therapeutic Agents, Elsevier.

Butler, N. D., S. Sen, L. B. Brown, M. Lin and A. M. Kunjapur (2023). "A platform for distributed production of synthetic nitrated proteins in live bacteria." Nature Chemical Biology **19**(7): 911-920.
Campos-Bermudez, V. A., F. P. Bologna, C. S. Andreo and M. F. Drincovich (2010). "Functional dissection of Escherichia coli phosphotransacetylase structural domains and analysis of key compounds involved in activity regulation." The FEBS Journal **277**(8): 1957-1966.
Cao, Y., T. Cheng, G. Zhao, W. Niu, J. Guo, M. Xian and H. Liu (2016). "Metabolic engineering of Escherichia coli for the production of hydroxy fatty acids from glucose." BMC Biotechnology **16**(1).
Carrillo, C., J. A. Teruel, F. J. Aranda and A. Ortiz (2003). "Molecular mechanism of membrane permeabilization by the peptide antibiotic surfactin." Biochimica et Biophysica Acta (BBA) - Biomembranes **1611**(1-2): 91-97.
Castro, T. G., M. Melle-Franco, C. E. A. Sousa, A. Cavaco-Paulo and J. C. Marcos (2023). "Non-Canonical Amino Acids as Building Blocks for Peptidomimetics: Structure, Function, and Applications." Biomolecules **13**(6): 981.
CDC, C. f. D. C. a. P. (2024). "Antimicrobial Resistance Threats in the United States, 2021-2022." Retrieved 12/09/2024, 2024, from https://www.cdc.gov/antimicrobial-resistance/data-research/threats/update-2022.html.
Chakraborty, S., S. Galla, X. Cheng, J.-Y. Yeo, B. Mell, V. Singh, B. Yeoh, P. Saha, A. V. Mathew, M. Vijay-Kumar and B. Joe (2018). "Salt-Responsive Metabolite, β-Hydroxybutyrate, Attenuates Hypertension." Cell Reports **25**(3): 677-689.e674.
Chandra Babu, K., R. Buchi Reddy, K. Mukkanti, K. Suresh, G. Madhusudhan and S. Nigam (2013). "Enantioselective Synthesis of Antiepileptic Agent, (−)-Levetiracetam, through Evans Asymmetric Strategy." Journal of Chemistry **2013**(1): 1-5.
Chapple, D. S., Mason, D. J., Joannou, C. L., Odell, E. W., Gant, V., & Evans, R. W. (1998). "Structure-function relationship of antibacterial synthetic peptides homologous to a helical surface region on human lactoferrin against Escherichia coli serotype O111." Infection and immunity **66**(6): 2434-2440.
Chen, C.-X., B. Jiang, C. Branford-White and L.-M. Zhu (2009). "Enantioselective reductive amination of α-keto acids by papain-based semisynthetic enzyme." Biochemistry (Moscow) **74**(1): 36-40.
Chen, E. H. L., C.-H. Wang, Y.-T. Liao, F.-Y. Chan, Y. Kanaoka, T. Uchihashi, K. Kato, L. Lai, Y.-W. Chang, M.-C. Ho and R. P. Y. Chen (2023). "Visualizing the membrane disruption action of antimicrobial peptides by cryo-electron tomography." Nature Communications **14**(1).
Chen, J., R. Zhu, J. Zhou, T. Yang, X. Zhang, M. Xu and Z. Rao (2021). "Efficient single whole-cell biotransformation for L-2-aminobutyric acid production through engineering of leucine dehydrogenase combined with expression regulation." Bioresource Technology **326**: 124665.
Chen, K., Q.-K. Kang, Y. Li, W.-Q. Wu, H. Zhu and H. Shi (2022). "Catalytic Amination of Phenols with Amines." Journal of the American Chemical Society **144**(3): 1144-1151.
Chen, L., X. Xin, Y. Zhang, S. Li, X. Zhao, S. Li and Z. Xu (2023). "Advances in Biosynthesis of Non-Canonical Amino Acids (ncAAs) and the Methods of ncAAs Incorporation into Proteins." Molecules **28**(18): 6745.

Chen, R. and A. E. Mark (2011). "The effect of membrane curvature on the conformation of antimicrobial peptides: implications for binding and the mechanism of action." Eur Biophys J **40**(4): 545-553.
Chen, X., Y. Cui, X. Cheng, J. Feng, Q. Wu and D. Zhu (2017). "Highly Atom Economic Synthesis of <scp>d</scp>-2-Aminobutyric Acid through an In Vitro Tri-enzymatic Catalytic System." ChemistryOpen **6**(4): 534-540.
Chen, Y., M. T. Guarnieri, A. I. Vasil, M. L. Vasil, C. T. Mant and R. S. Hodges (2007). "Role of peptide hydrophobicity in the mechanism of action of alpha-helical antimicrobial peptides." Antimicrob Agents Chemother **51**(4): 1398-1406.
Chiba, T. and T. Nakai (1987). "A New Synthetic Approach to the Carbapenem Antibiotic PS-5 from Ethyl (S)-3-Hydroxybutanoate." Chemistry Letters **16**(11): 2187-2188.
Chin, J. W., T. A. Cropp, J. C. Anderson, M. Mukherji, Z. Zhang and P. G. Schultz (2003). "An Expanded Eukaryotic Genetic Code." Science **301**(5635): 964-967.
Choudhari, S. K., F. Cerrone, T. Woods, K. Joyce, V. O. Flaherty, K. O. Connor and R. Babu (2015). "Pervaporation separation of butyric acid from aqueous and anaerobic digestion (AD) solutions using PEBA based composite membranes." Journal of Industrial and Engineering Chemistry **23**: 163-170.
Claassens, N. J., S. Burgener, B. Vögeli, T. J. Erb and A. Bar-Even (2019). "A critical comparison of cellular and cell-free bioproduction systems." Current Opinion in Biotechnology **60**: 221-229.
Clifford, K., D. Desai, C. Prazeres da Costa, H. Meyer, K. Klohe, A. S. Winkler, T. Rahman, T. Islam and M. H. Zaman (2018). "Antimicrobial resistance in livestock and poor quality veterinary medicines." Bull World Health Organ **96**(9): 662-664.
Cook, T. B., J. M. Rand, W. Nurani, D. K. Courtney, S. A. Liu and B. F. Pfleger (2018). "Genetic tools for reliable gene expression and recombineering in Pseudomonas putida." Journal of Industrial Microbiology and Biotechnology **45**(7): 517-527.
Cortay, J. C., D. Nègre, A. Galinier, B. Duclos, G. Perrière and A. J. Cozzone (1991). "Regulation of the acetate operon in Escherichia coli: purification and functional characterization of the IclR repressor." The EMBO Journal **10**(3): 675-679.
Cross, K. L., J. H. Campbell, M. Balachandran, A. G. Campbell, S. J. Cooper, A. Griffen, M. Heaton, S. Joshi, D. Klingeman, E. Leys, Z. Yang, J. M. Parks and M. Podar (2019). "Targeted isolation and cultivation of uncultivated bacteria by reverse genomics." Nat Biotechnol **37**(11): 1314-1321.
Cui, Y., Y. Gao and L. Yang (2024). "Transaminase catalyzed asymmetric synthesis of active pharmaceutical ingredients." Green Synthesis and Catalysis.
Daidone, I., A. Magliano, A. Di Nola, G. Mignogna, M. M. Clarkson, A. R. Lizzi, A. Oratore and F. Mazza (2011). "Conformational study of bovine lactoferricin in membrane-micking conditions by molecular dynamics simulation and circular dichroism." BioMetals **24**(2): 259-268.
Das, S., J. H. Glenn Iv and M. Subramanian (2010). "Enantioselective oxidation of 2-hydroxy carboxylic acids by glycolate oxidase and catalase coexpressed in methylotrophic Pichia pastoris." Biotechnology Progress **26**(3): 607-615.
Davies, J. (2006). "Where have All the Antibiotics Gone?" The Canadian journal of infectious diseases & medical microbiology **17**(5): 287-290.
de Carvalho, C. C. (2017). "Whole cell biocatalysts: essential workers from Nature to the industry." Microb Biotechnol **10**(2): 250-263.

Deepankumar, K., S. P. Nadarajan, S. Mathew, S. G. Lee, T. H. Yoo, E. Y. Hong, B. G. Kim and H. Yun (2015). "Engineering Transaminase for Stability Enhancement and Site-Specific Immobilization through Multiple Noncanonical Amino Acids Incorporation." ChemCatChem **7**(3): 417-421.
Dellero, Y., C. Mauve, E. Boex-Fontvieille, V. Flesch, M. Jossier, G. Tcherkez and M. Hodges (2015). "Experimental Evidence for a Hydride Transfer Mechanism in Plant Glycolate Oxidase Catalysis." Journal of Biological Chemistry **290**(3): 1689-1698.
Dennig, A., S. Gandomkar, E. Cigan, T. C. Reiter, T. Haas, M. Hall and K. Faber (2018). "Enantioselective biocatalytic formal α-amination of hexanoic acid to<scp>l</scp>-norleucine." Organic & Biomolecular Chemistry **16**(43): 8030-8033.
Dheman, N., N. Mahoney, E. M. Cox, J. J. Farley, T. Amini and M. L. Lanthier (2020). "An Analysis of Antibacterial Drug Development Trends in the US, 1980 - 2019." Clin Infect Dis.
Dhople, V., A. Krukemeyer and A. Ramamoorthy (2006). "The human beta-defensin-3, an antibacterial peptide with multiple biological functions." Biochimica et Biophysica Acta (BBA) - Biomembranes **1758**(9): 1499-1512.
Dias, R. D. O. and O. L. Franco (2015). "Cysteine-stabilized αβ defensins: From a common fold to antibacterial activity." Peptides **72**: 64-72.
Diêp Lê, K. H. and F. Lederer (1991). "Amino acid sequence of long chain alpha-hydroxy acid oxidase from rat kidney, a member of the family of FMN-dependent alpha-hydroxy acid-oxidizing enzymes." Journal of Biological Chemistry **266**(31): 20877-20881.
Diniz, M. S. D. F., M. M. Mourão, L. P. Xavier and A. V. Santos (2023). "Recent Biotechnological Applications of Polyhydroxyalkanoates (PHA) in the Biomedical Sector—A Review." Polymers **15**(22): 4405.
Dittrich, C. R., Vadali, R. V., Bennett, G. N., & San, K. Y. (2005). (2005). "Redistribution of metabolic fluxes in the central aerobic metabolic pathway of E. coli mutant strains with deletion of the ackA-pta and poxB pathways for the synthesis of isoamyl acetate. ." Biotechnology progress **21**(2): 627-631.
Dmitrieva-Posocco, O., A. C. Wong, P. Lundgren, A. M. Golos, H. C. Descamps, L. Dohnalová, Z. Cramer, Y. Tian, B. Yueh, O. Eskiocak, G. Egervari, Y. Lan, J. Liu, J. Fan, J. Kim, B. Madhu, K. M. Schneider, S. Khoziainova, N. Andreeva, Q. Wang, N. Li, E. E. Furth, W. Bailis, J. R. Kelsen, K. E. Hamilton, K. H. Kaestner, S. L. Berger, J. A. Epstein, R. Jain, M. Li, S. Beyaz, C. J. Lengner, B. W. Katona, S. I. Grivennikov, C. A. Thaiss and M. Levy (2022). "β-Hydroxybutyrate suppresses colorectal cancer." Nature **605**(7908): 160-165.
Domínguez De María, P. (2021). "Biocatalysis, sustainability, and industrial applications: Show me the metrics." Current Opinion in Green and Sustainable Chemistry **31**: 100514.
Drago-Serrano, M. E., Campos-Rodriguez, R., Carrero, J. C., & de la Garza, M. (2018). "Lactoferrin and peptide-derivatives: antimicrobial agents with potential use in nonspecific immunity modulation." Current pharmaceutical design **24**(10): 1067-1078.
Drayton, M., J. N. Kizhakkedathu and S. K. Straus (2020). "Towards Robust Delivery of Antimicrobial Peptides to Combat Bacterial Resistance." Molecules **25**(13): 3048.
Du, S., M. Wey and D. W. Armstrong (2023). "<scp>d</scp>-Amino acids in biological systems." Chirality **35**(9): 508-534.

Du, Y., L. Li, Y. Zheng, J. Liu, J. Gong, Z. Qiu, Y. Li, J. Qiao and Y.-X. Huo (2022). "Incorporation of Non-Canonical Amino Acids into Antimicrobial Peptides: Advances, Challenges, and Perspectives." Applied and Environmental Microbiology **88**(23).
Duminil, P., C. Oury, M. Hodges and N. Glab (2024). Determination of Phosphoglycolate Phosphatase Activity via a Coupled Reaction Using Recombinant Glycolate Oxidase, Springer US**:** 29-39.
Ebbensgaard, A., H. Mordhorst, M. T. Overgaard, F. M. Aarestrup and E. B. Hansen (2018). "Dissection of the antimicrobial and hemolytic activity of Cap18: Generation of Cap18 derivatives with enhanced specificity." PLoS One **13**(5): e0197742.
Eggers, J. and A. Steinbuchel (2013). "Poly(3-Hydroxybutyrate) Degradation in Ralstonia eutropha H16 Is Mediated Stereoselectively to (S)-3-Hydroxybutyryl Coenzyme A (CoA) via Crotonyl-CoA." Journal of Bacteriology **195**(14): 3213-3223.
El-Mansi, M., J.-N. Phue and J. Shiloach (2021). "Expression of the ace operon in Escherichia coli is triggered in response to growth rate-dependent flux-signal of ATP." FEMS Microbiology Letters **368**(2).
El-Sayed, A. S. A., M. A. Yassin and H. Ibrahim (2015). "Coimmobilization of <scp>l</scp>-methioninase and glutamate dehydrogenase: Novel approach for <scp>l</scp>-homoalanine synthesis." Biotechnology and Applied Biochemistry **62**(4): 514-522.
Elass-Rochard, E., A. Roseanu, D. Legrand, M. Trif, V. Salmon, C. Motas, J. Montreuil and G. Spik (1995). "Lactoferrin-lipopolysaccharide interaction: involvement of the 28-34 loop region of human lactoferrin in the high-affinity binding to Escherichia coli 055B5 lipopolysaccharide." Biochemical Journal **312**(3): 839-845.
Eliassen, L. T., G. Berge, A. Leknessund, M. Wikman, I. Lindin, C. Løkke, F. Ponthan, J. I. Johnsen, B. Sveinbjørnsson, P. Kogner, T. Flægstad and Ø. Rekdal (2006). "The antimicrobial peptide, lactoferricin B, is cytotoxic to neuroblastoma cells in vitro and inhibits xenograft growth in vivo." International Journal of Cancer **119**(3): 493-500.
Engelberg, Y. and M. Landau (2020). "The Human LL-37(17-29) antimicrobial peptide reveals a functional supramolecular structure." Nat Commun **11**(1): 3894.
Enjalbert, B., P. Millard, M. Dinclaux, J.-C. Portais and F. Létisse (2017). "Acetate fluxes in Escherichia coli are determined by the thermodynamic control of the Pta-AckA pathway." Scientific Reports **7**(1): 42135.
Enninful, G. N., R. Kuppusamy, E. K. Tiburu, N. Kumar and M. D. P. Willcox (2024). "Non-canonical amino acid bioincorporation into antimicrobial peptides and its challenges." Journal of Peptide Science **30**(6).
EuropeanCommission. (2024). "Safe and sustainable by design." Retrieved 24/07/2024, 2024, from https://research-and-innovation.ec.europa.eu/research-area/industrial-research-and-innovation/chemicals-and-advanced-materials/safe-and-sustainable-design_en#:~:text=The%20'safe%20and%20sustainable%20by,2022%20in%20a%20Commission%20Recommendation%20.
Fatema, N. and C. Fan (2023). "Studying lysine acetylation of citric acid cycle enzymes by genetic code expansion." Molecular Microbiology **119**(5): 551-559.
Fei, P., Y. Luo, N. Lai and H. Wu (2021). "Biosynthesis of (R)-3-hydroxybutyric acid from syngas-derived acetate in engineered Escherichia coli." Bioresource Technology **336**: 125323.

Feng, M., S. Fei, J. Xia, V. Labropoulou, L. Swevers and J. Sun (2020). "Antimicrobial Peptides as Potential Antiviral Factors in Insect Antiviral Immune Response." Front Immunol **11**: 2030.
Ferla, M. P. and W. M. Patrick (2014). "Bacterial methionine biosynthesis." Microbiology **160**(8): 1571-1584.
Fernandes, T., C. Osório, M. J. Sousa and R. Franco-Duarte (2023). "Contributions of Adaptive Laboratory Evolution towards the Enhancement of the Biotechnological Potential of Non-Conventional Yeast Species." Journal of Fungi **9**(2): 186.
Fernández-Vidal, M., Jayasinghe, S., Ladokhin, A. S., White, S. H. (2007). "Folding amphipathic helices into membranes: amphiphilicity trumps hydrophobicity." Journal of molecular biology **370**(3): 459-470.
Fishovitz, J., J. A. Hermoso, M. Chang and S. Mobashery (2014). "Penicillin-binding protein 2a of methicillin-resistant Staphylococcus aureus." IUBMB Life **66**(8): 572-577.
Fjell, C. D., J. A. Hiss, R. E. Hancock and G. Schneider (2011). "Designing antimicrobial peptides: form follows function." Nat Rev Drug Discov **11**(1): 37-51.
Fleming, A. (1922). "On a remarkable bacteriolytic element found in tissues and secretions." Proceedings of the Royal Society of London. Series B, Containing Papers of a Biological Character **93**(653): 306-317.
Fleming, A. (1929). "On the antibacterial action of cultures of a penicillium, with special reference to their use in the isolation of B. influenzae." British journal of experimental pathology **10**(3): 226.
Fort, A. G. and D. C. Spray (2009). "Trifluoroethanol reveals helical propensity at analogous positions in cytoplasmic domains of three connexins." Peptide Science **92**(3): 173-182.
France, S. P., L. J. Hepworth, N. J. Turner and S. L. Flitsch (2017). "Constructing Biocatalytic Cascades: In Vitro and in Vivo Approaches to de Novo Multi-Enzyme Pathways." ACS Catalysis **7**(1): 710-724.
Friberg, C., J. K. Haaber, M. Vestergaard, A. Fait, V. Perrot, B. R. Levin and H. Ingmer (2020). "Human antimicrobial peptide, LL-37, induces non-inheritable reduced susceptibility to vancomycin in Staphylococcus aureus." Sci Rep **10**(1): 13121.
Furukawa, N., A. Miyanaga, M. Togawa, M. Nakajima and H. Taguchi (2014). "Diverse allosteric and catalytic functions of tetrameric d-lactate dehydrogenases from three Gram-negative bacteria." AMB Express **4**(1).
Ganjave, S. D., H. Dodia, A. V. Sunder, S. Madhu and P. P. Wangikar (2022). "High cell density cultivation of E. coli in shake flasks for the production of recombinant proteins." Biotechnology Reports **33**: e00694.
Gao, H.-J., Q. Wu and G.-Q. Chen (2002). "Enhanced production of d-(â?')-3-hydroxybutyric acid by recombinantEscherichia coli." FEMS Microbiology Letters **213**(1): 59-65.
Gardete, S. and A. Tomasz (2014). "Mechanisms of vancomycin resistance in Staphylococcus aureus." Journal of Clinical Investigation **124**(7): 2836-2840.
Garzon-Posse, F., L. Becerra-Figueroa, J. Hernandez-Arias and D. Gamba-Sanchez (2018). "Whole Cells as Biocatalysts in Organic Transformations." Molecules **23**(6).
Gaudet, R. G., S. Zhu, A. Halder, B.-H. Kim, C. J. Bradfield, S. Huang, D. Xu, A. Mamiñska, T. N. Nguyen, M. Lazarou, E. Karatekin, K. Gupta and J. D. Macmicking (2021). "A human apolipoprotein L with detergent-like activity kills intracellular pathogens." Science **373**(6552): eabf8113.

Gauza-Włodarczyk, M., L. Kubisz and D. Włodarczyk (2017). "Amino acid composition in determination of collagen origin and assessment of physical factors effects." International Journal of Biological Macromolecules **104**: 987-991.
Gezae Daful, A., M. Loridon and M. R. Chandraratne (2024). Lactic Acid Production from Lignocellulosic Biomass, IntechOpen.
Ghislieri, D. and N. J. Turner (2013). "Biocatalytic Approaches to the Synthesis of Enantiomerically Pure Chiral Amines." Topics in Catalysis **57**(5): 284-300.
Gibson, D. G., L. Young, R.-Y. Chuang, J. C. Venter, C. A. Hutchison and H. O. Smith (2009). "Enzymatic assembly of DNA molecules up to several hundred kilobases." Nature Methods **6**(5): 343-345.
Gifford, J. L., H. N. Hunter and H. J. Vogel (2005). "Lactoferricin: a lactoferrin-derived peptide with antimicrobial, antiviral, antitumor and immunological properties." Cell Mol Life Sci **62**(22): 2588-2598.
Goettig, P., N. G. Koch and N. Budisa (2023). "Non-Canonical Amino Acids in Analyses of Protease Structure and Function." International Journal of Molecular Sciences **24**(18): 14035.
Gonzales, M. F., T. Brooks, S. U. Pukatzki and D. Provenzano (2013). "Rapid Protocol for Preparation of Electrocompetent Escherichia coli and <em>Vibrio cholerae</em&gt." Journal of Visualized Experiments(80).
Greco, I., A. P. Emborg, B. Jana, N. Molchanova, A. Oddo, P. Damborg, L. Guardabassi and P. R. Hansen (2019). "Characterization, mechanism of action and optimization of activity of a novel peptide-peptoid hybrid against bacterial pathogens involved in canine skin infections." Scientific Reports **9**(1).
Gregory, S. M., A. Cavenaugh, V. Journigan, A. Pokorny and P. F. F. Almeida (2008). "A Quantitative Model for the All-or-None Permeabilization of Phospholipid Vesicles by the Antimicrobial Peptide Cecropin A." Biophysical Journal **94**(5): 1667-1680.
Grishin, D. V., D. D. Zhdanov, M. V. Pokrovskaya and N. N. Sokolov (2020). "D-amino acids in nature, agriculture and biomedicine." All Life **13**(1): 11-22.
Gross, L. and J. Enck (2021). "Confronting plastic pollution to protect environmental and public health." PLOS Biology **19**(3): e3001131.
Gruber, P., M. P. C. Marques, B. O'Sullivan, F. Baganz, R. Wohlgemuth and N. Szita (2017). "Conscious coupling: The challenges and opportunities of cascading enzymatic microreactors." Biotechnology Journal **12**(7): 1700030.
Guan, L.-J., J. Ohtsuka, M. Okai, T. Miyakawa, T. Mase, Y. Zhi, F. Hou, N. Ito, A. Iwasaki, Y. Yasohara and M. Tanokura (2015). "A new target region for changing the substrate specificity of amine transaminases." Scientific Reports **5**(1): 10753.
Guevara-Martínez, M., M. Perez-Zabaleta, M. Gustavsson, J. Quillaguamán, G. Larsson and A. J. A. Van Maris (2019). "The role of the acyl-CoA thioesterase “YciA” in the production of (R)-3-hydroxybutyrate by recombinant Escherichia coli." Applied Microbiology and Biotechnology **103**(9): 3693-3704.
Guevara-Martínez, M., K. Sjöberg Gällnö, G. Sjöberg, J. Jarmander, M. Perez-Zabaleta, J. Quillaguamán and G. Larsson (2015). "Regulating the production of (R)-3-hydroxybutyrate in Escherichia coli by N or P limitation." Frontiers in Microbiology **6**.
Gulevich, A. Y., A. Y. Skorokhodova and V. G. Debabov (2021). "Optimization of (S)-3-Hydroxybutyric Acid Biosynthesis from Glucose through the Reversed Fatty Acid β-Oxidation Pathway by Recombinant Escherichia coli Strains." Applied Biochemistry and Microbiology **57**(2): 161-169.

Guo, F. and P. Berglund (2017). "Transaminase biocatalysis: optimization and application." Green Chemistry **19**(2): 333-360.
Guo, X., X. Miao, Y. An, T. Yan, Y. Jia, B. Deng, J. Cai, W. Yang, W. Sun, R. Wang and J. Xie (2024). "Novel antimicrobial peptides modified with fluorinated sulfono-γ-AA having high stability and targeting multidrug-resistant bacteria infections." European Journal of Medicinal Chemistry **264**: 116001.
Haag, A. F., B. Kerscher, S. Dall'Angelo, M. Sani, R. Longhi, M. Baloban, H. M. Wilson, P. Mergaert, M. Zanda and G. P. Ferguson (2012). "Role of Cysteine Residues and Disulfide Bonds in the Activity of a Legume Root Nodule-specific, Cysteine-rich Peptide." Journal of Biological Chemistry **287**(14): 10791-10798.
Haarr, M. B., K. T. Sriwong and E. O'Reilly (2024). "Commercial Transaminases for the Asymmetric Synthesis of Bulky Amines." European Journal of Organic Chemistry **27**(23).
Hallock, K. J., Lee, D. K., Ramamoorthy, A (2003). "MSI-78, an analogue of the magainin antimicrobial peptides, disrupts lipid bilayer structure via positive curvature strain." Biophysical journal **84**(5): 3052-3060.
Hanahan, D. (1983). "Studies on transformation of Escherichia coli with plasmids." Journal of Molecular Biology **166**(4): 557-580.
Hancock, R. E., & Lehrer, R. (1998). "Cationic peptides: a new source of antibiotics." Trends in biotechnology **16**(2): 82-88.
Hancock, R. E. W. (1997). "Peptide antibiotics." The Lancet **349**(9049): 418-422.
Hancock, R. E. W. P., A. (2002). "Clinical development of cationic antimicrobial peptides: from natural to novel antibiotics." Current drug targets-Infectious disorders **2**(1): 79-83.
Haney, E. F. and R. E. Hancock (2013). "Peptide design for antimicrobial and immunomodulatory applications." Biopolymers **100**(6): 572-583.
Hansen, K. B., Balsells, J., Dreher, S., Hsiao, Y., Kubryk, M., Palucki, M., ... & Grabowski, E. J. (2005). "First generation process for the preparation of the DPP-IV inhibitor sitagliptin. ." Organic process research & development **9**(5): 634-639.
Harden, A. (1901). "LXIV.—The chemical action of Bacillus coli communis and similar organisms on carbohydrates and allied compounds." J. Chem. Soc., Trans. **79**(0): 610-628.
Harris, R. C., M. J. Tallon, M. Dunnett, L. Boobis, J. Coakley, H. J. Kim, J. L. Fallowfield, C. A. Hill, C. Sale and J. A. Wise (2006). "The absorption of orally supplied β-alanine and its effect on muscle carnosine synthesis in human vastus lateralis." Amino Acids **30**(3): 279-289.
Harty, P. S., H. A. Zabriskie, J. L. Erickson, P. E. Molling, C. M. Kerksick and A. R. Jagim (2018). "Multi-ingredient pre-workout supplements, safety implications, and performance outcomes: a brief review." Journal of the International Society of Sports Nutrition **15**(1).
Haukland, H. H., H. Ulvatne, K. Sandvik and L. H. Vorland (2001). "The antimicrobial peptides lactoferricin B and magainin 2 cross over the bacterial cytoplasmic membrane and reside in the cytoplasm." FEBS Letters **508**(3): 389-393.
Hedayati Marzbali, M., I. G. Hakeem, T. Ngo, R. Balu, M. K. Jena, A. Vuppaladadiyam, A. Sharma, N. R. Choudhury, D. J. Batstone and K. Shah (2024). "A critical review on emerging industrial applications of chars from thermal treatment of biosolids." Journal of Environmental Management **369**: 122341.

Heerklotz, H. and J. Seelig (2007). "Leakage and lysis of lipid membranes induced by the lipopeptide surfactin." European Biophysics Journal **36**(4-5): 305-314.
Henry, R. J. (1943). "The mode of action of sulfonamides." Bacteriological reviews **7**(4): 175.
Hilde Ulvatne, L. H. V. (2001). "Bactericidal Kinetics of 3 Lactoferricins Against Staphylococcus aureus and Escherichia coli." Scandinavian Journal of Infectious Diseases **33**(7): 507-511.
Hilpert, K., R. Volkmer-Engert, T. Walter and R. E. Hancock (2005). "High-throughput generation of small antibacterial peptides with improved activity." Nat Biotechnol **23**(8): 1008-1012.
Hoek, K. S., J. M. Milne, P. A. Grieve, D. A. Dionysius and R. Smith (1997). "Antibacterial activity in bovine lactoferrin-derived peptides." Antimicrobial Agents and Chemotherapy **41**(1): 54-59.
Hoskin, D. W. and A. Ramamoorthy (2008). "Studies on anticancer activities of antimicrobial peptides." Biochim Biophys Acta **1778**(2): 357-375.
Hossain, F., H. Dohra and M. Yamazaki (2021). "Effect of Membrane Potential on Entry of Lactoferricin B-Derived 6-Residue Antimicrobial Peptide into Single Escherichia coli Cells and Lipid Vesicles." Journal of Bacteriology **203**(9).
Huang, Y., L. He, G. Li, N. Zhai, H. Jiang and Y. Chen (2014). "Role of helicity of α-helical antimicrobial peptides to improve specificity." Protein & Cell **5**(8): 631-642.
Hueber, A., Y. Gimbert, G. Langevin, J.-M. Galano, A. Guy, T. Durand, N. Cenac, J. Bertrand-Michel and J.-C. Tabet (2022). "Identification of bacterial lipo-amino acids: origin of regenerated fatty acid carboxylate from dissociation of lipo-glutamate anion." Amino Acids **54**(2): 241-250.
Hughes, G. and J. C. Lewis (2018). "Introduction: Biocatalysis in Industry." Chem Rev **118**(1): 1-3.
Humble, M. S., K. E. Cassimjee, V. Abedi, H. J. Federsel and P. Berglund (2012). "Key Amino Acid Residues for Reversed or Improved Enantiospecificity of an ω-Transaminase." ChemCatChem **4**(8): 1167-1172.
Humble, M. S., K. E. Cassimjee, M. Håkansson, Y. R. Kimbung, B. Walse, V. Abedi, H. J. Federsel, P. Berglund and D. T. Logan (2012). "Crystal structures of the Chromobacterium violaceumω-transaminase reveal major structural rearrangements upon binding of coenzyme PLP." The FEBS Journal **279**(5): 779-792.
Hunter, H. N., A. R. Demcoe, H. Jenssen, T. J. Gutteberg and H. J. Vogel (2005). "Human lactoferricin is partially folded in aqueous solution and is better stabilized in a membrane mimetic solvent." Antimicrob Agents Chemother **49**(8): 3387-3395.
Hwang, P. M., N. Zhou, X. Shan, C. H. Arrowsmith and H. J. Vogel (1998). "Three-Dimensional Solution Structure of Lactoferricin B, an Antimicrobial Peptide Derived from Bovine Lactoferrin." Biochemistry **37**(12): 4288-4298.
IMARC. (2024). "Europe Biocatalyst Market." Retrieved 29/07/2024, 2024, from https://www.imarcgroup.com/europe-biocatalyst-market.
Iqbal, A., R. S. Khan, K. Shehryar, A. Imran, F. Ali, S. Attia, S. Shah and M. Mii (2019). "Antimicrobial peptides as effective tools for enhanced disease resistance in plants." Plant Cell, Tissue and Organ Culture (PCTOC) **139**(1): 1-15.
Ishikawa, M., T. Kubo and S. Natori (1992). "Purification and characterization of a diptericin homologue from Sarcophaga peregrina (flesh fly)." Biochemical Journal **287**(2): 573-578.

Islam, M. Z., F. Hossain, M. H. Ali and M. Yamazaki (2023). "Relationship between antimicrobial peptides-induced cell membrane damage and bactericidal activity." Biophysical Journal **122**(24): 4645-4655.
Ivanković, A. (2017). "Review of 12 Principles of Green Chemistry in Practice." International Journal of Sustainable and Green Energy **6**(3): 39.
Iwata, R., S. Furumoto, C. Pascali, A. Bogni and K. Ishiwata (2003). "Radiosynthesis of O-[¹¹C]methyl-<scp>L</scp>-tyrosine and O-[¹⁸F]Fluoromethyl-<scp>L</scp>-tyrosine as potential PET tracers for imaging amino acid transport." Journal of Labelled Compounds and Radiopharmaceuticals **46**(6): 555-566.
Jain, N., S. W. Smith, S. Ghone and B. Tomczuk (2015). "Current ADC Linker Chemistry." Pharmaceutical Research **32**(11): 3526-3540.
Jallet, D., V. Soldan, R. Shayan, A. Stella, N. Ismail, R. Zenati, E. Cahoreau, O. Burlet-Schiltz, S. Balor, P. Millard and S. Heux (2024). "Integrative in vivo analysis of the ethanolamine utilization bacterial microcompartment in Escherichia coli." mSystems.
Jarmander, J., J. Belotserkovsky, G. Sjöberg, M. Guevara-Martínez, M. Pérez-Zabaleta, J. Quillaguamán and G. Larsson (2015). "Cultivation strategies for production of (R)-3-hydroxybutyric acid from simultaneous consumption of glucose, xylose and arabinose by Escherichia coli." Microbial Cell Factories **14**(1).
Javid-Majd, F. and J. S. Blanchard (2000). "Mechanistic Analysis of the argE-Encoded N-Acetylornithine Deacetylase." Biochemistry **39**(6): 1285-1293.
Jendrossek, D. and R. Handrick (2002). "Microbial Degradation of Polyhydroxyalkanoates." Annual Review of Microbiology **56**(1): 403-432.
Jiang, N., M. Wang, L. Song, D. Yu, S. Zhou, Y. Li, H. Li and X. Han (2023). "Polyhydroxybutyrate production by recombinant Escherichia coli based on genes related to synthesis pathway of PHB from Massilia sp. UMI-21." Microbial Cell Factories **22**(1).
Jiang, Y., B. Chen, C. Duan, B. Sun, J. Yang and S. Yang (2015). "Multigene Editing in the Escherichia coli Genome via the CRISPR-Cas9 System." Applied and Environmental Microbiology **81**(7): 2506-2514.
John Owonubi, S., N. M. Malima and N. Revaprasadu (2020). Metal Oxide–Based Nanocomposites as Antimicrobial and Biomedical Agents, Elsevier**:** 287-323.
John, R. A. (1995). "Pyridoxal phosphate-dependent enzymes." Biochimica et Biophysica Acta (BBA) - Protein Structure and Molecular Enzymology **1248**(2): 81-96.
Jones, G., P. Willett, R. C. Glen, A. R. Leach and R. Taylor (1997). "Development and validation of a genetic algorithm for flexible docking 1 1Edited by F. E. Cohen." Journal of Molecular Biology **267**(3): 727-748.
Jongkind, E. P. J., A. Fossey-Jouenne, O. Mayol, A. Zaparucha, C. Vergne-Vaxelaire and C. E. Paul (2022). "Synthesis of Chiral Amines via a Bi-Enzymatic Cascade Using an Ene-Reductase and Amine Dehydrogenase." ChemCatChem **14**(2).
Joo, H.-S. and M. Otto (2015). "Mechanisms of resistance to antimicrobial peptides in staphylococci." Biochimica et Biophysica Acta (BBA) - Biomembranes **1848**(11): 3055-3061.
Jumper, J., R. Evans, A. Pritzel, T. Green, M. Figurnov, O. Ronneberger, K. Tunyasuvunakool, R. Bates, A. Žídek, A. Potapenko, A. Bridgland, C. Meyer, S. A. A. Kohl, A. J. Ballard, A. Cowie, B. Romera-Paredes, S. Nikolov, R. Jain, J. Adler, T. Back, S.

Petersen, D. Reiman, E. Clancy, M. Zielinski, M. Steinegger, M. Pacholska, T. Berghammer, S. Bodenstein, D. Silver, O. Vinyals, A. W. Senior, K. Kavukcuoglu, P. Kohli and D. Hassabis (2021). "Highly accurate protein structure prediction with AlphaFold." Nature **596**(7873): 583-589.
Kakuda, H., K. Shiroishi, K. Hosono and S. Ichihara (1994). "Construction of Pta-Ack Pathway Deletion Mutants ofEscherichia coliand Characteristic Growth Profiles of the Mutants in a Rich Medium." Bioscience, Biotechnology, and Biochemistry **58**(12): 2232-2235.
Kaminski, H. M. and J. B. Feix (2011). "Effects of D-Lysine Substitutions on the Activity and Selectivity of Antimicrobial Peptide CM15." Polymers (Basel) **3**(4): 2088-2106.
Kampshoff, F., M. D. P. Willcox and D. Dutta (2019). "A Pilot Study of the Synergy between Two Antimicrobial Peptides and Two Common Antibiotics." Antibiotics **8**(2): 60.
Kamysz, E., E. Sikorska, M. Jaskiewicz, M. Bauer, D. Neubauer, S. Bartoszewska, W. Baranska-Rybak and W. Kamysz (2020). "Lipidated Analogs of the LL-37-Derived Peptide Fragment KR12-Structural Analysis, Surface-Active Properties and Antimicrobial Activity." Int J Mol Sci **21**(3).
Kang, J. H., M. K. Lee, K. L. Kim and K. S. Hahm (1996). "Structure–biological activity relationships of 11-residue highly basic peptide segment of bovine lactoferrin." International Journal of Peptide and Protein Research **48**(4): 357-363.
Karav, S., J. German, C. Rouquié, A. Le Parc and D. Barile (2017). "Studying Lactoferrin N-Glycosylation." International Journal of Molecular Sciences **18**(4): 870.
Katz, L. and R. H. Baltz (2016). "Natural product discovery: past, present, and future." J Ind Microbiol Biotechnol **43**(2-3): 155-176.
Kelly, S. A., S. Pohle, S. Wharry, S. Mix, C. C. R. Allen, T. S. Moody and B. F. Gilmore (2018). "Application of ω-Transaminases in the Pharmaceutical Industry." Chemical Reviews **118**(1): 349-367.
Kharissova, O. V., B. I. Kharisov, C. M. Oliva González, Y. P. Méndez and I. López (2019). "Greener synthesis of chemical compounds and materials." Royal Society Open Science **6**(11): 191378.
Kim, K.-R. and D.-K. Oh (2013). "Production of hydroxy fatty acids by microbial fatty acid-hydroxylation enzymes." Biotechnology Advances **31**(8): 1473-1485.
Kim, S.-K. and Y.-C. Park (2019). "Biosynthesis of ω-hydroxy fatty acids and related chemicals from natural fatty acids by recombinant Escherichia coli." Applied Microbiology and Biotechnology **103**(1): 191-199.
Klug, D. M., F. I. M. Idiris, M. A. T. Blaskovich, F. Von Delft, C. G. Dowson, C. Kirchhelle, A. P. Roberts, A. C. Singer and M. H. Todd (2021). "There is no market for new antibiotics: this allows an open approach to research and development." Wellcome Open Research **6**: 146.
Knaus, T., W. Böhmer and F. G. Mutti (2017). "Amine dehydrogenases: efficient biocatalysts for the reductive amination of carbonyl compounds." Green Chemistry **19**(2): 453-463.
Kohrer, C., & RajBhandary, U. L. (2013). "Proteins Carrying One or More Unnatural Amino Acids. In: Madame Curie Bioscience Database [Internet]. ." from https://www.ncbi.nlm.nih.gov/books/NBK6136/.
Kohrer, C., & RajBhandary, U. L. (2013). Proteins carrying one or more unnatural amino acids. Madame Curie Bioscience Database. Internet, Landes Bioscience.

Koszelewski, D., D. Clay, D. Rozzell and W. Kroutil (2009). "Deracemisation of α-Chiral Primary Amines by a One-Pot, Two-Step Cascade Reaction Catalysed by ω-Transaminases." European Journal of Organic Chemistry **2009**(14): 2289-2292.
Kumar, P., J. N. Kizhakkedathu and S. K. Straus (2018). "Antimicrobial Peptides: Diversity, Mechanism of Action and Strategies to Improve the Activity and Biocompatibility In Vivo." Biomolecules **8**(1).
Kutila, T., S. Pyörälä, H. Saloniemi and L. Kaartinen (2003). Acta Veterinaria Scandinavica **44**(1): 35.
Lam, J., P. Katti, M. Biete, M. Mungai, S. Ashshareef, K. Neikirk, E. Garza Lopez, Z. Vue, T. A. Christensen, H. K. Beasley, T. A. Rodman, S. A. Murray, J. L. Salisbury, B. Glancy, J. Shao, R. O. Pereira, E. D. Abel and A. Hinton (2021). "A Universal Approach to Analyzing Transmission Electron Microscopy with ImageJ." Cells **10**(9): 2177.
Lande, R., G. Chamilos, D. Ganguly, O. Demaria, L. Frasca, S. Durr, C. Conrad, J. Schroder and M. Gilliet (2015). "Cationic antimicrobial peptides in psoriatic skin cooperate to break innate tolerance to self-DNA." Eur J Immunol **45**(1): 203-213.
Lande, R., J. Gregorio, V. Facchinetti, B. Chatterjee, Y. H. Wang, B. Homey, W. Cao, Y. H. Wang, B. Su, F. O. Nestle, T. Zal, I. Mellman, J. M. Schroder, Y. J. Liu and M. Gilliet (2007). "Plasmacytoid dendritic cells sense self-DNA coupled with antimicrobial peptide." Nature **449**(7162): 564-569.
Lartey, P. A., H. N. Nellans and S. K. Tanaka (1994). New Developments in Macrolides: Structures and Antibacterial and Prokinetic Activities, Elsevier**:** 307-343.
Le, C.-F., C.-M. Fang and S. D. Sekaran (2017). "Intracellular Targeting Mechanisms by Antimicrobial Peptides." Antimicrobial Agents and Chemotherapy **61**(4): AAC.02340-02316.
Le, W., B. Chen, Z. Cui, Z. Liu and D. Shi (2019). "Detection of cancer cells based on glycolytic-regulated surface electrical charges." Biophysics Reports **5**(1): 10-18.
Lee, K.-H. (2002). "Development of Short Antimicrobial Peptides Derived from Host Defense Peptides or by Combinatorial Libraries." Current Pharmaceutical Design **8**(9): 795-813.
Lee, S.-H., S. J. Park, S. Y. Lee and S. H. Hong (2008). "Biosynthesis of enantiopure (S)-3-hydroxybutyric acid in metabolically engineered Escherichia coli." Applied Microbiology and Biotechnology **79**(4): 633-641.
Lee, T.-H., K. N. Hall and M.-I. Aguilar (2015). "Antimicrobial Peptide Structure and Mechanism of Action: A Focus on the Role of Membrane Structure." Current Topics in Medicinal Chemistry **16**(1): 25-39.
Lehninger, A. L., H. C. Sudduth and J. B. Wise (1960). "d-β-Hydroxybutyric Dehydrogenase of Mitochondria." Journal of Biological Chemistry **235**(8): 2450-2455.
Lehrer, R. I. (1998). Microbicidal Mechanisms, Oxygen-Independent, Elsevier**:** 1719-1725.
Leistner, R., Bloch, A., Sakellariou, C., Gastmeier, P., & Schwab, F (2014). "Costs and length of stay associated with extended-spectrum β-lactamase production in cases of Escherichia coli bloodstream infection." Journal of global antimicrobial resistance **2**(2): 107-109.
Lemeignan, B., P. Sonigo and P. Marlière (1993). "Phenotypic Suppression by Incorporation of an Alien Amino Acid." Journal of Molecular Biology **231**(2): 161-166.
León-Sicairos, N., C. Ordaz-Pichardo, J. C. Carrero and M. D. L. Garza (2017). Lactoferrin in the Battle against Intestinal Parasites: A Review, InTech.

Lewis, K. (2013). "Platforms for antibiotic discovery." Nat Rev Drug Discov **12**(5): 371-387.
Li, D., Y. Yang, R. Li, L. Huang, Z. Wang, Q. Deng and S. Dong (2021). "N-terminal acetylation of antimicrobial peptide L163 improves its stability against protease degradation." Journal of Peptide Science **27**(9).
Li, R.-H., J. Huang, C.-X. Liu, K. Yu, F. Guo, Y. Li, Z.-H. Chen, X. Wang, R.-X. Zhao, J.-Y. Zhang, J.-J. Liang, Y. Li, L. Lin, L. Sun, X.-Y. Li and B. Li (2023). "Genome-centric metagenomics provides new insights into metabolic pathways of polyhydroxyalkanoates biosynthesis and functional microorganisms subsisting on municipal organic wastes." Water Research **244**: 120512.
Li, X., C. Gao, W. Wei, W. Song, W. Meng, J. Liu, X. Chen, C. Gao, L. Guo, L. Liu and J. Wu (2023). "A Tri-Enzyme Cascade for Efficient Production of L-2-Aminobutyrate from L-Threonine." ChemBioChem **24**(15).
Lindqvist, Y. (1989). "Refined structure of spinach glycolate oxidase at 2 Å resolution." Journal of Molecular Biology **209**(1): 151-166.
Liscano, Y., J. Oñate-Garzón and J. P. Delgado (2020). "Peptides with Dual Antimicrobial–Anticancer Activity: Strategies to Overcome Peptide Limitations and Rational Design of Anticancer Peptides." Molecules **25**(18): 4245.
Liu, F., J. Zhou, M. Xu, T. Yang, M. Shao, X. Zhang and Z. Rao (2020). "One-Pot Biocatalytic Preparation of Enantiopure Unusual α-Amino Acids from α-Hydroxy Acids via a Hydrogen-Borrowing Dual-Enzyme Cascade." Catalysts **10**(12): 1470.
Liu, J., W. Kong, J. Bai, Y. Li, L. Dong, L. Zhou, Y. Liu, J. Gao, R. T. Bradshaw Allen, N. J. Turner and Y. Jiang (2022). "Amine dehydrogenases: Current status and potential value for chiral amine synthesis." Chem Catalysis **2**(6): 1288-1314.
Liu, N., J. Feng, X. Chen, Y. Luo, T. Lv, Q. Wu and D. Zhu (2023). "Reshaping the Substrate Binding Pocket of β-Amino Acid Dehydrogenase for the Synthesis of Aromatic β-Amino Acids." Organic Letters **25**(47): 8469-8473.
Liu, Q., S.-P. Ouyang, A. Chung, Q. Wu and G.-Q. Chen (2007). "Microbial production of R-3-hydroxybutyric acid by recombinant E. coli harboring genes of phbA, phbB, and tesB." Applied Microbiology and Biotechnology **76**(4): 811-818.
Liu, S. (2020). A molecular investigation of the synthesis of polyhydroxyalkanoates in Pseudomonas putida KT2440 and the recombinant production of 3-hydroxyalkanoic acids in Escherichia coli. PhD, University College Dublin.
Liu, Y., J. Zhou and Z. Sun (2024). "Direct synthesis of unnatural amino acids and modifications of peptides via LADA strategy." Chinese Chemical Letters **35**(1): 108553.
Lozano Terol, G., J. Gallego-Jara, R. A. Sola Martínez, M. Cánovas Díaz and T. De Diego Puente (2019). "Engineering protein production by rationally choosing a carbon and nitrogen source using E. coli BL21 acetate metabolism knockout strains." Microbial Cell Factories **18**(1).
Lu, J., H. Xu, J. Xia, J. Ma, J. Xu, Y. Li and J. Feng (2020). "D- and Unnatural Amino Acid Substituted Antimicrobial Peptides With Improved Proteolytic Resistance and Their Proteolytic Degradation Characteristics." Frontiers in Microbiology **11**.
Luo, W., J. Hu, J. Lu, H. Zhang, X. Wang, Y. Liu, L. Dong and X. Yu (2021). "One pot cascade synthesis of L-2-aminobutyric acid employing ω-transaminase from Paracoccus pantotrophus." Molecular Catalysis **515**: 111890.

Lv, B., W. Yin, J. Gao, H. Liu, K. Liu, J. Bai and Q. Yang (2018). "Neo-5,22E-Cholestadienol Derivatives from Buthus martensii Karsch and Targeted Bactericidal Action Mechanisms." Molecules **24**(1): 72.
Macheroux, P., Massey, V., Thiele, D. J., & Volokita, M. (1991). " Expression of spinach glycolate oxidase in Saccharomyces cerevisiae: purification and characterization." Biochemistry **30**(18): 4612-4619.
Madani, F., S. Lindberg, U. Langel, S. Futaki and A. Graslund (2011). "Mechanisms of cellular uptake of cell-penetrating peptides." J Biophys **2011**: 414729.
Malina, A. and Y. Shai (2005). "Conjugation of fatty acids with different lengths modulates the antibacterial and antifungal activity of a cationic biologically inactive peptide." Biochemical Journal **390**(3): 695-702.
Martínez-Rodríguez, S., J. M. Torres, P. Sánchez and E. Ortega (2020). "Overview on Multienzymatic Cascades for the Production of Non-canonical α-Amino Acids." Frontiers in Bioengineering and Biotechnology **8**.
Martínez, B. R., A.; Suárez, E. (2016). Antimicrobial Peptides Produced by Bacteria: The Bacteriocins. New weapons to control bacterial growth V. M. Villa T., Springer, Cham.**:** 15-38.
Mathew, S. and H. Yun (2012). "ω-Transaminases for the Production of Optically Pure Amines and Unnatural Amino Acids." ACS Catalysis **2**(6): 993-1001.
McCann, S. D., E. C. Reichert, P. L. Arrechea and S. L. Buchwald (2020). "Development of an Aryl Amination Catalyst with Broad Scope Guided by Consideration of Catalyst Stability." Journal of the American Chemical Society **142**(35): 15027-15037.
McMurry, L. P., R. E. Levy, S. B. (1980). "Active efflux of tetracycline encoded by four genetically different tetracycline resistance determinants in Escherichia coli." Proceedings of the national academy of sciences **77**(7): 3974-3977.
Mendez-Samperio, P. (2014). "Peptidomimetics as a new generation of antimicrobial agents: current progress." Infect Drug Resist **7**: 229-237.
Meng, Q., C. Ramírez-Palacios, N. Capra, M. E. Hooghwinkel, S. Thallmair, H. J. Rozeboom, A.-M. W. H. Thunnissen, H. J. Wijma, S. J. Marrink and D. B. Janssen (2021). "Computational Redesign of an ω-Transaminase from Pseudomonas jessenii for Asymmetric Synthesis of Enantiopure Bulky Amines." ACS Catalysis **11**(17): 10733-10747.
Mesa, J. A., L. Sierra-Fontalvo, K. Ortegon and A. Gonzalez-Quiroga (2024). "Advancing circular bioeconomy: A critical review and assessment of indicators." Sustainable Production and Consumption **46**: 324-342.
Michael, C. A., D. Dominey-Howes and M. Labbate (2014). "The antimicrobial resistance crisis: causes, consequences, and management." Front Public Health **2**: 145.
Michael Conlon, J., R. Al-Kharrge, E. Ahmed, H. Raza, S. Galadari and E. Condamine (2007). "Effect of aminoisobutyric acid (Aib) substitutions on the antimicrobial and cytolytic activities of the frog skin peptide, temporin-1DRa." Peptides **28**(10): 2075-2080.
Micsonai, A., É. Moussong, F. Wien, E. Boros, H. Vadászi, N. Murvai, Y.-H. Lee, T. Molnár, M. Réfrégiers, Y. Goto, Á. Tantos and J. Kardos (2022). "BeStSel: webserver for secondary structure and fold prediction for protein CD spectroscopy." Nucleic Acids Research **50**(W1): W90-W98.

Mierziak, J., M. Burgberger and W. Wojtasik (2021). "3-Hydroxybutyrate as a Metabolite and a Signal Molecule Regulating Processes of Living Organisms." Biomolecules **11**(3): 402.
Millard, P., B. Enjalbert, S. Uttenweiler-Joseph, J.-C. Portais and F. Létisse (2021). "Control and regulation of acetate overflow in Escherichia coli." eLife **10**.
Mohamed, M. F., A. Brezden, H. Mohammad, J. Chmielewski and M. N. Seleem (2017). "A short D-enantiomeric antimicrobial peptide with potent immunomodulatory and antibiofilm activity against multidrug-resistant Pseudomonas aeruginosa and Acinetobacter baumannii." Scientific Reports **7**(1).
Mohanrasu, K., R. Guru Raj Rao, V. Ananthi, G. Sivaprakash, G. H. Dinesh, T. A. Swetha, J. Jeyakanthan and A. Arun (2022). Microbial bio-based polymer nanocomposite for food industry applications, Elsevier**:** 331-354.
Moniruzzaman, M., M. Z. Islam, S. Sharmin, H. Dohra and M. Yamazaki (2017). "Entry of a Six-Residue Antimicrobial Peptide Derived from Lactoferricin B into Single Vesicles and Escherichia coli Cells without Damaging their Membranes." Biochemistry **56**(33): 4419-4431.
Moreira Brito, J. C., L. R. Carvalho, A. Neves De Souza, G. Carneiro, P. P. Magalhães, L. M. Farias, N. R. Guimarães, R. M. Verly, J. M. Resende and M. Elena De Lima (2022). "PEGylation of the antimicrobial peptide LyeTx I-b maintains structure-related biological properties and improves selectivity." Frontiers in Molecular Biosciences **9**.
Mouton, J. W., J. Meletiadis, A. Voss and J. Turnidge (2018). "Variation of MIC measurements: the contribution of strain and laboratory variability to measurement precision." Journal of Antimicrobial Chemotherapy **73**(9): 2374-2379.
Murray, C. J. L., K. S. Ikuta, F. Sharara, L. Swetschinski, G. Robles Aguilar, A. Gray, C. Han, C. Bisignano, P. Rao, E. Wool, S. C. Johnson, A. J. Browne, M. G. Chipeta, F. Fell, S. Hackett, G. Haines-Woodhouse, B. H. Kashef Hamadani, E. A. P. Kumaran, B. McManigal, S. Achalapong, R. Agarwal, S. Akech, S. Albertson, J. Amuasi, J. Andrews, A. Aravkin, E. Ashley, F.-X. Babin, F. Bailey, S. Baker, B. Basnyat, A. Bekker, R. Bender, J. A. Berkley, A. Bethou, J. Bielicki, S. Boonkasidecha, J. Bukosia, C. Carvalheiro, C. Castañeda-Orjuela, V. Chansamouth, S. Chaurasia, S. Chiurchiù, F. Chowdhury, R. Clotaire Donatien, A. J. Cook, B. Cooper, T. R. Cressey, E. Criollo-Mora, M. Cunningham, S. Darboe, N. P. J. Day, M. De Luca, K. Dokova, A. Dramowski, S. J. Dunachie, T. Duong Bich, T. Eckmanns, D. Eibach, A. Emami, N. Feasey, N. Fisher-Pearson, K. Forrest, C. Garcia, D. Garrett, P. Gastmeier, A. Z. Giref, R. C. Greer, V. Gupta, S. Haller, A. Haselbeck, S. I. Hay, M. Holm, S. Hopkins, Y. Hsia, K. C. Iregbu, J. Jacobs, D. Jarovsky, F. Javanmardi, A. W. J. Jenney, M. Khorana, S. Khusuwan, N. Kissoon, E. Kobeissi, T. Kostyanev, F. Krapp, R. Krumkamp, A. Kumar, H. H. Kyu, C. Lim, K. Lim, D. Limmathurotsakul, M. J. Loftus, M. Lunn, J. Ma, A. Manoharan, F. Marks, J. May, M. Mayxay, N. Mturi, T. Munera-Huertas, P. Musicha, L. A. Musila, M. M. Mussi-Pinhata, R. N. Naidu, T. Nakamura, R. Nanavati, S. Nangia, P. Newton, C. Ngoun, A. Novotney, D. Nwakanma, C. W. Obiero, T. J. Ochoa, A. Olivas-Martinez, P. Olliaro, E. Ooko, E. Ortiz-Brizuela, P. Ounchanum, G. D. Pak, J. L. Paredes, A. Y. Peleg, C. Perrone, T. Phe, K. Phommasone, N. Plakkal, A. Ponce-De-Leon, M. Raad, T. Ramdin, S. Rattanavong, A. Riddell, T. Roberts, J. V. Robotham, A. Roca, V. D. Rosenthal, K. E. Rudd, N. Russell, H. S. Sader, W. Saengchan, J. Schnall, J. A. G. Scott, S. Seekaew, M. Sharland, M. Shivamallappa, J. Sifuentes-Osornio, A. J. Simpson, N. Steenkeste, A. J. Stewardson, T. Stoeva, N. Tasak, A. Thaiprakong, G. Thwaites, C. Tigoi, C. Turner, P.

Turner, H. R. Van Doorn, S. Velaphi, A. Vongpradith, M. Vongsouvath, H. Vu, T. Walsh, J. L. Walson, S. Waner, T. Wangrangsimakul, P. Wannapinij, T. Wozniak, T. E. M. W. Young Sharma, K. C. Yu, P. Zheng, B. Sartorius, A. D. Lopez, A. Stergachis, C. Moore, C. Dolecek and M. Naghavi (2022). "Global burden of bacterial antimicrobial resistance in 2019: a systematic analysis." The Lancet **399**(10325): 629-655.
Musa, M. M., F. Hollmann and F. G. Mutti (2019). "Synthesis of enantiomerically pure alcohols and amines via biocatalytic deracemisation methods." Catalysis Science & Technology **9**(20): 5487-5503.
Musiejuk, M. and P. Kafarski (2023). "Engineering of Nisin as a Means for Improvement of Its Pharmacological Properties: A Review." Pharmaceuticals **16**(8): 1058.
Mutti, F. G., T. Knaus, N. S. Scrutton, M. Breuer and N. J. Turner (2015). "Conversion of alcohols to enantiopure amines through dual-enzyme hydrogen-borrowing cascades." Science **349**(6255): 1525-1529.
Ney, Y., M. Jawad Nasim, A. Kharma, L. Youssef and C. Jacob (2018). "Small Molecule Catalysts with Therapeutic Potential." Molecules **23**(4): 765.
Nguyen, L. T., J. K. Chau, N. A. Perry, L. De Boer, S. A. J. Zaat and H. J. Vogel (2010). "Serum Stabilities of Short Tryptophan- and Arginine-Rich Antimicrobial Peptide Analogs." PLoS ONE **5**(9): e12684.
Ni, R., S. Bhandari, P. R. Mitchell, G. Suarez, N. B. Patel, K. Lamb, K. S. Bisht and D. J. Merkler (2021). "Synthesis, Quantification, and Characterization of Fatty Acid Amides from In Vitro and In Vivo Sources." Molecules **26**(9): 2543.
Nijnik, A. and R. Hancock (2009). "Host defence peptides: antimicrobial and immunomodulatory activity and potential applications for tackling antibiotic-resistant infections." Emerg Health Threats J **2**: e1.
Nikawa, H. S., L. P.; Tenovuo, J.; Pang, K. M.; Hamada, T. (1993). "The fungicidal effect of human lactoferrin on Candida albicans and Candida krusei." Archives of oral biology **38**(12): 1057-1063.
Noh, H. J., S. Y. Lee and Y.-S. Jang (2019). "Microbial production of butyl butyrate, a flavor and fragrance compound." Applied Microbiology and Biotechnology **103**(5): 2079-2086.
Novick, S. J., N. Dellas, R. Garcia, C. Ching, A. Bautista, D. Homan, O. Alvizo, D. Entwistle, F. Kleinbeck, T. Schlama and T. Ruch (2021). "Engineering an Amine Transaminase for the Efficient Production of a Chiral Sacubitril Precursor." ACS Catalysis **11**(6): 3762-3770.
Nugent, T. C. and M. El-Shazly (2010). "Chiral Amine Synthesis – Recent Developments and Trends for Enamide Reduction, Reductive Amination, and Imine Reduction." Advanced Synthesis & Catalysis **352**(5): 753-819.
O'Neill, J. (2015). Antimicrobials in agriculture and the environment : reducing unnecessary use and waste. London, Review on Antimicrobial Resistance.
Oh, J. E., & Lee, K. H. (1999). "Synthesis of novel unnatural amino acid as a building block and its incorporation into an antimicrobial peptide." Bioorganic & medicinal chemistry **7**(12): 2985-2990.
Oh, W., D. Jeong and J. W. Park (2023). "An Artificial Compartmentalized Biocatalytic Cascade System Constructed With Enzyme-Caged Reticulate Nanoporous Membranes." Advanced Materials Interfaces **10**(17).
Ojo, A. O. and O. De Smidt (2023). "Lactic Acid: A Comprehensive Review of Production to Purification." Processes **11**(3): 688.

Oren, Z. and Y. Shai (2000). "Cyclization of a Cytolytic Amphipathic α-Helical Peptide and Its Diastereomer: Effect on Structure, Interaction with Model Membranes, and Biological Function." Biochemistry **39**(20): 6103-6114.
Ortega, C., R. López, J. Cacho and V. Ferreira (2001). "Fast analysis of important wine volatile compounds." Journal of Chromatography A **923**(1-2): 205-214.
Ortiz, E., J. Shezaf, Y.-H. Chang and M. J. Krische (2022). "Enantioselective Metal-Catalyzed Reductive Coupling of Alkynes with Carbonyl Compounds and Imines: Convergent Construction of Allylic Alcohols and Amines." ACS Catalysis **12**(14): 8164-8174.
Park, C. B. K., M. S. Kim, S. C. (1996). "A novel antimicrobial peptide frombufo bufo gargarizans." Biochemical and biophysical research communications **218**(1): 408-413.
Park, E., M. Kim and J. S. Shin (2010). "One-Pot Conversion of <scp>L</scp>-Threonine into <scp>L</scp>-Homoalanine: Biocatalytic Production of an Unnatural Amino Acid from a Natural One." Advanced Synthesis & Catalysis **352**(18): 3391-3398.
Parodi, A., D'Ambrosio, M., Mazzocchetti, L., Martinez, G. A., Samori, C., Torri, C., & Galletti, P. (2021). "Chemical recycling of polyhydroxybutyrate (PHB) into bio-based solvents and their use in a circular PHB extraction." ACS Sustainable Chemistry & Engineering **9**(37): 12575-12583.
Parthasarathy, A., M. A. Savka and A. O. Hudson (2019). "The Synthesis and Role of β-Alanine in Plants." Frontiers in Plant Science **10**.
Patel, V. R., G. G. Dumancas, L. C. K. Viswanath, R. Maples and B. J. J. Subong (2016). "Castor Oil: Properties, Uses, and Optimization of Processing Parameters in Commercial Production." Lipid Insights **9**: LPI.S40233.
Patil, S. T., L. Zhang, F. Martenyi, S. L. Lowe, K. A. Jackson, B. V. Andreev, A. S. Avedisova, L. M. Bardenstein, I. Y. Gurovich, M. A. Morozova, S. N. Mosolov, N. G. Neznanov, A. M. Reznik, A. B. Smulevich, V. A. Tochilov, B. G. Johnson, J. A. Monn and D. D. Schoepp (2007). "Activation of mGlu2/3 receptors as a new approach to treat schizophrenia: a randomized Phase 2 clinical trial." Nature Medicine **13**(9): 1102-1107.
Perez-Zabaleta, M., M. Guevara-Martínez, M. Gustavsson, J. Quillaguamán, G. Larsson and A. J. A. Van Maris (2019). "Comparison of engineered Escherichia coli AF1000 and BL21 strains for (R)-3-hydroxybutyrate production in fed-batch cultivation." Applied Microbiology and Biotechnology **103**(14): 5627-5639.
Perez-Zabaleta, M., G. Sjöberg, M. Guevara-Martínez, J. Jarmander, M. Gustavsson, J. Quillaguamán and G. Larsson (2016). "Increasing the production of (R)-3-hydroxybutyrate in recombinant Escherichia coli by improved cofactor supply." Microbial Cell Factories **15**(1).
Phue, J.-N. and J. Shiloach (2005). "Impact of dissolved oxygen concentration on acetate accumulation and physiology of E. coli BL21, evaluating transcription levels of key genes at different dissolved oxygen conditions." Metabolic Engineering **7**(5-6): 353-363.
Powers, J. P. and R. E. Hancock (2003). "The relationship between peptide structure and antibacterial activity." Peptides **24**(11): 1681-1691.
Prieto, A., I. F. Escapa, V. Martínez, N. Dinjaski, C. Herencias, F. De La Peña, N. Tarazona and O. Revelles (2016). "A holistic view of polyhydroxyalkanoate metabolism in Pseudomonas putida." Environmental Microbiology **18**(2): 341-357.

Qoronfleh, M. W. (1999). "Dissolved Oxygen Concentration Affects the Accumulation of HIV-1 Recombinant Proteins in Escherichia coli." Applied Biochemistry and Biotechnology **80**(2): 107-120.
Querinjean, P. M., P. L, Heremans, J. F. (1971). "Molecular weight, single-chain structure and amino acid composition of human lactoferrin." European journal of biochemistry **20**(3): 420-425.
Rai, D. K. and S. Qian (2017). "Interaction of the Antimicrobial Peptide Aurein 1.2 and Charged Lipid Bilayer." Scientific Reports **7**(1).
Rainard, P. (1987). "Bacteriostatic activity of bovine lactoferrin in mastitic milk. ." Veterinary microbiology **13**(2): 159-166.
Rekdal, Ø., Andersen, J., Vorland, L. H., & Svendsen, J. S. (1999). "Construction and synthesis of lactoferricin derivatives with enhanced antibacterial activity. ." Journal of Peptide Science: An Official Publication of the European Peptide Society **2**(1): 011501.
Rodríguez-Contreras, A., M. Calafell-Monfort and M. S. Marqués-Calvo (2012). "Enzymatic degradation of poly(3-hydroxybutyrate-co-4-hydroxybutyrate) by commercial lipases." Polymer Degradation and Stability **97**(4): 597-604.
Rodríguez-Melcón, C., C. Alonso-Calleja, C. García-Fernández, J. Carballo and R. Capita (2021). "Minimum Inhibitory Concentration (MIC) and Minimum Bactericidal Concentration (MBC) for Twelve Antimicrobials (Biocides and Antibiotics) in Eight Strains of Listeria monocytogenes." Biology **11**(1): 46.
Rosenfeld, Y., Lev, N., & Shai, Y. (2010). "Effect of the hydrophobicity to net positive charge ratio on antibacterial and anti-endotoxin activities of structurally similar antimicrobial peptides. ." Biochemistry **49**(5): 853-861.
Rossino, G., M. S. Robescu, E. Licastro, C. Tedesco, I. Martello, L. Maffei, G. Vincenti, T. Bavaro and S. Collina (2022). "Biocatalysis: A smart and green tool for the preparation of chiral drugs." Chirality **34**(11): 1403-1418.
Rounds, T. and S. K. Straus (2020). "Lipidation of Antimicrobial Peptides as a Design Strategy for Future Alternatives to Antibiotics." Int J Mol Sci **21**(24).
Rudat, J., B. R. Brucher and C. Syldatk (2012). "Transaminases for the synthesis of enantiopure beta-amino acids." AMB Express **2**(1): 11.
Ruf, J., A. Emberger-Klein and K. Menrad (2022). "Consumer response to bio-based products – A systematic review." Sustainable Production and Consumption **34**: 353-370.
Russmayer, H., H. Marx and M. Sauer (2019). "Microbial 2-butanol production with Lactobacillus diolivorans." Biotechnology for Biofuels **12**(1).
Ruth, K., A. Grubelnik, R. Hartmann, T. Egli, M. Zinn and Q. Ren (2007). "Efficient Production of (R)-3-Hydroxycarboxylic Acids by Biotechnological Conversion of Polyhydroxyalkanoates and Their Purification." Biomacromolecules **8**(1): 279-286.
Saito, S., R. Imai, Y. Miyahara, M. Nakagawa, I. Orita, T. Tsuge and T. Fukui (2022). "Biosynthesis of Poly(3-hydroxybutyrate-co-3-hydroxyhexanoate) From Glucose by Escherichia coli Through Butyryl-CoA Formation Driven by Ccr-Emd Combination." Frontiers in Bioengineering and Biotechnology **10**.
Samuelsen, Ã. R., H. H. Haukland, H. Ulvatne and L. H. Vorland (2004). "Anti-complement effects of lactoferrin-derived peptides." FEMS Immunology & Medical Microbiology **41**(2): 141-148.

Sani, M.-A., S. Rajput, D. W. Keizer and F. Separovic (2024). "NMR techniques for investigating antimicrobial peptides in model membranes and bacterial cells." Methods **224**: 10-20.
Savile, C. K., Janey, J. M., Mundorff, E. C., Moore, J. C., Tam, S., Jarvis, W. R., ... Devine, P. N. (2010). "Biocatalytic asymmetric synthesis of chiral amines from ketones applied to sitagliptin manufacture." Science **329**(5989): 305-309.
Sayer, C., M. N. Isupov, A. Westlake and J. A. Littlechild (2013). "Structural studies ofPseudomonasandChromobacteriumω-aminotransferases provide insights into their differing substrate specificity." Acta Crystallographica Section D Biological Crystallography **69**(4): 564-576.
Scavello, F., M. Amiche and J.-E. Ghia (2022). "Recent Advances in Multifunctional Antimicrobial Peptides as Immunomodulatory and Anticancer Therapy: Chromogranin A-Derived Peptides and Dermaseptins as Endogenous versus Exogenous Actors." Pharmaceutics **14**(10): 2014.
Schätzle, S., Höhne, M., Redestad, E., Robins, K., & Bornscheuer, U. T. (2009). (2009). "Rapid and sensitive kinetic assay for characterization of ω-transaminases." Analytical chemistry **81**(19): 8244-8248.
Schmid, A., Dordick, J. S., Hauer, B., Kiener, A., Wubbolts, M., & Witholt, B. (2001). "Schmid, A., Dordick, J. S., Hauer, B., Kiener, A., Wubbolts, M., & Witholt, B. (2001). Industrial biocatalysis today and tomorrow." Nature **409**(6817): 258-268.
Schmidtchen, A., M. Pasupuleti and M. Malmsten (2014). "Effect of hydrophobic modifications in antimicrobial peptides." Adv Colloid Interface Sci **205**: 265-274.
Schütze, A., D. Benndorf, S. Püttker, F. Kohrs and K. Bettenbrock (2020). "The Impact of ackA, pta, and ackA-pta Mutations on Growth, Gene Expression and Protein Acetylation in Escherichia coli K-12." Frontiers in Microbiology **11**.
Schuurmans, J. M., A. S. Nuri Hayali, B. B. Koenders and B. H. Ter Kuile (2009). "Variations in MIC value caused by differences in experimental protocol." Journal of Microbiological Methods **79**(1): 44-47.
Scott, M. G., D. J. Davidson, M. R. Gold, D. Bowdish and R. E. Hancock (2002). "The human antimicrobial peptide LL-37 is a multifunctional modulator of innate immune responses." J Immunol **169**(7): 3883-3891.
Sekurova, O. N., O. Schneider and S. B. Zotchev (2019). "Novel bioactive natural products from bacteria via bioprospecting, genome mining and metabolic engineering." Microb Biotechnol **12**(5): 828-844.
Sengupta, C., M. Ekka, S. Arora, P. D. Dhaware, R. Chowdhury and S. Raychaudhuri (2017). "Cross feeding of glucose metabolism byproducts of Escherichia coli human gut isolates and probiotic strains affect survival of Vibrio cholerae." Gut Pathogens **9**(1).
Shin, J.-S. and B.-G. Kim (2002). "Exploring the Active Site of Amine:Pyruvate Aminotransferase on the Basis of the Substrate Structure−Reactivity Relationship: How the Enzyme Controls Substrate Specificity and Stereoselectivity." The Journal of Organic Chemistry **67**(9): 2848-2853.
Siddique, M. S., A. B.; Ahmad, S.; Dogar, N. A. (2013). "Synthesis and biological evaluation of hydrazide based sulfonamides." J Sci Innovative Res **2**: 627-633.
Sikkema, W. D., A. J. Cal, U. I. Hathwaik, W. J. Orts and C. C. Lee (2023). "Polyhydroxyalkanoate production in Pseudomonas putida from alkanoic acids of varying lengths." PLOS ONE **18**(7): e0284377.

Sikorska, E., O. Stachurski, D. Neubauer, I. Małuch, D. Wyrzykowski, M. Bauer, K. Brzozowski and W. Kamysz (2018). "Short arginine-rich lipopeptides: From self-assembly to antimicrobial activity." Biochimica et Biophysica Acta (BBA) - Biomembranes **1860**(11): 2242-2251.
Simon, R. C., N. Richter, E. Busto and W. Kroutil (2014). "Recent Developments of Cascade Reactions Involving ω-Transaminases." ACS Catalysis **4**(1): 129-143.
Singh, T., P. Choudhary and S. Singh (2022). Antimicrobial Peptides: Mechanism of Action, IntechOpen.
Sinha, M., S. Kaushik, P. Kaur, S. Sharma and T. P. Singh (2013). "Antimicrobial Lactoferrin Peptides: The Hidden Players in the Protective Function of a Multifunctional Protein." International Journal of Peptides **2013**: 1-12.
Skalden, L., C. Peters, J. Dickerhoff, A. Nobili, H. J. Joosten, K. Weisz, M. Höhne and U. T. Bornscheuer (2015). "Two Subtle Amino Acid Changes in a Transaminase Substantially Enhance or Invert Enantiopreference in Cascade Syntheses." ChemBioChem **16**(7): 1041-1045.
Smirnova, M. P., N. I. Kolodkin, A. A. Kolobov, V. G. Afonin, I. V. Afonina, L. I. Stefanenko, V. M. Shpen', O. V. Shamova and A. A. Kolobov (2020). "Indolicidin analogs with broad-spectrum antimicrobial activity and low hemolytic activity." Peptides **132**: 170356.
SnapGene. from www.snapgene.com.
Sneideris, T., N. A. Erkamp, H. Ausserwöger, K. L. Saar, T. J. Welsh, D. Qian, K. Katsuya-Gaviria, M. L. L. Y. Johncock, G. Krainer, A. Borodavka and T. P. J. Knowles (2023). "Targeting nucleic acid phase transitions as a mechanism of action for antimicrobial peptides." Nature Communications **14**(1).
Son, H. F., I.-K. Kim and K.-J. Kim (2015). "Structural insights into domain movement and cofactor specificity of glutamate dehydrogenase from Corynebacterium glutamicum." Biochemical and Biophysical Research Communications **459**(3): 387-392.
Sorensen, M. S., S. P. L. (1940). "The proteins in whey." Compte rendu des Travaux du Laboratoire de Carlsberg, Ser. Chim. **23**(7): 55-99.
Soth, M., J. C. Hermann, C. Yee, M. Alam, J. W. Barnett, P. Berry, M. F. Browner, K. Frank, S. Frauchiger, S. Harris, Y. He, M. Hekmat-Nejad, T. Hendricks, R. Henningsen, R. Hilgenkamp, H. Ho, A. Hoffman, P.-Y. Hsu, D.-Q. Hu, A. Itano, S. Jaime-Figueroa, A. Jahangir, S. Jin, A. Kuglstatter, A. K. Kutach, C. Liao, S. Lynch, J. Menke, L. Niu, V. Patel, A. Railkar, D. Roy, A. Shao, D. Shaw, S. Steiner, Y. Sun, S.-L. Tan, S. Wang and M. D. Vu (2013). "3-Amido Pyrrolopyrazine JAK Kinase Inhibitors: Development of a JAK3 vs JAK1 Selective Inhibitor and Evaluation in Cellular and in Vivo Models." Journal of Medicinal Chemistry **56**(1): 345-356.
Spaar, A., C. Munster and T. Salditt (2004). "Conformation of peptides in lipid membranes studied by x-ray grazing incidence scattering." Biophys J **87**(1): 396-407.
Spehr, V., D. Frahm and T. F. Meyer (2000). "Improvement of the T7 expression system by the use of T7 lysozyme." Gene **257**(2): 259-267.
Špitalský, Z., I. Lacík, E. Lathová, I. Janigová and I. Chodák (2006). "Controlled degradation of polyhydroxybutyrate via alcoholysis with ethylene glycol or glycerol." Polymer Degradation and Stability **91**(4): 856-861.
Stanbury, P. F., Whitaker, A., & Hall, S. J. (2013). Principles of fermentation technology. Burlington MA, Elsevier.

Stark, M., L. P. Liu and C. M. Deber (2002). "Cationic hydrophobic peptides with antimicrobial activity." Antimicrob Agents Chemother **46**(11): 3585-3590.
Stella, L., C. Mazzuca, M. Venanzi, A. Palleschi, M. Didonè, F. Formaggio, C. Toniolo and B. Pispisa (2004). "Aggregation and Water-Membrane Partition as Major Determinants of the Activity of the Antibiotic Peptide Trichogin GA IV." Biophysical Journal **86**(2): 936-945.
Stewart, J. D. (2001). "Dehydrogenases and transaminases in asymmetric synthesis." Current Opinion in Chemical Biology **5**(2): 120-129.
Suh, J. Y., Lee, Y. T., Park, C. B., Lee, K. H., Kim, S. C., Choi, B. S. (1999). "Structural and functional implications of a proline residue in the antimicrobial peptide gaegurin." European journal of biochemistry **266**(2): 665-674.
Sun, C., L. Gu, M. A. Hussain, L. Chen, L. Lin, H. Wang, S. Pang, C. Jiang, Z. Jiang and J. Hou (2019). "Characterization of the Bioactivity and Mechanism of Bactenecin Derivatives Against Food-Pathogens." Frontiers in Microbiology **10**.
Sun, H., H. Zhang, E. L. Ang and H. Zhao (2018). "Biocatalysis for the synthesis of pharmaceuticals and pharmaceutical intermediates." Bioorg Med Chem **26**(7): 1275-1284.
Sykes, R. (2010). "The 2009 Garrod lecture: the evolution of antimicrobial resistance: a Darwinian perspective." J Antimicrob Chemother **65**(9): 1842-1852.
Takeuchi, M., S. Kishino, S. B. Park, A. Hirata, N. Kitamura, A. Saika and J. Ogawa (2016). "Efficient enzymatic production of hydroxy fatty acids by linoleic acid Δ9 hydratase from Lactobacillus plantarum AKU 1009a." Journal of Applied Microbiology **120**(5): 1282-1288.
Thakkar, K. N., S. S. Mhatre and R. Y. Parikh (2010). "Biological synthesis of metallic nanoparticles." Nanomedicine **6**(2): 257-262.
Torres, J. M. C., J. L.; Vielma, J. R. (2006). "DETECCIÓN DE LISOZIMA Y LACTOFERRINA POR WESTERN BLOT EN OVAS DE TRUCHA ARCOIRIS Oncorhynchus mykiss." Mundo Pecuario **2**(3): 57-59.
Tossi, A., L. Sandri and A. Giangaspero (2000). "Amphipathic, α-helical antimicrobial peptides." Biopolymers **55**(1): 4-30.
Tsuji, H. and F. Kondoh (2017). "Synthesis of meso-lactide by thermal configurational inversion and depolymerization of poly(l -lactide) and thermal configurational inversion of lactides." Polymer Degradation and Stability **141**: 77-83.
Ulvatne, H., Ã. R. Samuelsen, H. H. Haukland, M. Krã¤Mer and L. H. Vorland (2004). "Lactoferricin B inhibits bacterial macromolecular synthesis in Escherichia coli and Bacillus subtilis." FEMS Microbiology Letters **237**(2): 377-384.
Unden, G., S. Becker, J. Bongaerts, G. Holighaus, J. Schirawski and S. Six (1995). "O2-Sensing and O2-dependent gene regulation in facultatively anaerobic bacteria." Archives of Microbiology **164**(2): 81-90.
UnitedNations. (2015). "Transforming our world. The 2030 Agenda for Sustainable Development." A/RES/70/1 Retrieved 10/09/2024, from https://sdgs.un.org/2030agenda.
Van Meer, G., D. R. Voelker and G. W. Feigenson (2008). "Membrane lipids: where they are and how they behave." Nature Reviews Molecular Cell Biology **9**(2): 112-124.
Vance, J. E. (2015). "Phospholipid synthesis and transport in mammalian cells." Traffic **16**(1): 1-18.

Vaucher, R. A., S. da Motta Ade and A. Brandelli (2010). "Evaluation of the in vitro cytotoxicity of the antimicrobial peptide P34." Cell Biol Int **34**(3): 317-323.
Velkov, T., K. D. Roberts, R. L. Nation, P. E. Thompson and J. Li (2013). "Pharmacology of Polymyxins: New Insights into an 'Old' Class of Antibiotics." Future Microbiology **8**(6): 711-724.
Vicente, D., D. N. Proença and P. V. Morais (2023). "The Role of Bacterial Polyhydroalkanoate (PHA) in a Sustainable Future: A Review on the Biological Diversity." International Journal of Environmental Research and Public Health **20**(4): 2959.
Vikhrankar, S., S. Satbhai, P. Kulkarni, R. Ranbhor, V. Ramakrishnan and P. Kodgire (2024). "Enzymatic Routes for Chiral Amine Synthesis: Protein Engineering and Process Optimization." Biologics: Targets and Therapy **Volume 18**: 165-179.
Vogel, H. J., D. J. Schibli, W. Jing, E. M. Lohmeier-Vogel, R. F. Epand and R. M. Epand (2002). "Towards a structure-function analysis of bovine lactoferricin and related tryptophan- and arginine-containing peptides." Biochemistry and Cell Biology **80**(1): 49-63.
Voss, M., C. Xiang, J. Esque, A. Nobili, M. J. Menke, I. André, M. Höhne and U. T. Bornscheuer (2020). "Creation of (R)-Amine Transaminase Activity within an α-Amino Acid Transaminase Scaffold." ACS Chemical Biology **15**(2): 416-424.
Wahart, A. J. C., J. Staniland, G. J. Miller and S. C. Cosgrove (2022). "Oxidase enzymes as sustainable oxidation catalysts." Royal Society Open Science **9**(1).
Wakabayashi, H., T. Hiratani, K. Uchida and H. Yamaguchi (1996). "Antifungal Spectrum and Fungicidal Mechanism of an N-Terminal Peptide of Bovine Lactoferrin." Journal of Infection and Chemotherapy **1**(3): 185-189.
Wakabayashi, H., H. Matsumoto, K. Hashimoto, S. Teraguchi, M. Takase and H. Hayasawa (1999). "N-Acylated and <scp>d</scp> Enantiomer Derivatives of a Nonamer Core Peptide of Lactoferricin B Showing Improved Antimicrobial Activity." Antimicrobial Agents and Chemotherapy **43**(5): 1267-1269.
Wang, G., X. Li and Z. Wang (2016). "APD3: the antimicrobial peptide database as a tool for research and education." Nucleic Acids Res **44**(D1): D1087-1093.
Wang, J.-F., H.-L. Meng, Z.-Q. Xiong, S.-L. Zhang and Y. Wang (2014). "Identification of novel knockout and up-regulated targets for improving isoprenoid production in E. coli." Biotechnology Letters **36**(5): 1021-1027.
Wang, L., A. Brock, B. Herberich and P. G. Schultz (2001). "Expanding the Genetic Code of Escherichia coli." Science **292**(5516): 498-500.
Wang, L., P. Chen and W. Xiao (2021). "β-hydroxybutyrate as an Anti-Aging Metabolite." Nutrients **13**(10): 3420.
Wang, M., M. Xu, Y. Long, S. Fargue, N. Southall, X. Hu, J. C. McKew, C. J. Danpure and W. Zheng (2016). "High throughput cell-based assay for identification of glycolate oxidase inhibitors as a potential treatment for Primary Hyperoxaluria Type 1." Scientific Reports **6**(1): 34060.
Wang, Q., A. R. Parrish and L. Wang (2009). "Expanding the Genetic Code for Biological Studies." Chemistry & Biology **16**(3): 323-336.
Wang, Q., Y. Xu and J. Hu (2022). "Intracellular mechanism of antimicrobial peptide HJH-3 against Salmonella pullorum." RSC Advances **12**(23): 14485-14491.

Wang, X., L. Li, Y. Zheng, H. Zou, Y. Cao, H. Liu, W. Liu and M. Xian (2012). "Biosynthesis of long chain hydroxyfatty acids from glucose by engineered Escherichia coli." Bioresource Technology **114**: 561-566.
Wang, Z., B. Sundara Sekar and Z. Li (2021). "Recent advances in artificial enzyme cascades for the production of value-added chemicals." Bioresource Technology **323**: 124551.
Waterhouse, A., M. Bertoni, S. Bienert, G. Studer, G. Tauriello, R. Gumienny, F. T. Heer, A. Tjaart, C. Rempfer, L. Bordoli, R. Lepore and T. Schwede (2018). "SWISS-MODEL: homology modelling of protein structures and complexes." Nucleic Acids Research **46**(W1): W296-W303.
Weber, N., A. Hatsch, L. Labagnere and H. Heider (2017). "Production of (S)-2-aminobutyric acid and (S)-2-aminobutanol in Saccharomyces cerevisiae." Microbial Cell Factories **16**(1).
Weinstein, L. C., T. W.; Hudson, J. B.; Hartl, W. (1957). "The concurrent use of sulfonamides and antibiotics in the treatment of infections: in vivo and in vitro studies of the effect of sulfonamide-antibiotic combinations on the emergence of drug resistance." Annals of the New York Academy of Sciences **69**(3): 408.
Widney, K. A., D.-D. Yang, L. M. Rusch and S. D. Copley (2024). CRISPR-Cas9-assisted genome editing inE. colielevates the frequency of unintended mutations, Cold Spring Harbor Laboratory.
Wimley, W. C. (2010). "Describing the mechanism of antimicrobial peptide action with the interfacial activity model." ACS chemical biology **5**(10): 905-917.
Wojcieszak, R., T. Bonnotte, S. Paul, B. Katryniok and F. Dumeignil (2020). "Lactic Acid Conversion to Acrylic Acid Over Fluoride-Substituted Hydroxyapatites." Frontiers in Chemistry **8**.
Woo, S. Y. and H. Lee (2017). "Aggregation and insertion of melittin and its analogue MelP5 into lipid bilayers at different concentrations: effects on pore size, bilayer thickness and dynamics." Physical Chemistry Chemical Physics **19**(10): 7195-7203.
WorldBank. (2016). "By 2050, drug-resistant infections could cause global economic damage on par with 2008 financial crisis." Retrieved 23/03/21, 2021, from https://www.worldbank.org/.
Wu, C.-L., K.-L. Peng, B.-S. Yip, Y.-H. Chih and J.-W. Cheng (2021). "Boosting Synergistic Effects of Short Antimicrobial Peptides With Conventional Antibiotics Against Resistant Bacteria." Frontiers in Microbiology **12**.
Wu, G., F. W. Bazer, R. C. Burghardt, G. A. Johnson, S. W. Kim, D. A. Knabe, P. Li, X. Li, J. R. McKnight, M. C. Satterfield and T. E. Spencer (2011). "Proline and hydroxyproline metabolism: implications for animal and human nutrition." Amino Acids **40**(4): 1053-1063.
Xiang, Z. and L. Wang (2011). "Enantiospecific Synthesis of Genetically Encodable Fluorescent Unnatural Amino Acid <scp>l</scp>-3-(6-Acetylnaphthalen-2-ylamino)-2-aminopropanoic Acid." The Journal of Organic Chemistry **76**(15): 6367-6371.
Xiao, K., X.-H. Yue, W.-C. Chen, X.-R. Zhou, L. Wang, L. Xu, F.-H. Huang and X. Wan (2018). "Metabolic Engineering for Enhanced Medium Chain Omega Hydroxy Fatty Acid Production in Escherichia coli." Frontiers in Microbiology **9**.
Xiong, Y. Q., W. A. Hady, A. Deslandes, A. Rey, L. Fraisse, H. H. Kristensen, M. R. Yeaman and A. S. Bayer (2011). "Efficacy of NZ2114, a novel plectasin-derived cationic

antimicrobial peptide antibiotic, in experimental endocarditis due to methicillin-resistant Staphylococcus aureus." Antimicrob Agents Chemother **55**(11): 5325-5330.
Xu, J.-M., J.-Q. Li, B. Zhang, Z.-Q. Liu and Y.-G. Zheng (2019). "Fermentative production of the unnatural amino acid l-2-aminobutyric acid based on metabolic engineering." Microbial Cell Factories **18**(1).
Xu, J., X. Tang, Y. Zhu, Z. Yu, K. Su, Y. Zhang, Y. Dong, W. Zhu, C. Zhang, R. Wu and J. Liu (2020). "Structural studies reveal flexible roof of active site responsible for ω-transaminase CrmG overcoming by-product inhibition." Communications Biology **3**(1).
Xu, Y. Y., Samaranayake, Y. H., Samaranayake, L. P., & Nikawa, H. (1999). "In vitro susceptibility of Candida species to lactoferrin." Sabouraudia **37**(1): 35-51.
Yamauchi, K., H. Wakabayashi, K. Shin and M. Takase (2006). "Bovine lactoferrin: benefits and mechanism of action against infections." Biochem Cell Biol **84**(3): 291-296.
Yan, J., K. Wang, W. Dang, R. Chen, J. Xie, B. Zhang, J. Song and R. Wang (2013). "Two Hits Are Better than One: Membrane-Active and DNA Binding-Related Double-Action Mechanism of NK-18, a Novel Antimicrobial Peptide Derived from Mammalian NK-Lysin." Antimicrobial Agents and Chemotherapy **57**(1): 220-228.
Yang, X.-H., J.-H. Xie and Q.-L. Zhou (2014). "Chiral spiro iridium catalysts with SpiroPAP ligands: highly efficient for asymmetric hydrogenation of ketones and ketoesters." Organic Chemistry Frontiers **1**(2): 190.
Yang, Z.-P., D. J. Freas and G. C. Fu (2021). "Asymmetric Synthesis of Protected Unnatural α-Amino Acids via Enantioconvergent Nickel-Catalyzed Cross-Coupling." Journal of the American Chemical Society **143**(23): 8614-8618.
Ye, D., C. Yang, W. Ji, J. Zheng, J. Zhang, R. Xue, J. Gu, M. Chen, K. Yan and Y. Liu (2022). "Impact of the Expert Consensus on Carbapenem Consumption Trends and Patterns in Public Healthcare Institutes: An Interrupted Time Series Analysis, 2017–2020." Frontiers in Pharmacology **12**.
Yin, Q., Y. Shi, J. Wang and X. Zhang (2020). "Direct catalytic asymmetric synthesis of α-chiral primary amines." Chemical Society Reviews **49**(17): 6141-6153.
Yoo, Y.-C., R. Watanabe, Y. Koike, M. Mitobe, K.-I. Shimazaki, S. Watanabe and I. Azuma (1997). "Apoptosis in Human Leukemic Cells Induced by Lactoferricin, a Bovine Milk Protein-Derived Peptide: Involvement of Reactive Oxygen Species." Biochemical and Biophysical Research Communications **237**(3): 624-628.
Ypsilantis, K., A. Garypidou, A. Gikas, A. Kiapekos, J. C. Plakatouras and A. Garoufis (2023). "A New Unnatural Amino Acid Derived from the Modification of 4'-(p-tolyl)-2,2':6',2"-terpyridine and Its Mixed-Ligand Complexes with Ruthenium: Synthesis, Characterization, and Photophysical Properties." Chemistry **5**(1): 151-163.
Yun, E. J., S. Kwak, S. R. Kim, Y.-C. Park, Y.-S. Jin and K. H. Kim (2015). "Production of (S)-3-hydroxybutyrate by metabolically engineered Saccharomyces cerevisiae." Journal of Biotechnology **209**: 23-30.
Zhang, C. and S. A. Madbouly (2016). Plant Oil-Based Derivatives, Elsevier**:** 19-35.
Zhang, H., L. Zhao, P. Zhang, Y. Xie, X. Yao, X. Pan, Y. Fu, J. Wei, H. Bai, X. Shao, J. Ye and C. Wu (2024). "Effects of selenoprotein extracts from Cardamine hupingshanensis on growth, selenium metabolism, antioxidant capacity, immunity and intestinal health in largemouth bass Micropterus salmoides." Frontiers in Immunology **15**.
Zhao, C., L. Wang, D. Li, J. Li, Y. Ge, T. Liang, Y. Zhu and R. Yu (2021). "High-cell-density fermentation of <scp>Escherichia coli</scp> for expression of a recombinant

phenylalanine dehydrogenase mutant and its purification." Journal of Chemical Technology & Biotechnology **96**(1): 199-206.
Zhao, H., R. Sood, A. Jutila, S. Bose, G. Fimland, J. Nissen-Meyer and P. K. J. Kinnunen (2006). "Interaction of the antimicrobial peptide pheromone Plantaricin A with model membranes: Implications for a novel mechanism of action." Biochimica et Biophysica Acta (BBA) - Biomembranes **1758**(9): 1461-1474.
Zhou, F., Y. Xu, Y. Nie and X. Mu (2022). "Substrate-Specific Engineering of Amino Acid Dehydrogenase Superfamily for Synthesis of a Variety of Chiral Amines and Amino Acids." Catalysts **12**(4): 380.
Zou, H., L. Li, T. Zhang, M. Shi, N. Zhang, J. Huang and M. Xian (2018). "Biosynthesis and biotechnological application of non-canonical amino acids: Complex and unclear." Biotechnology Advances **36**(7): 1917-1927.
Zuend, S. J., M. P. Coughlin, M. P. Lalonde and E. N. Jacobsen (2009). "Scaleable catalytic asymmetric Strecker syntheses of unnatural α-amino acids." Nature **461**(7266): 968-970.

Appendix

Table S1. Quantification of amino and keto fatty acids used to screen the activity of commercial transaminases in deaminating L-alanine and using acetophenone as amino acceptor.

Transaminase	Concentration (mM)			
	Amino donor (L-ala)	Amino acceptor (AP)	Amino product (1-PEA)	Keto by-product (AP)
ATA-117	15.09	NA	NA	NA
ATA-217	14.94	NA	NA	NA
ATA-113	15.21	NA	NA	NA
CV_TA	10.58	NA	NA	NA
BL21_pET45b	9.703	NA	NA	NA

NA indicates that the compound could not be detected in the samples.

Table S2. Quantification of amino and keto fatty acids used to screen the activity of commercial transaminases in deaminating 3ABA and using acetophenone as amino acceptor.

Transaminase	Concentration (mM)				
	Amino donor (3ABA)	Amino acceptor (AP)	Amino product (1-PEA)	L-ala	Keto by-product (3OBA)
ATA-117	14.73	NA	NA	NA	4.05
ATA-217	15.74	NA	NA	NA	NA
ATA-113	15.99	NA	NA	NA	NA
CV_TA	14.37	NA	NA	2.12	NA
BL21_pET45b	14.16	NA	NA	0.84	NA

NA indicates that the compound could not be detected in the sample

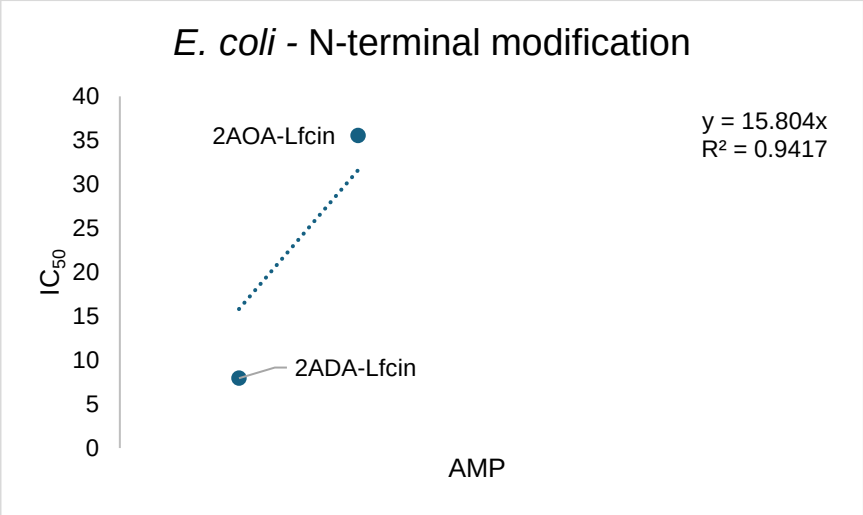
E. coli - N-terminal modification
y = 15.804x
R² = 0.9417
IC50
40
35
30
25
20
15
10
5
0
2AOA-Lfcin
2ADA-Lfcin
AMP

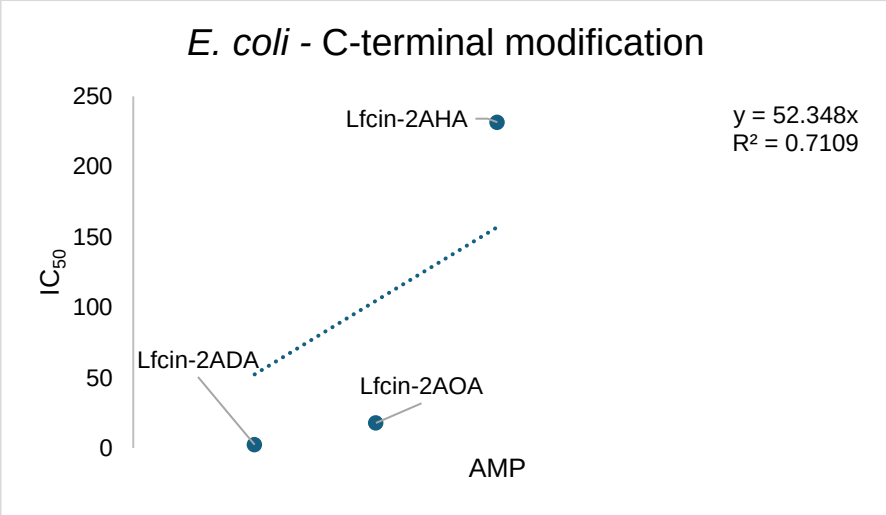
E. coli - C-terminal modification
y = 52.348x
R² = 0.7109
IC50
250
200
150
100
50
0
Lfcin-2AHA
Lfcin-2ADA
Lfcin-2AOA
AMP

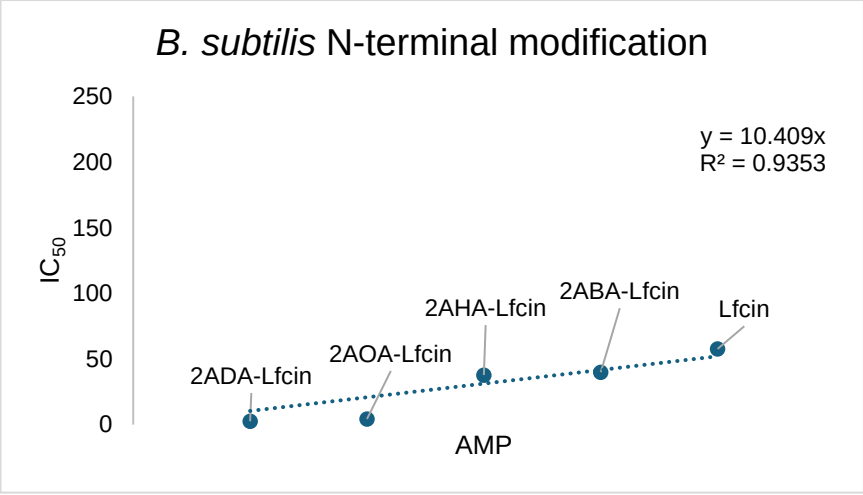
B. subtilis N-terminal modification
y = 10.409x
R² = 0.9353
IC50
250
200
150
100
50
0
2ADA-Lfcin
2AOA-Lfcin
2AHA-Lfcin
2ABA-Lfcin
Lfcin
AMP

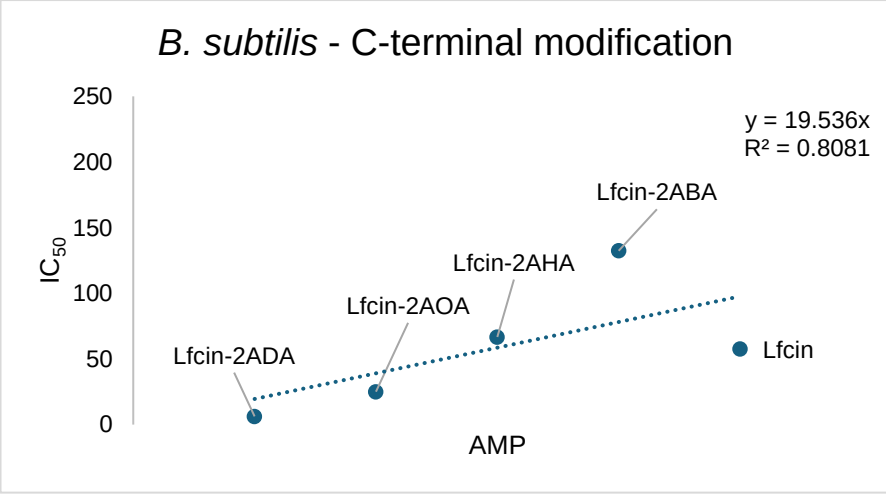
B. subtilis - C-terminal modification
y = 19.536x
R² = 0.8081
IC50
250
200
150
100
50
0
Lfcin-2ABA
Lfcin-2AHA
Lfcin-2AOA
Lfcin-2ADA
Lfcin
AMP

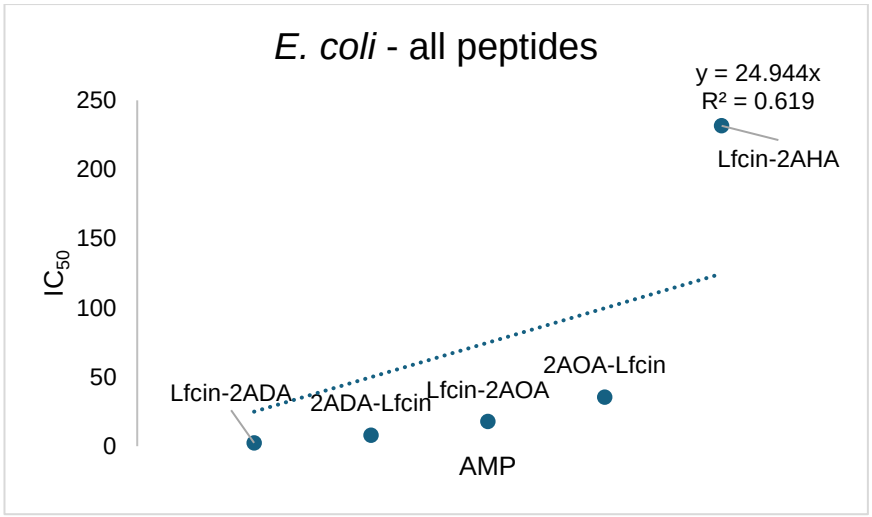

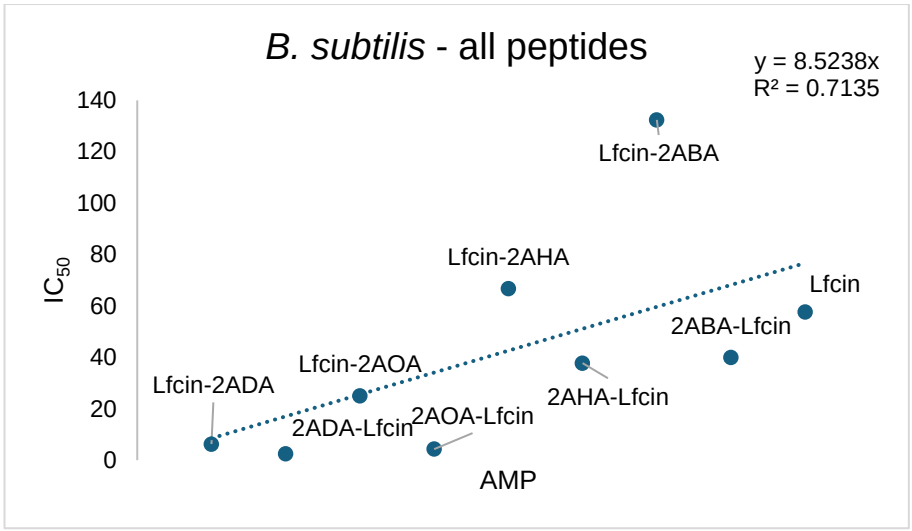

Figure S. 1. Relationship between the size of the acyl chain in the ncAA and the IC_{50}. The LFcin peptide series is shown in the X axis while the IC_{50} is shown in the Y axis. This was calculated for peptides where bacterial growth was inhibited in MIC and MBC.

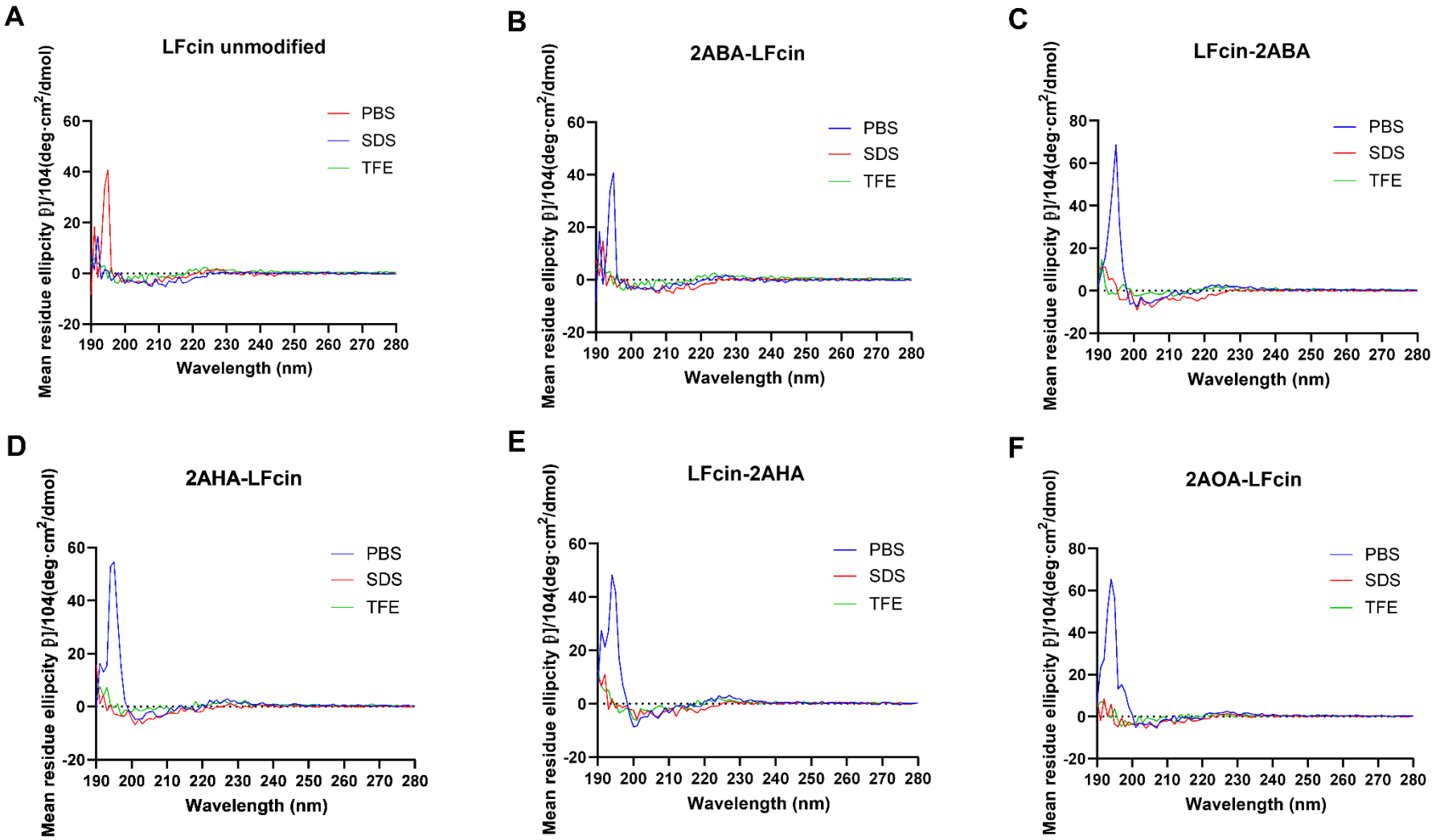
A
LFcin unmodified
B
2ABA-LFcin
C
LFcin-2ABA
D
2AHA-LFcin
E
LFcin-2AHA
F
2AOA-LFcin
PBS
SDS
TFE
Mean residue ellipcity β]/104(deg·cm²/dmol)
Wavelength (nm)
190 200 210 220 230 240 250 260 270 280

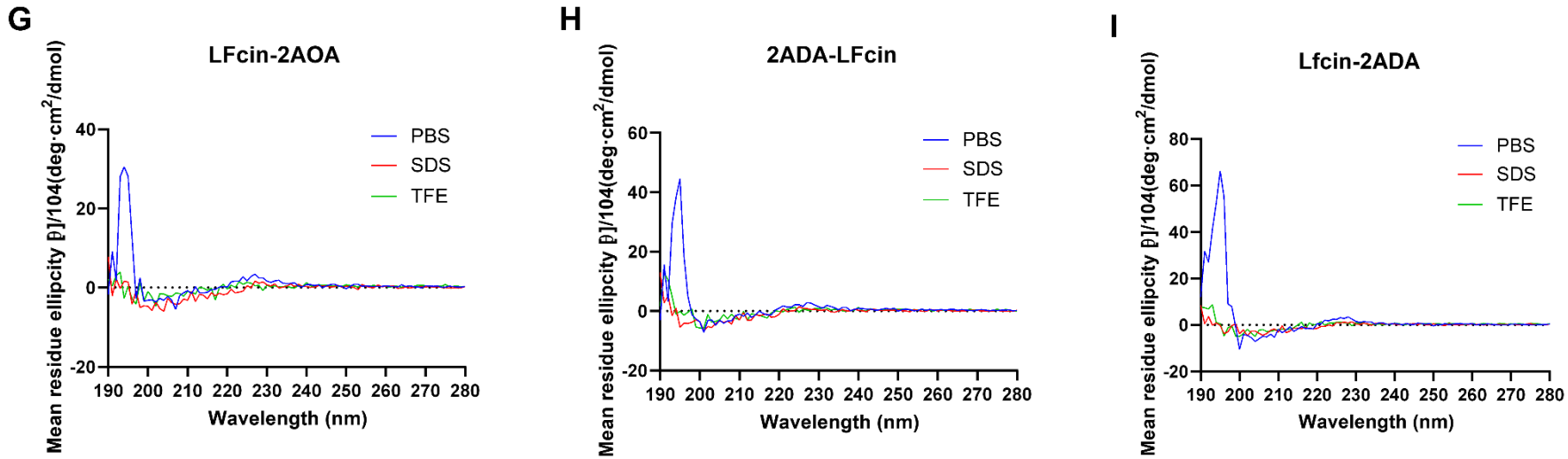

Figure S. 2. Circular dichroism (CD) spectra for LFcin peptide series. CD spectra for LFcin nonameric and LFcin modified C- and N-terminally with 2-aminobutyric acid (2ABA), 2-aminohexanoic acid (2AHA), 2-aminooctanoic (2AOA), and 2-aminodecanoic acid (2ADA).